

**STOCHASTIC ANALYSIS AND DESIGN
OF
VIBRATING BARRIERS
UNDER
SIMULATED GROUND MOTION
PROCESSES**

LAURA D'AMICO

PHD 2017

BLANK

Abstract

Vibration control techniques have developed remarkably over the past thirty years. These solutions are usually employed to protect new rather than existing structures, for which most of the available control devices may be costly and invasive to install. Recently, Vibrating Barriers (ViBas) have been proposed as a solution to protect both new and existing buildings. By exploiting the Structure-Soil-Structure-Interaction (SSSI) phenomenon, the ViBa is constructed away from the structures to be protected allowing the characteristics of the buildings to remain unaltered. The ViBa is envisaged as a vibrating mass placed into the soil, through which the control device interacts with the structure in its proximity and is therefore able to control vibrations for cluster of buildings.

Up until now the efficiency of the ViBa has only been demonstrated for simple cases of seismic deterministic input and stationary Gaussian stochastic processes. This research explores the multiple interactions between a building and a ViBa device in order to assess its performance in realistic earthquake scenarios. By means of Direct Stochastic methods, this research presents a methodology to design the ViBa validated through pertinent Monte Carlo Simulation. The effects of the input selection on the ViBa performance are investigated by analysis of the building-soil-ViBa system response under advanced stochastic Ground Motion Models (GMMs). In regard to this, a technique is proposed to simulate earthquake ground motions in agreement with seismic codes and reproducing the non-stationarity and natural variability typical of recorded earthquakes.

Initial investigations on the response of linear and non-linear structures, under the proposed ground motion and a traditional quasi-stationary and non-stationary model, have demonstrated that the choice of the ground motion has considerable influence over the study of the reliability of structures also for the simple case of linear behaving structures. From the analyses, the sensitivity of the distribution of the relevant response parameters (e.g. the peak displacement) to the GMMs is shown. All spectrum compatible models adopted fulfil the code provisions, however noticeable differences in the distribution of response parameters are observed. Moreover, studies on the sensitivity of structural responses to damping variation have been performed to address the significance of the GMM selection in relation to the assumptions on the structural damping. Finally, some drawbacks in the current seismic codes have also been identified.

In order to establish the methodology for the design of the ViBa under stochastic excitation, the discrete formulation for buildings-soil-ViBa-systems available in the frequency domain has been extended to the time domain. The methodology proposed in this work enables a simplified reliability assessment by defining the mean value of the maxima response displacements under stationary Gaussian stochastic seismic action firstly and successively verified for non-stationary input. From the investigations, the effectiveness of the ViBa is exhibited as having reductions of up to 37.80 % of the mean and up to 41.49% of the fractile 95% of the peak displacements.

BLANK

Table of Contents

LIST OF TABLES	VIII
LIST OF FIGURES	XIV
ABBREVIATIONS AND SYMBOLS	XXI
1 INTRODUCTION.....	1
1.1 MOTIVATIONS.....	2
1.2 RESEARCH AIM AND OBJECTIVES.....	3
1.3 ORIGINAL CONTRIBUTION.....	5
1.4 THESIS OUTLINE	8
2 ANALYSIS METHODS OF SEISMICALLY EXCITED LINEAR STRUCTURAL SYSTEMS	11
2.1 DETERMINISTIC SEISMIC ANALYSIS.....	11
2.1.1 <i>Equation of Motion and Response of Single Degree Of Freedom (SDOF) Systems</i>	<i>11</i>
2.1.1.1 Time Domain Analysis of SDOF Systems: Relative and Absolute Motion	12
2.1.1.2 Frequency Domain Analysis of SDOF Systems: Relative and Absolute Motion.....	16
2.1.2 <i>Equation of Motion and Response of Multi Degree Of Freedom (MDOF) Systems</i>	<i>20</i>
2.1.2.1 Time domain analysis of MDOF systems: Relative and Absolute Motion.....	20
2.1.2.2 Frequency domain analysis of MDOF systems: Relative and Absolute Motion	25
2.2 STOCHASTIC SEISMIC ANALYSIS.....	27
2.2.1 <i>Review of Theory of Probability and Stochastic Processes.....</i>	<i>27</i>
2.2.2 <i>Stochastic Seismic Ground Motion Processes.....</i>	<i>33</i>
2.2.3 <i>Spectral Characteristics of Stochastic Processes.....</i>	<i>36</i>
2.2.4.1 Spectral Representation of the Response of Structural Systems.....	40
2.2.4.2 First Passage Problem and Reliability	45
2.2.4.3 Peak Factor	50
3 GROUND MOTION MODELLING: RESPONSE SPECTRUM COMPATIBLE APPROACH.....	53
3.1 LITERATURE REVIEW	55
3.1.1 <i>Stationary and Quasi-Stationary Gaussian Stochastic Processes.....</i>	<i>61</i>
3.1.1.1 Problem Position.....	62
3.1.1.2 Closed-Form Expressions for the Parameters of the Jennings et al. (1969) Time- Modulating function	72
3.1.1.3 Numerical Application	74
3.1.2 <i>Non-Stationary Gaussian Stochastic Processes</i>	<i>80</i>
3.1.2.1 Problem Position.....	80
3.1.2.2 Numerical Application	87
3.2 CURRENT TRENDS IN GROUND MOTION MODELLING	90
3.2.1 <i>Problem Position.....</i>	<i>93</i>

3.2.2	<i>Simulation of Ground Motions with Imposed Natural Variability and Correlated Spectral Accelerations</i>	96
3.2.2.1	Numerical Application.....	100
3.3	CONCLUDING REMARKS.....	105
4	NUMERICAL COMPARATIVE STUDY OF LINEAR AND NON-LINEAR BENCHMARK STRUCTURES	107
4.1	PROPOSED TECHNIQUE TO DEFINE STOCHASTIC INPUT GROUND MOTIONS	107
4.2	STRUCTURAL RESPONSE AND ANALYSIS TOOLS	114
4.2.1.1	SMART 2008:2-Storey Reinforced Concrete Building	114
4.2.1.2	IASC 1996: 5-Storey Steel Frame.....	118
4.2.1.3	SAC building: 20-Storey Steel Frame.....	121
4.3	CONCLUDING REMARKS.....	125
5	STRUCTURE-SOIL-STRUCTURE-INTERACTION OVERVIEW	127
5.1	FUNDAMENTALS OF DYNAMIC SOIL-STRUCTURE-INTERACTION (SSI).....	128
5.1.1	<i>Overview of SSI in Earthquake Engineering</i>	128
5.1.2	<i>Soil-Structure-Interaction Effects and Methods of Analysis</i>	135
5.2	STATE OF THE ART OF STRUCTURE-SOIL-STRUCTURE-INTERACTION (SSSI)	137
5.2.1	<i>Discrete Models</i>	141
5.2.2	<i>Experimental Approach</i>	153
5.3	STATIONARY STOCHASTIC ANALYSIS OF SSSI SYSTEMS.....	155
5.4	CONCLUDING REMARKS.....	159
6	VIBRATION CONTROL OF A SINGLE STRUCTURE THROUGH THE VIBRATING BARRIER	161
6.1	LITERATURE REVIEW	164
6.1.1	<i>Passive Vibration Control Solution for Structures under Seismic Ground Motion: Vibrating Barriers</i>	166
6.1.2	<i>Design of the Vibrating Barrier under Harmonic Base Excitation: Frequency Domain Approach</i>	168
6.2	TIME DOMAIN ANALYSIS OF SINGLE STRUCTURES UNDER HARMONIC INPUT PROTECTED THROUGH THE VIBRATING BARRIER	176
6.3	NUMERICAL APPLICATIONS OF TIME DOMAIN DETERMINISTIC ANALYSES	180
6.3.1	<i>Design of the ViBa for the Control of the Simplified Structure of Cacciola and Tombari (2015)</i>	180
6.3.2	<i>Design of the ViBa for the Control of the SAC building 20-Storey Steel Frame</i>	188
6.4	DESIGN OF THE VIBRATING BARRIER FOR STATIONARY STOCHASTIC EXCITATION	195
6.5	NUMERICAL APPLICATION OF STOCHASTIC ANALYSIS AND DESIGN OF THE VIBRATING BARRIER.....	198
6.5.1	<i>Ground Motion Models Specifications</i>	198
6.5.2	<i>Parametric Study to Calibrate the ViBa and Monte Carlo Simulation Study</i>	205

6.5.2.1	Design of the ViBa for the Control of the Simplified Structure of Cacciola and Tombari (2015) under Gaussian Stochastic Excitation	207
6.5.2.2	Stochastic Response of the Simplified Structure of Cacciola and Tombari (2015) Protected with the ViBa	209
6.5.2.3	Design of the ViBa for the Control of the SAC Building 20-Storey Steel Frame under Gaussian Stochastic Excitation.....	221
6.5.2.4	Stochastic Response of the SAC Building 20-Storey Steel Frame Protected with the ViBa... ..	223
6.5.3	<i>Concluding Remarks</i>	234
7	CONCLUSIONS	237
7.1	REVIEW OF RESEARCH AIM AND OBJECTIVES	239
7.2	SUMMARY OF THE MAIN FINDINGS	242
7.3	FURTHER DEVELOPMENTS OF THE RESEARCH.....	243
	REFERENCES	246
	APPENDIX	265

List of Tables

Chapter 3

Table 3.1.	Target response spectrum parameters of definition: Type 1, Type A....	77
Table 3.2.	Target response spectrum parameters of definition: Type 1, Type B....	87
Table 3.3.	Target response spectrum parameters of definition: Type 1, Type A..	100

Chapter 4

Table 4.1.	Target response spectrum parameters of definition: Type 1, Type D..	109
Table 4.2.	SMART 2008 structural responses: displacement statistics [m].	117
Table 4.3.	5-storey building structural responses: displacement statistics [m].....	120
Table 4.4.	SAC building linear model structural responses: displacement statistics [m].	122
Table 4.5.	SAC building non-linear model structural responses: displacement statistics [m].....	124

Chapter 5

Table 5.1.	Stiffness coefficients for one-dimensional discrete foundation soil-interaction (Richart et al. 1970, Gazetas 1983, Wolf 1988).	142
Table 5.2.	Expression of coupling functions for foundation-soil-foundation interaction (Mulliken and Karabalis 1998).....	143

Chapter 6

Table 6.1.	First two natural frequencies of the system one building-soil-ViBa under investigation.	173
------------	---	-----

Table 6.2.	Mechanical parameters for the experimental tests on a single structure protected through ViBa device (Cacciola and Tombari 2015).	174
Table 6.3.	Values of the transfer function of the building's horizontal DOF at selected frequencies in coupled and uncoupled conditions under the hypothesis of viscous damping.	186
Table 6.4.	Mechanical parameters for the SAC building and ViBa device.	189
Table 6.5.	First two natural frequencies of the simplified SAC building-soil-ViBa system modelled on MATLAB.	189
Table 6.6.	Geotechnical properties of the soil deposit adopted to model the SAC building-Soil-ViBa system in SAP2000.	191
Table 6.7.	First two natural frequencies of the SAC building-soil-ViBa system modelled on SAP2000 in coupled and uncoupled conditions.	191
Table 6.8.	Values of the selected frequencies of the harmonic input forcing the system SAC building-soil-ViBa.	192
Table 6.9.	Target response spectrum parameters of definition: Type 2, soil D. ...	200
Table 6.10.	ViBa's parameters for different ratios m_{ViBa} / m obtained by the design under stationary stochastic excitation for the protection of the structure of Cacciola and Tombari (2015) through ViBa.	207
Table 6.11.	Coupled and uncoupled natural frequencies of the system building-soil-ViBa for different ratios m_{ViBa} / m	209
Table 6.12.	Monte Carlo Simulation: mean of the displacements of the building protected with ViBa for $m_{ViBa} / m = 0.5$	211
Table 6.13.	Monte Carlo Simulation: fractile 5% of the displacements of the building protected with ViBa for $m_{ViBa} / m = 0.5$	211

Table 6.14.	Monte Carlo Simulation: fractile 50% of the displacements of the building protected with ViBa for $m_{ViBa} / m = 0.5$	211
Table 6.15.	Monte Carlo Simulation: fractile 95% of the displacements of the building protected with ViBa for $m_{ViBa} / m = 0.5$	211
Table 6.16.	Monte Carlo Simulation: mean of the displacements of the building protected with ViBa for $m_{ViBa} / m = 1.05$	213
Table 6.17.	Monte Carlo Simulation: fractile 5% of the displacements of the building protected with ViBa for $m_{ViBa} / m = 1.05$	213
Table 6.18.	Monte Carlo Simulation: fractile 50% of the displacements of the building protected with ViBa for $m_{ViBa} / m = 1.05$	213
Table 6.19.	Monte Carlo Simulation: fractile 95% of the displacements of the building protected with ViBa for $m_{ViBa} / m = 1.05$	213
Table 6.20.	Monte Carlo Simulation: mean of the displacements of the building protected with ViBa for $m_{ViBa} / m = 1.5$	215
Table 6.21.	Monte Carlo Simulation: fractile 5% of the displacements of the building protected with ViBa for $m_{ViBa} / m = 1.5$	215
Table 6.22.	Monte Carlo Simulation: fractile 50% of the displacements of the building protected with ViBa for $m_{ViBa} / m = 1.5$	215
Table 6.23.	Monte Carlo Simulation: fractile 95% of the displacements of the building protected with ViBa for $m_{ViBa} / m = 1.5$	215
Table 6.24.	Monte Carlo simulation: mean of the displacements of the building protected with ViBa for $m_{ViBa} / m = 2$	217

Table 6.25. Monte Carlo simulation: fractile 5% of the displacements of the building protected with ViBa for $m_{ViBa} / m = 2$	217
Table 6.26. Monte Carlo simulation: fractile 50% of the displacements of the building protected with ViBa for $m_{ViBa} / m = 2$	217
Table 6.27. Monte Carlo simulation: fractile 95% of the displacements of the building protected with ViBa for $m_{ViBa} / m = 2$	217
Table 6.28. Percentage differences between the reductions predicted through the design under stationary stochastic excitation and Monte Carlo Simulation study of the response of Cacciola and Tombari (2015) structure.	219
Table 6.29. Modal participation coefficients for the SSSI systems under investigation.	220
Table 6.30. Summary of the highest reductions of the mean value and fractiles of the distribution of the peak displacements of the simplified system of Cacciola and Tombari (2015).	220
Table 6.31. ViBa's parameters for different ratios m_{ViBa} / m obtained by the design under stationary stochastic excitation for the protection of the structure of the SAC building through ViBa.	221
Table 6.32. Natural frequencies of the simplified SAC building-soil-ViBa system for different ratios m_{ViBa} / m	223
Table 6.33. Monte Carlo Simulation: mean of the displacements of the simplified SAC building protected with ViBa for $m_{ViBa} / m = 0.5$	225
Table 6.34. Monte Carlo Simulation: fractile 5% of the displacements of the simplified SAC building protected with ViBa for $m_{ViBa} / m = 0.5$	225

Table 6.35.	Monte Carlo Simulation: fractile 50% of the displacements of the simplified SAC building protected with ViBa for $m_{ViBa} / m = 0.5$	225
Table 6.36.	Monte Carlo Simulation: fractile 95% of the displacements of the simplified SAC building protected with ViBa for $m_{ViBa} / m = 0.5$	225
Table 6.37.	Monte Carlo simulation: mean of the displacements of the simplified SAC building protected with ViBa for $m_{ViBa} / m = 1$	227
Table 6.38.	Monte Carlo Simulation: fractile 5% of the displacements of the simplified SAC building protected with ViBa for $m_{ViBa} / m = 1$	227
Table 6.39.	Monte Carlo Simulation: fractile 50% of the displacements of the simplified SAC building protected with ViBa for $m_{ViBa} / m = 1$	227
Table 6.40.	Monte Carlo Simulation: fractile 95% of the displacements of the simplified SAC building protected with ViBa for $m_{ViBa} / m = 1$	227
Table 6.41.	Monte Carlo simulation: mean of the displacements of the simplified SAC building protected with ViBa for $m_{ViBa} / m = 1.5$	229
Table 6.42.	Monte Carlo simulation: fractile 5% of the displacements of the simplified SAC building protected with ViBa for $m_{ViBa} / m = 1.5$	229
Table 6.43.	Monte Carlo simulation: fractile 50% of the displacements of the simplified SAC building protected with ViBa for $m_{ViBa} / m = 1.5$	229
Table 6.44.	Monte Carlo simulation: fractile 95% of the displacements of the simplified SAC building protected with ViBa for $m_{ViBa} / m = 1.5$	229
Table 6.45.	Monte Carlo simulation: mean of the displacements of the simplified SAC building protected with ViBa for $m_{ViBa} / m = 2$	231

Table 6.46.	Monte Carlo simulation: fractile 5% of the displacements of the simplified SAC building protected with ViBa for $m_{ViBa} / m = 2$	231
Table 6.47.	Monte Carlo simulation: fractile 50% of the displacements of the simplified SAC building protected with ViBa for $m_{ViBa} / m = 2$	231
Table 6.48.	Monte Carlo simulation: fractile 95% of the displacements of the simplified SAC building protected with ViBa for $m_{ViBa} / m = 2$	231
Table 6.49.	Percentage differences between the reductions predicted through the design under stationary stochastic excitation and Monte Carlo Simulation study of the response of the simplified SAC building model.	233
Table 6.50.	Summary of the highest reductions of the mean value and fractiles of the distribution of the peak displacements of the simplified SAC building model.	234

List of Figures

Chapter 2

- Figure 2.1. 2 DOF frame subjected to single support excitation at the base..... 44
- Figure 2.2. Geometrical and Non-Geometrical and Spectral moments of the response of a 2 DOF system under quasi-stationary input under the assumption of: a) 5% and b) 1% of the structural damping..... 44
- Figure 2.3. a) The Husid functions of the accelerograms simulated by the Jennings et al. (1969) time modulating function with the proposed parameters; b) the generalized Husid function (Theoretical) and the mean value obtained from simulated accelerograms (MCS)..... 74

Chapter 3

- Figure 3.1. Comparison between different peak factor's definitions adopted in the compared models for $T_s = 10 s$ 77
- Figure 3.2. Comparison between the selected power spectral density functions. 78
- Figure 3.3. Comparison of the mean ensemble of the simulated response spectra
79
- Figure 3.4. Evolutionary power spectral density function according to a) Preumont (1985); b) Preumont (1985) after 5 iterations; c) Cacciola (2010); d) Cacciola (2010) after 5 iterations. 89
- Figure 3.5. Comparison of the ensemble of the simulated response spectra before and after 5 iterations. 90
- Figure 3.6. Comparison between simulated and target response spectra: a) $\varepsilon(\omega_k) = 1$; b) $\varepsilon(\omega_k)$ uncorrelated; c) $\varepsilon(\omega_k)$ correlated (from D'Amico et al. 2012). 102

Figure 3.7.	Trajectories of simulated ground motion accelerograms: a) $\varepsilon(\omega_k) = 1$; b) $\varepsilon(\omega_k)$ uncorrelated; c) $\varepsilon(\omega_k)$ correlated (from D'Amico et al. 2012).....	102
Figure 3.8.	Correlations of the log-response spectral acceleration values: a) Inoue and Cornell (1990) target correlation; b) $\varepsilon(\omega_j) = 1$; c) $\varepsilon(\omega_j)$ uncorrelated; d) $\varepsilon(\omega_j)$ correlated (from D'Amico et al. 2012).	103
Figure 3.9.	Iterative scheme to simulate response-spectrum-compatible accelerograms according to the proposed technique.	104
Figure 3.10.	SMART 2008 convergence of the output displacement statistics a) mean; b) fractile 5%; median; d) fractile 95%.....	118
Chapter 4		
Figure 4.1.	Evolutionary PSD functions: a) C& P model, b) quasi-stationary; c) non-stationary; d) non-stationary with imposed variability.....	110
Figure 4.2.	Mean instantaneous frequency of the ground motion models adopted in the numerical comparative study on the structural response of benchmark buildings.	111
Figure 4.3.	Simulated time-histories a) quasi-stationary; b) non-stationary; c) non-stationary with imposed variability.	112
Figure 4.4.	Response spectral accelerations with damping ratio variation plotted versus: a) period; b) frequency.	113
Figure 4.5.	Difference percentage of the response spectra for 1% and 2% damping evaluated with respect to the simulated 5% damped response spectra....	114
Figure 4.6.	SMART 2008 structure: SAP2000 model.....	115
Figure 4.7.	Geometrical data of the SMART 2008 structure [m].....	116

Figure 4.8.	SMART 2008 output displacements: a) probability density function; b) cumulative density function.	116
Figure 4.9.	5-storey building: SAP2000 model.....	119
Figure 4.10.	5-storey building output displacements: a) probability density function; b) cumulative density function.....	119
Figure 4.11.	5-storey building convergence of the output displacement statistics a) mean; b) fractile 5%; median; d) fractile 95%.	120
Figure 4.12.	SAC building: SAP 2000 model.....	121
Figure 4.13.	SAC building linear model output displacements: a) probability density function; b) cumulative density function.	122
Figure 4.14.	SAC building linear model convergence of the output displacement statistics: a) mean; b) fractile 5%; median; d) fractile 95%.	123
Figure 4.15.	Moment-rotation relationship for moment resisting column-beam connection of the analysed node at the roof.	123
Figure 4.16.	SAC building non-linear model output displacements: a) probability density function; b) cumulative density function.....	124
Figure 4.17.	SAC building non-linear model convergence of the output displacement statistics: a) mean; b) fractile 5%; median; d) fractile 95%.	125

Chapter 5

Figure 5.1.	Model with: a) SDOF system on elastic soil deposit; b) idealised discrete system with representation of the translational and rotational springs and dashpots; c) components of motion (Kramer 1996).	129
Figure 5.2.	a) Lumped parameters representation of the building and its foundation; b) SDOF systems placed on independent foundations according to Mulliken and Karabalis (1998).....	144

Figure 5.3.	Discrete model for structure-soil-structure-interaction according to Alexander et al. (2012).	145
Figure 5.4.	Effect on the translational DOF of the building due to: a) the rotation of the foundation; b) the horizontal acceleration at the base; c) the deformation of the structure.	147
Figure 5.5.	Power Spectral Density functions of the response for a) building 1; b) building 2 according to Alexander et al. (2012).	158
 Chapter 6		
Figure 6.1.	Discrete model used for the vibration control of a single structure through ViBa according to Cacciola and Tombari (2015).	171
Figure 6.2.	Transfer functions of the undamped for different mass ratios system of the: a) structure; b) ViBa (Cacciola and Tombari 2015).	174
Figure 6.3.	Transfer functions of the damped system for different mass ratios and null ViBa loss factor of the: a) structure; b) ViBa (Cacciola and Tombari 2015).	175
Figure 6.4.	Discrete model adopted to study in the time domain the vibration control of a single structure through ViBa.	178
Figure 6.5.	Comparison of the transfer functions of the: (a) structure and (b) ViBa for the Viscous Model (VM) and Hysteretic model (HM).	182
Figure 6.6.	Flowchart of the proposed procedure to establish the equivalent viscous damping model of the investigated system from the hysteretic model of Cacciola and Tombari (2015).	183
Figure 6.7.	Displacement time-histories of the simplified structure of Cacciola and Tombari (2015) under harmonic input in coupled and uncoupled conditions.	187
Figure 6.8.	Transfer functions of: a) simplified SAC building; b) ViBa.	190

Figure 6.9. FE model in SAP2000 of the SAC building and soil underneath: a) uncoupled; b) coupled with ViBa.....	191
Figure 6.10. Displacement time-histories of the SAC building modelled on MATLAB under harmonic input in coupled and uncoupled conditions.....	193
Figure 6.11. Displacement time-histories of the SAC modelled on SAP2000 under harmonic input in coupled and uncoupled conditions.....	194
Figure 6.12. Evolutionary PSD functions: a) C&P model, b) quasi-stationary; c) non-stationary; d) non-stationary and imposed variability.....	199
Figure 6.13. Mean instantaneous frequency of the response-spectrum-compatible ground motion models adopted in the SSSI investigations.	200
Figure 6.14. Trajectories of simulated ground motion accelerograms: a) quasi-stationary; b) non-stationary; c) non-stationary with imposed variability.	201
Figure 6.15. Comparison between simulated and target response spectra: a) stationary; b) non-stationary; c) non-stationary with imposed variability.	202
Figure 6.16. Ground motion models' peak ground acceleration: a) mean; b) fractile 5%; c) median; d) fractile 95%.....	204
Figure 6.17. a) Probability density function and b) cumulative density function of the peak ground acceleration of the quasi-stationary, non-stationary and non-stationary with variability ground motions.....	204
Figure 6.18. Surface plots of the parametric study to reduce the displacements relative to the foundation of the structure of Cacciola and Tombari (2015) for: a) $m_{ViBa} / m = 0.5$; b) $m_{ViBa} / m = 1.05$; c) $m_{ViBa} / m = 1.5$; d) $m_{ViBa} / m = 2$	208
Figure 6.19. Transfer functions of the ViBa and the modified Cacciola and Tombari (2015) prototype building for different values of m_{ViBa} / m	210

Figure 6.20. Convergence of the response of the building protected with ViBa: a) mean; b) fractile 5%; c) median; d) fractile 95% for $m_{ViBa} / m = 0.5$	212
Figure 6.21. a) Probability density function; b) cumulative density function of the response of the building protected with ViBa for $m_{ViBa} / m = 0.5$	212
Figure 6.22. Convergence of the response of the building protected with ViBa: a) mean; b) fractile 5%; c) median; d) fractile 95% for $m_{ViBa} / m = 1.05$	214
Figure 6.23. a) Probability density function; b) cumulative density function of the response of the building protected with ViBa for $m_{ViBa} / m = 1.05$	214
Figure 6.24. Convergence of the response of the building protected with ViBa: a) mean; b) fractile 5%; c) median d) fractile 95% for $m_{ViBa} / m = 1.5$	216
Figure 6.25. a) Probability density function; b) cumulative density function of the response of the building protected with ViBa for $m_{ViBa} / m = 1.5$	216
Figure 6.26. Convergence of the response of the building protected with ViBa: a) mean; b) fractile 5%; c) median d) fractile 95% for $m_{ViBa} / m = 2$	218
Figure 6.27. a) Probability density function and b) cumulative density function of the response of the building protected with ViBa $m_{ViBa} / m = 2$	218
Figure 6.28. Surface plots of the parametric study to reduce the displacements relative to the foundation of the SAC building for: a) $m_{ViBa} / m = 0.5$ b) $m_{ViBa} / m = 1$; c) $m_{ViBa} / m = 1.5$; d) $m_{ViBa} / m = 2$	222
Figure 6.29. Transfer functions for the ViBa and the simplified SAC building benchmark for different values of m_{ViBa} / m	224
Figure 6.30. Convergence of the response of the simplified SAC building protected with ViBa: a) mean; b) fractile 5%; c) median d) fractile 95% for $m_{ViBa} / m = 0.5$	226

Figure 6.31. a) Probability density function; b) cumulative density function of the response of the simplified SAC building simplified model protected with ViBa for $m_{ViBa} / m = 0.5$ 226

Figure 6.32. Convergence of the response of the simplified SAC building protected with ViBa: a) mean; b) fractile 5%; c) median d) fractile 95% for $m_{ViBa} / m = 1.228$

Figure 6.33. a) Probability density function; b) cumulative density of the response of the simplified SAC building simplified model protected with ViBa for $m_{ViBa} / m = 1$ 228

Figure 6.34. Convergence of the response of the simplified SAC building protected with ViBa: a) mean; b) fractile 5%; c) median d) fractile 95% for $m_{ViBa} / m = 1.5$ 230

Figure 6.35. a) Probability density function; b) cumulative density of the response of the simplified SAC building simplified model protected with ViBa for $m_{ViBa} / m = 1.5$ 230

Figure 6.36. Convergence of the response of the building protected with ViBa: a) mean; b) fractile 5%; c) median d) fractile 95% for $m_{ViBa} / m = 2$ 232

Figure 6.37. a) Probability density function; b) cumulative density function of the response of the simplified SAC building simplified model protected with ViBa for $m_{ViBa} / m = 2$ 232

Abbreviations and Symbols

ViBa	Vibrating Barrier
SDOF	Single Degree Of Freedom
MDOF	Multi Degree Of Freedom
GMM	Ground Motion Modelling
SSI	Soil Structure Interaction
SSSI	Structure Soil Structure Interaction
EC2	Eurocode 2
EC8	Eurocode 8
PSD	Power Spectral Density
EPSD	Evolutionary Power Spectral Density
KT	Kanai-Tajimi
CP	Clough- Penzien
QS	Quasi Stationary
NS	Non Stationary
NSV	Non Stationary with Variability
NUPEC	Nuclear Power Engineering Corporation
FEM	Finite Element Method
BEM	Boundary Element Method
CDF	Cumulative Distribution Function
PDF	Probability Density Function
GSM	Geometrical Spectral Moments
NGSM	Non Geometrical Spectral Moments
RV	Random Variable
SRM	Spectral Representation Method
ARMA	Auto Regressive Moving Average
HWF	Harmonic Wavelet Transform
PGA	Peak Ground Acceleration
SMP	Strong Motion Phase
TD	Total Duration
KNJD	K-Net Japanese Database
EGMD	European Ground Motion Database
FDA	Frequency Domain Analysis
EOM	Equation Of Motion
VM	Viscous Model
HM	Hysteretic Model
$\text{Re}[\cdot]$	Real part of a complex number
$\text{Im}[\cdot]$	Imaginary part of a complex number
\in	Set membership
\mathfrak{R}_0^+	Set of positive real numbers
$ \cdot $	Absolute value

$\mathcal{F}[\cdot]$	Fourier Transform operator
$\mathcal{F}^{-1}[\cdot]$	Inverse Fourier Transform operator
$i = \sqrt{-1}$	Imaginary unit
m	Mass [kg]
c	Viscous damping coefficient [Ns/m]
k	Stiffness [N/m]
t	Generic time instant [s]
Δt	Time interval [s]
t_0	Time after which the motion begins [s]
τ	Time shift [s]
$u(t)$	Relative displacement time-history [m]
$\dot{u}(t)$	Relative velocity time-history [m/s]
$\ddot{u}(t)$	Relative acceleration time-history [m/s ²]
$u_{abs}(t)$	Absolute displacement time-history [m]
$\dot{u}_{abs}(t)$	Absolute velocity time-history [m/s]
$\ddot{u}_{abs}(t)$	Absolute acceleration time-history [m/s ²]
$\ddot{u}_g(t)$	Ground acceleration time-history [m/s ²]
ζ_0	Damping ratio
ω	Circular frequency [rad/s]
T	Period [s]
ω_0	Natural frequency [rad/s]
T_0	Natural period [s]
$\bar{\omega}_0$	Natural frequency of damped vibrations [rad/s]
$h(t - \tau)$	Damped unit-impulse response function of an oscillator of unitary mass
D	Matrix of the structural properties of order 2×2 for SDOF systems
y(t)	State space vector of order 2×1 for SDOF systems
v	Incidence vector of order 2×1 for relative motion for SDOF systems
$\Theta(t - \tau)$	State transition matrix (fundamental or transition matrix) of order 2×2 for SDOF systems
$\gamma_0(\Delta t)$	Loading matrix for the numerical integration of the EOM of order 2×2 for SDOF systems
$\gamma_1(\Delta t)$	Loading matrix for the numerical integration of the EOM of order 2×2 for SDOF systems
L(Δt)	Loading matrix for the numerical integration of the EOM of order 2×2 for SDOF systems
I	Identity matrix of order 2×2 for SDOF systems
$\mathbf{v}^{(1)}$	Incidence vector for absolute motion of SDOF systems
$\mathbf{v}^{(2)}$	Incidence vector for absolute motion of SDOF systems
$X(\omega)^*$	Complex conjugate of $X(\omega)$

$U(\omega)$	Fourier Transform of the relative displacement [ms]
$\dot{U}(\omega)$	Fourier Transform of the relative velocity [m]
$\ddot{U}(\omega)$	Fourier Transform of the relative acceleration [m/s]
$U_{abs}(\omega)$	Fourier Transform of the absolute displacement [ms]
$\dot{U}_{abs}(\omega)$	Fourier Transform of the absolute velocity [m]
$\ddot{U}_{abs}(\omega)$	Fourier Transform of the absolute acceleration [m/s]
$\ddot{U}_g(\omega)$	Fourier Transform of the seismic acceleration [m/s]
k_{dyn}	Dynamic stiffness
$H(\omega)$	Transfer function
$RSD(\omega_0, \zeta_0)$	Displacement response spectrum [m]
$RSV(\omega_0, \zeta_0)$	Pseudo-velocity response spectrum [m/s]
$RSA(\omega_0, \zeta_0)$	Pseudo-acceleration response spectrum [m/s ²]
t_f	Duration of the earthquake ground motion [s]
n	Number of degree of freedom
M	Mass matrix of order $n \times n$
C	Damping matrix of order $n \times n$
K	Stiffness matrix of order $n \times n$
\tilde{K}	Complex stiffness matrix of order $n \times n$ accounting of hysteretic damping
u(t)	Displacement vector of order $n \times 1$
$\dot{u}(t)$	Velocity vector of order $n \times 1$
$\ddot{u}(t)$	Acceleration vector of order $n \times 1$
τ	Incidence vector of order $n \times 1$
D_N	Matrix of the structural properties system of order $2n \times 2n$ for MDOF systems
y_N(t)	State space vector of order $2n \times 1$ for MDOF systems
V_N	Incidence matrix for relative motion of order $2n \times 1$ for MDOF systems
$\Theta_N(t - \tau)$	State transition matrix (fundamental or transition matrix) of order $2n \times 2n$ for MDOF systems
$\gamma_{0,N}(\Delta t)$	Loading matrix for the numerical integration of the EOM of order $2n \times 2n$ for MDOF systems
$\gamma_{1,N}(\Delta t)$	Loading matrix for the numerical integration of the EOM of order $2n \times 2n$ for MDOF systems
L_N(Δt)	Loading matrix for the numerical integration of the EOM of order $2n \times 2n$ for MDOF systems
I_n	Identity matrix of order $n \times n$
V_N⁽¹⁾	Incidence vector for absolute motion of order $2n \times 1$ for MDOF systems
V_N⁽²⁾	Incidence vector for absolute motion of order $2n \times 1$ for MDOF systems

$q_i(t)$	Modal displacement of the i -th DOF
ϕ_i	Eigen-vector of the the i -th modal shape
ω_i	Natural frequency of i -th mode of vibration [rad/s]
ζ_i	Damping ratio of i -th mode of vibration
$\mathbf{q}(t)$	Modal displacement vector of order $n \times 1$
$\dot{\mathbf{q}}(t)$	Modal velocity vector of order $n \times 1$
$\ddot{\mathbf{q}}(t)$	Modal acceleration vector of order $n \times 1$
Φ	Modal matrix of order $n \times n$
Ω	Spectral matrix of order $n \times m$
Ξ	Generalised damping matrix of order $n \times m$
$\mathbf{U}(\omega)$	Fourier Transform of the relative displacement vector of order $n \times 1$ [ms]
$\dot{\mathbf{U}}(\omega)$	Fourier Transform of the relative velocity vector of order $n \times 1$ [m]
$\ddot{\mathbf{U}}(\omega)$	Fourier Transform of the relative acceleration vector of order $n \times 1$ [m/s]
$\mathbf{U}_{abs}(\omega)$	Fourier Transform of the absolute displacement vector of order $n \times 1$ [ms]
$\dot{\mathbf{U}}_{abs}(\omega)$	Fourier Transform of the absolute velocity vector of order $n \times 1$ [m]
$\ddot{\mathbf{U}}_{abs}(\omega)$	Fourier Transform of the absolute acceleration vector of order $n \times 1$ [m/s]
\mathbf{Q}	Influence vector relating to the inertial forces
\mathbf{Q}_K	Influence vector relating to the elastic forces
\mathbf{Q}_C	Influence vector relating to the dissipative forces
\mathbf{K}_{dyn}	Dynamic stiffness matrix of order $n \times n$
$\tilde{\mathbf{K}}_{dyn}$	Complex dynamic stiffness matrix of order $n \times n$ accounting of hysteretic damping
$\mathbf{H}(\omega)$	Transfer function vector of order $n \times 1$
$P(\cdot)$	Probability measure
$F_X(x)$	Cumulative Distribution Function
$p_X(x)$	Probability Density Function
$M_X(\theta)$	Characteristic function
θ	Real parameter
$m_j[X]$	Statistical moments
$k_j[X]$	Cumulants of random variables
μ_X	Mean value of random variables
$E[\cdot]$	Expected value of random variables
$E[X^2]$	Mean squared value of random variables
$m_j[f(X)]$	Central moments of random variables

σ_x^2	Variance of random variables
σ_x	Standard deviation of random variables
$m_{jk}[XY]$	Cross moments of random variables
$m_{jk}[f(X)f(Y)]$	Cross central moments of random variables
σ_{XY}	Covariance of random variables
ρ_{XY}	Correlation coefficient of random variables
$X(t)$	Stochastic process
$K_{XX}(t_l, t_m)$	Auto-covariance function for non-stationary processes
$K_{XY}(t_l, t_m)$	Cross-covariance function for non-stationary processes
$R_{XX}(t_l, t_m)$	Auto-correlation function for non-stationary processes
$R_{XY}(t_l, t_m)$	Cross-correlation function for non-stationary processes
$R_{XX}(\tau)$	Auto-correlation function for stationary processes
$G(\omega, t)$	One-sided non-stationary power spectral density function
$S(\omega, t)$	Two-sided non-stationary power spectral density function
$G(\omega)$	One-sided stationary power spectral density function
$S(\omega)$	Two-sided stationary power spectral density function
$S_{KT}(\omega)$	Stationary Kanai-Tajimi power spectrum
$S_{CP}(\omega)$	Stationary Clough-Penzien spectrum
$S_{CP}(\omega, t)$	Non-stationary Clough-Penzien spectrum
ω_g, ω_f	Constant stiffness parameters of a filter to model seismic ground motion spectra
ζ_g, ζ_f	Constant damping parameters of a filter to model seismic ground motion spectra
$\omega_g(t), \omega_f(t)$	Time-variant stiffness parameters of a filter to model seismic ground motion spectra
$\zeta_g(t), \zeta_f(t)$	Time-variant damping parameter of a filter to model seismic ground motion spectra
$a(\omega, t)$	Time-frequency modulating function
$a(t)$	Time modulating function
$\lambda_{i,X}$	Geometrical spectral moments
$\lambda_{i,X}(t)$	Non geometrical spectral moments
$\omega_{1,X}$	Central frequency of a power spectral density function [rad/s]
$\omega_{2,X}$	Radius of gyration of a power spectral density function about the frequency origin [rad/s]
δ_x	Bandwidth factor of a stationary stochastic process
ω_s	Radius of gyration of a power spectral density function about the central frequency [rad/s]
$U(t)$	Displacement response process [m]
$\dot{U}(t)$	Velocity response process [m/s]

$\ddot{U}(t)$	Acceleration response process [m/s ²]
$U_{\max}(t)$	Process of the maxima amplitude of [m]
$G_{UU}(\omega)$	Unilateral power spectral density function of the response displacement stochastic process [m ² /s]
$G_{\ddot{u}_g \ddot{u}_g}(\omega)$	Unilateral power spectral density function of the seismic acceleration [m ² /s ³]
$H(\omega, t)$	Duhamel's convolution integrals
$\dot{H}(\omega, t)$	Duhamel's convolution integrals
$h(t - \tau)$	Response to the Dirac delta function
$\dot{h}(t - \tau)$	First derivative of the response to the Dirac delta function
$L(t)$	Probability of survival
N_U	Number of out-crossings of a given barrier
α_U	Hazard function
$\nu_{ U }^+$	Expected rate of barrier up-crossings of a double symmetric barrier [1/s]
ν_U^+	Expected rate of barrier up-crossings of a single barrier [1/s]
$\bar{\eta}_U$	The reduced threshold level
T_s	Time observing window of a stochastic process and the strong motion phase for ground motion processes
p	Probability of not exceedance of a barrier
ζ_s	Fictitious damping
ζ_a	Adjusted damping
γ	The Euler constant
t_1	Initial time of the SMP
t_2	Final time of the SMP
β	Parameter determining the decay of the time modulating function of Jennings et al. (1969).
$H(t)$	The Husid function
N_a	Number of harmonics superimposed to generate a signal
$\Delta\omega$	Size interval of a discretized frequency domain
$\phi_i^{(r)}$	Independent random phases uniformly distributed over the interval [0, 2 π]
a_g	The design ground acceleration [m/s ²]
S	Soil factor
T_B	Frist period specified for defining target response spectra relatively to the soil type
T_C	Second period specified for defining target response spectra relatively to the soil type
T_D	Third period specified for defining target response spectra relatively to the soil type
\overline{RSA}	Mean value of simulated response spectra
RSA^R	Pseudo-acceleration response spectrum for recorded ground

	motions [m/s ²]
$\ddot{u}_g^R(t)$	Recorded ground motion accelerogram [m/s ²]
$\alpha(\omega)$	Set of uncorrelated random variables
$\varepsilon(\omega)$	Set of correlated log-normal random variables
$\beta(\omega)$	Set of correlated Gaussian random variables
$RSA^{+\sigma}$	Mean acceleration response spectrum + standard deviation [m/s ²]
$RSA^{-\sigma}$	Mean acceleration response spectrum- standard deviation [m/s ²]
ω_{t_0}	Frequency at $t=0$ describing the time-varying frequency content of the ground motion
ω_F	Frequency describing the time-varying frequency content of the ground motion at the final time
$\ddot{u}_g^{BC}(t)$	Baseline corrected artificial time history [m/s ²]
$\Delta\%$	Difference percentage
m_f	Mass of a building foundation [Kg]
m_{ViBa}	Mass of the ViBa [Kg]
$m_{f,ViBa}$	Mass of the foundation of the ViBa [Kg]
k_f	Stiffness of a building's foundation [N/m]
k_{ViBa}	Stiffness of the ViBa [N/m]
$k_{f,ViBa}$	Stiffness of the foundation of the ViBa [N/m]
η_f	Loss factor of the foundation of a building's foundation
$\eta_{f,ViBa}$	Loss factor of the foundation of the ViBa
η_{SSSI}	Loss factor of the soil deposit affected by the SSSI
c_f	Viscous damping coefficient of the foundation of a building's foundation [Ns/m]
$c_{f,ViBa}$	Viscous damping coefficient of the foundation of the ViBa [Ns/m]
c_{SSSI}	Viscous damping coefficient of the soil deposit affected by the SSSI [Ns/m]
$\mathbf{U}(t)$	Stochastic absolute displacement vector of order $n \times 1$ [m]
$\dot{\mathbf{U}}(t)$	Stochastic absolute velocity vector of order $n \times 1$ [m/s]
$\ddot{\mathbf{U}}(t)$	Stochastic absolute acceleration vector of order $n \times 1$ [m/s ²]
$U_g(t)$	Ground displacement stochastic process [m]
$\dot{U}_g(t)$	Ground velocity stochastic process [m/s]
U_b	Stochastic response process of the horizontal relative displacements between the the top floor of the building and the foundation [m]
X_{U_b}	Fractile of the distribution of the peak response with probability p of not exceedance [m]
λ_{0,U_b}	zero-th order geometrical spectral moment of the response process U_b [m ²]

η_{U_b}	Peak factor relative to the response process of the building to protect with ViBa
α	Vector listing the ViBa design parameters for deterministic design
β	Vector listing the ViBa design parameters for stochastic design
G	Shear modulus [Pa]
ρ_s	Density of soil [kg/m ³]
d	Generic distance [m]
Π	Dissipated energy [J]
V	Potential energy [J]
K	Kinetic energy [J]

Acknowledgements

This thesis would have not come to completion without the support of my supervisors, colleagues, and members of staff, friends and my family.

I would like to thank my principal supervisor, Dr. Pierfrancesco Cacciola, for the support and guidance received and his valuable example of commitment to research. I would like to express my gratitude to my other supervisors Dr. Andreas Lampropoulos and Dr. Kevin Stone, and to Dr. Alessandro Tombari.

I gratefully acknowledge the Doctoral College for the constant presence and help during these years and the University of Brighton for the PhD scholarship, providing me with the invaluable opportunity to embark on a life-changing challenge.

I would like to express my gratitude to my colleagues for sharing so much of our own experiences about our PhD journey, in particular to Adeni Abigo and Sabrina Barbosa, Richard Kulczak, Panajota Nenaj, Hamed Mahjorian Dehkordi, Salam Alrekabi, Mohammed Haloob Al Majidi, Yahya Ibraheem, Nagham Al Qaysi, Johan Coronado and to the visiting students Annalisa Chiodi and Gabriele Testa.

Sincere thanks to the students of the module of Random Vibrations, especially to Polly Morris, for their simulating brightness during the lectures and appreciation for my work.

A huge thank you to Katrina Rumsby, Tim Dance, Tristan Bristow, Neil Stawarz and Julia Siddi who made of Clyde Road my second home, where I could always relieve from a hard day, and to John Godwin, Katie Kunningham, Jon Ward, Carla Halpin, Andrew Murphy and Sarah West.

I thank my parents, who have often been waiting for my late phone calls after work, to my brother Dario and to all my best friends back home, Arianna Laudini, Federica Currò, Maria Andrea Bruzzaniti, Mara Giuffrida, Serena Laudini and Cecilia Villari, to all of them for their love and encouragement.

Declaration

I declare that the research contained in this thesis, unless otherwise formally indicated within the text, is the original work of the author. The thesis has not been previously submitted to this or any other university for a degree, and does not incorporate any material already submitted for a degree.

Signature

Laura D'Amico

Date

28/03/2017

To Salvatore, Mattia and Dario.

BLANK

1 Introduction

Due to their large unpredictability, earthquakes continue to be a cause of damage and collapse of engineering facilities as well as loss of lives. Engineers thus seek to reduce the damage induced by the seismic action on structures by enhancing both the accuracy of ground motion modelling and by employing control strategies able to reduce the vibrations induced in the structural systems.

A new approach in vibration control has been initiated recently by introducing a novel solution called Vibrating Barriers (ViBas), which is supported and further investigated in this work. The ViBa is a massive device embedded into the soil and detached from the structure to protect, it is designed to adsorb a portion of the energy of the ground motion by exploitation of the Structure-Soil-Structure-Interaction phenomenon.

In the context of this research, the typical vibration control systems are referred to as “local” devices. This definition highlights the position of the control devices within the structure being protected. In fact, local devices are embedded into the systems therefore changing the structural characteristics. The ViBa, on the contrary, is disconnected from the buildings and might act as a “global” solution thus able to protect several structures simultaneously.

This research addresses the study of Vibrating Barriers under stochastic excitation, in particular the focus is on developing a technique to design the ViBa for broad band Gaussian response-spectrum-compatible excitation, and on the study of its efficiency for advanced model of the seismic action forcing benchmark structures.

1.1 Motivations

The vibration control solutions developed in the last decades have greatly improved the earthquake resistance of structures. Regardless of this, vibration control systems are not typically used due to the possible high costs involved and, moreover, due to the impracticality of retro-fitting them into buildings. In earthquake prone developed countries, vibration control has been a successful solution to enhance the seismic performance of buildings, however the impact of severe earthquakes can be even more catastrophic in poor areas (e.g. Haiti 2010, Nepal 2015, Ecuador 2016).

Nowadays, another aspect of concern in seismic engineering is the growth of densely urbanized cities, where numerous buildings stand closely spaced to each other becoming more affected by the Structure-Soil-Structure-Interaction (SSSI). The SSSI, whose awareness has become more established in the last decades, is due to the superposition of seismic waves travelling from the fault to the buildings' foundations, reflected and diffracted and moreover altered by the vibrating structures. The effects of the SSSI phenomenon can be either beneficial or detrimental and consequently the vibrations induced within the buildings in a neighbourhood may reduce or increase the responses predicted by the design process. Although the early studies of the SSSI phenomenon date back to the 1970's, its application to design engineering facilities has been beyond the possibility of software and computer performances for a long time, until the recent developments in computational science. This research tackles the vibration control problem by exploiting the beneficial effects of the SSSI among structural systems, the aim being to contribute to the field of vibration control by investigating some of the current gaps in knowledge relative to the ViBa solution. The innovative Vibrating Barrier as a "global" solution in seismic protection of structures, may introduce a decisive change in the approach to design and urbanization of cities. The ViBa has been proposed in order to provide simultaneous protection to more buildings, it is potentially able to provide a communal solution for entirely safer cities and to offer protection for new as well as existing structures in a neighbourhood. As all the new

technologies, the ViBa needs further study and validation, specifically, with regard to its efficiency under broad band artificial accelerograms.

1.2 Research Aim and Objectives

The scope of this work is to define a methodology to design the ViBa under Gaussian stochastic excitation and assess its efficiency in protecting single buildings. In this regard, the design is firstly performed considering the input as a stationary Gaussian stochastic process to readily derive the design parameters of the device. Successively, the ViBa's performance is verified by pertinent Monte Carlo Simulation study to take into account advanced ground motion models, including amplitude and frequency non-stationarity as well as natural variability.

The ViBa has been designed and tested experimentally so far under the assumption of deterministic seismic loading and stationary Gaussian stochastic ground motions (Cacciola and Tombari 2014, Cacciola et al. 2015, Cacciola and Tombari 2015, Tombari et al. 2016). By undertaking the stochastic approach, which guarantees high reliability of the outcomes, the investigations on the ViBa's efficiency, its design and applications performed in this work adopt stochastic models of the seismic action underpinning the hypotheses of non-stationarity in amplitude and frequency content. Both amplitude and frequency content of earthquakes change in time, representing a complex scenario to be realistically reproduced by pertinent stochastic simulation techniques. In accordance to the theory of random vibrations, the aim of this research is to define a methodology being reliable, simple and pertinent to the seismic code requirements.

In order to perform the investigations of this research, the following objectives have been pursued:

- To identify from the literature review on Gaussian stochastic ground motions processes for generating time histories pertinently to the seismic codes requirements, the gaps in knowledge concerning the modelling of the non-stationarity in amplitude and frequency content of response-spectrum-compatible ground motions.

- To investigate the effects of the frequency non-stationarity and variability of the earthquake ground motions on linear and non-linear systems by developing a versatile ground motion model adaptable to different hypotheses for unbiased comparisons of the systems' responses due to different earthquakes models.
- To assess the effects of the assumptions of the structural damping on responses to ground motion models holding different hypothesis.
- To identify limitations of the current Eurocode 8 with respect to seismic stochastic analyses of the response of structural systems.
- To understand from literature, the advantages and limitations of modelling discrete Structure-Soil-Structure-Interaction systems and the lack of contributions concerning the stochastic analysis of the phenomenon.
- To set the conditions to apply a simplified methodology to perform the design of the ViBa under stationary Gaussian stochastic excitation of Structure-Soil-Structure-Interaction systems, i.e. to develop a procedure to determine viscous damping matrices from hysteretic models.
- To validate via Monte Carlo Simulation of the response of Structure-Soil-Structure-Interaction systems, the proposed methodology to design the ViBa for protecting structures with different dynamic characteristics, encompassing a spread scenario of natural frequencies, forced by the simulated earthquake time histories.

1.3 Original Contribution

In order to establish a solid base for the investigations carried out in this work, the Ground Motion Modelling (GMM) of the seismic action is undertaken aiming to establish reliable earthquake models for the studies on SSSI systems. A modification of the techniques proposed by Cacciola and Zentner (2012) and D'Amico et al. (2012) has been introduced to simulate response-spectrum-compatible accelerograms, i.e. in agreement with seismic codes, and to realistically describe the non-stationarity and the natural variability typical of recorded earthquakes.

The contribution achieved in this regard can be summarized as follows:

- Proposing a model for simulating fully non-stationary response-spectrum-compatible time histories accounting for the natural variability of real earthquakes through log-normal distributed random variables (Cacciola, D'Amico and Zentner 2014). This model is the modification of the previous work on the simulation of response-spectrum-compatible ground motion with correlated spectral correlations (D'Amico, Cacciola and Zentner 2012, Zentner, D'Amico and Cacciola 2013) and guarantees the spectrum compatibility achievement with both target \pm standard deviation response spectra.

With the aim of understanding the influence of the ground motion selection on the structural responses of real linear and non-linear behaving structures, a comparative study of real benchmarks has been performed providing the followings findings (Cacciola, D'Amico and Zentner 2014):

- Although the codes provisions are fulfilled, the distributions of relevant response parameters, such as the peak displacements, are sensitive to the ground motion model adopted. The weakness of the response-spectrum-compatible criteria currently available in the seismic codes is evidenced.

- The response of structures having damping ratio smaller than the nominal 5% (used as a target value by the international codes) is sensitive to the non-stationary model adopted.
- The current accepted understanding that the non-stationarity of the ground motion models is more relevant for non-linear behaving structures in comparison with the linear case should be revised.
- Quasi-stationary models do not always lead to over-conservative response when compared to non-stationary models, as it is dependent on the strategy used to generate the accelerograms.

This research demonstrates that the choice of the ground motion can considerably change the structural design, through investigations which have been carried out in order to understand the implications of the ground motion simulation strategy adopted on the design of buildings without accounting for the SSSI. In particular, the responses of selected structures to non-stationary inputs, are compared to the response obtained accounting for the input modelled as quasi-stationary stochastic process. It has been demonstrated that although the code provisions are fulfilled, the distributions of the peak displacement of the response are sensitive to the GMM adopted and to the damping variation of the structural systems.

Furthermore, in this work the ViBa's performance are analysed for the case of coupled building-soil-ViBa systems. A methodology to design the control devices is addressed with the purpose to enable the assessment of the reliability of structures-soil-ViBa systems. The reliability of the systems under investigation is addressed by defining the mean of the peak displacements for stationary stochastic input. Successively, the design is verified for the case of non-stationary and fully non-stationary ground motions (D'Amico, Cacciola and Zentner 2012; Cacciola, D'Amico and Zentner 2013; Zentner, D'Amico and Cacciola 2013). From the investigations, the effectiveness of the ViBa is highlighted showing a reduction of up to 37.80% of the mean value of the peak displacements.

In order to perform stochastic analysis, the ViBa parameters have been determined to calibrate the control device to protect a single building. The investigations have been

carried out under the assumptions that the building, the soil and the ViBa behave linearly by the following steps:

- Three sets of response-spectrum-compatible ground motions have been selected, one from the stationary and non-stationary stochastic models available from literature and a further non-stationary one, whose extension is proposed in this work. Namely, a versatile fully non-stationary response-spectrum-compatible power spectral density with random coefficients, named as *non-stationary with imposed variability* model (Cacciola, D'Amico and Zentner 2013). The ground motion models, the quasi-stationary, non-stationary and non-stationary with imposed variability, are simulated via the spectral representation methods and compatible with Eurocode 8.
- The discrete model of the ViBa's protection of single buildings as proposed in literature by Cacciola and Tombari (2015) is investigated. Specifically, the cases of ViBa coupled with one building under different scenarios accounting of varied mass of the ViBa are analysed. The discrete model under investigation, originally proposed for frequency domain analysis, is extended in this work to the time domain. In order to establish the dynamic equilibrium of the system in the time domain the equivalent viscous damping model of the system from the hysteretic model provided by Cacciola and Tombari (2015) has been established.
- In order to define the equivalent viscous damping model of the investigated SSSI systems, the proposed problem of minimization, stated with reference to target transfer functions proposed by Cacciola and Tombari (2015), has been pursued and successfully applied.
- A parametric study has been adopted to perform the design of the ViBa for protecting one building under Gaussian stationary stochastic excitation.
- A Monte Carlo Simulation study of the structural response has been employed to verify the accuracy of the design approach and to highlight the limits of the simplified GMM.

1.4 Thesis Outline

The investigations undertaken in this thesis focus on: (i) the stochastic ground motion modelling and development of the current trends for earthquake simulation methods, (ii) the analysis in the time domain of the response of discrete SSSI systems constituted by the ViBa coupled with a single building, and (iii) the control of vibrations induced by Gaussian stochastic input: stationary, quasi-stationary, non-stationary and fully non-stationary ground motions with imposed variability.

In Chapter 2, the deterministic equations of motion for seismic structural analysis have been introduced in both frequency and time domain; the governing equations of the dynamic equilibrium are reported for Single Degree Of Freedom (SDOF) and Multi-Degree-Of-Freedom (MDOF) systems. The step-by-step numerical solution adopted to solve the equations of motion is described as well as the background of theory of probability and the fundamentals of random vibrations. Namely, the concept of Power Spectral Density (PSD) function for ground motion modelling and stochastic analysis of the structural response are introduced. Finally, the first passage problem and the peak factor formulation adopted to design the ViBa are described.

Chapter 3 encompasses the literature review on response-spectrum-compatible ground motion models and presents the simulation technique proposed in this work to generate fully-non-stationary accelerograms. The technique follows the current trends in modelling the earthquake ground motion by taking into account the seismological parameters available from databases. A versatile PSD function is proposed by which the variability of the earthquake phenomenon, i.e. variability of the spectral accelerations about their mean value, is embedded to the basic development of the model.

In Chapter 4 a comparative study on the response of structural systems to the proposed response-spectrum-compatible accelerograms is presented. The purpose of this Chapter is to comprehend the implications of ground motion model selection on the response of linear behaving systems. Therefore, the response of three benchmark buildings is investigated by means of probability density functions and cumulative

distribution functions of the peak displacements obtained by Monte Carlo Simulation technique.

In Chapter 5, an overview of the background concepts of Soil-Structure-Interaction (SSI) and the main theories and relevant analytical studies on the SSSI phenomenon are presented; the focus of the review is on the formulation of discrete models for SSSI systems. Specifically, the SSSI discrete models proposed are based on the general Winkler spring approach, that is used in the following chapters. The basic theory presented in Chapter 5 is used to develop the ViBa structure-soil-structure discrete model

In Chapter 6, the procedure to perform the design of the ViBa under Gaussian stochastic excitation for reducing the vibrations of a single structure is presented. In order to determine the equations of motion of the investigated system in the time domain, the analytical formulation available in literature is extended from the traditional frequency domain. This Chapter presents the methodology proposed to perform the design of the ViBa, which encompasses the design of the device for stationary input and to verify its efficiency under quasi-stationary and fully non-stationary stochastic inputs. The synthetic accelerograms forcing the system have been modelled according to the method proposed in Chapter 3. Moreover, the proposed methodology is applied to design the ViBa for protecting a real benchmark structure, the results are presented in a numerical application.

In Chapter 7, the findings of this research are discussed and recommendations for future works are provided.

BLANK

2 Analysis Methods of Seismically Excited Linear Structural Systems

In order to analyse the response of engineering systems, to characterise the soil underneath and the external forces acting upon them, extensively used deterministic and stochastic methods are available in structural dynamics.

The methods adopted for the investigations of the presented work are described in this Chapter in which, deterministic methods and techniques to perform analyses of linear Single Degree Of Freedom Systems (SDOF) and Multi Degree of Freedom Systems (MDOF) are described both in the time and frequency domain. Direct analysis and Monte Carlo Simulation procedures have been employed to perform the analyses, therefore the fundamentals of random vibrations theory are also introduced. Specifically the basics probability theory is reviewed to set the background of the stochastic modelling of earthquake ground motions and reliability analysis.

2.1 Deterministic Seismic Analysis

In the following sections, the differential equations of motion for linear structural systems under dynamic loading are presented. The numerical techniques adopted in order to integrate the equations of motion of SDOF and MDOF are described in the time and frequency domain. Lastly the definition of the response spectra widely adopted for designing structures follows.

2.1.1 Equation of Motion and Response of Single Degree Of Freedom (SDOF) Systems

In order to define the dynamic equilibrium of a mass subjected to general external forces, the dynamic equilibrium can be directed to a static balance among inertial, elastic and dissipative forces by using *D'Alembert's Principle*. Pertinently, the equation of motion in the time and frequency domain analysis are presented

hereafter. In the description of the methods, both relative and absolute motions are considered for single support excitation.

2.1.1.1 Time Domain Analysis of SDOF Systems: Relative and Absolute Motion

The equation of motion of a quiescent linear SDOF system with lumped mass free to move in the horizontal direction and corresponding initial conditions are

$$m[\ddot{u}(t) + \ddot{u}_g(t)] + c\dot{u}(t) + ku(t) = 0 \quad (2.1)$$

$$u(t_0) = 0; \dot{u}(t_0) = 0 \quad (2.2)$$

where the positive quantities m , c and k are the mass, the viscous damping coefficient and the stiffness respectively; the instant t_0 of the initial conditions is the time after which the motion begins; the functions $u(t)$, $\dot{u}(t)$ and $\ddot{u}(t)$ are respectively the relative displacement, velocity and acceleration time histories of the oscillator mass relatively to the oscillator base; $\ddot{u}_g(t)$ is the ground acceleration acting on the base support.

After rearranging the terms in equation (2.1), it follows

$$m\ddot{u}(t) + c\dot{u}(t) + ku(t) = -m\ddot{u}_g(t) \quad (2.3)$$

According to the definition of the natural frequency of the system given by

$$\omega_0 = \sqrt{\frac{k}{m}} \quad (2.4)$$

and the damping coefficient

$$c = 2\zeta_0\sqrt{km} = 2\zeta_0\omega_0 m \quad (2.5)$$

where ζ_0 is the adimensional damping ratio, by dividing equation (2.3) by m it follows the canonical form of the SDOF equilibrium, that is

$$\ddot{u}(t) + 2\zeta_0\omega_0\dot{u}(t) + \omega_0^2u(t) = -\ddot{u}_g(t) \quad (2.6)$$

The response of structures under general dynamic loading, is given by the Duhamel's integral by representing the input as the summation of a train of instantaneous impulses. For seismic ground motion, the general Duhamel's convolution integral for a SDOF system is

$$u(t) = \int_{t_0}^t h(t-\tau)\ddot{u}_g(\tau)d\tau \quad t > t_0 \quad (2.7)$$

where $h(t-\tau)$ is the damped unit-impulse response function of an oscillator of unitary mass is given by

$$h(t-\tau) = \frac{1}{\bar{\omega}_0} \sin[\bar{\omega}_0(t-\tau)] \exp[-\zeta_0\omega_0(t-\tau)] \quad (2.8)$$

where $\bar{\omega}_0 = \omega_0\sqrt{1-\zeta_0^2}$ is the damped natural frequency of the system with damping ratio $\zeta_0 \ll 1$ typical of engineering structures.

In order to perform the direct integration of equation (2.1), several numerical methods have been established, known as step-by-step procedures (see e.g. Bathe 1996).

In this work the exact solution of equation (2.7) is found via the step-by-step numerical method considering linear interpolation of the excitation (Chopra 2007). This numerical procedure for linear systems is highly efficient when: (i) the excitation is discretized for short intervals of time, (ii) the input changes linearly within the time step. The method is presented more in depth after specifying the equations of motion in the state space.

Nodal State space

The second order differential equations of motion in (2.1) are rewritten in the state space as a set of coupled first order differential equations as follows (see e.g. Newland 1989)

$$\dot{\mathbf{y}}(t) = \mathbf{D}\mathbf{y}(t) + \mathbf{v}\ddot{u}_g(t) \quad \mathbf{y}(t_0) = \mathbf{y}_0 \quad (2.9)$$

where \mathbf{D} is the 2×2 matrix of the structural properties of the system, $\mathbf{y}(t)$ is the 2×1 state space vector describing the state of the system at any time instant and \mathbf{v} is the incidence vector of order 2×1 , these respectively read

$$\mathbf{y}(t) = \begin{bmatrix} u(t) \\ \dot{u}(t) \end{bmatrix} \quad \mathbf{D} = \begin{bmatrix} 0 & 1 \\ -\omega_0^2 & -2\zeta_0\omega_0 \end{bmatrix} \quad \mathbf{v} = \begin{bmatrix} 0 \\ 1 \end{bmatrix} \quad (2.10)$$

Taking into account the initial conditions of a quiescent oscillator, the Duhamel's convolution integral seen in equation (2.7) in the state space reads

$$\mathbf{y}(t) = \mathbf{\Theta}(t-t_0)\mathbf{y}(t_0) + \int_{t_0}^t \mathbf{\Theta}(t-\tau)\mathbf{v}\ddot{u}_g(\tau)d\tau \quad t > t_0 \quad (2.11)$$

where $\mathbf{\Theta}(t-\tau) = \exp[\mathbf{D}(t-\tau)]$ is the 2×2 state transition matrix (fundamental or transition matrix), which governs the transient part of the response (see e.g. Meirovitch 1976).

Numerical evaluation of dynamic response: step-by-step methods

The Duhamel's integral in equation (2.11) can be calculated at each consecutive time interval Δt by assuming the excitation to be linearly interpolated within the interval, it follows that the response at each time step t_{k+1} is given by

$$\mathbf{y}(t_{k+1}) = \mathbf{\Theta}(\Delta t)\mathbf{y}(t_k) + \boldsymbol{\gamma}_0(\Delta t)\mathbf{v}\ddot{u}_g(t_k) + \boldsymbol{\gamma}_1\mathbf{v}\ddot{u}_g(t_{k+1}) \quad (2.12)$$

where $\boldsymbol{\gamma}_0(\Delta t)$ and $\boldsymbol{\gamma}_1(\Delta t)$ are the 2×2 matrices expressed as follows

$$\boldsymbol{\gamma}_0(\Delta t) = \left(\mathbf{\Theta}(\Delta t) - \frac{\mathbf{L}(\Delta t)}{\Delta t} \right) \mathbf{D}^{-1}; \quad \boldsymbol{\gamma}_1(\Delta t) = \left(\frac{\mathbf{L}(\Delta t)}{\Delta t} - \mathbf{I} \right) \mathbf{D}^{-1} \quad (2.13)$$

where \mathbf{I} is the identity matrix of dimensions 2×2 , as well as $\mathbf{L}(\Delta t)$ and $\mathbf{\Theta}(\Delta t)$ that are given by

$$\begin{aligned}\mathbf{L}(\Delta t) &= (\mathbf{\Theta}(\Delta t) - \mathbf{I})\mathbf{D}^{-1} \\ \mathbf{\Theta}(\Delta t) &= \exp(\mathbf{D}\Delta t)\end{aligned}\tag{2.14}$$

In order to perform the direct integration of the equations of motion of a structural system a variety of methods are alternatively available in literature by step procedures (Houbolt 1950, Newmark 1959, Wilson 1968, Hilbert et al. 1977). The step-by-step methods have the advantage to allow response analysis whether for linear and non-linear structures, furthermore these can be easily extended for multi degree of freedom systems.

The step-by-step procedure presented in equations (2.12)-(2.14) has been selected for its accuracy and stability; it provides an *exact method*, whose source of error lies only on the truthfulness of the input's linearity (see e.g. Borino e Muscolino 1986), therefore it suits the case of seismic ground motion loading functions appropriately. Moreover, the algorithm is *unconditionally stable* being the error bounded at each time step.

Let the absolute displacements of the lumped mass be given by the summation

$$u_{abs}(t) = u(t) + u_g(t).\tag{2.15}$$

The dynamic equilibrium in equation (2.1) can be rewritten in terms of absolute motion by substitution of equation (2.15) and its first and second derivative, that gives

$$m\ddot{u}_{abs}(t) + c[\dot{u}_{abs}(t) - \dot{u}_g(t)] + k[u_{abs}(t) - u_g(t)] = 0\tag{2.16}$$

rearranging the equation above it follows that

$$m\ddot{u}_{abs}(t) + c\dot{u}_{abs}(t) + ku_{abs}(t) = ku_g(t) + c\dot{u}_g(t)\tag{2.17}$$

which in the canonical form reads

$$\ddot{u}_{abs}(t) + 2\zeta_0\omega_0\dot{u}_{abs}(t) + \omega_0^2u_{abs}(t) = \omega_0^2u_g(t) + 2\zeta_0\omega_0\dot{u}_g(t)\tag{2.18}$$

The expression of equation (2.18) in the state space is rearranged as follows

$$\dot{\mathbf{y}}(t) = \mathbf{D}\mathbf{y}(t) + \mathbf{v}^{(1)}u_g(t) + \mathbf{v}^{(2)}\dot{u}_g(t); \quad \mathbf{y}(t_0) = \mathbf{0} \quad (2.19)$$

where $\mathbf{y}(t) = [u(t) \quad \dot{u}(t)]^T$ is the vector of the state space variables, \mathbf{D} is the matrix seen in equation (2.10), $\mathbf{v}^{(1)}$ and $\mathbf{v}^{(2)}$ are the incidence vectors reading

$$\mathbf{v}^{(1)} = \begin{bmatrix} 0 \\ \omega_0^2 \end{bmatrix}; \quad \mathbf{v}^{(2)} = \begin{bmatrix} 0 \\ 2\zeta_0\omega_0 \end{bmatrix} \quad (2.20)$$

The solution of equation (2.19) by means of the Duhamel's convolution integral is provided by the expression

$$\mathbf{y}(t) = \Theta(t-t_0)\mathbf{y}_0(t) + \int_{t_0}^t \Theta(t-\tau) \left[\mathbf{v}^{(1)}u_g(\tau) + \mathbf{v}^{(2)}\dot{u}_g(\tau) \right] d\tau \quad t > t_0 \quad (2.21)$$

which according to the step-by-step procedure seen in equation (2.12) is solved numerically by the following

$$\begin{aligned} \mathbf{y}(t_{k+1}) = & \Theta(\Delta t)\mathbf{y}(t_k) + \gamma_0(\Delta t) \left[\mathbf{v}^{(1)}u_g(t_k) + \mathbf{v}^{(2)}\dot{u}_g(t_k) \right] \\ & + \gamma_1(\Delta t) \left[\mathbf{v}^{(1)}u_g(t_{k+1}) + \mathbf{v}^{(2)}\dot{u}_g(t_{k+1}) \right] \end{aligned} \quad (2.22)$$

where the matrix $\Theta(\Delta t)$ and the operators $\gamma_0(\Delta t)$ and $\gamma_1(\Delta t)$ are given in equations (2.13)-(2.14).

2.1.1.2 Frequency Domain Analysis of SDOF Systems: Relative and Absolute Motion

Earthquake time histories can be decomposed into their frequency components by considering the ground motion as the summation of harmonic functions (see e.g. Shinozuka 1988). Hence, the response of a SDOF system can be seen as the combination of the outputs to several periodical excitations, which are defined for every frequency of a domain. The spectral characteristics of both input and output can be captured by Fourier Transform through the well-known pair of integrals

generally used to interchange time and frequency domain. The Fourier Transform and its inverse are denoted respectively by the operators $\mathcal{F}[\cdot]$ and $\mathcal{F}^{-1}[\cdot]$.

By taking the Fourier Transform of equation (2.1), the dynamic equilibrium of the relative motion of a SDOF system in the frequency domain follows as

$$m[\ddot{U}(\omega) + \ddot{U}_g(\omega)] + c\dot{U}(\omega) + kU(\omega) = 0 \quad (2.23)$$

where $U(\omega)$, $\dot{U}(\omega)$ and $\ddot{U}(\omega)$ are respectively the Fourier Transforms of the relative displacement, velocity and acceleration response and $\ddot{U}_g(\omega)$ of the ground acceleration.

According to equations (2.4) and (2.5), equation (2.23) rewritten in the canonical form reads

$$m[\ddot{U}(\omega) + \ddot{U}_g(\omega)] + 2\zeta_0\omega_0\dot{U}(\omega) + \omega_0^2U(\omega) = 0 \quad (2.24)$$

After substituting into equation (2.24) the followings

$$\dot{U}(\omega) = i\omega U(\omega); \quad \ddot{U}(\omega) = -\omega^2U(\omega) \quad (2.25)$$

dividing by m and after simple algebra it becomes

$$(\omega_0^2 - \omega^2 + 2i\zeta_0\omega_0\omega)U(\omega) = -\ddot{U}_g(\omega) \quad (2.26)$$

in which $i = \sqrt{-1}$ is the imaginary unit, $k_{dyn} = (\omega_0^2 - \omega^2 + 2i\zeta_0\omega_0\omega)$ is the dynamic stiffness whose inverse is the transfer function, which reads

$$H(\omega) = \frac{1}{(\omega_0^2 - \omega^2 + 2i\zeta_0\omega_0\omega)} \quad (2.27)$$

From equation (2.26) the absolute value of the displacements is given by

$$|U(\omega)| = |H(\omega)| |\ddot{U}_g(\omega)| \quad (2.28)$$

The response of the SDOF in the time domain is obtained from the frequency domain by taking the inverse Fourier transform of equation (2.28), that is

$$\mathcal{F}^{-1}[U(\omega)] = u(t) = \frac{1}{2\pi} \int_{-\infty}^{+\infty} H(\omega) \ddot{U}_g(\omega) e^{i\omega t} d\omega \quad (2.29)$$

Assuming the unitary input excitation, for which $u(t) \equiv h(t)$, the equation above becomes

$$u(t) = \frac{1}{2\pi} \int_{-\infty}^{+\infty} H(\omega) e^{i\omega t} d\omega \equiv h(t) \quad (2.30)$$

from which the definition of the transfer function as the dual damped unit-impulse response function in the frequency domain, according to the Fourier Transformation

$$H(\omega) = \int_{-\infty}^{+\infty} h(t) e^{-i\omega t} dt \quad (2.31)$$

where the function $h(t)$ is given in equation (2.8).

The equilibrium of the mass of a SDOF in terms of absolute motion is obtained by Fourier Transform of equation (2.18)

$$\ddot{U}_{abs}(\omega) + 2\zeta_0\omega_0 [\dot{U}_{abs}(\omega) - \dot{U}_g(\omega)] + \omega_0^2 [U_{abs}(\omega) - U_g(\omega)] = 0 \quad (2.32)$$

from which

$$-\omega^2 U_{abs}(\omega) + 2i\zeta_0\omega_0\omega U_{abs}(\omega) + \omega_0^2 U_{abs}(\omega) = \omega_0^2 U_g(\omega) + 2\zeta_0\omega_0 \dot{U}_g(\omega) \quad (2.33)$$

and after rearranging gives

$$(\omega_0^2 - \omega^2 + 2i\zeta_0\omega_0\omega) U_{abs}(\omega) = \omega_0^2 U_g(\omega) + 2\zeta_0\omega_0 \dot{U}_g(\omega) \quad (2.34)$$

By substituting the first expression seen in equation (2.25) into equation (2.34), after simple algebra it follows that

$$\left(\omega_0^2 - \omega^2 + 2i\zeta_0\omega_0\omega\right)U_{abs}(\omega) = \left(\omega_0^2 + 2i\zeta_0\omega_0\omega\right)U_g(\omega) \quad (2.35)$$

By defining the transfer function for the response motion in absolute displacements as

$$H_{abs}(\omega) = k_{dyn}^{-1} \left(\omega_0^2 + 2i\zeta_0\omega_0\omega\right), \quad (2.36)$$

from equation (2.35) the modulus of the absolute response displacements follows

$$|U_{abs}(\omega)| = |H_{abs}(\omega)| |U_g(\omega)| \quad (2.37)$$

where $U_g(\omega)$ is the Fourier Transform of the ground displacement record.

Response Spectra

In earthquake engineering, a response spectrum represents the absolute maxima of the responses of an elastic SDOF system of varying natural frequency, forced by a ground motion time-history for a fixed value of the damping ratio (see e.g. Housner and Jennings 1982). The response spectra are expressed in terms of maxima of the absolute acceleration, velocity and displacement by means of equations (2.1)-(2.5).

Under the hypotheses of a lightly damped SDOF system, the pseudo-acceleration response spectrum $RSA(\omega_0, \zeta_0)$ is obtained as follows

$$RSA(\omega_0, \zeta_0) = \max_{0 \leq t \leq t_f} \left| 2\zeta_0\omega_0\dot{u}(t) + \omega_0^2 u(t) \right| \cong \omega_0^2 \max_{0 \leq t \leq t_f} |u(t)| \quad (2.38)$$

where t_f is the duration of the earthquake ground motion and the displacement response spectrum is

$$\max_{0 \leq t \leq t_f} |u(t)| = RSD(\omega_0, \zeta_0) \quad (2.39)$$

From equation (2.38) and (2.39), the pseudo-velocity response spectrum follows as

$$RSV(\omega_0, \zeta_0) = \omega_0 RSD(\omega_0, \zeta_0) \quad (2.40)$$

The response spectra are suggested by the seismic codes to perform simplified analysis as linear static and response spectrum analysis.

2.1.2 Equation of Motion and Response of Multi Degree Of Freedom (MDOF) Systems

In this section, the equation of motion in the time and frequency domain are introduced by expanding the formulations in section 2.1.1 presented for SDOF systems under seismic excitations acting on a single support.

2.1.2.1 Time domain analysis of MDOF systems: Relative and Absolute Motion

The second order linear differential equation of motion for SDOF seen in equation (2.1) expanded for n -degree of freedom systems reads

$$\mathbf{M}[\ddot{\mathbf{u}}(t) + \mathbf{u}_g(t)] + \mathbf{C}\dot{\mathbf{u}}(t) + \mathbf{K}\mathbf{u}(t) = \mathbf{0} \quad (2.41)$$

where \mathbf{M} , \mathbf{C} , and \mathbf{K} are the $n \times n$ mass, damping and stiffness matrices, $\mathbf{u}(t)$, $\dot{\mathbf{u}}(t)$ and $\ddot{\mathbf{u}}(t)$ are respectively the $n \times 1$ vectors of the displacement, velocity and acceleration relative to the foundation.

In the equation above the vector of the ground acceleration as allocated to the n degree of freedom can be written as

$$\mathbf{u}_g(t) = \boldsymbol{\tau}\ddot{u}_g(t) \quad (2.42)$$

in which $\boldsymbol{\tau}$ is the $n \times 1$ incidence vector, whose elements are unitary relatively to the degrees of freedom activated by the ground motion's components or otherwise equal to zero; $\ddot{u}_g(t)$ is the ground motion acceleration acting on the support.

Nodal State space

Equation (2.41) is rewritten in the state space following the structure seen in equation (2.9) for SDOF systems; for MDOF the matrices seen in equation and

(2.10) are expanded in order to include all the degrees of freedom of the structural system then the dynamic equilibrium reads

$$\dot{\mathbf{y}}_N(t) = \mathbf{D}_N \mathbf{y}_N(t) + \mathbf{V}_N \ddot{\mathbf{u}}_g(t) \quad \mathbf{y}_N(t_0) = \mathbf{y}_{0,N} \quad (2.43)$$

where the subscript N stands for *nodal* and distinguishes the formulation for MDOF from SDOF; \mathbf{D}_N is the $2n \times 2n$ matrix of the structural properties of the system, $\mathbf{y}_N(t)$ is the matrix of the $2n \times 1$ unknown vectors displacements and velocities at any time instant and \mathbf{V}_N is the $2n \times 1$ incidence matrix, these are

$$\mathbf{y}_N(t) = \begin{bmatrix} \mathbf{u}(t) \\ \dot{\mathbf{u}}(t) \end{bmatrix} \quad \mathbf{D}_N = \begin{bmatrix} \mathbf{0}_n & \mathbf{I}_n \\ -\mathbf{M}^{-1}\mathbf{K} & -\mathbf{M}^{-1}\mathbf{C} \end{bmatrix} \quad \mathbf{V}_N = \begin{bmatrix} \mathbf{0} \\ \mathbf{M}^{-1}\boldsymbol{\tau} \end{bmatrix} \quad (2.44)$$

where \mathbf{I}_n and $\mathbf{0}_n$ are respectively the identity and zero matrix of dimension $n \times n$ and $\boldsymbol{\tau}$ the $n \times 1$ incidence vector with same order as the vector $\mathbf{0}$.

Expanding equation (2.11), the Duhamel's integral in the nodal state space for MDOF systems reads

$$\mathbf{y}_N(t) = \boldsymbol{\Theta}_N(t-t_0)\mathbf{y}(t_0) + \int_{t_0}^t \boldsymbol{\Theta}_N(t-\tau)\mathbf{V}_N \ddot{\mathbf{u}}_g(\tau) d\tau \quad (2.45)$$

where $\boldsymbol{\Theta}_N(t-\tau) = \exp[\mathbf{D}_N(t-\tau)]$ is the $2n \times 2n$ transition matrix.

The numerical evaluation of the integral in equation (2.45) by the step-by-step method seen in equation (2.12) for the case of relative motion, for MDOF systems becomes

$$\mathbf{y}_N(t_{k+1}) = \boldsymbol{\Theta}_N(\Delta t)\mathbf{y}(t_k) + \boldsymbol{\gamma}_{0,N}(\Delta t)\mathbf{V}_N \ddot{\mathbf{u}}_g(t_k) + \boldsymbol{\gamma}_{1,N}(\Delta t)\mathbf{V}_N \ddot{\mathbf{u}}_g(t_{k+1}) \quad (2.46)$$

where $\boldsymbol{\gamma}_{0,N}(\Delta t)$ and $\boldsymbol{\gamma}_{1,N}(\Delta t)$ are the $2n \times 2n$ loading matrices which expression is obtained from expansion of equations (2.13) and $\boldsymbol{\Theta}_N(\Delta t) = \exp(\mathbf{D}_N \Delta t)$.

The dynamic equilibrium for viscous damped MDOF systems in terms of absolute motion, is derived by means of the following position

$$\mathbf{u}_{abs}(t) = \mathbf{u}(t) + \mathbf{u}_g(t) \quad (2.47)$$

By substituting equation (2.47), its first and second derivative into equation (2.41), the equilibrium is restated as

$$\mathbf{M}\ddot{\mathbf{u}}_{abs}(t) + \mathbf{C}\left[\dot{\mathbf{u}}_{abs}(t) - \dot{\mathbf{u}}_g(t)\right] + \mathbf{K}\left[\mathbf{u}_{abs}(t) - \mathbf{u}_g(t)\right] = \mathbf{0} \quad (2.48)$$

After rearranging the equation above the following form of the dynamic equilibrium is obtained

$$\mathbf{M}\ddot{\mathbf{u}}_{abs}(t) + \mathbf{C}\dot{\mathbf{u}}_{abs}(t) + \mathbf{K}\mathbf{u}_{abs}(t) = \mathbf{K}\mathbf{u}_g(t) + \mathbf{C}\dot{\mathbf{u}}_g(t) \quad (2.49)$$

which after substituting equation (2.42) becomes

$$\mathbf{M}\ddot{\mathbf{u}}_{abs}(t) + \mathbf{C}\dot{\mathbf{u}}_{abs}(t) + \mathbf{K}\mathbf{u}_{abs}(t) = \mathbf{K}\boldsymbol{\tau}u_g(t) + \mathbf{C}\boldsymbol{\tau}\dot{u}_g(t) \quad (2.50)$$

To the terms on the right hand side, the following influence vectors are substituted

$$\mathbf{Q}_K = \mathbf{K}\boldsymbol{\tau}; \quad \mathbf{Q}_C = \mathbf{C}\boldsymbol{\tau} \quad (2.51)$$

Replacing the equation above to equation (2.50) it is obtained that

$$\mathbf{M}\ddot{\mathbf{u}}_{abs}(t) + \mathbf{C}\dot{\mathbf{u}}_{abs}(t) + \mathbf{K}\mathbf{u}_{abs}(t) = \mathbf{Q}_K u_g(t) + \mathbf{Q}_C \dot{u}_g(t) \quad (2.52)$$

In order to define the equations of the absolute motion of MDOF systems in the state variables space, according to equation (2.19), equation (2.43) is restated as

$$\dot{\mathbf{y}}_N(t) = \mathbf{D}_N \mathbf{y}_N(t) + \mathbf{V}_N^{(1)} u_g(t) + \mathbf{V}_N^{(2)} \dot{u}_g(t); \quad \mathbf{y}_N(t_0) = \mathbf{y}_{N,0} \quad (2.53)$$

where \mathbf{D}_N is a $2n \times 2n$ matrix and $\mathbf{V}_N^{(1)}$ and $\mathbf{V}_N^{(2)}$ $2n \times 1$ the incidence matrices, which read

$$\mathbf{D}_N = \begin{bmatrix} \mathbf{0}_n & \mathbf{I}_n \\ -\mathbf{M}^{-1}\mathbf{K} & -\mathbf{M}^{-1}\mathbf{C} \end{bmatrix}; \mathbf{V}_N^{(1)} = \begin{bmatrix} \mathbf{0} \\ \mathbf{M}^{-1}\mathbf{Q}_K \end{bmatrix}; \mathbf{V}_N^{(2)} = \begin{bmatrix} \mathbf{0} \\ \mathbf{M}^{-1}\mathbf{Q}_C \end{bmatrix} \quad (2.54)$$

Adopting the step-by-step procedure for numerical integration of the system of equations of motion that formally coincides to equation (2.22), it follows that

$$\begin{aligned} \mathbf{y}_N(t_{k+1}) = & \mathbf{\Theta}_N(\Delta t)\mathbf{y}(t_k) + \boldsymbol{\gamma}_{0,N}(\Delta t) \left[\mathbf{V}_N^{(1)}u_g(t_k) + \mathbf{V}_N^{(2)}\dot{u}_g(t_k) \right] + \\ & + \boldsymbol{\gamma}_{1,N}(\Delta t) \left[\mathbf{V}_N^{(1)}u_g(t_{k+1}) + \mathbf{V}_N^{(2)}\dot{u}_g(t_{k+1}) \right] \end{aligned} \quad (2.55)$$

where the matrices $\boldsymbol{\gamma}_{0,N}(\Delta t)$ and $\boldsymbol{\gamma}_{1,N}(\Delta t)$ are the $2n \times 2n$ loading matrices, whose expression is obtained from expansion of equations (2.13), $\mathbf{\Theta}_N(\Delta t) = \exp(\mathbf{D}_N\Delta t)$ is the transition matrix.

Modal space

When a structural system holds many DOF it is convenient to decouple the linear differential equations of motion seen in (2.41). In order to perform analysis of the response of MDOF systems and avoid high computational costs, the significant DOF are selected from vibration frequency analysis by which the mode shapes of the systems are determined. The analysis of the dynamic response is successively achieved by means of the modes superposition method.

The modal analysis and response superposition is performed by projecting equation (2.41) to the *modal space* of the generalized coordinates, which relate to the original nodal space through the transformation

$$\mathbf{u}(t) = \sum_{i=1}^n q_i(t)\phi_i = \mathbf{\Phi}\mathbf{q}(t) \quad (2.56)$$

where $q_i(t)$ are the modal contribution of the i -th degree of freedom, ϕ_i are real vectors which define the i -th modal shape; $\mathbf{q}(t)$ is the $n \times 1$ vector of unknown modal displacements and $\mathbf{\Phi}$ is $n \times n$ the modal matrix given as solution of the following eigen problem

$$\mathbf{K}\Phi = \mathbf{M}\Phi\Omega^2 \quad (2.57)$$

where, Ω is the diagonal matrix of order $n \times n$ listing the natural frequencies of the mode shapes.

The modal matrix Φ has properties of orthonormality expressed as $\Phi^T \mathbf{M} \Phi = \mathbf{I}_n$ and orthogonality, for which $\Phi^T \mathbf{K} \Phi = \Omega^2$ holds. The equation of motion in the nodal space see in equation (2.41) can be uncoupled by means equation (2.56) to obtain a system of $m \leq n$ reduced equations, with m the number of modes, that is

$$\begin{aligned} \ddot{\mathbf{q}}(t) + \Xi \dot{\mathbf{q}}(t) + \Omega^2 \mathbf{q}(t) &= \Phi^T \mathbf{M} \tau \ddot{u}_g(t) \\ \mathbf{q}_0 &= \Phi^T \mathbf{M} \mathbf{u}_0; \dot{\mathbf{q}}_0 = \Phi^T \mathbf{M} \dot{\mathbf{u}}_0 \end{aligned} \quad (2.58)$$

where, $\mathbf{q}(t)$, $\dot{\mathbf{q}}(t)$ and $\ddot{\mathbf{q}}(t)$ are the $n \times 1$ vectors of unknown modal displacement, velocity and acceleration; Ω , \mathbf{M} and Ξ are matrices of $n \times m$ order, called respectively the spectral, generalised mass and damping matrices.

The generalised modal damping matrix is usually assumed to be diagonal according to equation

$$\Xi = \Phi^T \mathbf{C} \Phi \equiv \text{Diag}[2\zeta_i \omega_i] \quad (2.59)$$

where ζ_i and ω_i denotes the damping ratio and the natural frequency for the i -th mode.

From equation (2.59) the damping matrix \mathbf{C} can be obtained by the following inverse relationship

$$\begin{aligned} \mathbf{C} &= (\Phi^T)^{-1} \Xi \Phi^{-1} \quad \forall m = n \\ \mathbf{C} &= \mathbf{M} \Phi \Xi \Phi^T \mathbf{M} \quad \forall m < n \end{aligned} \quad (2.60)$$

This approach allows to model the damping of structural systems when insufficient information is available by assigning the values ζ_i relying on the knowledge of typical values.

2.1.2.2 Frequency domain analysis of MDOF systems: Relative and Absolute Motion

By applying the Fourier Transform to the equations of motion of MDOF systems in the time domain, the dynamic equilibrium in the frequency domain is derived.

Firstly, the equations of the relative motion with respect to the foundation are introduced, which from equation (2.23) after Fourier Transformation gives

$$(\mathbf{K} - \omega^2 \mathbf{M} + i\omega \mathbf{C}) \mathbf{U}(\omega) = -\mathbf{M} \boldsymbol{\tau} \ddot{U}_g(\omega) \quad (2.61)$$

where $\mathbf{U}(\omega)$ is the $n \times 1$ displacements response vector and $\mathbf{K}_{dyn} = (\mathbf{K} - \omega^2 \mathbf{M} + i\omega \mathbf{C})$ is the $n \times m$ dynamic stiffness matrix.

From equation (2.61) the vector $\mathbf{U}(\omega)$ is obtained as

$$\mathbf{U}(\omega) = (\mathbf{K} - \omega^2 \mathbf{M} + i\omega \mathbf{C})^{-1} \mathbf{Q} \ddot{U}_g(\omega) \quad (2.62)$$

in which $\mathbf{Q} = -\mathbf{M} \boldsymbol{\tau}$ is the influence vector.

From the dynamic stiffness and influence vector positions the definition of the complex transfer function follows as

$$\mathbf{H}(\omega) = \mathbf{K}_{dyn}^{-1} \mathbf{Q} \quad (2.63)$$

and equation (2.62) becomes

$$|\mathbf{U}(\omega)| = |\mathbf{H}(\omega)| |\ddot{U}_g(\omega)| \quad (2.64)$$

The Duhamel's integral, presented for SDOF systems in equation (2.29), is obtained by means of the inverse Fourier Transform of equation (2.62), that is

$$\mathcal{F}^{-1}[\mathbf{U}(\omega)] = \mathbf{u}(t) = \frac{1}{2\pi} \int_{-\infty}^{+\infty} \mathbf{H}(\omega) \ddot{U}_g(\omega) e^{i\omega t} d\omega \quad (2.65)$$

Likewise, to solve the governing equation of MDOF systems for the absolute displacements, the Fourier Transform of equation (2.50) is taken by accounting of the relation between the Fourier Transform of the velocity and acceleration and displacements in equation (2.25), that gives

$$-\omega^2 \mathbf{M} \mathbf{U}_{abs}(\omega) + i\omega \mathbf{C} \mathbf{U}_{abs}(\omega) + \mathbf{K} \mathbf{U}_{abs}(\omega) = \mathbf{K} \boldsymbol{\tau} U_g(\omega) + \mathbf{C} \boldsymbol{\tau} \dot{U}_g(\omega) \quad (2.66)$$

Rearranging equation (2.66) the following expression holds

$$\left(\mathbf{K} + i\omega \mathbf{C} - \omega^2 \mathbf{M} \right) \mathbf{U}_{abs}(\omega) = \mathbf{K} \boldsymbol{\tau} U_g(\omega) + \mathbf{C} \boldsymbol{\tau} \dot{U}_g(\omega) \quad (2.67)$$

where $\mathbf{Q}_K = \mathbf{K} \boldsymbol{\tau}$ and $\mathbf{Q}_C = \mathbf{C} \boldsymbol{\tau}$ are the incidence matrices respectively related to the elastic dynamic force and the dissipative force triggered by the ground motion.

By substituting $\dot{U}_g(\omega) = i\omega U_g(\omega)$ into equation (2.67), the latter can be more conveniently expressed as

$$\left(\mathbf{K} + i\omega \mathbf{C} - \omega^2 \mathbf{M} \right) \mathbf{U}_{abs}(\omega) = \left(\mathbf{K} + i\omega \mathbf{C} \right) \boldsymbol{\tau} U_g(\omega) \quad (2.68)$$

Being the transfer function in absolute displacements given by

$$\mathbf{H}_{abs}(\omega) = \mathbf{K}_{dyn}^{-1} \left(\mathbf{K} + i\omega \mathbf{C} \right) \boldsymbol{\tau}, \quad (2.69)$$

the absolute displacement vector $\mathbf{U}_{abs}(\omega)$ is

$$\left| \mathbf{U}_{abs}(\omega) \right| = \left| \mathbf{H}_{abs}(\omega) \right| \left| U_g(\omega) \right| \quad (2.70)$$

where the dynamic force $U_g(\omega)$ is the Fourier Transform of the ground displacement.

2.2 Stochastic Seismic Analysis

A stochastic approach for structural earthquake engineering consists by modelling recorded seismic events, the accelerograms, as stochastic processes which vary with time. In the following sections, the fundamentals of the theory of random vibrations for zero-mean Gaussian stochastic processes is firstly presented, followed by the basics of linear vibration analysis for SDOF and MDOF systems in the time and frequency domain. Furthermore, the main concepts of direct stochastic analysis are reported, with particular focus on the integral formulation of the second order statistics of the response and the formulation of the first-passage problem for failure analysis.

2.2.1 Review of Theory of Probability and Stochastic Processes

The theory of stochastic processes is based on the theory of probability, whose basics concepts, e.g. the axioms of probability, the derivation and the generalised definitions of the statistical and central moments of random variables, can be found in several textbooks (see e.g. Lutes and Sarkani 2004). Hereafter only those concepts required to the definition of stochastic processes are reviewed.

The statistical characteristics of a random variable are fully defined by the knowledge of the CDF or the PDF; other quantities used to describe a random variable are the *statistical moments*, whose knowledge up to the infinite order fully defines the PDF. Particularly significant in statistics is the *Normal or Gaussian distribution* of random variables, which is fully defined by the statistical moments up to the second order. According to the *central limit theorem*, the *Gaussian distribution* fully defines a random event of independent infinite random variables by the following statement: for independent random variables in the infinite domain, the sum of their PDFs is normally distributed whatsoever their distribution (see e.g. Freedman et al. 1978).

The expression of this PDF for mono-dimensional random variables is given by

$$p_X(x) = \frac{1}{\sqrt{2\pi}\sigma_X} \exp\left\{-\frac{1}{2}\left(\frac{x-\mu_X}{\sigma_X}\right)^2\right\} \quad (2.71)$$

Henceforth only Gaussian stochastic processes are considered.

Introducing the stochastics operator $E[\cdot]$, the general expression of the statistical moments of j -th order can be presented as follows

$$m_j[X] = E[X^j] = \int_{-\infty}^{+\infty} x^j p_X(x) dx \quad (2.72)$$

The first moment is the expected value or *mean value* which is

$$m_1[X] = E[X] = \int_{-\infty}^{+\infty} x p_X(x) dx \equiv \mu_X \quad (2.73)$$

The second order moment known as the *mean-squared value* of the random variables

$$m_2[X] = E[X^2] = \int_{-\infty}^{+\infty} x^2 p_X(x) dx \quad (2.74)$$

whose square root is the root-mean-square value or rms.

The moments of random variables are alternatively defined by the *central moments*, which are given as follows

$$m_j[f(X)] = E\left[(X - \mu_X)^j\right] = \int_{-\infty}^{+\infty} (x - \mu_X)^j p_X(x) dx \quad (2.75)$$

The second order central moment is the variance σ_X^2 , which according to the definition in equation (2.75) reads

$$\sigma_X^2 = E\left[(X - \mu_X)^2\right] = E\left[X^2 - 2\mu_X E(X) + \mu_X^2\right] = E(X^2) - \mu_X^2 \quad (2.76)$$

The presented concepts refers to *mono-dimensional* random variables for which a random event is described by a single random variable. When a random event is described by more random variables, its CDF and PDF are *multi-dimensional* joint functions.

As any function of a random variable is a random variable, any random event which is function of two random variables can be referred as a bi-dimensional random variable.

According to equation (2.72), the *cross moments* of order $j+k$ of bi-dimensional random variables can be defined as

$$m_{jk}[XY] = E[X^j Y^k] = \int_{-\infty}^{+\infty} \int_{-\infty}^{+\infty} x^j y^k p_{X,Y}(x, y) dx dy \quad (2.77)$$

A stochastic process $X(t)$ is an ensemble of random functions of time $X^{(j)}(t)$, which are the samples of the process. Equally, a stochastic process can be seen as the family of sets of random variables with associated PDFs, $\{X(t_1), X(t_2), \dots, X(t_n)\}$, relatively to any particular time instant.

Gaussian stochastic processes are fully defined by their mean and second order statistical moments. According to equation (2.73), the mean value of the process $X(t)$ is

$$\mu_X(t) = E[X(t)] = \int_{-\infty}^{+\infty} x p_{X(t)}(x, t) dx \quad (2.78)$$

where x is the value of the random variable belonging to a set relative to the generic time t .

Similarly to equation (2.74), the second order cross-product of two random variables from the same process at two different time instants, $X(t_l)$ and $X(t_m)$, is called *auto-correlation* function and reads

$$R_{XX}(t_l, t_m) = E[X(t_l)X(t_m)] = \int_{-\infty}^{+\infty} \int_{-\infty}^{+\infty} x_l x_m p_{X(t_l)X(t_m)}(x_l, x_m, t_l, t_m) dx_l dx_m \quad (2.79)$$

When the random variables are extracted from two different stochastic processes, $X(t_l)$ and $Y(t_m)$, at different time instants, likewise in equation (2.77), the second order cross-product is the *cross-correlation* function

$$R_{XY}(t_l, t_m) = E[X(t_l)Y(t_m)] = \int_{-\infty}^{+\infty} \int_{-\infty}^{+\infty} x_l y_m p_{X(t_l)Y(t_m)}(x_l, y_m, t_l, t_m) dx_l dy_m \quad (2.80)$$

According to the expression of the central moments of RVs, seen in equation (2.75), the expression of the second order central moments for random variables of the same stochastic process at two different time instants is the *auto-covariance function*, that is

$$\begin{aligned} K_{XX}(t_l, t_m) &= E\left\{[X(t_l) - \mu_X(t_l)][X(t_m) - \mu_X(t_m)]\right\} = \\ &= E[X(t_l)X(t_m)] - \mu_X(t_l)\mu_X(t_m) \end{aligned} \quad (2.81)$$

where $E[X(t_l)X(t_m)]$ is the joint second order moment seen in equation (2.80), $\mu_X(t_l)$ and $\mu_X(t_m)$ are the mean values of the random variables according to equation (2.78).

Similarly, to equation (2.81), considering a pair of random variables drawn from different stochastic processes, the expressions of the second order central moment provides the so called *cross-covariance* function, that reads

$$\begin{aligned} K_{XY}(t_l, t_m) &= E\left\{[X(t_l) - \mu_X(t_l)][Y(t_m) - \mu_Y(t_m)]\right\} \\ &= E[X(t_l)Y(t_m)] - \mu_X(t_l)\mu_Y(t_m) \end{aligned} \quad (2.82)$$

Henceforth, zero-mean Gaussian stochastic processes are considered, the covariance functions equal the correlation functions, as equation (2.79) coincides with (2.81) and equation (2.80) with (2.82).

The auto-correlation function can be rewritten for any time instant t by arranging the time t_m as the summation of the previous time instant and a time shift τ , that is

$$t_m = t_l + \tau \quad (2.83)$$

by which it holds

$$R_{XX}(t_l, t_m) \equiv R_{XX}(t, \tau) \quad (2.84)$$

For *stationary* processes the auto-correlation function, through equation (2.83) particularises into

$$R_{XX}(t_l, t_m) = R_{XX}(t_l, t_l + \tau) \equiv R_{XX}(\tau) \quad (2.85)$$

Accordingly, the second order moment, the auto and cross-correlation functions can be expressed in the frequency domain by the Fourier Transform procedure, however these numerical integrals are unbounded unless the integrand of the Fourier Transform tends to zero as the time tends towards infinite, as a result these relations are not employable.

In order to apply the Fourier Transform procedure to stationary processes, a special truncated version of the original process is introduced; satisfying the Dirichlet condition, which are expressed as

$$\int_{-\infty}^{+\infty} |R_{XX}(\tau)| d\tau < \infty, \quad (2.86)$$

by means of the Wiener-Khinchine expressions, a new function of the frequency is characterised as the Fourier Transform of the auto-correlation function, called Power Spectral Density (PSD) function, that reads

$$S_{XX}(\omega) = \frac{1}{2\pi} \int_{-\infty}^{+\infty} R_{XX}(\tau) e^{-i\omega\tau} d\tau \quad (2.87)$$

by inverse transformation, from the PSD function, the auto-correlation function is given as follows

$$R_{XX}(\tau) = \int_{-\infty}^{+\infty} S_{XX}(\omega) e^{i\omega\tau} d\omega \quad (2.88)$$

The PSD function is commonly adopted in earthquake engineering applications due to its physical interpretation according to the Parseval theorem, by which the PSD relates to the energy of the earthquake as following (see e.g. Thomson 1993)

$$S_{XX}(\omega) = \lim_{T \rightarrow \infty} \frac{1}{T} X(\omega) X^*(\omega) \quad (2.89)$$

where T is the period of the harmonics, $X(\omega)$ is the Fourier transform of the a ground motion record and $X(\omega)^*$ its complex conjugate.

By means of the Fourier analysis only the average spectral decomposition of the signal is provided, therefore equations (2.87) and (2.89) cannot be straightforwardly expanded for time-frequency representation of deterministic time series. In this regard, different methods of joint-time frequency distribution can be found in literature. Among these, the expression of the Evolutionary Power Spectral Density function holds (see e.g. Cohen 1989)

$$S_{XX}(\omega, t) = \frac{1}{2\pi} \int_{-\infty}^{+\infty} R_{XX}(t, \tau) e^{-i\omega\tau} d\tau \quad (2.90)$$

where $R_{XX}(t, \tau)$ is the central auto-correlation function of the non-stationary stochastic process $X(t)$.

According to the physical nature of the earthquake phenomenon, whose amplitude and frequency content vary with time, time-frequency dependant PSD functions more realistically characterise the ground motion as a stochastic process. Nevertheless, the selection of the time instants at which the frequency content changes and the evolution of the frequency itself, are difficult to mathematically

define. For the class of oscillatory processes developed by Priestley (1965), the generalisation of the classic Fourier analysis provides pertinent relationships between the evolutionary PSD and the corresponding correlation functions, aspect particularly significant in earthquake ground motion modelling (see e.g. Shinozuka and Deodatis 1988, Deodatis 1996). Presented in the next section, Priestley's *evolutionary spectrum* is commonly considered for stochastic modelling of earthquake ground motion.

2.2.2 Stochastic Seismic Ground Motion Processes

Following the background of theory of probability, the fundamental of seismic ground motion modelling are provided in this section. Firstly, the theory of the evolutionary spectra adopted in this work to model non-stationary ground motions is presented. Successively, the first models, white noise and filtered white noise for seismic ground motions are described.

Evolutionary spectra for seismic ground motions

Priestley's (1965) theory of "evolutionary spectra" provides a pertinent expression of non-stationary PSD functions for stochastic processes whose characteristics change slowly over the time. Expressing the process whether in terms of the one and two-sided evolutionary PSD function, it holds

$$\begin{aligned} G(\omega, t) &= 0 & \omega < 0, \\ G(\omega, t) &= 2S(\omega, t) = |a(\omega, t)|^2 G(\omega) & \omega \geq 0; \end{aligned} \quad (2.91)$$

where $G(\omega, t)$ and $S(\omega, t)$ are respectively related evolutionary one-sided and two-sided PSD functions; $G(\omega)$ is a one-sided stationary process and $a(\omega, t)$ is a slowly varying deterministic time-frequency modulating function.

Despite the processes defined by equation (2.91) have separable counterparts, these still retain both amplitude and frequency variation with time. Real earthquake ground motions are fully non-stationary (or non-separable) stochastic processes, which can be simplified by assuming that only the amplitude of the process varies with respect

to time, (i.e. $a(\omega, t) = a(t)$), generally known as quasi-stationary, separable or also uniformly modulated. Accordingly, for quasi-stationary processes equation (2.91) modifies as follows

$$\begin{aligned} G(\omega, t) &= 0, & \omega < 0; \\ G(\omega, t) &= 2S(\omega, t) = |a(t)|^2 G(\omega), & \omega \geq 0. \end{aligned} \quad (2.92)$$

Several authors proposed time modulating functions generally calibrated on different arrays of accelerograms (e.g. Bogdanoff et al. 1961, Shinozuka and Sato 1967, Jennings et al. 1969).

Equation (2.92) can be particularised by assuming $|a(t)| = 1$ reducing to the form for stationary processes, that gives

$$\begin{aligned} G(\omega) &= 0, & \omega < 0; \\ G(\omega) &= 2S(\omega), & \omega \geq 0. \end{aligned} \quad (2.93)$$

Equation (2.93) is a considerable simplification in representing the seismic action. Initially, the stochastic earthquake models used for earthquake engineering applications were stationary models, which were obtained by filtering PSD functions with constant amplitude, known as white noises (WN).

White noise and filtered white noise for seismic ground motions

A widely used model for stationary stochastic processes in engineering applications is the Kanai-Tajimi (KT) power spectrum. The KT spectrum models the free field seismic acceleration as a filtered white noise process (Kanai 1957), this reads

$$S_{KT}(\omega) = \frac{1 + 4\zeta_g^2 \left(\frac{\omega}{\omega_g}\right)^2}{\left\{1 - \left(\frac{\omega}{\omega_g}\right)^2\right\}^2 + 4\zeta_g^2 \left(\frac{\omega}{\omega_g}\right)^2} \quad (2.94)$$

where ω_g and ζ_g respectively represent the stiffness and the damping of the soil which is assumed as an oscillator of infinite mass filtering a white noise process.

The Kanai-Tajimi spectrum at the zero frequency begins with a non-zero value, as a consequence, the velocity and the displacement integrals are unbounded. In order to overcome this physical inconsistency, the Clough-Penzien spectrum (CP) was introduced to suppresses the values of the spectrum as the frequency tends to zero, through a high-pass filter (Clough and Penzien 1993), that is

$$S_{CP}(\omega) = S_{KT}(\omega) \times \frac{\left(\frac{\omega}{\omega_f}\right)^4}{\left\{1 - \left(\frac{\omega}{\omega_f}\right)^2\right\}^2 + 4\zeta_f^2 \left(\frac{\omega}{\omega_f}\right)^2} \quad (2.95)$$

where ω_f and ζ_f are the stiffness and the damping of the soil, assumed as an oscillator of infinite mass and filtering the response process, the KT spectrum, of a second SDOF system in series.

The KT and CP functions are stationary spectra, whose constant parameters depend on the soil properties. The non-stationary version of the CP spectrum has been formulated by considering time varying frequency parameters of the spectrum (see e.g. Deodatis 1996), which gives

$$S_{CP}(\omega, t) = \frac{1 + 4\zeta_g^2(t) \left(\frac{\omega}{\omega_g(t)}\right)^2}{\left\{1 - \left(\frac{\omega}{\omega_g(t)}\right)^2\right\}^2 + 4\zeta_g^2(t) \left(\frac{\omega}{\omega_g(t)}\right)^2} \times \frac{\left(\frac{\omega}{\omega_f(t)}\right)^4}{\left\{1 - \left(\frac{\omega}{\omega_f(t)}\right)^2\right\}^2 + 4\zeta_f^2(t) \left(\frac{\omega}{\omega_f(t)}\right)^2} \quad (2.96)$$

where the time-variant functions, $\omega_g(t)$ and $\omega_f(t)$ are natural frequencies, $\zeta_g(t)$ and $\zeta_f(t)$ are damping ratio, which account of the frequency content of the seismic waves propagating throughout the soil.

2.2.3 Spectral Characteristics of Stochastic Processes

In this section, the spectral characteristics of a generic stochastic processes $X(t)$ are presented. Under the hypothesis of stationarity, the *geometrical spectral moments* are introduced followed by the *non-geometrical spectral moments* whereas accounting for the non-stationarity of stochastic processes.

Geometrical Spectral Moments (GSM)

The geometrical spectral moments are widely employed for the failure assessment of engineering structural systems. These quantities are related to the second order statistics of stochastic processes; therefore, they enable to determine the probability density functions of structural response's measures (e.g. largest absolute value of the response or peak).

Vanmarke (1972) introduced the representation of stationary stochastic process $X(t)$ by the so called geometrical spectral moments

$$\lambda_{i,X} = \int_0^{+\infty} \omega^i G_{XX}(\omega) d\omega \quad i=0,1,2\dots \quad (2.97)$$

which for $i=0,1,2$ gives respectively the zero-th, the first and the second order geometrical spectral moments.

From the geometrical spectral moments, other parameters with the dimension of a circular frequency can be defined

$$\omega_{i,X} = \left(\frac{\lambda_{i,X}}{\lambda_{0,X}} \right)^{\frac{1}{i}} \quad (2.98)$$

The quantity $\omega_{1,X}$ is called *central frequency* of the stochastic process, it is seen as the centroid of PSD function with respect to the frequency origin; the quantity $\omega_{2,X}$ is the radius of gyration of the PSD about the frequency origin and represents where the spectral mass is located.

The spread of the frequency content about the central frequency $\omega_{1,X}$ is quantified by the bandwidth factor δ_X , interpreted as the variability in frequency content of the PSD function, this reads

$$\delta_X = \sqrt{1 - \frac{\lambda_{1,X}^2}{\lambda_{0,X}\lambda_{2,X}}} = \frac{\omega_s}{\omega_{2,X}} \quad (2.99)$$

where the frequency $\omega_s = \sqrt{\omega_{2,X}^2 - \omega_{1,X}^2}$ is the radius of gyration of the PSD function about the central frequency $\omega_{1,X}$.

The interpretation of $\omega_{1,X}$, $\omega_{2,X}$ and ω_s is respectively of the mean, the mean square and the standard deviation of the stochastic process $\lambda_{0,X}^{-1}G(\omega)$, according to the analogy between a probability density function and the PSD function normalised to the zero-th order spectral moment $\lambda_{0,X}$ (Vanmarke 1972).

By taking first and second derivatives of the Wiener-Khinchine relations in equation (2.88), for $\tau = 0$ the correspondence between the second order statistics for the zero-th and second geometrical spectral moments of the unilateral PSD holds

$$R_{XX}(0) = \sigma_X^2 = \int_0^{+\infty} G_{XX}(\omega) d\omega = \lambda_{0,X} \quad (2.100)$$

$$R_{\dot{X}\dot{X}}(0) = \sigma_{\dot{X}}^2 = \int_0^{+\infty} \omega^2 G_{XX}(\omega) d\omega = \lambda_{2,X} \quad (2.101)$$

Differently, the first order spectral moment does not hold any interpretation

$$R_{\dot{X}\dot{X}}(0) = \int_0^{+\infty} \omega G_{XX}(\omega) d\omega = \lambda_{1,X} \quad (2.102)$$

To note that the cross-correlation function between the stochastic process and its first derivative is null.

Time-dependent Geometrical Spectral Moments

The geometrical spectral moments presented in equations (2.100)-(2.102) can be straightforwardly expanded time-dependent PSD function; these are called transient spectral moments, which read

$$\lambda_{i,X}(t) = \int_0^{+\infty} \omega^i G_{XX}(\omega, t) d\omega \quad i=0,1,2... \quad (2.103)$$

The relationships between the transient spectral moments and the second order statistics, as seen in equations (2.100)-(2.102) for stationary processes, are not fully satisfied, only the zero-th order transient spectral moment is related to the variance of the process

$$\lambda_{0,X}(t) = \sigma_X^2(t) = \int_0^{+\infty} G_{XX}(\omega, t) d\omega \quad (2.104)$$

To evaluate the transient spectral moments according to a geometrical definition is conceptually acceptable nevertheless may induce to divergent solutions (Michealov et al. 1999b). The transient spectral moments are valuable to determine the bandwidth measures as the central frequency and the bandwidth factor, for instance under the hypotheses of evolutionary processes.

For non-stationary stochastic processes, equation (2.98) can be intuitively restated and expanded accounting of the definition of the time-variant spectral moments in equation (2.103) as follows

$$\omega_i = \left(\frac{\int_0^{\infty} \omega G(\omega, t) d\omega}{\int_0^{\infty} G(\omega, t) d\omega} \right)^{\frac{1}{i}} \quad (2.105)$$

For $i=1$, equation (2.105) is referred as mean instantaneous frequency, representing the change in mean value of the frequencies of the signal with time (see e.g. Spanos et al. 2007).

For non-stationary processes the bandwidth factor seen in equation (2.99) is a function of time

$$\delta_x(t) = \sqrt{1 - \frac{\lambda_{1,x}^2(t)}{\lambda_{0,x}(t)\lambda_{2,x}(t)}} \quad (2.106)$$

The definition of the central frequency and bandwidth parameter have been object of extensive studies with focus on the definition of the spectral characteristics of the response of structural systems subjected to random processes. The definition of the geometrical and non-geometrical spectral moments has been object of several investigations in structural safety and reliability (Caddemi et al. 2001), in the next section an introduction to the problem is presented.

2.2.4 Stochastic Response of Structural Systems

In this section the concepts relatively to general stochastic processes presented in paragraph 2.2.3 are particularised for structural systems under stochastic seismic ground motions. The representation of the response stochastic processes of engineering systems under random excitation has been tackled by several authors by describing the spectral characteristics of the response process (see e.g. Vanmarke 1972, Corotis et al. 1972, Der Kiureghian 1980, Di Paola 1985, Di Paola and Petrucci 1990, Spanos and Miller 1994, Mickealov et al. 1999a; Mickealov et al. 1999b, Caddemi et al. 2004, Barbato and Conte 2008, Barbato and Vasta 2010, Cacciola and Muscolino 2011, Muscolino and Alderucci 2015). In the next sections the geometrical and non-geometrical spectral moments of the structural response are

presented, and their applicability in reliability analysis introduced with reference to the first passage problem. For sake of clarity, the stochastic equations of motion for SDOF systems in the frequency domain are introduced.

2.2.4.1 Spectral Representation of the Response of Structural Systems

According to equations (2.26)-(2.28) the equilibrium of a SDOF oscillator under seismic action represented by the simpler case of stationary PSD function, see equation (2.93), is

$$G_{UU}(\omega) = |H(\omega)|^2 G_{\ddot{u}_g \ddot{u}_g}(\omega) \quad (2.107)$$

where $G_{UU}(\omega)$ is the unilateral PSD function of the response displacement, $H(\omega)$ is the transfer function of the oscillator and $G_{\ddot{u}_g \ddot{u}_g}(\omega)$ is the PSD of the seismic acceleration input ground motion.

GSMs of the structural response of linear structural system

Let consider the stationary stochastic response $U(t)$ of a damped SDOF system. According to the definition of the geometrical spectral moments for Gaussian stochastic processes seen in equation (2.97), the geometrical spectral moments of $U(t)$ read

$$\lambda_{i,U} = \int_0^{+\infty} \omega^i G_{UU}(\omega) d\omega \quad (2.108)$$

where the unilateral PSD function $G_{UU}(\omega)$ according to the equation (2.89) can be written as follows

$$G_{UU}(\omega) = E \left[U(\omega) U^*(\omega) \right] \quad (2.109)$$

where $U(\omega)$ and $U^*(\omega)$ are the Fourier transform of each realisation $u(t)$ of process $U(t)$ and its complex conjugate.

According to equation (2.27) and (2.28), which present the response of the damped SDOF oscillator under seismic ground motion, equation (2.109) can be expanded as follows

$$E[U(\omega)U^*(\omega)] = E\left[\left(H(\omega)\ddot{U}_g(\omega)\right)\left(H(\omega)\ddot{U}_g(\omega)\right)^*\right] \quad (2.110)$$

$$E[U(\omega)U^*(\omega)] = H(\omega)H^*(\omega)E\left[\ddot{U}_g(\omega)\ddot{U}_g^*(\omega)\right] \quad (2.111)$$

where $\ddot{U}_g(\omega)$ is the Fourier transform of the realisation $\ddot{u}_g(t)$ representing the seismic acceleration at the base of the system and $\ddot{U}_g^*(\omega)$ is the complex conjugate.

According to Parseval's theorem and equation (2.27)

$$G_{\ddot{u}_g\ddot{u}_g}(\omega) = E\left[\ddot{U}_g(\omega)\ddot{U}_g^*(\omega)\right] \quad (2.112)$$

After rearranging equation (2.111) and substituting it in the definition of PSD of the input ground motion, it follows that

$$G_{UU}(\omega) = E\left[U(\omega)U^*(\omega)\right] = H(\omega)H^*(\omega)G_{\ddot{u}_g\ddot{u}_g}(\omega) \quad (2.113)$$

For the expression above, equation (2.108) becomes

$$\lambda_{i,U} = \int_0^{+\infty} \omega^i |H(\omega)|^2 G_{\ddot{u}_g\ddot{u}_g}(\omega) d\omega \quad i=0,1\dots \quad (2.114)$$

The equation above allows to pursue the problem of defining the reliability of structural systems.

NGSMs of the response of linear structural system

In structural engineering the transient geometrical definition of the spectral characteristics of a stochastic response process is also not appropriate for the case of SDOF system subjected to the simple Gaussian white noise process. (Corotis et al. 1972). An important contribution has been provided by Di Paola (1985) by establishing a relation between the variances and covariances of the response of non-

stationary evolutionary processes and a real auxiliary process. Another contribution for evaluating the NGSMS of the stochastic response of structural systems has been provided by Cacciola and Muscolino (2011). The authors proposed to determine the spectral characteristics by assuming the input process to be the summation of a number of zero-mean independent uniformly modulated Gaussian processes, according to the model of Conte and Peng (1997). Therefore, Cacciola and Muscolino (2011) introduced the formulation of the non-stationary spectral moments in the nodal space as a linear function of the time-dependent modal non-geometric spectral moments “purged” by participation factors, which for any modal DOF have the following structure

$$\lambda_{0,U}(t) = \int_0^{\infty} H_j(\omega, t) H_j^*(\omega, t) G_j(\omega) d\omega \quad (2.115)$$

$$\lambda_{1,U}(t) = -i \int_0^{\infty} H_j(\omega, t) \dot{H}_j^*(\omega, t) G_j(\omega) d\omega \quad (2.116)$$

$$\lambda_{2,U}(t) = \int_0^{\infty} \dot{H}_j(\omega, t) \dot{H}_j^*(\omega, t) G_j(\omega) d\omega \quad (2.117)$$

where $G_j(\omega)$ is the PSD function of the seismic acceleration process, $H(\omega, t)$ and $\dot{H}(\omega, t)$ are the Duhamel's convolution integrals representing the response of SDOF oscillator forced by the deterministic complex function $\exp(-i\omega t)a_j(t)$, these are

$$H(\omega, t) = \exp(i\omega t) \int_0^t h(t-\tau) \exp(-i\omega\tau) a_j(\tau) d\tau \quad (2.118)$$

$$\dot{H}(\omega, t) = \exp(i\omega t) \int_0^t \dot{h}(t-\tau) \exp(-i\omega\tau) a_j(\tau) d\tau \neq \frac{\partial H(\omega, t)}{\partial t} \quad (2.119)$$

in which $h(t-\tau)$ is the response to the Dirac delta function seen in equation (2.8) and $\dot{h}(t-\tau)$ its first derivative.

Closed-form solutions of the evaluation of the NGSM have been proposed by Barbato and Conte (2013) for fully non-stationary input considered as a superposition of time modulated coloured noise processes.

Numerical application

The time-dependent geometrical spectral moments are widely employed for engineering applications although the approximation that they may introduce in the evaluation of the second order moments of the response process (see e.g. Michealov et al. 1999b). In order to understand the implications of their use for time-frequency dependant stochastic response process, a numerical application regarding the system depicted in Figure 2.1 is presented hereafter. The input is assumed to be an uniformly modulated stochastic process modelled according to Bogdanoff-Goldberg-Bernard (BGB) modulating function and the stationary response-spectrum-compatible PSD function proposed by Cacciola et al. (2004). The time-dependant geometrical spectral moment of the structural response are evaluated according to equation (2.103), the non-geometrical spectral moment through equations (2.115)-(2.119); specifically the latter equations are particularised for the BGB time modulating function by close form solutions for equations (2.118) and (2.119).

The system adopted for this numerical example is the 2-storey linear frame with lumped masses at each beam shown in Figure 2.1; the system has 2 DOF relatively to the horizontal displacements, its natural frequencies are $\omega_1 = 21.30$ rad/s and $\omega_2 = 51.83$ rad/s, the damping is assumed to be viscous and modelled according to equations (2.59) and (2.60).

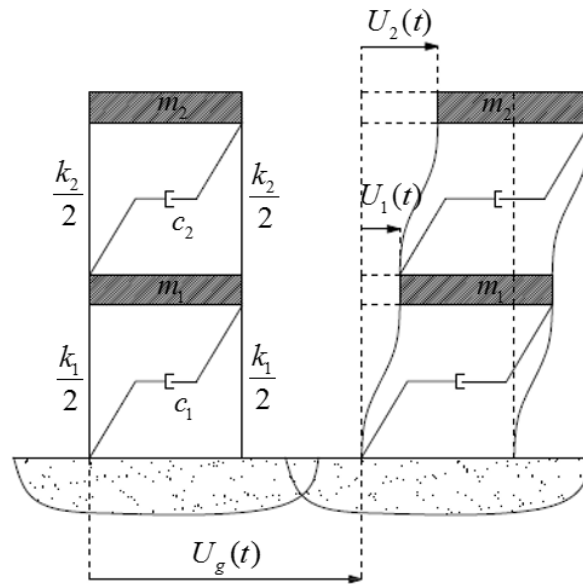


Figure 2.1. 2 DOF frame subjected to single support excitation at the base.

In Figure 2.2 the comparison of the zero-th order geometrical and non-geometrical spectral moments of the response of the first floor is illustrated; two different values of damping of the system are compared, namely the 5% and the 1% of the damping ratio are considered.

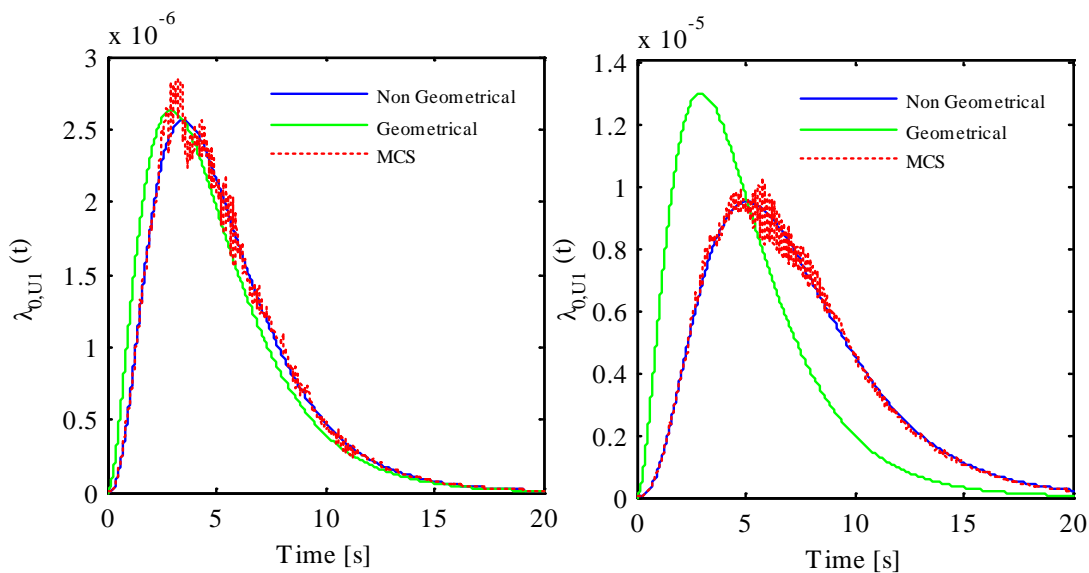


Figure 2.2. Geometrical and Non-Geometrical and Spectral moments of the response of a 2 DOF system under quasi-stationary input under the assumption of: a) 5% and b) 1% of the structural damping.

Figure 2.2 shows that for the system with 1% of the damping whose transient response is more dominant, the geometrical approximation unsuccessfully predicts the time dependant variance of the displacement response process. The results are validated by Monte Carlo Simulation, that satisfactorily agrees with the formulation of the non-geometrical definition of the spectral moments adopted.

2.2.4.2 First Passage Problem and Reliability

For some engineering systems, the failure is assumed to occur when the response exceeds some threshold for the first time; for these systems, the *first passage problem* is formulated in order to predict the stochastic response with a certain probability to not exceed a barrier, i.e. fixed threshold.

The probability that a process has not yet crossed a barrier, can be related to the distribution of the maxima values of the response process $U(t)$ during a specified time interval. The local maxima of $U(t)$ over the fixed time interval are called peaks, and the process of the extreme value or absolute peak, i.e. maxima amplitude of $U(t)$, is defined as follows

$$U_{\max}(t) = \max_{0 \leq s \leq t} |U(s)| \quad (2.120)$$

The distribution of $U_{\max}(t)$ is related to the time of first passage of a double barrier, denoted with T_b , therefore the cumulative distribution function of the extreme value $U_{\max}(t)$ can be equivalently expressed as, that is

$$F_{U_{\max}}(b) = P[U_{\max}(t) \leq b] = P[T_b(t) > t] = L(t) \quad (2.121)$$

where $L(t)$ is sometimes called the probability of survival (Lutes and Sarkani 2007), with reference to the critical value of a barrier b , which is related to the failure mode of the system.

The distribution used for counting time-dependant phenomena is the Poisson distribution, then assuming the barrier's crossing as a Poisson point process¹ the probability of survival is

$$L(t) = A \exp(-\alpha_U t) \quad (2.122)$$

where α_U is the hazard function and A is the probability that the process is below the barrier at time $t = 0$, which can be assumed equal to 1.

In order to identify the hazard function, the number of peaks crossing a given threshold have to be quantified by the *expected rate of barrier up-crossings*, which converted in terms of probability of an up-crossing is given as follows

$$v_U^+(b, t) = \lim_{\Delta t \rightarrow 0} \frac{P(\text{an upcrossing of } b \text{ in } [t, t+\Delta t])}{\Delta t} \quad (2.123)$$

where Δt is the infinitesimal time increment in the counting interval of the up-crossing, which can be either zero or one and b is the barrier level.

The probability of an up-crossing of a barrier by the process $U(t)$ depends on the process itself, on its first derivative $\dot{U}(t)$, and on the level of the barrier. By considering the time interval over which the peaks occur to be infinitesimal, the process $\dot{U}(t)$ can be assumed to be constant; under this hypothesis the probability that the process $U(t)$ up-crosses a single barrier in the time interval $[t, t+\Delta t]$ is (Lutes and Sarkani 2004)

$$P(\text{an upcrossing of } b \text{ in } [t, t+\Delta t]) \approx \int_0^{\infty} (\dot{u} \Delta t) p_{U(t), \dot{U}(t)}(b, \dot{u}) d\dot{u} \quad (2.124)$$

Substituting equation (2.124) into equation (2.123) the mean rate of conditional up-crossing reads

¹ The Poisson distribution approximates well broad band processes and/or high level of the barrier, in some other instances it may lead to erroneous values of the first passage probability (Lutes and Sarkani 2007), however it tends to be very conservative for narrow band processes (Vanmarke 1972).

$$\nu_U^+(b, t) = \int_0^{\infty} \dot{u} p_{U(t), \dot{U}(t)}(b, \dot{u}) d\dot{u} \quad (2.125)$$

Under the hypothesis of stationarity, the stochastic process and its derivative process are uncorrelated; furthermore if the process $U(t)$ is Gaussian, $U(t)$ and $\dot{U}(t)$ are also independent and the conditioning event is negligible; therefore due to the independency between random variables, the joint probability density function $p_{U(t), \dot{U}(t)}$ can be rewritten as the product of the marginal probability density functions $p_{U(t)}(b)$ and $p_{\dot{U}(t)}(\dot{x})$; it follows the fundamental definition of the mean rate of unconditional up-crossing as (see e.g. Vanmarke 1972)

$$\nu_U^+(b) = p_{U(t)}(b) \int_0^{\infty} \dot{u} p_{\dot{U}(t)}(\dot{u}) d\dot{u} \quad (2.126)$$

The main approximation of the first passage problem is neglecting the conditioning event expressed in equation (2.125) which allows to replace the hazard function as follows

$$\alpha_U = \nu_{|U|}^+ = 2\nu_U^+ \quad (2.127)$$

where $\nu_{|U|}^+$ refers to the double symmetric barrier and ν_U^+ to the single barrier problem.

The mean rate of up crossing of the barrier is obtained from equation (2.126) by replacing $p_{\dot{U}(t)}$ with the expression of the probability density function for zero mean Gaussian processes presented in equation (2.71), that is

$$\nu_U^+(b) = \frac{\sigma_{\dot{U}}}{2\pi\sigma_U} \exp\left[-\frac{1}{2}\left(\frac{b}{\sigma_U}\right)^2\right] \quad (2.128)$$

where the following position can be made,

$$\bar{\eta}_U = \frac{b}{\sigma_U} \quad (2.129)$$

which is known as the *reduced threshold level*.

Equation (2.128) can be rewritten in terms of the geometrical spectral moments according to equations (2.100) and (2.101) as follows

$$\nu_U^+(b) = \frac{1}{2\pi} \left(\frac{\lambda_{2,U}}{\lambda_{0,U}} \right)^{1/2} \exp\left(-\frac{1}{2} \frac{b^2}{\lambda_{0,U}} \right) \quad (2.130)$$

Moreover, when the barrier $b=0$, the mean rate of up-crossing of the zero level, $\nu_U^+(0) = \nu_0^+$ is obtained, that is

$$\nu_0^+ = \frac{1}{2\pi} \left(\frac{\lambda_{2,U}}{\lambda_{0,U}} \right)^{1/2} = \frac{\omega_{2,U}}{2\pi} \quad (2.131)$$

Therefore after substituting equation (2.131) and (2.129) in equation (2.130), for the double barrier problem the mean rate of up crossing with positive slope follows as

$$\nu_{|U|}^+(b) = 2\nu_0^+ \exp\left(-\frac{\bar{\eta}_U^2}{2} \right) \quad (2.132)$$

The cumulative distribution function of the extreme values according to equations (2.121), (2.122) and (2.130)-(2.129) is

$$F_{U_{\max}}(b) = \exp\left[-2\nu_0 t \exp\left(-\frac{\bar{\eta}_U^2}{2} \right) \right] \quad (2.133)$$

For wide band processes groups of up-crossings tend to immediately follow one another forming “clumps”, instead for very narrow band processes the clumps tend to be clustered. Equation (2.130) is generally adopted for sufficiently high thresholds’ level, case in which the clump size is small. In order to improve the definition of the formulation of the problem of first passage for low thresholds’ level,

as well as for narrow band processes, the mean clump duration interval between the end and the start of two consecutive clumps is accounted, that is

$$E[T_0] = \frac{1}{2\nu_0} \frac{\exp\left(\frac{\bar{\eta}_U^2}{2}\right) - 1}{1 - \exp\left(-\frac{\pi}{2} \delta_U \bar{\eta}_U\right)} \quad (2.134)$$

where T_0 is the time interval between the end and the start of two consecutive clumps.

The mean rate of up-crossing in equation (2.122) is replaced with $1/E[T_0]$, which is the inverse of equation (2.134), that gives

$$\nu_{|U|}^+(b) = 2\nu_0 \frac{1 - \exp\left(-\sqrt{\frac{\pi}{2}} \bar{\eta}_U \delta_U\right)}{\exp\left(\frac{\bar{\eta}_U^2}{2}\right) - 1}, \quad (2.135)$$

Through equation above, the cumulative distribution function of the extreme values in equation (2.122) can be expresses as

$$F_{U_{\max}}(b) = \exp\left[-2\nu_0 t \frac{1 - \exp\left(-\sqrt{\frac{\pi}{2}} \bar{\eta}_U \delta_U\right)}{\exp\left(\frac{\bar{\eta}_U^2}{2}\right) - 1}\right] \quad (2.136)$$

When the assumption of stationary structural response is far from reality, the dependency of the spectral moments and the bandwidth factor to the time cannot be neglected in the formulation of the first passage problem; hence the function in equation (2.122) is rewritten for non-stationary response processes as follows (Corotis et al 1972)

$$L(t) = A \exp\left(-\int_0^{t_f} \alpha_U(b, t) dt\right) \quad (2.137)$$

where A is usually assumed equal to 1 and p is the probability of the barrier to not be exceeded.

When the non-stationarity of the response is considered, the hazard function is time dependant and in order to solve the first passage problem expressed by equation (2.137), the computation of the non-geometrical spectral moments is required (see e.g. Barbato 2011). On the other hand, under the assumption of stationary stochastic processes, the solution of the first passage problem of a given barrier according to equation (2.122) is achievable by evaluation of the geometrical spectral moments, leading to a simplified solution, which being the approach adopted in this work is presented more in depth in the next section.

2.2.4.3 Peak Factor

Let consider equation (2.122) and a threshold u_{\max} below which the peak of the response of a slightly damped system remains with probability p , within the duration T_s . The structural reliability of a system, whose peak of the response is the process $U_{\max}(t)$, can be assessed by solving the following equation

$$F_{U_{\max}}(u_{\max}) = p \quad (2.138)$$

where u_{\max} is the maximum of $|U(t)|$ with probability p of not being exceeded, unknown of the first passage problem.

Assuming the threshold level as the value of the maximum of the response u_{\max} equation (2.129) can be written

$$u_{\max} = \eta_U(T_s, p, \delta_U) \sigma_U \quad (2.139)$$

where η_U is the peak factor relating the peak response to the variance of the response process and T_s is the time observing window.

The definition for η_U is derived by Vanmarke (1972) for stationary Gaussian stochastic processes under the hypothesis of up crossing in clumps for low threshold level by taking into account of the actual clump duration. By substituting equation (2.136), in which $\bar{\eta}_U \equiv \eta_U(T_s, p, \delta_U) = u_{\max} / \sigma_U$, into equation (2.138) it follows that

$$\eta_U(T_s, p, \delta_U) = \sqrt{2 \ln \left\{ 2\nu_0 T_s (-\ln p)^{-1} \left[1 - \exp \left(-\delta_U^{1.2} \sqrt{\frac{\pi}{2}} \eta_U(T_s, p, \delta_U, \omega_0, \zeta_0) \right) \right] \right\}} \quad (2.140)$$

In order to solve the iterative equation above the value of the peak factor on the right hand side is assigned under the assumption of high level of the barrier, which value is derived through the same procedure by equation (2.133), that provides the following upper limit of the peak factor

$$\eta_{U,upp}(T_s, p) = \sqrt{2 \ln \left[2\nu_0 T_s (-\ln p)^{-1} \right]} \quad (2.141)$$

Finally by substituting equation (2.141) into (2.140) the approximated peak factor reads

$$\eta_U(T_s, p, \delta_U) = \sqrt{2 \ln \left\{ 2\nu_0 T_s (-\ln p)^{-1} \left[1 - \exp \left(-\delta_U^{1.2} \sqrt{\pi \ln \left[2\nu_0 T_s (-\ln p)^{-1} \right]} \right) \right] \right\}} \quad (2.142)$$

where the mean rate of zero up-crossing ν_0 is determined according to equation (2.131) and the bandwidth factor δ_U via equation (2.99).

Under the hypothesis of stationarity, the peak factor plays a fundamental role in ground motion modelling and spectrum compatibility with the seismic codes, which is discussed in Chapter 3. Moreover, the formulation of the first passage problem for a selected fractile of the peak distribution, has enabled to perform the design of the ViBa within the development of this work, as presented in Chapter 6.

BLANK

3 Ground Motion Modelling: Response Spectrum Compatible Approach

The uncertainty of seismic waves constitutes the rationale for embarking upon the definition of the ground motion via the probabilistic approach. This approach has provided a number of methodologies for modelling of earthquakes based on the principles of random vibrations presented in Chapter 2. Accordingly, in this Chapter ground motions modelled as zero-mean Gaussian stochastic processes are considered.

The definition of the seismic load for seismic assessment of structures is regulated by international code provisions; the seismic codes impose criteria in order to regulate the use of both real and artificial time-histories through mandatory requirements regarding the response spectra obtained from the time-histories adopted; the conditions established by the seismic codes are denoted as *response-spectrum-compatibility* criteria. To satisfy the spectrum compatibility requirements real ground motion time-histories, properly selected, are modified generally by scaling techniques. On the other hand, when artificial ground motions are used the time-histories have to be generated from response-spectrum-compatible Power Spectral Density (PSD) functions. However, the international seismic codes do not provide any method to generate response-spectrum-compatible synthetic signals and how to establish response-spectrum-compatible PSD functions. Therefore, the question of which PSD functions are more appropriate to describe the complex nature of the seismic ground motion, in conjunction with the regulations' requirements, is still an open issue. Which hypotheses and methods more realistically address the description of the ground motion phenomenon has been the subject of discussion over the last four decades. In this Chapter the developments of response-spectrum-compatible ground motion modelling from the 1970s up until now, are reviewed by encompassing the early proposed stationary models and the more advanced stochastic processes accounting for the frequency non-stationarity, the so called fully non-stationary processes. The contributions provided by this work

are comprised of the current trends, which embed seismological parameters obtained from databases of real earthquakes, to the models.

From a review of the state of the art methodologies, the common drawback observed concerns the variability of the frequency content that accelerograms generated by the current methodologies do not manifest. In fact, even if real accelerograms possess the same magnitude and epi-central distance, their frequency content variation with time is different. The distinctive characteristics of each single record induce the variability of the ground motion parameters (e.g. variability of the response spectral ordinates about their mean or median value), which are estimated, for instance, by analysis of data from sets of real records available in databases. Synthetic time-histories, being determined from a single power spectral density function, possess similar joint-time frequency distribution and present a marginal spread about their simulated mean response spectrum. Few authors have attempted to reproduce the natural variability of real accelerograms for simulating artificial time-histories. In light of this gap in knowledge, this work proposes enhanced evolutionary fully non-stationary stochastic processes with random variables simulated by pertinent techniques, which are embedded to the proposed PSD function.

In this Chapter the proposed technique to simulate advanced fully non-stationary response-spectrum-compatible ground motions is presented and discussed. Non-stationary and fully non-stationary PSD functions are derived from a single versatile ground motion stochastic process, which is able to model the time-frequency variation and additionally, the variability of the frequency content among the simulated accelerograms. The proposed procedure requires the definition of an Evolutionary Power Spectral Density (EPSD) function with random parameters, by which the variability of the time frequency content is imposed. The random variables featuring the variability of the simulated earthquakes are calibrated on a set of recorded earthquakes taking into account the realistic standard deviation of response spectral accelerations at different periods.

Moreover, in this Chapter the implications of the ground motion selection on the design of structural systems is investigated; a thorough analysis of the structural

response of the selected structures subjected to the ground motion models under investigation is analysed in a comparative study on the responses of benchmark buildings. The response-spectrum-compatible stochastic input processes under investigation are: one among the traditional quasi-stationary ground motion models, a fully non-stationary with imposed variability ground motion presented hereafter. From the analysis of the structural response of the benchmark buildings, the spectrum compatibility criteria mandated by Eurocode 8 have been examined and some drawbacks in the definition of the required conditions highlighted. Specifically, the different ground motion models although satisfying the same code compatibility criteria, may lead to different statistics of the responses of buildings with damping ratios different from the nominal 5%, which is also applicable for linear behaving structures nevertheless the general widespread acceptance.

3.1 Literature Review

One of the main challenges in stochastic ground motion modelling is to include the time-frequency variation typical of real earthquakes. This is due to the established understating regarding the influence that the frequency content carried by the earthquake, has on engineering structures. The non-stationary frequency content of earthquakes has been found to be relevant for the seismic assessment of structures by several authors. Researchers have observed over the years that the dynamic response of non-linear structures is highly influenced by the non-stationary behaviour of the input (see e.g. Yeh and Wen 1990, Papadimitriou and Beck 1990, Beck and Papadimitriou 1993, Wang et al. 2002, Spanos et al. 2007a, Spanos et al. 2007b, Giaralis and Spanos 2010, Spanos and Kougiumtzoglou 2011, Spanos and Giaralis 2013). Papadimitriou and Beck (1990) and Beck and Papadimitriou (1993) demonstrated analytically the influence of the frequency non-stationarity of the seismic action on the response of both linear and non-linear structural systems. Their investigations proved that non-linear systems can be substantially affected by the temporal non-stationarity in the frequency content of the input due to the moving resonance effect, i.e. the time variation of the natural period of the system, which tracks the decrease of the dominant frequency of the ground motion. Moreover, the

authors pointed out that also for linear system the influence of the frequency non-stationarity can be important in spite of the general acceptance in the scientific community.

In order to perform structural analyses accounting of a full description of the earthquake non-stationarity, many researchers and professionals have been pursuing the use of real records. However, to find sets of real accelerograms that are compatible to a prescribed target response spectrum is impracticable and the modification of the records becomes crucial. Researchers have debated the underlying assumptions of scaling procedures of natural accelerograms and simulation of artificial ground motions in comparison (see e.g. Iervolino et al. 2010), however the evidences provided so far do not allow a conclusion to be drawn on the discussion.

Natural records are customarily more attractive to practitioners as these are easily accessible through databases; recorded earthquakes signals are selected and scaled by adopting rather simplified criteria established by the international seismic codes (Katsanos et al. 2010). Recorded time-histories describe the complex frequency content of the ground motion as they hold the phasing of the seismic waves characterised by the real path from the fault to the site. It is recognised that the use of scaled recorded accelerograms presents several benefits (Watson-Lamprey and Abrahamson 2006), however it might provide misleading information for selected records inconsistent with soil conditions, a situation that may lead to an exaggeration of the displacement demand and energy input (Naeim and Lew 1995). Moreover, real earthquakes are selected from limited databases, which scarcely provide several accelerograms consistent with a specific local site condition (Hancock et al. 2008). Additionally, real records are generally affected by a level of noise due to the signal's registration process, whose corrections may otherwise influence the original characteristics of the record itself (Boore and Bommer 2005), this aspect induces a certain level of subjectivity to the models. Despite the enrichment of databases, the availability of recorded earthquakes is still limited in comparison to the theoretical infinite number of time-histories that can be simulated by digital techniques by means of random vibration theory (see e.g. Shinozuka and Deodatis 1996).

Moreover, simulations more realistic than stochastic processes and fields, have been introduced by describing the ground motion as a simulated stochastic propagating wave (Shinozuka and Deodatis 1988). Despite the limitations in capturing the realistic time variation of the frequency content of real earthquakes encountered by the stochastic approach, the latter has been acknowledged for providing a high level of reliability for engineering applications (see e.g. Vanmarke 1996, Kostic et al. 2013). The simulation of artificial time-histories involves two considerable difficulties: (i) capturing the frequency non-stationarity typical of real earthquakes through PSD functions, which have a joint time-frequency dependency, and (ii) complying with the seismic codes requirements by defining response-spectrum-compatible PSD functions linked to the target response spectra.

For initially seeing the ground acceleration at a given location as a sample of random process, Housner (1947) is considered one of the pioneers of the stochastic engineering approach to ground motion modelling. Next, Kanai (1957) and Tajimi (1960), proposed to model the earthquake as a filtered white noise. Following on from the model of Kanai and Tajimi, Clough and Penzien (1975) established a stationary power spectrum from filtering the Kanai-Tajimi spectrum, as described more in depth in Chapter 2. Over the years the modelling of the ground motion has been improved by modulating the time amplitude first, by the use of time-modulating functions as by the models of Bogdanoff et al. (1961), Shinozuka and Sato (1967) and Jennings et al. (1969). In order to take into account both amplitude and frequency non-stationarity, Saragoni and Hart (1974) proposed a fully non-stationary ground motion model of a filtered Gaussian white noise modulated by juxtaposed time segments of gamma functions, whose properties differ from segment to segment. A comprehensive review on stochastic processes for earthquake ground motions was provided by Shinozuka and Deodatis (1988); the authors' work encompassed filtered white noises, filtered Poisson processes along with the simulation technique introduced by the authors and co-workers, and moreover the theory to model and simulate ground motions using stochastic wave models extending the definition of Priestley's oscillatory process. For modelling and simulating non-stationary ground motions directly from recorded earthquakes,

Deodatis and Shinozuka (1988) proposed an auto-regressive model based on the definition of the auto-correlation function for evolutionary oscillatory processes, from which time-frequency slowly varying modulating functions were obtained along with the parameters and time variant parametric functions of the Kanai-Tajimi spectrum, which was adopted as the stationary counterpart of the evolutionary process. Based on the analysis of earthquake accelerograms, Papadimitriou and Beck (1990) proposed a filtered wide band process, with time-variant amplitude and time-parametric functions of the frequency non-stationarity accounting of the dominant contribution from the P, S and surface waves carried by the ground motion. Yeh and Wen (1990) proposed a model by adopting simultaneously time and frequency modulating functions and generalising the Kanai-Tajimi spectrum. Similarly, another attempt was provided by Fan and Amadi (1990), who employed the Kanai-Tajimi model to capture the non-stationarity of real earthquakes, followed by Rofoeei et al. (2001) who adopted the handy Moving Time Window technique to obtain the ground frequency function from records for reproducing the frequency non-stationarity. An important contribution for modelling non-stationary earthquake stochastic vector processes was provided by one of the models proposed in Deodatis (1996), in which the evolutionary Clough-Penzien spectrum was generalised by employing ground frequency function and time-varying soil damping parameters, previously determined for a real seismic record according to Deodatis and Shinozuka (1988). Since the dissemination of databases along with the increasing number of strong-motion networks installed worldwide, analytical modelling and data gathered from real records have been merged to provide valuable information to calibrate ground motion models. Among the physical models of PSD functions defined by using the data from databases, the work of Sabetta and Pugliese (1996) is found. The authors proposed a fully non-stationary ground motion as a function of magnitude distance and site geology. Recorded time-histories were linked to a stochastic definition of the seismic action by Conte and Peng (1997) directly deriving PSD functions from real records according to the theory of sigma oscillatory processes proposed. According to Conte and Peng (1997) the seismic ground motion is seen as a finite summation of independent uniformly modulated zero-mean Gaussian stochastic process. The fully non-stationary model enables to

capture the intensity and frequency content of real records by using the proposed extension of the Thomson's spectrum estimation method. A notable contribution to the field of ground motion modelling, has been provided by the review paper on the modelling, generation of synthetic records' statistical estimation of Shinozuka et al. (1999). The authors presented the modelling of earthquake wave motion for near field earthquakes by physically-consistent models, which are pertinent to a seismic source and accounting of uncertainties of both medium and source. Moreover, Shinozuka et al. (1999) presented seismologically-consistent source models, pertinently to a specific earthquake, along with techniques for statistical analyses of the temporal and spatial statistics of the ground motion. Spanos et al. (2005) proposed a procedure applied to estimate the evolutionary spectrum of a non-stationary stochastic process, capturing the non-stationarity of an earthquake record by using harmonic wavelet transform. Successively, Spanos et al. (2007) introduced a technique for time-frequency analysis and representation of earthquake signals by means of adaptive chirplet decomposition, in conjunction with the employment of the Wigner-Ville distribution. Through parametric PSD functions, Rezaeian and Der Kiureghian (2008) formulated a non-stationary ground motion model able to capture the characteristic of a real seismic events, the stochastic process proposed is a modulated filtered white-noise with time-varying parameters, which is directly related to the earthquake and the site characteristics. The models herein presented encompass the representation of stationary, quasi-stationary and fully non-stationary ground motions, from which samples of time-histories can be simulated via different simulation techniques (see e.g. Grigoriu 1995, Shinozuka and Deodatis 1996, Spanos et al. 2002).

Time-history representation of the seismic action is undertaken for a broad number of engineering applications to perform either deterministic and probabilistic analyses. A rigorous assessment of non-linear multi degree of freedom systems often requires the use of input time-histories to predict the level of damage and dissipation of the system energy due to cyclic loading. Time-history analysis results a desirable alternative to complex procedures for the assessment of non-linear structural

systems, for instance when a rigorous stochastic approach might be cumbersome for high computational effort involved.

When time-history analysis is carried out, practicing engineers have to deal with the seismic prescriptions, which according to the international regulatory agencies impose the so-called spectrum compatibility criteria (see e.g. Eurocode 8 2010). Specifically, the code prescriptions impose a matching between a specific prescribed site-specific target response spectrum and the mean or median value of the response spectra derived from a set of natural or synthetic accelerograms. The spectral matching refers to a specified range of periods related to the first natural period of the structure and must be guaranteed within a prefixed tolerance, e.g. above the 90% of the reference spectrum for the EC8. The mean simulated response spectrum is obtained according to equation (2.38), which expresses the peak response of linear SDOF systems with fixed damping ratio, forced by a time-history from a selected scaled record or generated by simulation techniques. If the time-histories are response-spectrum-compatible, the simulated accelerograms are suitable for design purposes. The ground motion models of the seismic action formerly mentioned, are not generally compatible with the code requirements, made exclusion of the model of Deodatis (1996), in which a technique to achieve the spectrum compatibility was also proposed.

In the context of stochastic ground motion modelling by following the response-spectrum-compatible approach, the simulation of time-histories compatible with a given spectrum is a complex inverse problem. It consists of seeking the representation of the stochastic process whose realisations, the accelerograms, determine an output established beforehand; the mean response spectrum fulfilling the requirements. The solution to the aforementioned inverse problem is not a single one, since an infinite set of realisations and their simulated mean response spectrum can satisfy the prescribed matching. To guarantee the frequency non-stationarity and satisfy the seismic codes' requirements of spectrum compatibility is a more complex issue which is circumvented rather than pursuing a direct approach to the problem as tackled by assuming the hypothesis of stationarity. The approach for modelling the ground motion as a stationary process was provided in the early 1970s by a robust

relationship between the target response spectrum and the power spectral density function. This relationship is still used by practitioners and researchers to develop more advanced response-spectrum-compatible ground motion models as sought in this research. It has to be emphasized that the evaluation of the response-spectrum-compatible power spectral density function possesses the twofold aspects: (i) allowing the generation of artificial accelerograms through equation (3.43), and (ii) allowing the direct stochastic analysis.

In the following sections an overview of development of the relevant response-spectrum-compatible ground motion models is attempted (Cacciola and D'Amico 2015). Namely the stationary, quasi-stationary and fully non-stationary stochastic processes are discussed.

3.1.1 Stationary and Quasi-Stationary Gaussian Stochastic Processes

Assuming the seismic ground acceleration as a realisation of a zero-mean Gaussian separable random process, the early response-spectrum-compatible stochastic models of the seismic action consider only the intensity of the ground motion to change with time. These models are obtained by modulating a stationary process describing the frequency content of the motion, through a deterministic time dependant envelope function (see e.g. equation (2.92)). These uniformly modulated stochastic processes are a special case of non-stationary processes and are generally known as quasi-stationary models. The underlying assumption of separable ground acceleration process enables to model independently the stationary frequency-dependant counterpart and the time-dependent envelope. The uniformly modulated processes represent an approximation for the earthquake ground motion that generally is non-stationary in both intensity and frequency content. To assume stationary spectral shapes of the stochastic ground motion has been considered satisfactory for analysis of linear structures, in which only the spectral components in proximity of the natural periods are significant (Shinozuka 1988).

In the framework of response-spectrum-compatible Gaussian stochastic processes several procedures have been proposed for determining quasi-stationary power spectral density functions. Herein the models formulated by Vanmarcke and

Gasparini (1977), Kaul (1978), Sundararajan (1980), Pfaffinger (1983), Preumont (1980), Der Kiureghian and Neuenhofer (1992), Park (1995), Cacciola et al. (2004) are addressed. The list is not fully comprehensive and the readers can refer for further references to the review papers of Ahmadi (1979) and Cacciola (2011).

3.1.1.1 Problem Position

In order to address the problem of simulating artificial accelerograms compatible to a given response spectrum, firstly it is necessary to determine the generally known response-spectrum-compatible power spectral density function. Under the hypothesis of zero-mean Gaussian stationary ground motion process Vanmarcke and Gasparini (1977) pointed out the fundamental relationship between the target response spectrum and the power spectral density function of the ground motion through the “first passage problem” presented in Chapter 2, that according to equation (2.139) for response spectral accelerations reads

$$RSA(\omega_0, \zeta_0) = \omega_0^2 \eta_U(T_s, p, \delta_U, \omega_0, \zeta_0) \sigma_U \quad (3.1)$$

where $RSA(\omega_0, \zeta_0)$ is the pseudo-acceleration response spectrum for a given damping ratio ζ_0 and natural circular frequency ω_0 , η_U is the dimensionless peak factor characterised by the time observing window T_s the probability of not exceedance p , and the bandwidth factor δ_U ; σ_U is the standard deviation of the displacement response process related to the zero-order stationary spectral moment $\lambda_{0,U}$ as seen in equation (2.114).

In the last four decades, equation (3.1) has been used by several authors to define the response-spectrum-compatible power spectral density function. The methods proposed in literature mainly differentiate from each other for the hypothesis adopted to define the peak factor and for the approximations involved in the evaluation of the response spectral moments.

The authors who firstly introduced the implicit relationship for the evaluation of the response-spectrum-compatible power spectral density function were Vanmarcke and

Gasparini (1977); the formula proposed is nowadays still used by researchers and practitioners. To reach this objective Vanmarke and Gasparini (1977) proposed an approximate expression of the standard deviation of the response displacement

$$\sigma_U = \frac{1}{\omega_0^2} \left\{ \left[G(\omega_0) \omega_0 \left(\frac{\pi}{4\zeta_0} - 1 \right) \right] + \int_0^{\omega_0} G(\omega) d\omega \right\}^{1/2} \quad (3.2)$$

Equation (3.2) is determined under the hypothesis of small damping ratio ζ_0 and approximating the energy transfer function with its value $|H(0)|^2 = 1/\omega_0^4$ in the range of frequencies between 0 and ω_0 . Furthermore, they adopted the peak factor expression provided under the hypothesis of independent out-crossing of given barriers (see e.g. Vanmarke 1976), through its upper bound value (relatively to damping higher of the 10%) that is,

$$\eta_{U,upp} = \sqrt{2 \ln \left(\frac{2N_U}{-\ln p} \right)} \quad (3.3)$$

and for a lower bound valid for undamped systems

$$\eta_{U,low} = 1 + 0.25 \ln \left(\frac{N_U}{-\ln p} \right) \quad (3.4)$$

In equations (3.3) and (3.4) p is the value of the not exceeding probability chosen equal to 0.5, determining the median value of the peak factor; it is noted that by this assumption the median is approximated with the mean; N_U is the number of out-crossings of the given barrier over the fixed time observing window T_s assumed equal to the strong motion phase of the ground motion process, that is

$$N_U = \nu_0 T_s \quad (3.5)$$

where ν_0 is the mean out-crossings rate of the zero level seen in equation (2.131), depending on the zero-th and second order spectral moment. The dependence of the peak factor from the power-spectral density function of the response is overcome by approximating the response spectral moments with their solution for the white noise

input leading to the following formula (Der Kiureghian 1980)

$$N_U = \frac{T_s}{2\pi} \omega_0 \quad (3.6)$$

Finally the stationary response-spectrum-compatible unilateral power spectral density function can be expressed by using equations.(3.1), (3.2)and (3.3) as follows

$$G(\omega_0) = \frac{1}{\omega_0 \left(\frac{\pi}{4\zeta_s} - 1 \right)} \left[\frac{RSA^2(\omega_0, \zeta_0)}{\eta_U^2} - \int_0^{\omega_0} G(\omega) d\omega \right] \quad (3.7)$$

In which also the damping ratio ζ_0 has been substituted with the fictitious damping ζ_s to take into account of the transient part of the response process

$$\zeta_s = (1 - e^{-2\zeta_0 \omega_0 t})^{-1} \zeta_0 \quad (3.8)$$

which tends to the natural damping of the oscillator once the steady state response has developed.

Furthermore, the two authors developed the computer software SIMQKE (Gasparini and Vanmarke 1976), providing a practical tool to simulate time-histories from a response-spectrum-compatible power spectral density function which is implemented as

$$G(\omega_i) = \frac{4\zeta_s}{\omega_i \pi} \left(\frac{RSA^2(\omega_i, \zeta_0)}{\eta_U^2} - \Delta\omega \sum_{k=1}^{i-1} G(\omega_k) \right) \quad (3.9)$$

in which a more accurate expression of the peak factor is adopted under the hypothesis of barrier out-crossings in clumps, that is

$$\eta_U(T_s, p, \delta_U, \omega_0, \zeta_0) = \sqrt{2 \ln \left\{ \frac{\omega_0 T_s}{\pi(-\ln p)} \left[1 - \exp \left[-\delta_U \sqrt{\pi \ln \left(\frac{\omega_0 T_s}{\pi(-\ln p)} \right)} \right] \right] \right\}} \quad (3.10)$$

where δ_U is the bandwidth factor seen in equation (2.99) which for white noise input process is approximated by the following

$$\delta_U = \sqrt{1 - \frac{\lambda_{1,U}^2}{\lambda_{0,U}\lambda_{2,U}}} \cong \sqrt{\frac{4\zeta_0}{\pi}} \quad (3.11)$$

After selecting a time modulating function, the software employs the proposed power spectral density function for simulating synthetic accelerograms via superposition of random harmonic functions through equation (3.43).

Another contribution to determine a simplified expression of the power spectral density function compatible with a given response spectrum has been provided by Kaul (1978); the author adopted the peak factor in equation (3.3) in conjunction with the hypothesis that the response spectral moments are determined under the hypothesis of white noise input process. Therefore, N_U is determined according to equation (3.6) and the zero-order response spectral moments is given as following

$$\lambda_{0,U} = \frac{\pi}{4\zeta_0\omega_0^3} G(\omega_0) \quad (3.12)$$

After some simple algebra the following stationary power spectral density function is determined

$$G(\omega_0) = \frac{4\zeta_e}{\pi\omega_0} \frac{RSA^2(\omega_0, \zeta_0)}{\eta_U^2} \quad (3.13)$$

where the damping of the oscillator has been adjusted as suggested by Rosenblueth and Elorduy (1969) as follows

$$\zeta_a = \zeta_0 + \frac{2}{\omega_0 t_f} \quad (3.14)$$

In which t_f is the time duration of the stochastic process. As Kaul (1978) assumed the process as stationary t_f is coincident with T_s .

Equation (3.14) has been used by Der Kiureghian and Neuenhofer (1992) in order to investigate a response spectrum methodology for multi-support seismic excitation, in which a constant value of the peak factor was adopted. Currently their stationary

power spectral density function formula is adopted in Eurocode 8 part 2 (2010), recommended for the seismic analysis of bridges, that is

$$G(\omega_0) = 2\omega_0^2 \left(\frac{2\zeta_0\omega_0}{\pi} + \frac{4}{\pi T_s} \right) \left[\frac{RSD^2(\omega_0, \zeta_0)}{2.5^2} \right] \quad \omega \geq 0 \quad (3.15)$$

where $RSD(\omega_0, \zeta_0) = RSA(\omega_0, \zeta_0) / \omega_0^2$ is the displacement response spectrum.

Sundararajan (1980) introduced an iterative method for defining the response-spectrum-compatible power spectral density function, differently from the direct approaches followed by Vanmarke and Gasparini (1977), Kaul (1978) and Der Kiureghian and Neuenhofer (1992). The iterative procedure established by Sundararajan (1980) starts from a trial solution of the first passage problem given in equation (3.1) and variance of the response process given by equation (3.12)

$$G(\omega_0) = \frac{4\zeta_0\omega_0}{\pi} \frac{RSV^2(\omega_0, \zeta_0)}{\eta_U^2} \quad (3.16)$$

where $RSV(\omega_0, \zeta_0) = RSA(\omega_0, \zeta_0) / \omega_0$ is the velocity response spectrum and the peak factor is assumed independent of the input according to the hypothesis of small damping. Davenport (1964) and Amin and Gungor (1971) formulae have been considered suitable to this purpose. However, in the numerical analysis conducted by the authors a constant value $\eta_U = 3$ has been selected.

After determining the first trial solution of the power spectral density function approximate as piecewise of linear functions, the author expressed the variance of the displacement response accordingly as

$$\sigma_U = \sum_{k=0}^N \int_{\omega_k}^{\omega_{k+1}} \frac{G(\omega)}{(\omega_0^2 - \omega^2)^2 + 4\zeta_0^2 \omega_0^2 \omega^2} d\omega \quad k = 1, \dots, N \quad (3.17)$$

in which the integrals have been determined in closed-form, that is

$$\int_{\omega_k}^{\omega_{k+1}} \frac{G(\omega)}{(\omega_0^2 - \omega^2)^2 + 4\zeta_0^2 \omega_0^2 \omega^2} d\omega = \frac{G_k}{(\omega_{k+1} - \omega_k)} [\omega_{k+1} J(\omega_k, \omega_{k+1}) - K(\omega_k, \omega_{k+1})] + \frac{G_k}{(\omega_{k+1} - \omega_k)} [\omega_k J(\omega_k, \omega_{k+1}) - K(\omega_k, \omega_{k+1})] \quad (3.18)$$

where $J(\omega_k, \omega_{k+1})$ and $K(\omega_k, \omega_{k+1})$ are the solutions of the integrals determined analytically, given by the following equations

$$J(\omega_k, \omega_{k+1}) = \int_{\omega_k}^{\omega_{k+1}} \frac{1}{(\omega_0^2 - \omega^2)^2 + 4\zeta_0^2 \omega_0^2 \omega^2} d\omega \quad (3.19)$$

$$K(\omega_k, \omega_{k+1}) = \int_{\omega_k}^{\omega_{k+1}} \frac{\omega_0}{(\omega_0^2 - \omega^2)^2 + 4\zeta_0^2 \omega_0^2 \omega^2} d\omega \quad (3.20)$$

The iterative procedure proceeds by the comparison of the target response spectrum and the approximate response spectrum evaluated through the semi-analytical expression of the variance of the response displacement. The values G_k are then updated scaling their values by the ratio of the square of the target response spectrum and the approximate response spectrum.

In the same year Preumont (1980) coupled direct and iterative solutions in order to solve the inverse problem of response-spectrum-compatible ground motion processes obtained from given response spectra; following the approach used by Kaul (1978) and Sundararajan (1980) the suggested solution is given as

$$G(\omega_0) = \frac{4\zeta_e}{\pi\omega_0} \frac{RSA^2(\omega_0, \zeta_0)}{\eta_U^2} \quad (3.21)$$

in which the semi-empirical peak factor given in equations (3.10) and (3.11) is employed, considering the adjusted spread factor $\delta_U^{1.2}$ (Vanmarcke 1972). The fictitious damping ζ_s given by equation (3.8) is also used.

The approximate solution given in equation (3.21) provides accurate results for low and intermediate frequencies. Therefore the author considered the solution proposed by Vanmarcke and Gasparini (1977) given by equation (3.2) with the adjusted spread

factor as further improvement of equation (3.10). As the peak factor evaluation depends on the whole power spectral density function, which is intrinsically related to the spectral characteristics of the unknown response process (see equations, (2.114), (3.5), (2.131) and (3.11)), the author developed an algorithm which enables to update the spectral characteristics of the response process every frequency step of definition of the frequency domain. The iterative scheme mainly differs from the procedure proposed by Sundararajan (1980) as not only the zero-th order spectral moment is updated at each step but also the peak factor. To this aim the first and second order spectral moments are also updated in the iterative scheme. Using a stepwise representation of the power spectral density function as

$$G(\omega_k) = \frac{1}{2} [G(\omega_k) + G(\omega_{k+1})] \quad k = 1, \dots, N \quad (3.22)$$

The spectral moments of the response are analytically determined according the following formula

$$\lambda_{i,U} = \sum_{k=0}^N \int_{\omega_k}^{\omega_{k+1}} \frac{\omega^i G(\omega)}{(\omega_0^2 - \omega^2)^2 + 4\zeta_0^2 \omega_0^2 \omega^2} d\omega \quad k = 1, \dots, N \quad (3.23)$$

And approximating the first term for $i=0,1,2$ as

$$\lambda_{0,U} = \int_{\omega_k}^{\omega_{k+1}} |H(\omega)|^2 G(\omega) d\omega \cong \frac{\pi G(\omega_0)}{4\zeta_0 \omega_0^3} \varphi(\omega_k, \omega_{k+1}, \omega_0, \zeta_0) \quad (3.24)$$

$$\lambda_{1,U} = \int_{\omega_k}^{\omega_{k+1}} \omega |H(\omega)|^2 G(\omega) d\omega \cong \frac{\pi G(\omega_0)}{4\zeta_0 \omega_0^2 \sqrt{1 - \zeta_0}} \theta(\omega_k, \omega_{k+1}, \omega_0, \zeta_0) \quad (3.25)$$

$$\lambda_{2,U} = \int_{\omega_k}^{\omega_{k+1}} \omega^2 |H(\omega)|^2 G(\omega) d\omega \cong \frac{\pi G(\omega_0)}{4\zeta_0 \omega_0} \psi(\omega_k, \omega_{k+1}, \omega_0, \zeta_0) \quad (3.26)$$

where $\varphi(\omega_k, \omega_{k+1}, \omega_0, \zeta_0)$, $\theta(\omega_k, \omega_{k+1}, \omega_0, \zeta_0)$ and $\psi(\omega_k, \omega_{k+1}, \omega_0, \zeta_0)$ are determined in closed-form.

In the scenario of iterative methods to define the power spectral density function from a known response spectrum, Pfaffinger (1983) proposed a procedure in which a discretization by piecewise polynomials is numerically implemented. The free

parameters are determined iteratively by a least square fit. The peak factor used is the expression provided by Davenport (1964), assuming the statistical independence of the out-crossings of a given barrier, that is

$$\eta_U = \sqrt{2 \ln(2N_U)} + \frac{\gamma}{\sqrt{2 \ln(2N_U)}} \quad (3.27)$$

where $\gamma = 0.5772$ is the Euler constant and N_U given by equation (3.6).

The unilateral response-spectrum-compatible power spectral density function is discretized in the interval $\omega_k < \omega < \omega_{k+1}$ and obtained by summation of the piecewise polynomials as follows

$$G(\omega) = \sum_{k=1}^N p_k P_k(\omega) \quad k = 1, \dots, N \quad (3.28)$$

where p_i are either free parameters or have to be assigned to satisfy specified conditions, and $P_i(\omega)$ are the interpolation polynomials.

According to the approximation given equation (3.28) the standard deviation and mean out-crossings rate of the zero level are obtained from the following equations, respectively

$$\sigma_U = \left(\sum_{i=1}^N p_i I_{0,i}(\omega_0, \zeta_0) \right)^{1/2} \quad (3.29)$$

and

$$v_U = \frac{1}{2\pi} \left[\frac{\sum_{i=1}^N p_i I_{2,i}(\omega_0, \zeta_0)}{\sum_{i=1}^N p_i I_{0,i}(\omega_0, \zeta_0)} \right]^{1/2} \quad (3.30)$$

where $I_{2,j,i}$ is given by

$$I_{2j,i}(\omega_0, \zeta_0) = \int_{\omega_k}^{\omega_{k+1}} \frac{\omega^{2j} P_k(\omega)}{(\omega_0^2 - \omega^2)^2 + 4\zeta_0^2 \omega_0^2 \omega^2} d\omega \quad j=0,1 \quad (3.31)$$

That has been derived analytically. The parameters p_i and the polynomial coefficients are finally determined through a least square fitting.

Based on the model proposed by Pfaffinger (1993), Park (1995) defined a method to derive the equivalent power spectral density function from a given target response spectrum. The approach to the modelling consists of assuming the bilateral power spectral density function as the summation of Dirac's delta functions with unknown amplitudes, that is

$$S(\omega) = \sum_{j=1}^m S(\omega_j) \Delta\omega_j \delta(\omega_j) = \sum_{j=1}^m p_j \delta(\omega_j) \quad (3.32)$$

where $S(\omega)$ is the unknown two-sided power spectral density function, $\delta(\omega_j)$ are Dirac's delta functions for each component, $\Delta\omega_j$ is the incremental frequency step and p_j are the discretized power components.

Therefore, by superimposing a series of Dirac's delta functions the resulting process is a wide-band, which is generally the case of real earthquakes.

The discretized target response spectrum is obtained as a superposition of the components of the power and of the response spectrum in itself as following

$$RSA^2(\omega_k, \zeta_0) = \sum_{j=1}^m p_j RSA_{k,j}^2(\omega_k, \omega_j, \zeta_0) \quad k=1,2,\dots,m \quad (3.33)$$

where $RSA(\omega_k, \zeta_0)$ is the discretized target response spectrum, $RSA_{k,j}(\omega_k, \omega_j, \zeta_0)$ is the peak acceleration response of a single degree of freedom system with natural frequency ω_k , damping ratio ζ_0 and forced by narrowband $\delta(\omega_j)$ Dirac's delta functions. $RSA_{k,j}(\omega_k, \omega_j, \zeta_0)$ is determined using the peak factor approximation by Davenport (1964) with N_U given by equation (3.6) and equivalent duration T_e defined as

$$T_e = \frac{\int_0^{t_f} a(t) dt}{\max[a(t)]} \quad (3.34)$$

where $a(t)$ is a selected time modulating function and t_f is the total duration of the earthquake.

The unknown coefficients p_j defining the power spectral density function are evaluated by minimizing the following penalty function

$$\sum_{k=1}^n \left[RSA^2(\omega_k, \zeta_0) - \sum_{j=1}^m p_j RSA_{k,j}^2(\omega_k, \omega_j, \zeta_0) \right]^2 \quad p_j \geq 0; \quad (3.35)$$

where n represents the number of frequencies discretizing the target response spectrum.

Following the approach proposed by Vanmarcke and Gasparini (1977), Cacciola et al. (2004) developed a handy and accurate recursive expression for determining the power spectral density function compatible with a given response spectrum

$$G(\omega_i) = 0, \quad \forall 0 \leq \omega \leq \omega_\alpha$$

$$G(\omega_i) = \frac{4\zeta_0}{\omega_i \pi - 4\zeta_0 \omega_{i-1}} \left(\frac{RSA(\omega_i, \zeta_0)^2}{\eta_U^2(\omega_i, \zeta_0)} - \Delta \omega \sum_{k=1}^{i-1} G(\omega_k) \right), \quad \forall \omega > \omega_\alpha \quad (3.36)$$

where $\omega_\alpha \cong 1$ rad/s which is the lowest bound of the existence domain of the peak factor η_U evaluated according to Vanmarcke (1976), which for white noise input reads

$$\eta_U(\omega_0, \zeta_0) = \sqrt{2 \ln \left\{ \frac{\omega_0 T_s}{\pi(-\ln p)} \left[1 - \exp \left[-\delta_U^{1.2} \sqrt{\pi \ln \left(\frac{\omega_0 T_s}{\pi(-\ln p)} \right)} \right] \right] \right\}} \quad (3.37)$$

and bandwidth factor according to Der Kiureghian (1980), that is

$$\delta_U = \left[1 - \frac{1}{1 - \zeta_0^2} \left(1 - \frac{2}{\pi} \arctan \frac{\zeta_0}{\sqrt{1 - \zeta_0^2}} \right)^2 \right]^{1/2} \quad (3.38)$$

Recently Di Paola and Navarra (2009) proposed a closed-form expression for the response-spectrum-compatible power spectral density function whose parameters are defined through a best fitting of the model proposed by Cacciola et al. (2004).

Interestingly Giaralis and Spanos (2010) investigated the lowest bound of the existence domain of the peak factor, evaluated according to the expression seen in equation (2.142); the authors specified the conditions that have to be simultaneously satisfied, that are

$$\begin{aligned} \ln \left[2\nu_{0,U} T_s (-\ln p)^{-1} \right] &\geq 0 \\ \ln \left\{ 2\nu_{0,U} T_s (-\ln p)^{-1} \left[\exp \left(\delta_{i,U}^{1,2} \right) \sqrt{\pi \ln(2\nu_{0,U} T_s (-\ln p)^{-1})} \right] \right\} &\geq 0 \end{aligned} \quad (3.39)$$

where $\nu_{0,U}$ is the mean-rate of up-crossing of the zero level according to equation (2.131).

With numerical evaluation of the scheme introduced for different input PSD, the WN, KN, and CP spectrum, the authors validated the condition asserted in literature, that the value of the peak factor is not sensitive to the shape of the PSD function of the input process.

3.1.1.2 Closed-Form Expressions for the Parameters of the Jennings et al. (1969) Time-Modulating function

In this work the time modulating function proposed by Jennings et al. (1969) has been chosen for its suitability in modelling response-spectrum-compatible stochastic processes. The Jennings et al. (1969) function is able to facilitate the achievement of the spectrum compatibility criteria due to the shape determined by the constant tract over a selected time interval.

The expression of the Jennings et al. (1969) function is given by

$$a(t) = \begin{cases} \left(\frac{t}{t_1}\right)^2 & t < t_1 \\ 1 & t_1 \leq t \leq t_2 \\ \exp[-\beta(t-t_2)] & t > t_2 \end{cases} \quad (3.40)$$

where the parameters t_1 , t_2 and β are respectively the initial and the final time of the strong motion T_s and a parameter determining the decay of the function from t_2 until vanishing of the acceleration.

In this work the values of the expressions for the parameters t_1 , t_2 and β in equation (3.40) are evaluated in closed-form solution by imposing that the energy of the stochastic ground motion reaches the values of the 5% and 95% respectively in t_1 and t_2 . Namely by the use of the generalized Husid function extended for stochastic processes as proposed by Cacciola and Deodatis (2011)

$$H(t) = \frac{\int_0^t \int_0^\infty a(t)^2 G(\omega) d\omega dt}{\int_0^{t_f} \int_0^\infty a(t)^2 G(\omega) d\omega dt} \quad (3.41)$$

and imposing that $H(t_1) = 0.05$ and $H(t_2) = 0.95$, equation (3.41) leads to the following analytical values of the Jennings et al. (1969) function parameters as function of the duration of the stationary part T_s , that is

$$\beta = \frac{9}{T_s}; t_1 = \frac{2.5}{\beta}; t_2 = \frac{11.5}{\beta} \quad (3.42)$$

Demonstration of the validity of the formula derived is provided by Figure 2.3 in which plot a) shows the Husid functions evaluated from non-stationary accelerograms simulated from a stochastic ground motion process with amplitude non-stationarity modelled according to the Jennings et al. (1969) and the proposed parameters and their mean value.

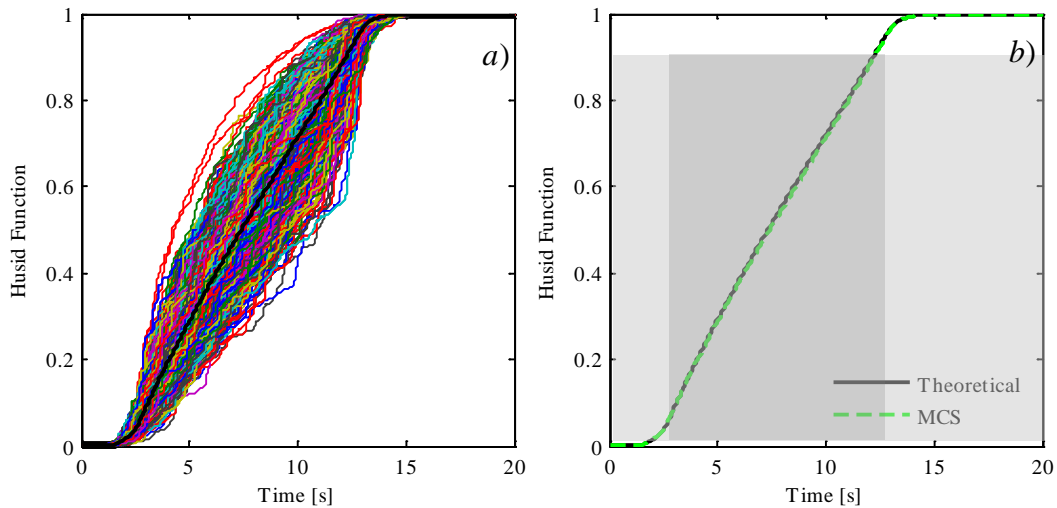


Figure 2.3. a) The Husid functions of the accelerograms simulated by the Jennings et al. (1969) time modulating function with the proposed parameters; b) the generalized Husid function (Theoretical) and the mean value obtained from simulated accelerograms (MCS).

More over plot b) presents the generalized Husid function according to Cacciola and Deodatis (2011), named as theoretical, compared to the mean value of the Husid functions simulated by MCS. The shaded area in Figure 2.3 b) in dark grey shows a time length of 10 s which is the value of the strong motion adopted for illustrative purposes.

Henceforth the parameters in equation (3.42) are adopted for modelling the time non-stationarity when the Jennings et al. (1969) function is employed.

3.1.1.3 Numerical Application

The direct models presented in section 3.1.1.1., are hereafter applied to simulate artificial quasi-stationary accelerograms compatible to a selected acceleration response spectrum provided by Eurocode 8. The spectrum compatibility achieved by model in comparison is illustrated; the stationary power spectral density functions compared are: Gasparini and Vanmarcke (1976), Vanmarcke and Gasparini (1977), Kaul (1978), Preumont (1980), Der Kiureghian and Neuenhofer (1992) and Cacciola et al. (2004).

Once the stochastic processes have been modelled by defining the PSD functions for the specific site, the simulation of time-histories can be performed by the *Spectral Representation Method* (SRM) (see e.g. Shinozuka and Jan 1972, Shinozuka and Deodatis 1991). Through the Monte Carlo Simulation method, it is possible to define the time-histories by summation of N_a harmonics with weighted amplitude and uniformly distributed random phase. For one dimensional uni-variate stochastic processes, the sample of the accelerogram is given by

$$\ddot{u}_g^{(r)}(t) = \sum_{i=1}^{N_a} \sqrt{2G(i\Delta\omega, t)\Delta\omega} \cos(i\Delta\omega t + \varphi_i^{(r)}) \quad (3.43)$$

where $\Delta\omega$ is the size interval of the discretized frequency domain, $G(i\Delta\omega, t)$ is the power spectral density function seen in equation (2.91)-(2.93) and $\varphi_i^{(r)}$ are independent random phases uniformly distributed over the interval $[0, 2\pi)$.

The response spectral acceleration as defined by EC8 for the 5% damping ratio are given by

$$\begin{aligned} RSA(T_0) &= a_g S \left[1 + \frac{T_0}{T_B} (1.5) \right] & 0 \leq T_0 \leq T_B \\ RSA(T_0) &= 2.5 a_g S & T_B \leq T_0 \leq T_C \\ RSA(T_0) &= 2.5 a_g S \left[\frac{T_C}{T_0} \right] & T_C \leq T_0 \leq T_D \\ RSA(T_0) &= 2.5 a_g S \left[\frac{T_C T_D}{T_0^2} \right] & T_D \leq T_0 \leq 4s \end{aligned} \quad (3.44)$$

where a_g is the design ground acceleration; S is the soil factor, T_0 is the natural period and T_B , T_C and T_D are the periods specified relatively to the soil type.

According to the Eurocode 8 the mean response-spectrum of the simulated time-histories has to match the target response spectrum within the following prescribed tolerance along the prefixed range of periods

$$\max \left\{ \frac{RSA(T_0) - \overline{RSA}(T_0)}{RSA(T_0)} \times 100 \right\} \leq 10\% \quad (3.45)$$

where $\overline{RSA}(T_0)$ is the mean response-spectrum of at least three simulated accelerograms and $RSA(T_0)$ is the target response spectrum.

Furthermore, according to the EC8 prescriptions the following conditions has to be verified

$$\overline{RSA}(0) > a_g S \quad (3.46)$$

where the period $T_0 = 0$ represents the ideal condition of an infinitely rigid SDOF which mass follows the acceleration of the ground.

The minimum duration of the stationary part recommended by the Eurocode 8 is of 10 s, which is the value used in this numerical application to define the Jennings et al. (1969) time modulating function through equation (3.40) and (3.42), which give values of $\beta = 0.9$, $t_1 = 2.78$ s and $t_2 = 12.78$ s. Figure 3.1 elucidates the differences among the peak factor values assumed in the models under investigation. The expression provided in the Eurocode 8 part 2, for which the peak factor is equal to 2.5, induces higher energy content compared with the others. From Figure 3.1 it can be observed that the constant value 2.5 is below the other peak factors in the range between 10-100 rad/s, therefore the power spectral density function suggested by the Eurocode 8, i.e. the model of Der Kiureghian and Neuenhofer (1992), results to be overestimated.

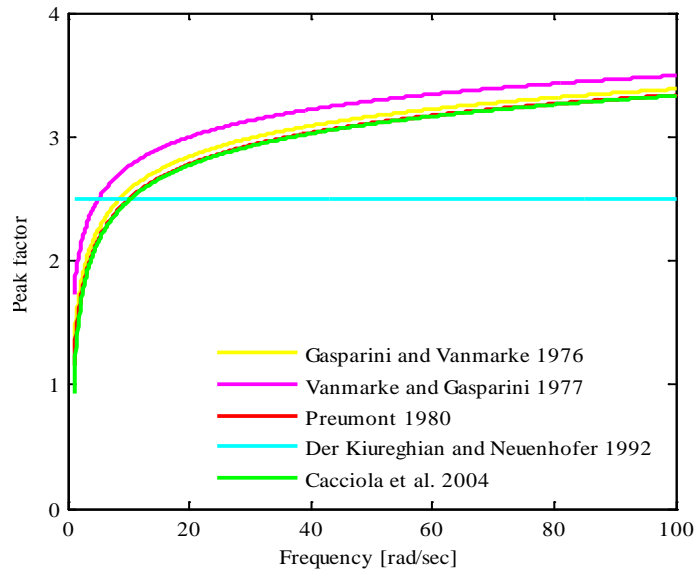


Figure 3.1. Comparison between different peak factor's definitions adopted in the compared models for $T_s = 10$ s.

Note that the peak factor relatively to the model of Kaul (1978) is identical to the peak factor presented for Vanmarcke and Gasparini (1977), thus it is has not been include in Figure 3.1.

The parameters chosen in this numerical application corresponding to ground Type A and Type 1 response spectra, are reported in the following table.

Parameter	Value
S	1
a_g	0.1 g
T_B	0.15 s
T_C	0.4 s
T_D	2.00 s

Table 3.1. Target response spectrum parameters of definition: Type 1, Type A.

Figure 3.2 shows the power spectral density functions of the selected models, which have been numerically evaluated adopting a frequency step of 0.1 rad/s.

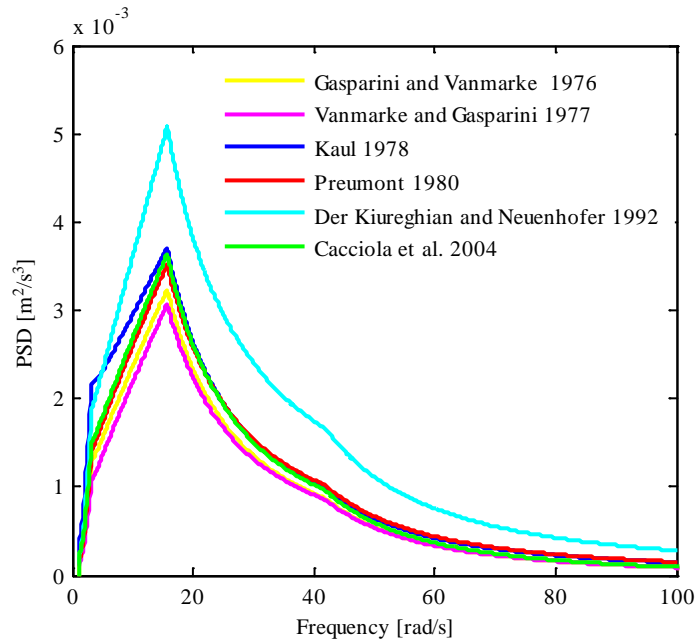


Figure 3.2. Comparison between the selected power spectral density functions

From Figure 3.2 small differences between all the models are noticeable; apart from Der Kiureghian and Neuenhofer (1992) and Kaul (1978), all the other power spectral density functions tend to similar values outside a certain range of frequencies, in which the amplitude of the functions tends to be negligible.

A number of 100 accelerograms have been generated through equation (3.43) via SRM, by superposition of harmonics with random phases uniformly distributed between 0 and 2π , and through equation (2.92) applied for quasi-stationary PSD functions. The accelerograms are generated using a time sampling step of 0.01 s and 0.1 rad/s for the frequency domain discretisation. Figure 3.3 displays the mean ensemble of the simulated response spectra obtained as the peak acceleration of oscillators with periods between 0 and 4 s, forced by the simulated time-histories.

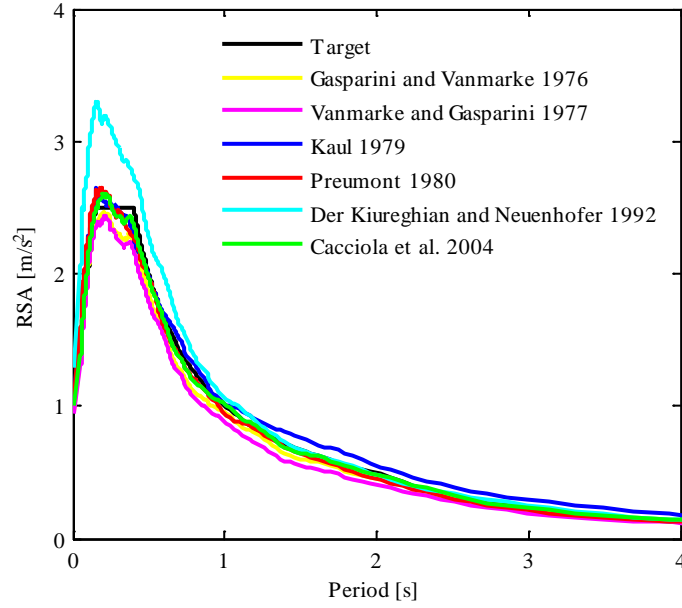


Figure 3.3. Comparison of the mean ensemble of the simulated response spectra

From Figure 3.3 it is observed that the model proposed by Eurocode 8, i.e. Der Kiureghian and Neuenhofer (1992) leads to a mean simulated response spectrum significantly above the recommended one, however it is response-spectrum-compatibles as it fulfils the provisions conditions presented in equations (3.45) and (3.46). No iterations have been adopted in order to improve the matching between the prescribed response spectrum and the mean simulated stochastic response spectral accelerations, which generally can be pursued by the following iterative scheme

$$G_0^{(1)}(\omega_0) = G_0(\omega_0); \quad G_0^{(j)}(\omega_0) = G_0^{(j-1)}(\omega_0) \left[\frac{RSA(\omega_0, \zeta_0)}{RSA^{(j-1)}(\omega_0, \zeta_0)} \right]^2 \quad (3.47)$$

where $RSA^{(j-1)}$ is the approximate pseudo-acceleration response spectrum determined at the j -th iteration and RSA the target response spectrum.

3.1.2 Non-Stationary Gaussian Stochastic Processes

The ground motion time-histories generated from quasi-stationary stochastic processes and presented in the previous sections, have only their amplitude variable with time. Although this approach is generally considered convenient for the seismic analysis of traditional linear behaving structures, it does not lead to a comprehensive description of the seismic phenomenon.

The change of the earthquake's frequency content with time recognised of primary importance especially for non-linear engineering structures (see e.g. Yeh and Wen 1990, Wang et al. 2002, Spanos et al. 2007a, Spanos et al. 2007b, Giaralis and Spanos 2010, Spanos and Giaralis 2013, Spanos and Kougoumtzoglou 2011) and can also influence the response of linear structure, as demonstrated by Papadimitriou and Beck (1990) and Beck and Papadimitriou (1993) and further investigated in this Chapter. In light of these evidences, the influence of the frequency variation with time should equally be considered significant as the amplitude time-dependency. In the next sections the few procedures proposed for modelling response-spectrum-compatible ground motion stochastic processes are presented.

3.1.2.1 Problem Position

Assuming the ground acceleration as zero-mean Gaussian non-stationary non-separable process, the evaluation of response-spectrum-compatible PSD functions could be undertaken by the first passage problem presented in equation (2.137) (see e.g. Corotis et al. 1972). From equation (2.137), the inverse stochastic problem can be arranged (Cacciola 2011), by seeing the target response spectrum as the barrier with some probability p of not being exceeded and the PSD function as the unknown of equation (2.137), that gives

$$\exp \left[- \int_0^{t_f} \alpha_U (RSA(\omega_0, \zeta_0), t) dt \right] = p \quad (3.48)$$

where t_f is the time interval in which the ground motion possesses not negligible energy and α_U is the hazard function seen in equation (2.135) and p is the probability of not exceedance.

The hazard function can be rewritten in terms of the target response spectrum by substituting of equations (2.129) and (2.131) into equation (2.135), that gives

$$\alpha_U(RSA(\omega_0, \zeta_0), t) = \frac{1}{\pi} \sqrt{\frac{\lambda_{2,U}(t)}{\lambda_{0,U}(t)}} \frac{1 - \exp\left(-\sqrt{\frac{\pi}{2}} \frac{RSA(\omega_0, \zeta_0) / \omega_0^2}{\sqrt{\lambda_{0,U}(t)}} \delta_U(t)\right)}{\exp\left(\frac{(RSA(\omega_0, \zeta_0) / \omega_0^2)^2}{2\lambda_{0,U}(t)}\right) - 1} \quad (3.49)$$

where $\lambda_{i,U}(t)$ are the time variant spectral moments and $\delta_U(t)$ the bandwidth factor of the response process; the latter according to equation (2.99) can be rewritten as

$$\delta_U(t) = \sqrt{1 - \frac{\lambda_{1,U}^2(t)}{\lambda_{0,U}(t)\lambda_{2,U}(t)}} \quad (3.50)$$

Ideally by equations (3.48)-(3.50) and the definition of the non-stationary spectral moments of the response presented in Chapter 2, the evolutionary power spectral density function pertinent to the codes prescriptions could be derivable. However, this approach has not yet been attempted. To solve this inverse problem could be computationally burdensome, the convergence not assured and moreover it may lead to physically unacceptable results. In this section, the approaches which were alternatively undertaken are presented.

In the framework of Gaussian response-spectrum-compatible non-stationary ground motion models, very few procedures have been proposed in literature (see e.g. Spanos and Vargas Loli 1985, Preumont 1985, Cacciola 2010, Cacciola and Deodatis 2011, Giaralis and Spanos 2012). Herein the ground motion models developed by Spanos and Vargas Loli (1985), Preumont (1985), and Cacciola (2010) are described; moreover, the explicit formulae among those proposed, i.e. Cacciola (2010) and Preumont (1985), are compared in a numerical application.

Spanos and Vargas Loli (1985) for the first time developed the relationship between the evolutionary power spectral density function and a known response spectrum. The authors defined an approximate analytical expression whose parameters were derived from an optimization procedure; the link between the power spectral density function and the target response spectrum is based on the following relationship

$$RSV(\omega_0, \zeta_0) = r\sigma_{\dot{U}_{\max}}(\omega_0, \zeta_0) \quad (3.51)$$

where $RSV(\omega_0, \zeta_0)$ is the velocity target response spectrum, $\sigma_{\dot{U}_{\max}}$ is the maximum of the standard deviation of the response velocity and r is a scaling factor which value is taken equal to $\sqrt{\pi/2}$.

The variance of the velocity response process is approximated by the authors by

$$\sigma_{\dot{U}}^2(t) \approx \omega_0^2 \sigma_U^2(t) = \pi \exp(-2\zeta_0 \omega_0 t) \int_0^t \exp(2\zeta_0 \omega_0 t) S(\omega, t) dt \quad (3.52)$$

where $S(\omega, t)$ is the bilateral power spectral density function to be determined.

In order to determine the power spectral density function from equation (3.51) the authors assumed the evolutionary power spectrum as a linear combination of separable functions through the following mathematical model

$$S(\omega, t) = \sum_{k=1}^N C_k t^2 \exp(-\alpha_k t) S_k(\omega) \quad (3.53)$$

where $S_k(\omega)$ is the Kanai-Tajimi power spectral density function seen in equation (2.94) whose parameters ζ_k and ω_k have to be determined along with N , C_k and α_k . By substituting equation (3.53) into (3.52) the maximum of $\sigma_{\dot{U}}^2(t)$ is given by

$$\sigma_{\dot{U}_{\max}}^2 = \frac{\pi}{2\zeta_0 \omega_0} \sum_{k=1}^m C_k t^{*2} \exp(-\alpha_k t^*) S_k(\omega_0) \quad (3.54)$$

Therefore by mean of equation (3.54) and (3.51), the relationship between the velocity target response spectrum and the evolutionary power spectral density function is expressed by the equation

$$RSV^2(\omega_0, \zeta_0) = r^2 \frac{\pi}{2\zeta_0\omega_0} \sum_{k=1}^m C_k t_k^{*2} \exp(-\alpha_k t_k^*) S_k(\omega_0) \quad (3.55)$$

The differences between the target spectrum on the left hand side and the right hand side of the above formula, are minimized through the Levenberg-Marquardt procedure by best fitting of the constant parameters $t_1^*, t_2^*, \dots, t_n^*, C_k, \alpha_k, \zeta_k, \omega_k$.

After defining the evolutionary power spectral density function samples of ground motions process are generated by equation (3.43). An iterative procedure is required in order to ensure the matching of the simulated and target response spectra.

The approach undertaken by Spanos and Vergas Loli (1985) has been followed by Giaralis and Spanos (2009) to simulate artificial ground motions by using Auto Regressive Moving Average simulation method (ARMA). The spectrum compatibility matching is guaranteed though a proposed iterative numerical procedure by means of Harmonic Wavelet Transform (HWF) combined with high pass filtering methods for baseline corrections.

In the same year, the relevance of the non-stationarity of the frequency content in the modelling of the ground motion has been recognised in the simulation of time-histories by Preumont (1985). The author defined an empirical model of the non-separable power spectral density function which assumes that the high frequency components are magnified in the early part of the time-history. Specifically, the following expression of the evolutionary spectrum is proposed

$$G(\omega, t) = G(\omega) t^2 e^{-\alpha(\omega)t} \quad (3.56)$$

with

$$\alpha(\omega) = \alpha_0 + \alpha_1\omega + \alpha_2\omega^2 \quad (3.57)$$

where α_0 , α_1 and α_2 are adjustable parameters.

The parameters in equation (3.57) are calibrated in order to impose the equality between the energy of the separable and non-separable process; this energy balance, which ensures the matching of the mean simulated and target response spectra for each frequency, reads

$$G^{SC}(\omega) \int_0^{\infty} a(t)^2 dt = G(\omega) \int_0^{\infty} t^2 e^{-\alpha(\omega)t} dt = G(\omega) \frac{2}{\alpha(\omega)^3} \quad (3.58)$$

where $G^{SC}(\omega)$ is the stationary response-spectrum-compatible power spectral density function and $a(t)$ is the time modulating function (see e.g. equation (3.40)).

Therefore through equation (3.40), the function $G(\omega)$ in equation (3.56) is readily determined as follows

$$G(\omega) = \frac{\int_0^{\infty} a^2(t) dt}{\int_0^{\infty} t^2 e^{-\alpha(\omega)t} dt} G^S(\omega) = \frac{\alpha(\omega)^3}{2} G^S(\omega) \int_0^{\infty} a^2(t) dt \quad (3.59)$$

Once $a(t)$ is defined, the evolutionary power spectral density function is pursued by means of equations (3.56) and (3.57) in which the coefficients α_0 , α_1 and α_2 are suitably determined.

An alternative approach has been proposed by Cacciola (2010), that allows the straightforward evaluation of a non-separable power spectral density function compatible with a target response spectrum. In the model proposed by Cacciola (2010), the non-stationary response-spectrum-compatible evolutionary ground motion process is given by the superposition of two independent contributions. The first one, is a fully non-stationary known counterpart, which takes into account of the time variability of both intensity and frequency content; the second one, is a corrective term represented by a quasi-stationary zero-mean Gaussian process, that

adjusts the non-stationary signal in order to make it response-spectrum-compatible. Therefore, the ground motion can be split in two contributions:

$$\ddot{u}_g(t) = \ddot{u}_g^R(t) + \ddot{u}_g^C(t) \quad (3.60)$$

Taking into account the statistical independence of the two contributions, the evolutionary response-spectrum-compatible power spectral density function can be expressed as

$$G(\omega, t) = G^R(\omega, t) + G^C(\omega, t) \quad (3.61)$$

where $G^R(\omega, t)$ is the joint time-frequency distribution of the recorded accelerogram and $G^C(\omega, t)$ is the separable power spectral density function representing the corrective term given by

$$G^C(\omega, t) = a^2(t)G(\omega) \quad (3.62)$$

Specifically, $G^R(\omega, t)$ is attained by the fully non-stationary model of Conte and Peng (1997), which hypothesizes the stochastic ground motion as a series of zero-mean independent uniformly modulated Gaussian processes as

$$G(\omega, t) = \sum_{j=1}^N |a_j(t)|^2 G_j(\omega) \quad (3.63)$$

where

$$a_j(t) = \alpha_j (t - \mathcal{G}_j)^{\beta_j} \exp(-\gamma_j (t - \mathcal{G}_j)) U(t - \mathcal{G}_j) \quad j = 1, \dots, N \quad (3.64)$$

where $U(t - \mathcal{G}_j)$ is the unit step function and $G_j(\omega)$ a stationary counterpart obtained as

$$G_j(\omega) = \frac{\nu_j}{\pi} \left[\frac{1}{\nu_j^2 + (\omega + \eta_j)^2} + \frac{1}{\nu_j^2 + (\omega - \eta_j)^2} \right] \quad j = 1, \dots, N \quad (3.65)$$

in which the parameters N , α_j , β_j , γ_j , ϑ_j , η_j , ν_j are determined by a best fit procedure in order to minimize the differences between the analytical model and the joint time-frequency distribution of a real earthquake.

In order to define the corrective term $G^C(\omega, t)$ according to the quasi-stationary model described in the previous section, $a(t)$ is the modulating function given in equation (3.40), whose parameters are calibrated by the knowledge of the recorded accelerograms and $G(\omega)$ is determined modifying equation (3.36) as follows

$$G^C(\omega_i) = \begin{cases} 0, & 0 \leq \omega \leq \omega_\alpha \\ \frac{4\zeta_0}{\omega_i\pi - 4\zeta_0\omega_{i-1}} \times & \\ \times \left(\frac{RSA(\omega_i, \zeta_0)^2 - RSA^R(\omega_i, \zeta_0)^2}{\eta_U^2(\omega_i, \zeta_0)} - \Delta\omega \sum_{k=1}^{i-1} G^C(\omega_k) \right) & \omega > \omega_\alpha \end{cases} \quad (3.66)$$

where η_U is the peak factor defined in equation (3.10) and RSA^R is the pseudo-acceleration response spectrum for the recorded ground motions $\ddot{u}_g^R(t)$.

Equation (3.66) is defined for $RSA(\omega_i, \zeta_0) > RSA^R(\omega_i, \zeta_0)$, as a consequence a preliminary scaling procedure might be required.

It has to be emphasized that, due to the mathematical structure of the model proposed by Conte and Peng (1997), equation (3.61) can be rewritten in the form

$$\begin{aligned} G(\omega, t) &= G^R(\omega, t) + G^C(\omega, t) = \\ &= \sum_{j=1}^N |a_j(t)|^2 G_j(\omega) + a_0^2(t) G(\omega) = \sum_{j=0}^N |a_j(t)|^2 G_j(\omega). \end{aligned} \quad (3.67)$$

The equation above allows a compact representation of the evolutionary response-spectrum-compatible power spectral density function. It is noted that, in the formulation proposed by Cacciola (2010), the non-stationary frequency content is

not modelled through empirical analytical formulas but it is selected from real records.

3.1.2.2 Numerical Application

In this section, the non-stationary ground motion stochastic processes holding an explicit formulation of the evolutionary power spectral density function are compared in a numerical example, namely the models proposed by Preumont (1985) and Cacciola (2010) are considered.

The spectrum compatibility of the two procedures is illustrated by considering a target response spectrum as prescribed by Eurocode 8 and presented in equation (3.44). The response spectrum for Type B soil and Type 1 seismicity is selected, whose recommended parameters are presented in Table 3.2.

Parameter	Value
S	1.2
a_g	0.35 g
T_B	0.15 s
T_C	0.5 s
T_D	2.00 s

Table 3.2. Target response spectrum parameters of definition: Type 1, Type B.

To implement the model proposed by Preumont (1985), the constant values in equation (3.57) required to fulfil the PSD definition in equation (3.56), have been set equal to $\alpha_0 = 0.3$, $\alpha_1 = 0.01$ and $\alpha_2 = 0$. These constants were defined by the author through the proposed calibration procedure by considering a total duration of the process $t_f = 20$ s and the time modulating function of Jennings et al. (1969), which set for a strong motion of $T_s = 13$ s, beginning at $t_1 = 2$ s and ending at $t_2 = 15$ s.

To apply the procedure proposed by Cacciola (2010), the evolutionary power spectrum established by Conte and Peng (1997) for El Centro 1940 earthquake (north-south component SOOE (N-S) of the Imperial Valley) is implemented firstly. According to the author, the Jennings et al. (1969) modulating function is defined to model the amplitude non-stationarity of the process. The author evaluated the

Jennings et al. (1969) model parameters by specifying the Husid function for the selected record which total duration is $t_f = 30$ s. Cacciola (2010) obtained the initial and final time of the strong motion respectively of $t_1 = 1.65$ s and $t_2 = 25.51$ s, as a consequence the strong motion duration is $T_s = 23.86$ s. The parameter defining the decay of the modulating function was determined according to a reduction of the 95% of the amplitude of the signal for $t = t_f$, that is presented as $\beta = 3 / (t_f - t_2)$.

Finally, a number of 100 time-histories were generated via Monte Carlo Simulation method by equation (3.43), in order to evaluate the mean of simulated response spectra for comparison of the spectrum compatibility achieved by the two models.

The evolutionary power spectral density functions proposed by the authors are displayed in Figure 3.4 a) and c).

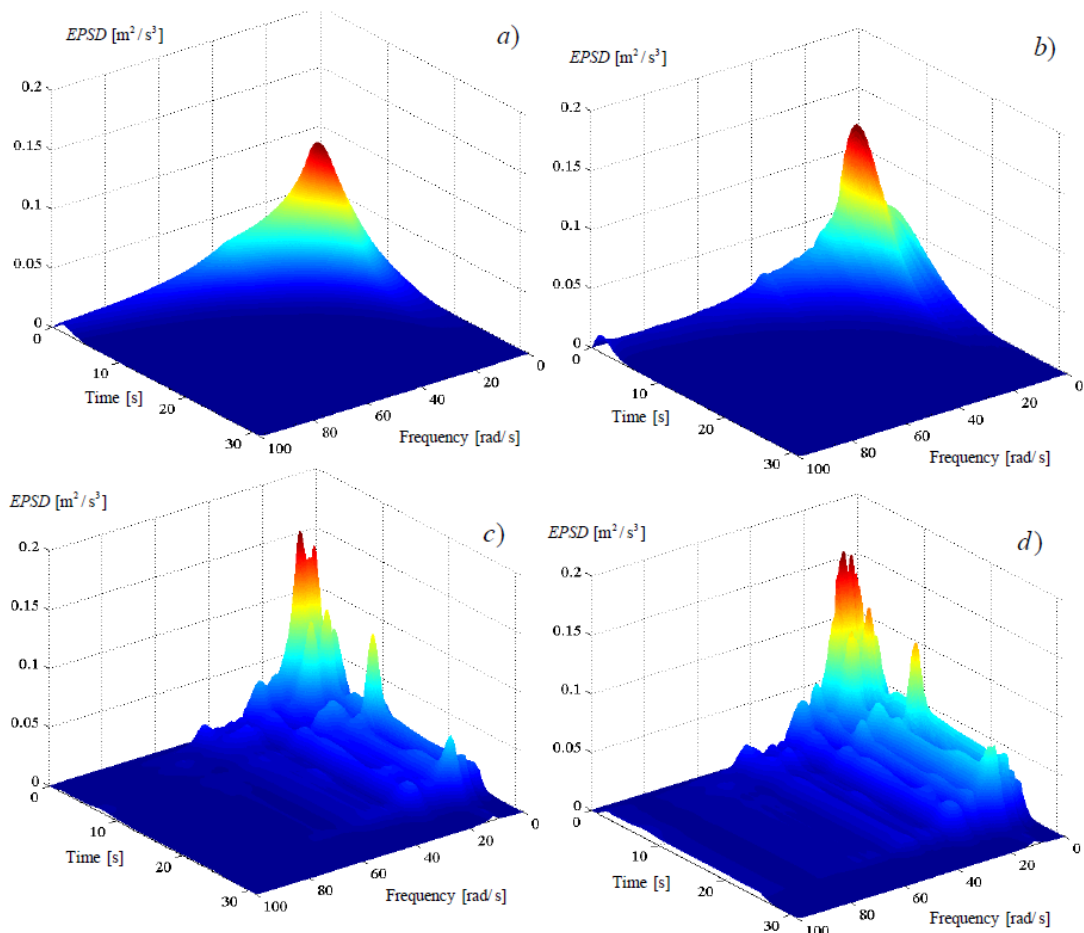


Figure 3.4. Evolutionary power spectral density function according to a) Preumont (1985); b) Preumont (1985) after 5 iterations; c) Cacciola (2010); d) Cacciola (2010) after 5 iterations.

Generally, due to the non-stationarity and the approximations involved in the models, the iterative scheme as seen in equation (3.47) is required, therefore Figure 3.4 b) and d) show the iterated power spectral density functions.

Markedly, it should be observed that although the different joint time-frequency distribution both models can be used according to the seismic provisions for simulating ground motion accelerograms and evidently tending to reach the spectrum compatibility criteria as shown in Figure 3.5.

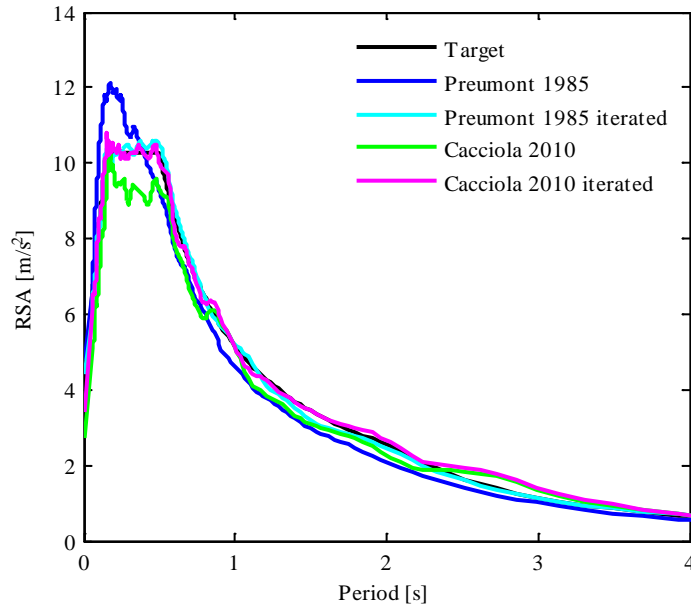


Figure 3.5. Comparison of the ensemble of the simulated response spectra before and after 5 iterations.

Figure 3.5 shows that both models reached the required spectrum compatibility over the recommend range of period, after the limited number of 5 iterations.

3.2 Current Trends in Ground Motion Modelling

For decades, the stochastic ground motion modelling has been successfully employed for engineering purposes. Besides, samples of accelerograms simulated through a pertinent stochastic approach do not exhibit the same dispersion as real ground motion parameters, such as the Peak Ground Acceleration (PGA), Arias Intensity (AI), Cumulative Absolute Velocity (CAV) and the spread about the mean/median response spectra (see e.g. Cacciola and Zentner 2012). Therefore, the developments in the simulation of ground motion models keeps moving towards bridging the gap existing between the engineering and the seismological approach. Effectively, considerable research effort has been devoted to include seismological observations into the simulation of earthquakes ground motions. In Boore (2003), a review of the available ground motion combining seismological models and engineering notions is provided, along with a proposed method for simulation by characterisation of the ground motion's amplitude spectrum through parametric or functional descriptions combined with a random phase spectrum. Investigations to

describe the earthquake non-stationarity by phase spectrum modelling have been tackled by several authors in the past years, and recent developments have further investigated the topic by employing seismological data (see e.g. Shrinkade and Gupta 2011, Peng and Li 2013). Concerning the modelling of the amplitude spectra of the ground motion by establishing PSD functions, a few methodologies have been proposed in the last twenty years to describe the seismic action for specific sites and use information from databases. As the work of Sabetta and Pugliese (1996), by which the authors' contributed to the field with one of the milestones in the definition of empirical physical amplitude spectra. Sabetta and Pugliese (1996) proposed a method to capture the frequency non-stationarity of earthquakes from the Italian Strong Motion Database (ISMD) and enabled a procedure to correlate the simulation parameters with earthquake magnitude, source distance, and soil conditions. More recently, Pousse et al. (2006) simulated accelerograms according to an evolutionary power spectral density function possessing random variables; the random variables were calibrated by empirical attenuation equations established from the K-Net Japanese Database (KNJD). In this context, an important contribution was provided by Rezaeian and Der Kiureghian (2010) introducing site-based models; the authors presented a method for simulating synthetic ground motions, whereby the seismic stochastic process is modelled by a modulated filtered white-noise with random parameters. The parameters embedded to the model are random variables calibrated on a set of real earthquakes this the site characteristics relatively to the records are reflected by the process. All these models can have a different impact on the calculation of the seismic risk for a facility. For instance, Vetter and Taflanidis (2014) recently compared the site-based model proposed by Rezaeian and Der Kiureghian (2010) to a source based model presented by the authors. Their work aimed to characterise the seismic risk associated to each model and thus, to provide insight on the differences between them by means of a probabilistic global sensitivity analysis framework.

Since the models of Sabetta and Pugliese (1996), Pousse et al. (2006) and Rezaeian and Der Kiureghian (2010) do not satisfy the spectrum compatibility criteria imposed by the international code provisions, these proposed methodologies cannot

be used directly for design purpose, unless adapted via proper calibration or filtering procedures. Recently, Cacciola and Zentner (2012) presented a methodology to simulate high variable fully non-stationary response-spectrum-compatible accelerograms. The authors introduced a random PSD function calibrated to determine not only the matching between the target and the mean simulated response spectrum, but also between target and simulated mean \pm standard deviation response spectra. The authors analysed a set of accelerograms from the European Ground Motion Database (EGMD), from which the standard deviation of the response spectral accelerations has been defined. Additionally, in this scenario of new trends of ground motion modelling, studies on the correlation of ground motion intensity parameters have been carried out and showed the significance of the spectral correlations in the assessment of seismic reliability of structures (see e.g. Baker 2007). Research has been accomplished to address the correlations between response spectral accelerations at multiple periods from data records (see e.g. Inoue and Cornell 1990, Baker and Cornell 2005, Baker and Jayaram 2008). In the context of response-spectrum-compatible ground motion modelling, the correlation among spectral accelerations at multiple periods was taken into consideration by few authors. In this respect, Wang (2011) established a methodology to select natural accelerograms, whereas D'Amico et al. (2012) and Zentner et al. (2013) proposed simulation techniques to generate synthetic accelerograms with correlated response spectral correlations. Ni et al. (2013), proposed also a fully non-stationary response-spectrum-compatible model capturing the variability of real ground motions as well as the correlated spectral correlations by using the Hilbert-Huang Transform and optimisation procedures. Formerly by adopting the same approach, Ni et al. (2011) proposed also a method to generate tri-directional time-histories guaranteeing the compatibility with a target response spectrum and maintaining the amplitude and frequency non-stationarity of the real selected records.

In the next sections, PSD functions with embedded random variables calibrated from seismological data are presented, being these techniques falling within the context of the current trends to simulate fully non-stationary ground motion time-histories.

3.2.1 Problem Position

The simulation of time-histories via Spectral Representation Method, pertinently to the random phase criteria (Shinozuka 1987), entails the description of the time-frequency distribution of the PSD functions to play a key role in the advancement of the modelling of the earthquake non-stationarity. It has to be noticed that the power spectral density function is a deterministic function which leads to simulate ground motion time-histories with very similar joint-time frequency distribution. To accommodate a more realistic description of the seismic acceleration phenomenon, PSD functions with “uncertain coefficients” are employed to enable an aleatory characterisation of the energy content considering the variability of the spectral coordinates of the ground motion (e.g. Fourier Transforms of the simulated signals, response spectral accelerations). To neglect the variability manifested by real records can lead to misrepresentative response analyses of structural systems under simulated ground motions. To this regard, the response-spectrum-compatible models proposed by Cacciola and Zentner (2012), D’Amico et al. (2012) are hereafter presented.

Cacciola and Zentner (2012) firstly introduced a method for simulating artificial earthquakes compatible with a given response-spectrum taking into account the natural variability through a pertinent evolutionary power spectrum with random coefficients. The distribution of the random coefficients has been determined by the further matching with a target mean \pm standard deviation response spectra. Specifically, in order to match the target spectra, the authors proposed the following random spectrum with random parameters

$$S(\omega, t, \alpha) = \alpha(\omega)^2 |a(\omega, t)|^2 S(\omega) \quad (3.68)$$

where $\alpha(\omega)$ is a set of uncorrelated Gaussian random variables, $|a(\omega, t)|$ is the non-separable time frequency modulating function, $S(\omega)$ is a stationary power spectral density function.

The stationary PSD function $S(\omega)$ suggested by the authors, is determined pertinently to the condition on the energy balance proposed by Preumont (1985) introduced in section 3.1.2.1. By using equations (3.58) and (3.59), Cacciola and Zentner (2012) extended the procedure of Preumont (1985) to deal with alternative time-frequency dependent modulating functions by the following generalised corrective term

$$S(\omega) = \frac{\int_0^{\omega_{cut}} a^2(t) dt}{\int_0^{\omega_{cut}} |a(\omega, t)|^2 dt} S^{SC}(\omega) \quad (3.69)$$

The non-separable time-frequency modulating function in equation (3.69) is obtained modifying the Clough-Penzien model seen in equation (2.96) as follows

$$a(\omega, t) = a(t)^2 S_{CP}(\omega, t) \quad (3.70)$$

The non-separable $S_{CP}(\omega, t)$ spectrum is modulated according to the following function

$$a(t) = a_1 t^{a_2} \exp(-a_3 t^{a_4}) \quad (3.71)$$

where the parameters a_1, a_2, a_3 and a_4 have been calibrated by least-squares approach to minimize the differences between the ground motion parameters of the formulated model and those extracted from the European Strong Motion Database, namely, $a_1 = 2.24$, $a_2 = 1.85$, $a_3 = 0.13$ and $a_4 = 1.58$.

The time variant parameters of the non-separable CP spectrum seen equation (2.96), characterise the non-stationary frequency content of the non-separable time frequency modulating function $|a(\omega, t)|$ in equation (3.70); namely the natural frequency and damping ratio depending on the soil conditions, these have been assumed pertinently to El Centro earthquake (Fan and Ahmadi 1990), these are

$$\omega_g(t) = \pi \left(3 + 19.01 \left(e^{-0.0625t} - e^{-0.15t} \right) \right) \quad (3.72)$$

and

$$\omega_f(t) = 0.1\omega_g(t) \quad (3.73)$$

The damping ratios $\zeta_g = \zeta_f = 0.6$ have been considered constant.

In order to guarantee the spectrum compatibility achievement, the authors established a relation between the response spectral accelerations and the random variables from equation (3.68), this is

$$RSA(\omega_j, \zeta_0, \alpha) = \alpha(\omega_j)RSA(\omega_j, \zeta_0) \quad (3.74)$$

where $\alpha(\omega_j)$ are the frequency dependant random variables for fixed $\omega_j \in [0, \Omega]$, which are assumed to be Gaussian distributed.

By taking mathematical expectation of equation (3.74) the random variables the spectrum compatibility condition lead to impose that

$$\mu_\alpha = \mu_\alpha(\omega_j) = 1 \quad (3.75)$$

From squaring the terms in equation (3.74), taking mathematical expectation and imposing the condition on the mean value the standard deviation $\sigma_\alpha = \sigma_\alpha(\omega_j)$ is obtained, that is

$$\sigma_\alpha(\omega_j) = \frac{RSA^{+\sigma}(\omega_j, \zeta_0)}{RSA(\omega_j, \zeta_0)} - 1 \quad \forall \omega_j \in [0, \Omega] \quad (3.76)$$

where $RSA^{+\sigma}(\omega_j, \zeta_0)$ is the mean + standard deviation acceleration response spectrum. Analogous expression can be found considering the $RSA^{-\sigma}$ spectrum.

The ground motions are simulated by the simulation formula given in equation (3.43) and modified as following

$$\ddot{u}_g^{(r)}(t) = \sum_{k=1}^{N_h} \sqrt{\alpha^{(r)}(k\Delta\omega)^2 |a(k\Delta\omega, t)|^2 2S(k\Delta\omega)\Delta\omega} \cos(k\Delta\omega t + \varphi_k^{(r)}) \quad (3.77)$$

where $|a(k\Delta\omega, t)|$ is given by equation (3.70) and $2S(k\Delta\omega) = G(k\Delta\omega)$ assumed according to Cacciola et al. (2004).

The value of the stationary component $G(\omega)$ is updated through the iterative scheme in equation (3.47) and the standard deviation $\sigma_\alpha(\omega)$ through the following iterative scheme

$$\sigma_\alpha^{(j)}(\omega_k) = \sigma_\alpha^{(j-1)}(\omega_k) \frac{RSA^{+\sigma}(\omega_k, \zeta_0)}{RSA^{+\sigma(j-1)}(\omega_k, \zeta_0)} \quad (3.78)$$

where $\sigma_\alpha^{(j)}(\omega)$ is the standard deviation at the j -th iteration.

3.2.2 Simulation of Ground Motions with Imposed Natural Variability and Correlated Spectral Accelerations

In this section, the non-stationary evolutionary PSD function for modelling the seismic action proposed by D'Amico et al. (2012) is introduced. The model is able to reproduce the natural variability of the response spectral accelerations along with a prescribed correlation of the spectral coordinates at different periods. The variability and the correlations are pertinent to seismological data, which can be provided by databases of earthquakes' records. The ground motion proposed by D'Amico et al. (2012) enhances the ground motion formulated by Cacciola and Zentner (2012), presented in section 3.1.2. The model provides a versatile procedure, which is adaptable to various models of the spectral correlations at different periods.

According to the definition of the evolutionary PSD function with random parameters in equation (3.68), D'Amico et al. (2012) characterized a response-spectrum-compatible stochastic process by a set of correlated log-normal random variable $\varepsilon(\omega_j)$. The random variables are assumed to be log-normally distributed according to the observations on empirical values of response spectral accelerations (Somerville 1993); the random variables $\varepsilon(\omega_j)$ are therefore expressed as follows

$$\varepsilon(\omega_j) = \exp[\beta(\omega_j)] \quad j = 1, \dots, n \quad (3.79)$$

where $\beta(\omega_j)$, $j=1,\dots,n$ is a set of correlated Gaussian random variables possessing mean value $\mu_\beta = \mu_\beta(\omega_j)$, standard deviations $\sigma_\beta = \sigma_\beta(\omega_j)$ and correlation $\rho_{\beta(\omega_i)\beta(\omega_j)}$. The mean value and standard deviation of $\varepsilon(\omega_j)$ are respectively $\mu_\varepsilon = \mu_\varepsilon(\omega_j)$ and $\sigma_\varepsilon = \sigma_\varepsilon(\omega_j)$.

In agreement with the model proposed by Cacciola and Zentner (2012) for Gaussian uncorrelated random variables, the values of μ_β , σ_β and $\rho_{\beta(\omega_i)\beta(\omega_j)}$ are specified to the different case of correlated log-normal random variables, for which in analogy to equation (3.74) holds that

$$RSA(\omega_j, \zeta_0, \varepsilon) = \varepsilon(\omega_j)RSA(\omega_j, \zeta_0) \quad (3.80)$$

where $RSA(\omega_j, \zeta_0, \varepsilon)$ is the response spectrum pertinent to a proposed evolutionary power spectrum in equation (3.68). Taking the mathematical expectation of equation (3.80)

$$E[RSA(\omega_j, \zeta_0, \varepsilon)] = E[\varepsilon(\omega_j)]RSA(\omega_j, \zeta_0) \quad (3.81)$$

and imposing the coincidence between the target response spectrum $RSA(\omega_j, \zeta_0)$ and the mean value $E[RSA(\omega_j, \zeta_0, \varepsilon)]$ it follows that

$$\mu_\varepsilon = E[\varepsilon(\omega_j)] = 1 \quad \forall \omega_j \in [0, \infty] \quad (3.82)$$

Since also the following relationship holds

$$\mu_\varepsilon = e^{\mu_\beta + \frac{\sigma_\beta^2}{2}} \quad (3.83)$$

By combining equation (3.82) and (3.83) the following expression is obtained

$$\mu_\beta = -\frac{\sigma_\beta^2}{2} \quad \forall \omega_j \in [0, \infty] \quad (3.84)$$

The value of the standard deviation is determined by using the target mean + standard deviation response spectrum seen in equation (3.76) and updated with equation (3.78) to reach the spectrum compatibility.

The value of $\sigma_\varepsilon = \sigma_\varepsilon(\omega_j)$ is derived from the definition of the second order central moment presented in equation (2.76) for the random variables $\varepsilon(\omega_j)$, that is

$$\sigma_\varepsilon^2 = E(\varepsilon^2) - \mu_\varepsilon^2 \quad (3.85)$$

which after substitution of equations (3.79) and (3.83) gives

$$\sigma_\varepsilon^2 = e^{2\mu_\beta + 2\sigma_\beta^2} - e^{2\mu_\beta + \sigma_\beta^2} \quad (3.86)$$

after rearranging the terms of the expression above it gives the variance as follows

$$\sigma_\varepsilon^2 = \left(e^{\sigma_\beta^2} - 1 \right) e^{2\mu_\beta + \sigma_\beta^2} \quad (3.87)$$

Finally, after substituting equation (3.84) into the above equation, the relation from which the standard deviation of the Gaussian random variables is provided as follows

$$\sigma_\beta(\omega_j) = \sqrt{\ln(1 + \sigma_\varepsilon^2(\omega_j))} \quad (3.88)$$

where $\sigma_\varepsilon^2(\omega_j)$ is the value evaluated from the simulated response spectra and updated at every iteration according to equation (3.78) in order to impose the variability to the mean simulated \pm standard deviation response spectral acceleration.

The correlation of spectral accelerations $\rho_{\ln RSA(\omega_i) \ln RSA(\omega_j)}$ is defined in literature in terms of the log-normal response spectra of the spectral accelerations (see e.g. Inoue and Cornell 1990, Baker and Jayaram 2008), by taking the logarithm of equation (3.80) it reads

$$\ln RSA(\omega_k, \zeta_0, \varepsilon) = \ln \varepsilon(\omega_k) + \ln RSA(\omega_k, \zeta_0) \quad (3.89)$$

which by substituting equation (3.79) enables to define the correlation coefficients $\rho_{\beta(\omega_i)\beta(\omega_j)}$, which can be shown to be coincident with the selected correlation of spectral accelerations, that is

$$\rho_{\beta(\omega_i)\beta(\omega_k)} = \rho_{\ln \varepsilon(\omega_i)\ln \varepsilon(\omega_k)} = \rho_{\ln RSA(\omega_i)\ln RSA(\omega_k)} \quad \forall \omega_k \in [0, \infty] \quad (3.90)$$

To define the EPSD function the correlated log-normal RVs $\varepsilon(\omega)$, possessing median value μ_ε and standard deviation σ_ε , are simulated.

The log-normal random variables are defined from the Gaussian normal distributed numbers according to equation (3.79) by the knowledge of their mean value (3.82), whilst the correlation is introduced through the correlation matrix obtained from the attenuation relationship of Ionue and Cornell (1990) in terms of natural periods.

In order to correlate the RVs $\varepsilon(T)$ at different periods, the Cholesky's decomposition is employed. The decomposition enables to evaluate a symmetric and positive definite square matrix, \mathbf{A} , with a single triangular factorisation given by

$$\mathbf{L} \times \mathbf{L}^T = \mathbf{A} \quad (3.91)$$

where \mathbf{L} is a lower triangular matrix and \mathbf{L}^T is its transpose.

The components of the matrix \mathbf{L} are given by the following coefficients

$$L_{ii} = \left(a_{ii} - \sum_{k=1}^{i-1} L_{ik}^2 \right)^{\frac{1}{2}}; L_{ji} = \frac{1}{L_{ji}} \left(a_{ij} - \sum_{k=1}^{i-1} L_{ik} L_{jk} \right) \quad j = i+1, i+2, \dots, N \quad (3.92)$$

where a_{ii} and a_{ij} are the elements of \mathbf{A} .

The correlated Gaussian random variables β_i in (3.79) are obtained by the product

$$\begin{bmatrix} \beta_1 \\ \beta_2 \\ \cdot \\ \cdot \\ \cdot \\ \beta_n \end{bmatrix} = \mathbf{L} \begin{bmatrix} \alpha_1 \\ \alpha_2 \\ \cdot \\ \cdot \\ \cdot \\ \alpha_n \end{bmatrix} \sigma_\beta \quad (3.93)$$

where α_i are uncorrelated RVs with σ_β standard deviation.

3.2.2.1 Numerical Application

In this section, the method for generating fully non-stationary response-spectrum-compatible earthquakes according to the evolutionary PSD function with uncertain parameters proposed by D'Amico et al. (2012) is presented by a numerical example for illustrative purposes. In order to apply the proposed procedure D'Amico et al. (2012) adopted the non-separable Clough-Penzien spectrum in equation (2.96) and modified it according to equations (3.70) and (3.71).

The spectrum compatibility criteria are chosen in accordance to the target EC8 response spectrum for a 5% damping seen in equation (3.44). The parameters characterising the target response spectral accelerations are for ground Type A and spectrum Type 1 are reported in Table 3.3.

Parameter	Value
S	1.
a_g	0.1 g
T_B	0.15 s
T_C	0.4 s
T_D	2.00 s

Table 3.3. Target response spectrum parameters of definition: Type 1, Type A.

For illustrative purpose the variability of the target response spectrum has been set as follows that

$$RSA^{+\sigma}(T) = 1.5RSA(T) \quad (3.94)$$

and

$$RSA^{-\sigma}(T) = 0.5RSA(T) \quad (3.95)$$

Therefore, equations (3.84) and (3.88)

$$\sigma_{\beta}(\omega_k) = \sqrt{\ln(1.25)} = 0.4724; \quad \mu_{\beta}(\omega_k) = -0.1116 \quad (3.96)$$

The correlation of spectral accelerations $\rho_{\ln RSA(\omega_i) \ln RSA(\omega_k)}$ proposed by Inoue and Cornell (1990) has been also selected, that is

$$\rho_{\beta(\omega_i)\beta(\omega_k)} = \rho_{\ln RSA(T_i) \ln RSA(T_k)} = 1 - 0.33 \left| \ln \left(\frac{T_i}{T_k} \right) \right|; \quad 0.1 \leq T_i, T_k \leq 4s \quad (3.97)$$

In order to apply the procedure, the evolutionary Clough-Penzien model is modified according to Cacciola and Zentner (2012) as presented in equations (3.70)-(3.73) is used. The procedure has been applied for simulating a number of 500 artificial accelerograms compatible with mean and mean \pm standard deviation response spectra assuming: (i) log-normally distributed correlated random variables $\varepsilon(\omega_k)$, (ii) log-normal uncorrelated random variables $\varepsilon(\omega_k)$, (iii) with no imposed variability $\varepsilon(\omega_k)=1$, the corresponding response spectral are presented in Figure 3.6.

Pertinently to Eurocode 8, consistency is achieved by satisfying the conditions presented in equations (3.45) and (3.46). The accuracy of the proposed procedure was demonstrated by the authors according to Figure 3.6, in which the confident match between the mean simulated response spectrum and the target one for the three cases is illustrated. Figure 3.6 b) and c) show that also the imposed target mean \pm standard deviation response spectra are matched by the simulated response spectra, confirming the accuracy of the convergence criteria defined by equation (3.47).

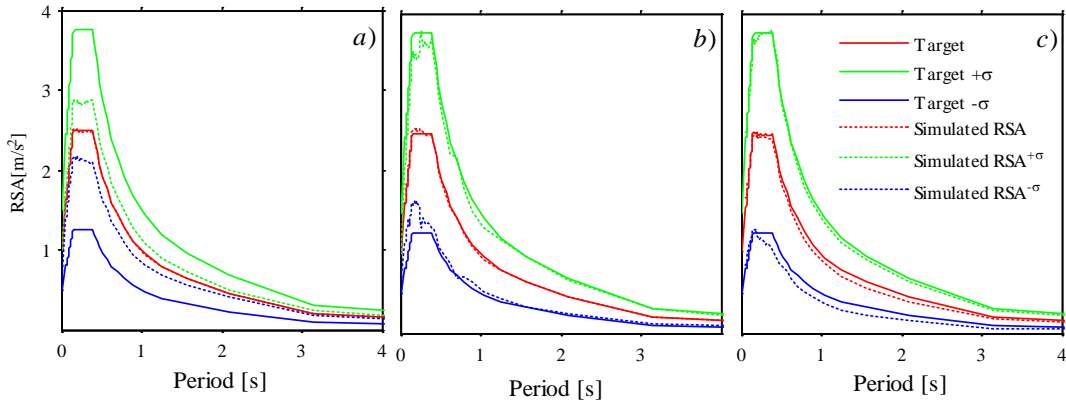


Figure 3.6. Comparison between simulated and target response spectra: a) $\varepsilon(\omega_k) = 1$; b) $\varepsilon(\omega_k)$ uncorrelated; c) $\varepsilon(\omega_k)$ correlated (from D'Amico et al. 2012).

Pertinent trajectories are reported in Figure 3.7 from D'Amico et al. (2012), which shows: for the case in which $\varepsilon(\omega_k) = 1$ the accelerograms are very similar, while by considering a random evolutionary spectrum not only large variability in the peak values is observed but also with regard to the frequency content.

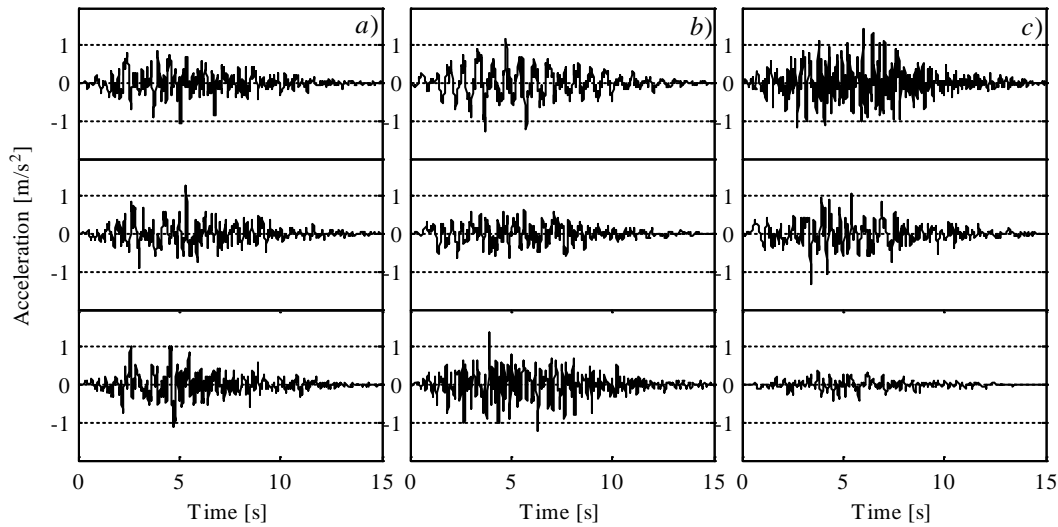


Figure 3.7. Trajectories of simulated ground motion accelerograms: a) $\varepsilon(\omega_k) = 1$; b) $\varepsilon(\omega_k)$ uncorrelated; c) $\varepsilon(\omega_k)$ correlated (from D'Amico et al. 2012).

The acceleration response spectral correlation at different periods imposed according to the model of Inoue and Cornell (1990) is presented in the comparison between Figure 3.8 a) and d) show. The correlations between the log-response spectral acceleration values at different periods compared in the subplots in Figure 3.8, show:

a) the target model of Inoue and Cornell (1990) presented in equation (3.97); b), c), and d) the correlation coefficients respectively for the case of $\varepsilon(\omega_k)=1$, uncorrelated $\varepsilon(\omega_k)$ and correlated $\varepsilon(\omega_k)$.

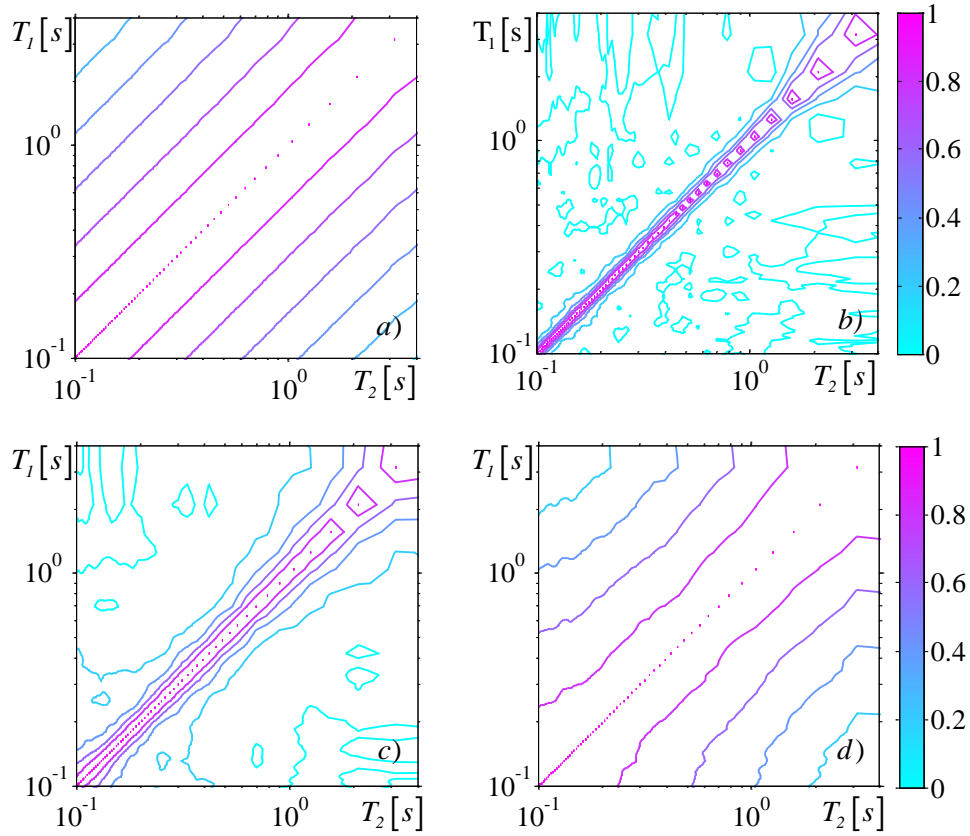


Figure 3.8. Correlations of the log-response spectral acceleration values: a) Inoue and Cornell (1990) target correlation; b) $\varepsilon(\omega_j)=1$; c) $\varepsilon(\omega_j)$ uncorrelated; d) $\varepsilon(\omega_j)$ correlated (from D’Amico et al. 2012).

The correlated response spectral accelerations simulated by the procedure proposed by D’Amico et al. (2012) are smoother as for real earthquakes response spectra.

In the flowchart in Figure 3.9 the steps and the equations used to implement the ground motion simulation method presented in this section are summarised. The random variables $\varepsilon(\omega)$ employed to simulate ground motions with imposed variability adopted in this work are uncorrelated RV, named $\alpha(\omega)$, which are simulated without accounting of the correlation, which can be imposed as seen in equation (3.93).

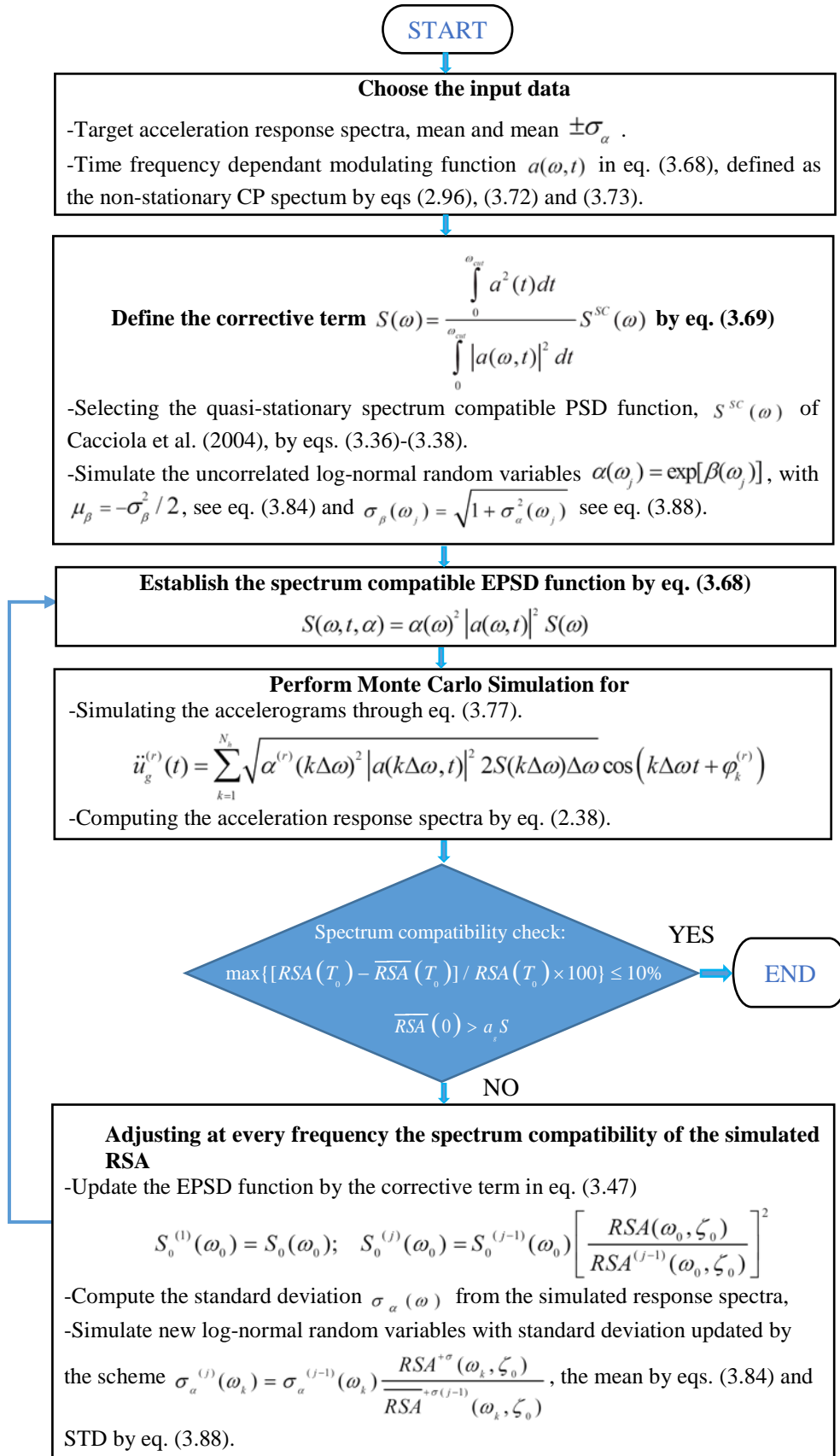


Figure 3.9. Iterative scheme to simulate response-spectrum-compatible accelerograms according to the proposed technique.

3.3 Concluding Remarks

In this Chapter an overview of the response-spectrum-compatible quasi-stationary and non-stationary stochastic processes for modelling the seismic ground motion has been firstly conducted. The review presented in this Chapter has enabled to appreciate the implications of adopting selected quasi-stationary and non-stationary response-spectrum-compatible ground motions in terms of spectrum compatibility achievement and convergence to a target spectrum of the mean simulated spectra for different models. In the framework of the simulation of response-spectrum-compatible accelerograms, the quasi-stationary ground motion models are still widely used as a vehicle for pre-design structures and/or control devices in a probabilistic sense, although neglecting the non-stationary frequency characteristic of the seismic ground motion.

In this Chapter a technique to simulate response-spectrum-compatible accelerograms is also proposed. The procedure aims at reproduce some of the features observed by the analysis of real accelerograms, specifically the variability of the acceleration response spectra. Through embedded random variables pertinently simulated in order to add realistic features to the simulated accelerograms, a parametrised evolutionary PSD function is established without loss of characteristics of a basic model. The proposed simulation follows the techniques proposed by Cacciola and Zentner (2012) and D'Amico et al. (2012), which have been described in the Chapter. The latter allows to define from a single parametrized evolutionary power spectral density function a number of three response-spectrum-compatible stochastic processes, which encompass the hypotheses of: non-stationarity, non-stationarity with imposed variability of the spectral accelerations and non-stationarity with imposed variability and correlation of the spectral accelerations at different periods. Correlated response spectral accelerations of simulated ground motions, are smoother than in uncorrelated models (Wang 2011), thus it can be observed that the correlation of the spectral acceleration might affect more the structural systems with close modes of vibration (D'Amico 2012).

The influence of the earthquake ground motion amplitude and frequency content variation with time on the structural response, is object of the investigations presented in the next Chapters. Due to the characteristics of the benchmark structures investigated in the next Chapters, i.e. modes of vibration, the correlation of the spectral acceleration has been excluded. Thus, Chapter 4 presents the stochastic analysis of the response of opportunely selected benchmark buildings to the response spectrum compatible earthquakes simulated according to the proposed technique summarised by means of the flowchart in Figure 3.9.

4 Numerical Comparative Study of Linear and Non-Linear Benchmark Structures

In this Chapter, the analysis of the response of structures to Gaussian response-spectrum-compatible stochastic ground motion models is performed through a Monte Carlo Simulation study; namely the response-spectrum-compatible stochastic processes adopted in this investigation are the quasi-stationary and non-stationary models along with the novel non-stationary model with imposed variability. For the first time, this work shows that different ground motions, modelled to hold the same response spectrum for 5% damping, peak ground acceleration (PGA), strong motion phase (SMP) and total duration (TD), lead to significant discrepancies in the structural responses even for proportionally damped linear behaving structures, although all the models satisfy the response-spectrum compatibility criteria.

Three benchmark structures have been selected to finalize the study, specifically the linear SMART 2008 nuclear building (Lermitte et al. 2008), IASC 1996 5-storey building linear steel frame (Djajakesukma et al. 2002, Samali 2007), and linear and non-linear SAC 1996 20-storey building structure (Othori et al. 2004). The structures have been selected to consider a spread scenario from high to low fundamental frequencies. The results clearly show a weakness of the current response-spectrum-compatible criteria mandated by the international seismic codes and points out that more robust conditions for the simulation of artificial earthquake ground motions are needed (Cacciola et al. 2014).

4.1 Proposed Technique to Define Stochastic Input Ground Motions

In this section, the one-dimensional stochastic inputs, namely the quasi-stationary, non-stationary and non-stationary model with imposed variability are described.

According to the method proposed to simulate ground motions with imposed variability, the quasi-stationary and non-stationary models are defined as particular

cases of equation (3.68). The random variables characterizing the model with imposed variability have been simulated according to the procedure in section 3.2.2, accounting of the variability only (i.e. without imposing the spectral correlation at different periods).

Therefore, from a versatile model for response-spectrum-compatible PSD functions, the three processes under investigation are simulated by setting different values of the random variables $\alpha(\omega)$ and of the time frequency modulating function $a(\omega, t)$. Specifically: (i) the quasi-stationary model assumes the random function $\alpha(\omega) = 1$ and $a(\omega, t) = a(t)$, the latter is the Jennings et al. (1969) model, (ii) in the non-stationary model the random variables are set $\alpha(\omega) = 1$ and the joint time-frequency modulating function $a(\omega, t)$, and (iii) the non-stationary model with imposed variability is characterised by assuming $\alpha(\omega)$ log-normally distributed, with $\mu_\alpha = 1$ and standard deviation $\sigma_{\alpha(\omega)}$, determined according to equation (3.76) without accounting of the correlation among the spectral accelerations, and a mean + standard deviation target response spectrum which reads

$$RSA^{+\sigma}(T) = 1.5RSA(T) \quad (4.1)$$

The mean/median response spectrum along its variability should be determined from the same earthquake database for performance based design studies. However, due to the lack of data in the EC8 provision with regard to the variability of the response spectral accelerations, for demonstrative purposes a feasible value of the response spectra standard deviation has been used in this comparative study.

Regarding the formulation of the quasi-stationary model, among the stationary PSD reviewed in this Chapter, the model proposed by Cacciola et al. (2004) has been chosen. The handy recursive expression of the power spectral density function compatible with a given response spectrum is presented in equation (3.36), approximated peak factor determined under the hypothesis of a barrier out-crossing in clumps as presented in equation (3.37)-(3.38) is adopted assuming smooth shape of the PSD function and values of the structural damping $\zeta_0 \ll 1$.

The modulating function $a(t)$ to model the quasi-stationary input is given by equation (3.40), whose parameters, namely t_1 , t_2 and β , closed-form expressions are presented in section 3.1.1.2. The parameters are evaluated once T_s has been set (e.g. using the minimum value from EC8 equal to 10 s). Therefore, by setting the duration of the stationary part $T_s=10$ s, the values are obtained are: $\beta=0.9$, $t_1=2.78$ s and $t_2=12.78$ s.

The elastic response spectrum used is the Type 1 spectrum for soil of Type D whose parameter of definition are reported in the table below.

Parameter	Value
S	1.35
a_g	0.32 g
T_B	0.20 s
T_C	0.80 s
T_D	2.00 s

Table 4.1. Target response spectrum parameters of definition: Type 1, Type D.

In order to simulate non-stationary and non-stationary with imposed variability processes, the non-separable frequency dependent modulating function $a(\omega, t)$ is selected as the evolutionary Clough-Penzien spectrum seen in equation (2.96) according to equation (3.70). In order to characterize the time-dependant parameters of the CP evolutionary spectrum, the frequency $\omega_g(t)$ has been assumed to be a linear function according to the investigations on the analysis of a large number of accelerograms carried out by Rezaeian and Der Kiureghian (2008), who proposed the expression of the filter frequency of the CP spectrum as follows

$$\omega_g(t) = \omega_{t_0} - (\omega_{t_0} - \omega_{t_f}) \frac{t}{t_f} \quad (4.2)$$

where ω_{t_0} is the frequency at the time instant $t=0$ and ω_{t_f} is the frequency at final time t_f .

Specifically the frequencies of the evolutionary CP spectrum determined through equation (4.2) are $\omega_{t_0} = 20$ rad/s and $\omega_{t_f} = 5$ rad/s while the frequency $\omega_f(t)$ is

determined consequently through equation (3.73). Under the assumptions for soft soil the values of the damping parameters have been selected as $\zeta_g = 0.2$ and $\zeta_f = 0.6$ (after Der Kiureghian and Neuenhofer 1992). The damping parameters are assumed to be time invariant on the basis of the investigations on recorded time-histories, revealing that the time bandwidth factor variation is relatively insignificant (Rezaeian and Der Kiureghian 2008). The evolutionary power spectral density functions used for the simulations of the artificial accelerograms are depicted in Figure 4.1.

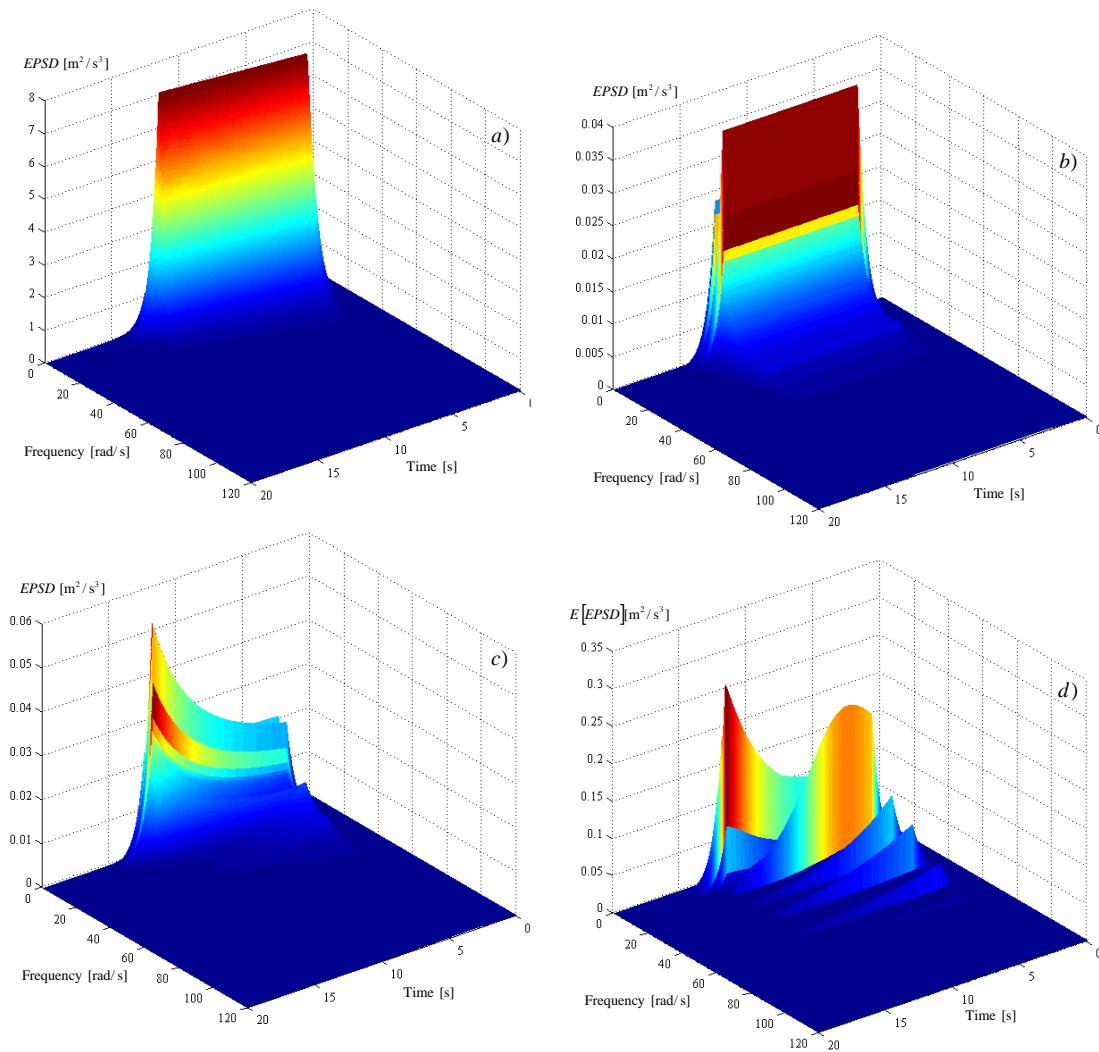


Figure 4.1. Evolutionary PSD functions: a) C& P model, b) quasi-stationary; c) non-stationary; d) non-stationary with imposed variability.

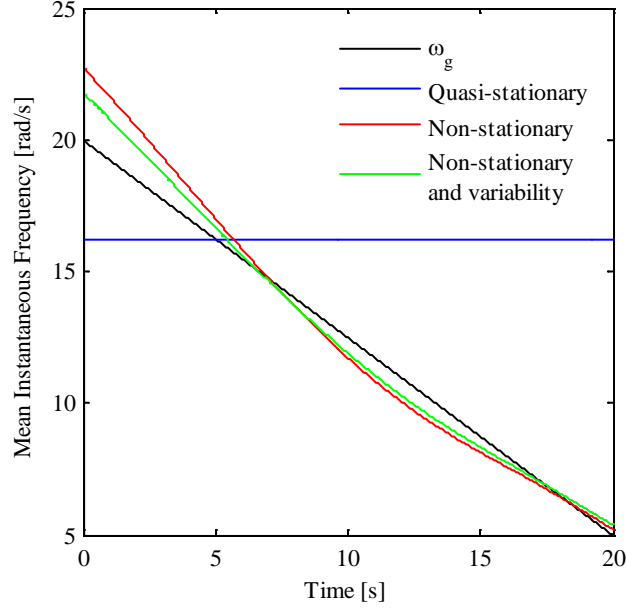


Figure 4.2. Mean instantaneous frequency of the ground motion models adopted in the numerical comparative study on the structural response of benchmark buildings.

Figure 4.2 shows the variation of the mean instantaneous frequency versus the time in order to highlight the differences in terms of non-stationary frequency content of the models adopted, determined according to the expression in equation (2.105).

A number of 500 response-spectrum-compatible ground motion time-histories were generated according to equation (3.77) by setting $N_a=1000$, $\Delta\omega = 0.1$ rad/s and total duration of 20 s. Samples from the quasi-stationary, the non-stationary and non-stationary with imposed variability sets are displayed in Figure 4.3.

The time-histories are baseline corrected (Preumont 1984) adding a polynomial function to the original simulated accelerogram as follows

$$\ddot{u}_g^{BC}(t) = \ddot{u}_g(t) + a_1 + a_2t + a_3t^2 + a_4t^3 \quad (4.3)$$

where $\ddot{u}_g^{BC}(t)$ is the corrected accelerogram, a_1 , a_2 , a_3 , a_4 and a_5 are the polynomial coefficients determined to impose zero end value to the ground motion velocity and displacement time-histories.

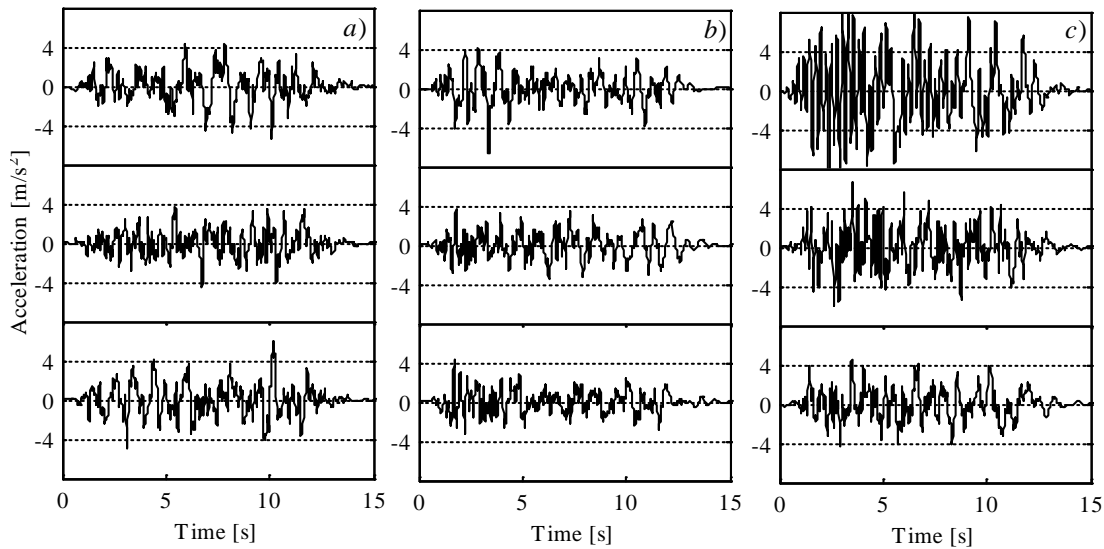


Figure 4.3. Simulated time-histories a) quasi-stationary; b) non-stationary; c) non-stationary with imposed variability.

The average response spectral accelerations of the ensemble of the artificial accelerograms satisfies equation (3.45) as required by EC8 in the range between of periods between 0 and 4s as shown in Figure 4.4. Furthermore, the average of the PGA calculated from the set of artificial accelerograms are: 4.77, 4.62 and 4.97 m/s^2 respectively for the quasi-stationary, non-stationary and non-stationary with imposed variability models, all satisfying the Eurocode 8 condition to be greater than the value $a_g S=4.23 \text{ m/s}^2$ (see equation (3.46)). Remarkably, the three sets of accelerograms fulfil all the requirements of the response spectrum compatibility criteria provided by the Eurocode 8 and possess, within negligible differences (i.e. below 5%), the same 5% damping mean response spectrum and duration of the stationary (amplitude region) part of 10 s. In Figure 4.4 the mean response spectra from the same set of accelerograms for various damping ratios are also depicted. Note that according to Eurocode provisions the accelerograms have to be compatible with the response spectrum defined for 5% damping ratio, even if the structure that need to be analysed possesses a damping ratio different from 5% (Eurocode 8, 2010). The response spectra, for values of damping ratio different from the 5%, are purged by the difference between the non-stationary models and the quasi-stationary one calculated for 5% damping ratio. As a consequence, the difference among them fairly represents the differences between the models as all the sets of accelerograms

possess the same identical mean response spectrum for 5% damping. Interestingly, note that for different damping ratios various differences arise especially in the case of light damping (e.g. <2%).

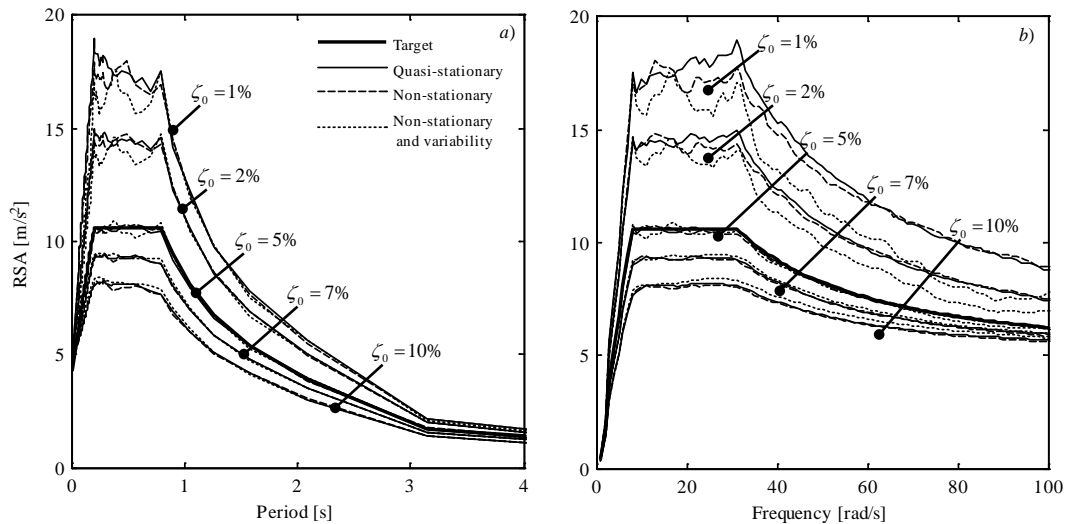


Figure 4.4. Response spectral accelerations with damping ratio variation plotted versus: a) period; b) frequency.

This is likely due to the fact that light damped system possesses a narrow band transfer function and therefore they are more sensitive to local non-stationary contribution of the input. It has to be emphasized that for the simplest linear decaying non-stationary models adopted in this application, can be observed differences respect the non-stationary case of about 20% especially for higher frequencies (see Figure 4.5). Clearly, alternative non-stationary models may provide different results. It is therefore necessary to clarify that on purpose the differences between the results from various ground motion models are labelled as $\Delta\%$ and not as a percentage error. Nowadays, it cannot be stated which is the most accurate model among them. The (amplitude and frequency) non-stationary model selected in this work is only one of the possible feasible models available in literature, and up to now does not exist any non-stationary model universally recognized as the most appropriate for engineering applications.

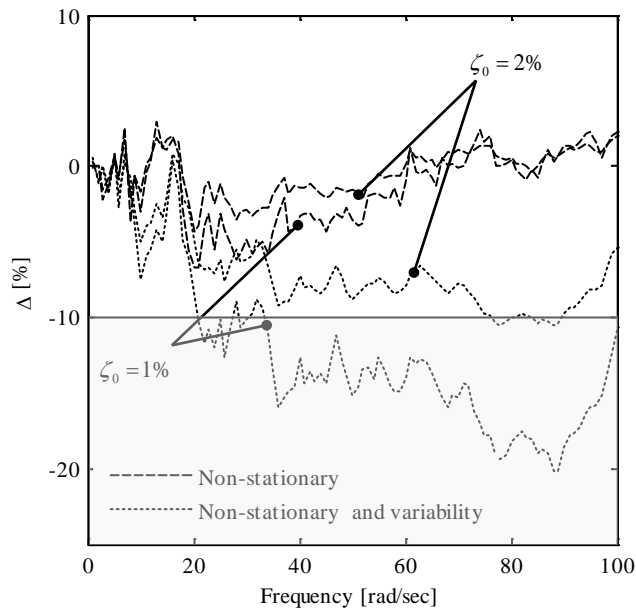


Figure 4.5. Difference percentage of the response spectra for 1% and 2% damping evaluated with respect to the simulated 5% damped response spectra.

4.2 Structural Response and Analysis Tools

In this section, the responses of the three benchmarks are presented, the SMART 2008 reinforced concrete building, the IASC 1996 and the SAC 1996 steel building were carefully chosen to represent respectively rigid, medium and slender structures. The buildings were studied assuming a linear behaviour, whereas the moment resisting frame, the SAC building, has been investigated also in the non-linear range.

4.2.1.1 SMART 2008:2-Storey Reinforced Concrete Building

This structure designed for the “Seismic Design and best estimate methods assessment for Reinforced Concrete Building subjected to Torsion” is known as SMART 2008 project (Lermitte et al. 2008). The reinforced concrete building has been built at CEA Seismic Laboratory of Saclay in France, meeting the seismic French nuclear regulations as well as EC2 and EC8 prescriptions. The model has been implemented in SAP2000 v15.0.1 assuming linear behaviour with a damping ratio equal to 2% for all the modes, Figure 4.6 shows the Finite Element model of the SMART 2008 structure.

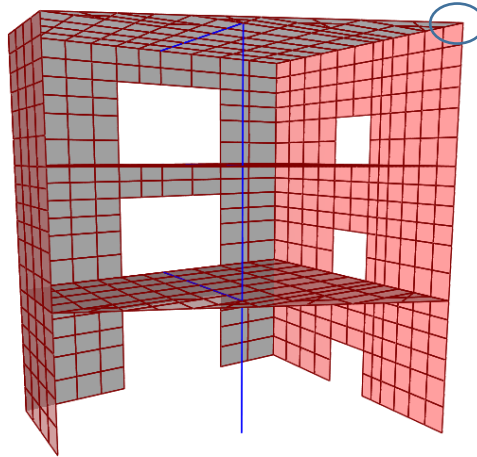


Figure 4.6. SMART 2008 structure: SAP2000 model.

The building is half of a 3-storey structure with trapezoidal plan, pertinent geometrical data are given in Figure 4.7.

The mass of the structure includes the self-weight of the building and the additional loads that are of 12 Tons for the first and the second slab and 11 Tons for the roof. The modulus of elasticity and the unit weight used in the numerical analysis are 3.2×10^{10} N/m² and 2460 kg/m³, respectively (Lermitte et al. 2008). The first two natural frequencies of the structure are 8.9 Hz and 15.9 Hz. The structure has been forced by the three set of accelerograms acting along the x-direction according to the reference system shown in Figure 4.7.

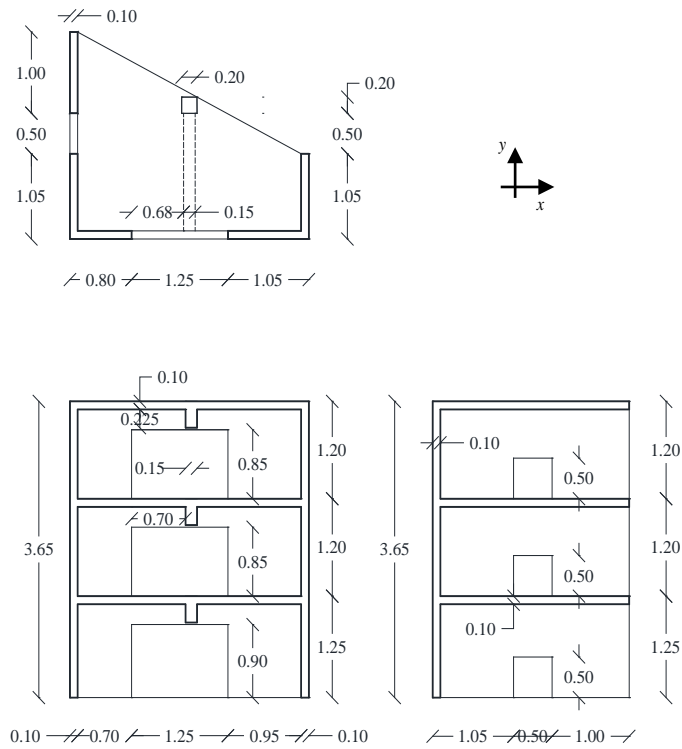


Figure 4.7. Geometrical data of the SMART 2008 structure [m].

In Figure 4.8 the distribution of the maxima of the displacement in the x-direction of the selected node (see circled joint in Figure 4.6) are represented.

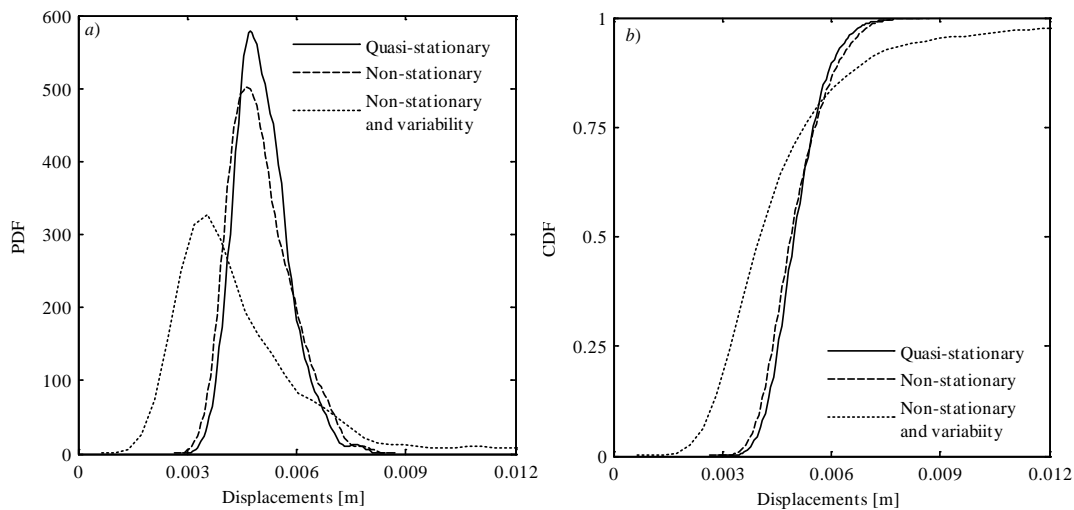


Figure 4.8. SMART 2008 output displacements: a) probability density function; b) cumulative density function.

Relevant statistical response quantities are displayed in Table 4.2. Differences in absolute value of the non-stationary model (Δ_{NS}) and non-stationary with imposed

variability model (Δ NSV) respect to the quasi-stationary model are also reported in Table 4.2.

SMART 2008	Mean	Fractile 5%	Fractile 50%	Fractile 95%
Quasi-stationary	0.0051	0.0040	0.0050	0.0064
Non-stationary	0.0050	0.0039	0.0049	0.0066
Non-stationary and variability	0.0046	0.0025	0.0039	0.0088
Δ NS %	0.8676	3.2997	1.8624	4.1451
Δ NSV %	8.1265	37.1894	20.5808	38.5640

Table 4.2. SMART 2008 structural responses: displacement statistics [m].

It can be observed that the non-stationary model does not provide significant differences with respect to the quasi-stationary case, whereas the non-stationary with imposed variability model presents significant differences in all the relevant statistics. Remarkably, as might be expected, the highest difference is detected for the fractiles and in particular the 95% fractile of the non-stationary with imposed variability model with a value of the 38% higher than the correspondent one for quasi-stationary process.

The convergence of the fractiles of the response is also reported in Figure 3.10. It is noted that Eurocode 8 requires a minimum of 3 accelerograms for the time-history analysis and suggest to use the average of the response quantities if a minimum number of 7 accelerograms are used.

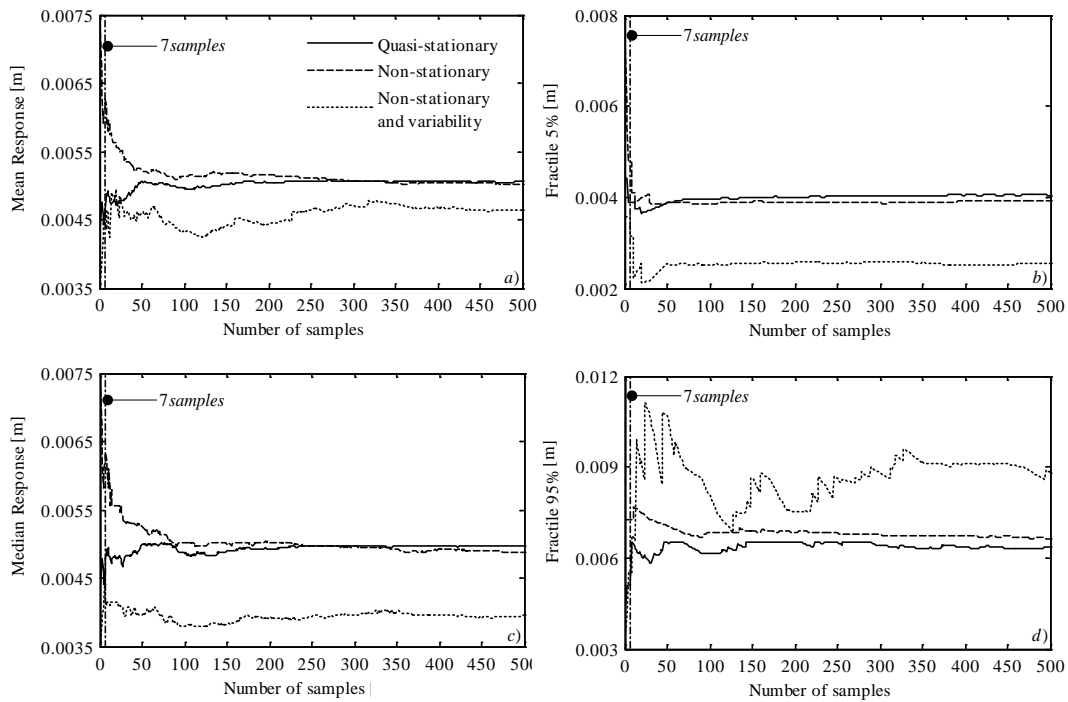


Figure 3.10. SMART 2008 convergence of the output displacement statistics a) mean; b) fractile 5%; median; d) fractile 95%.

From Figure 3.10 it is evident that even for the simplest quasi-stationary case the suggested numbers of accelerograms do not lead to stable statistics.

4.2.1.2 IASC 1996: 5-Storey Steel Frame

The second benchmark structure to be analysed is a 5-storey steel frame IASC 1996 whose stiffness matrix is (Samali 2007, Djajakesukma et al. 2002)

$$K = \begin{bmatrix} 4270 & -3124 & 64 & -1 & 15 \\ -3124 & 6174 & -3156 & 65 & 9 \\ 64 & -3156 & 6174 & -3156 & 74 \\ -1 & 65 & -3156 & 6172 & -3079 \\ 15 & 9 & 74 & -3079 & 2978 \end{bmatrix} \quad (4.4)$$

The structure has been modelled in MATLAB assuming equally concentrated masses at each floor level of 1042 Kg and with damping ratio of 0.2% for all the modes. The first natural frequency is 4.27 Hz. The structure has been forced by the three sets of

accelerograms in the x direction of the referring system shown in the equivalent SAP2000 model depicted in Figure 4.9. The distributions of the maxima displacement of the top floor along the x direction are shown in Figure 4.10

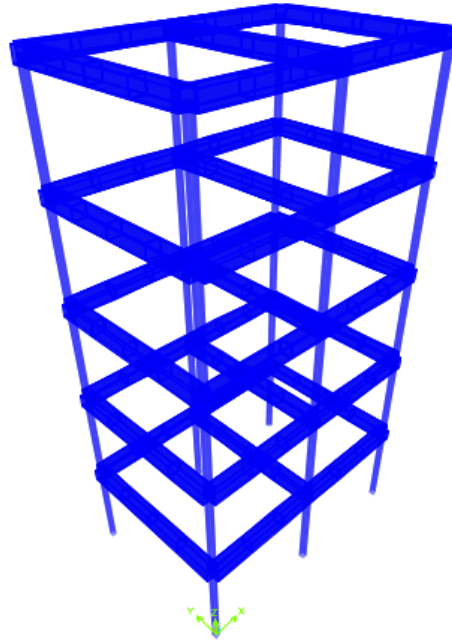


Figure 4.9. 5-storey building: SAP2000 model.

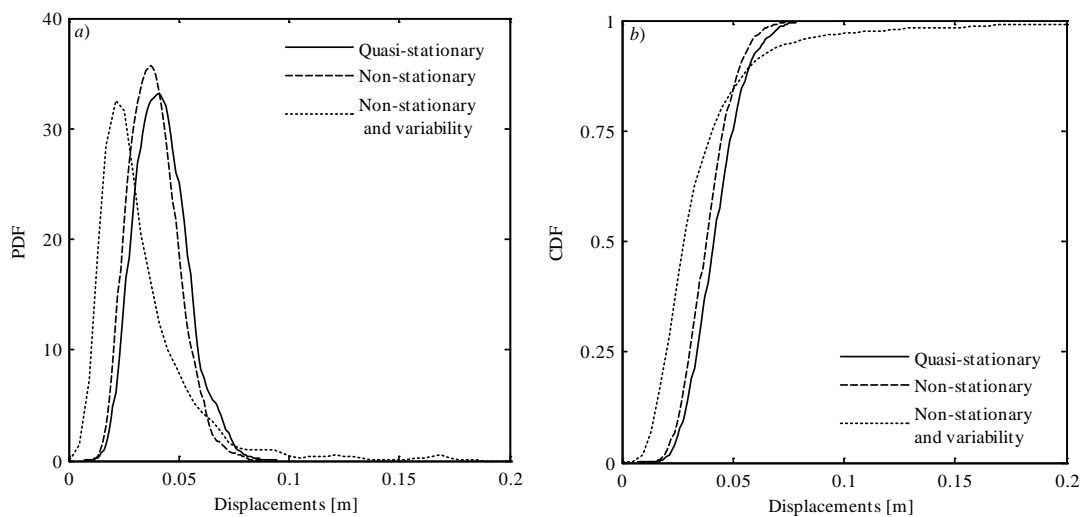


Figure 4.10. 5-storey building output displacements: a) probability density function; b) cumulative density function.

Relevant response data are summarized in Table 4.3. In this case significant differences can be observed with respect to all the fractiles and mean values. Proof of convergence is also reported in Figure 4.11.

5-storey building	Mean	Fractile 5%	Fractile 50%	Fractile 95%
Quasi-stationary	0.0423	0.0260	0.0415	0.0633
Non-stationary	0.0387	0.0234	0.0377	0.0579
Non-stationary and variability	0.0356	0.0139	0.0268	0.0762
Δ NS %	8.4710	9.7425	9.1024	8.5655
Δ NSV %	15.993	46.5767	35.2950	20.3271

Table 4.3. 5-storey building structural responses: displacement statistics [m].

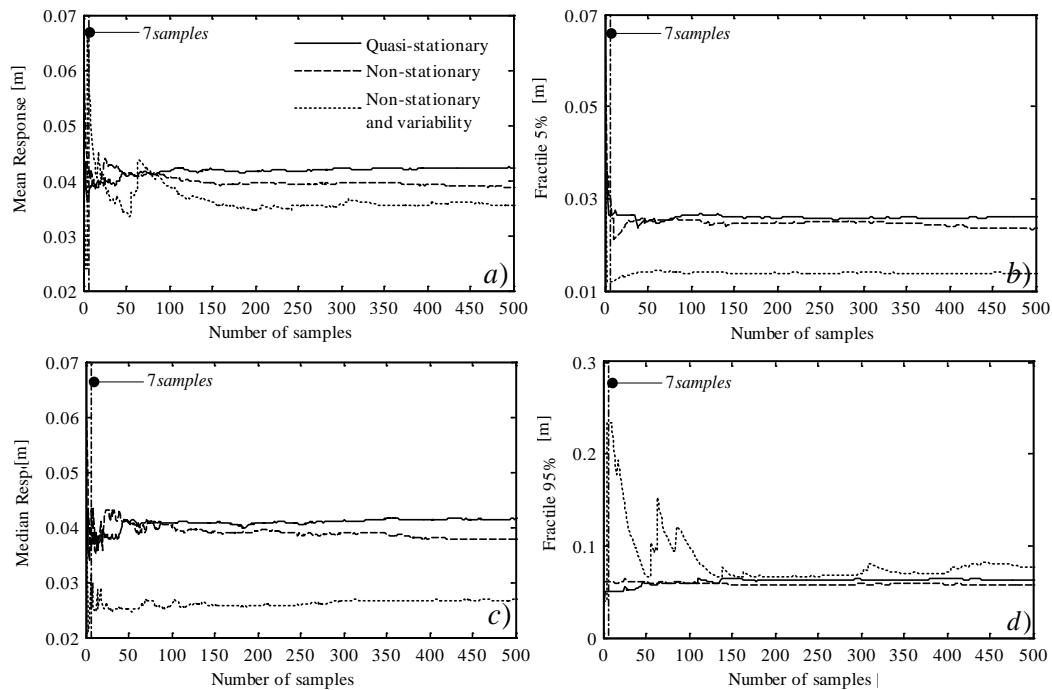


Figure 4.11. 5-storey building convergence of the output displacement statistics a) mean; b) fractile 5%; median; d) fractile 95%.

4.2.1.3 SAC building: 20-Storey Steel Frame

The third benchmark structure analysed is the moment resisting frame for the SAC Phase 2 Steel project designed by Brandow & Johnston Associates (1996). The SAC joint venture aimed to study structural control strategies for non-linear 3, 9 and 20-storey buildings. The 20-storey steel frame shown in Figure 4.12 has been selected and modelled in SAP2000 pertinently with the regulation for the Los Angeles, California region.

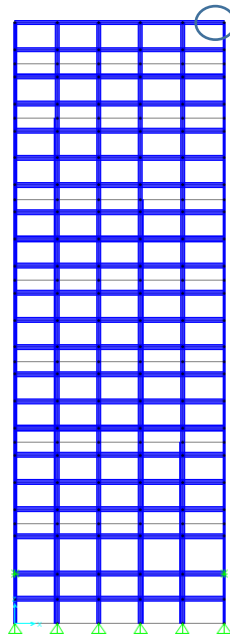


Figure 4.12. SAC building: SAP 2000 model.

The study of the structural response is performed through the 2-dimensional analysis of the moment resisting frame. Geometrical details are reported in Othori et al. (2004). Pertinently with the benchmark presentation the first five natural frequencies of the reproduced model are 0.261 Hz, 0.75 Hz, 1.30 Hz, 1.83 Hz, 2.4 Hz; 2% damping is assigned to the first and fifth frequency according to proportionally damped Rayleigh model.

The linear case is analysed first. Figure 4.13 shows the distributions of the displacement of the top floor for the three different set of accelerograms.

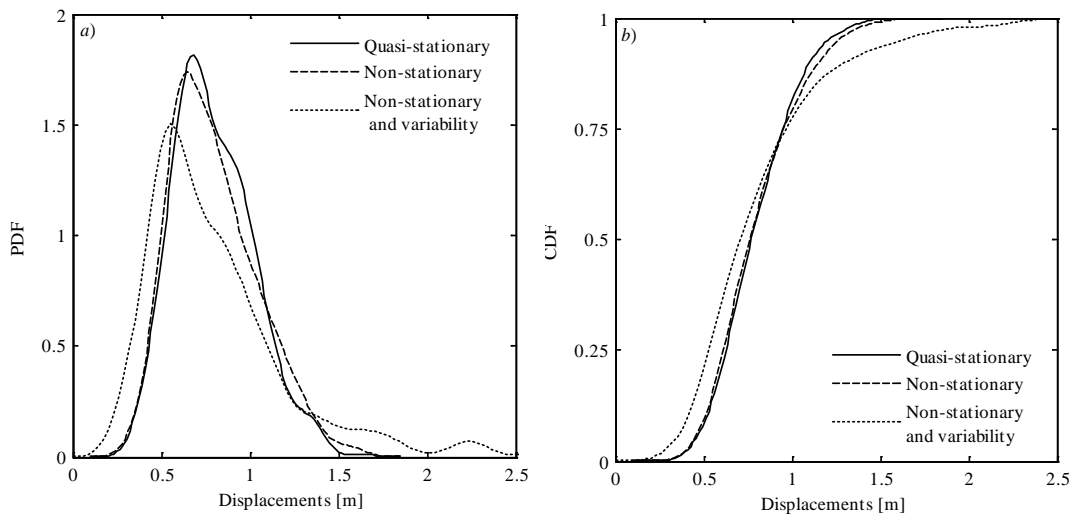


Figure 4.13. SAC building linear model output displacements: a) probability density function; b) cumulative density function.

Relevant results regarding the statistics of the structural response are reported in Table 4.4.

SAC building linear model	Mean	Fractile 5%	Fractile 50%	Fractile 95%
Quasi-stationary	0.7951	0.4747	0.7593	1.1804
Non-stationary	0.7977	0.4746	0.7590	1.2488
Non-stationary and variability	0.7990	0.3743	0.7020	1.6365
Δ NS %	0.3362	0.0212	0.0368	5.7908
Δ NSV %	0.4916	21.1422	7.5480	38.6425

Table 4.4. SAC building linear model structural responses: displacement statistics [m].

Negligible discrepancies can be observed between the quasi-stationary and the non-stationary model, while the non-stationary model with imposed variability provided, as expected, significant differences in the tails leading to a value of the 95% fractile of the response of 38%, also in this case higher than the correspondent one for quasi-stationary input process. This is in contrast with the common understanding that quasi-stationary models lead to over-conservative response with respect to the non-stationary ones. In the light of these results, this general idea should be revised, depending on how the accelerograms are generated. Proof of convergence for the linear model is also reported in Figure 4.14.

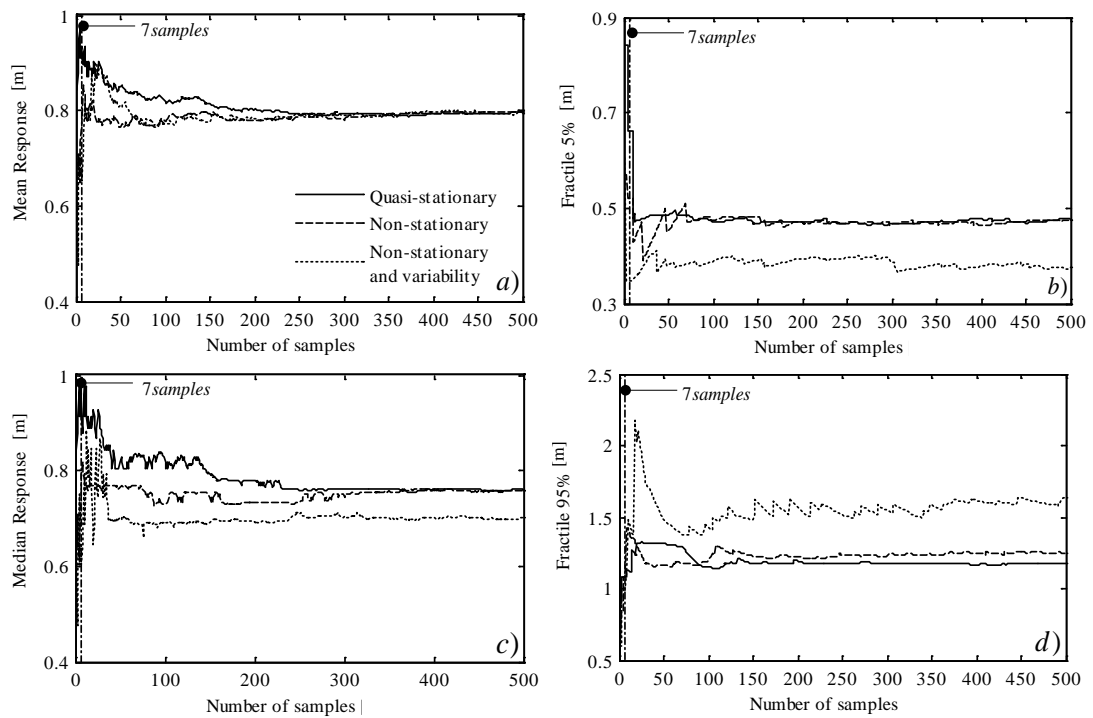


Figure 4.14. SAC building linear model convergence of the output displacement statistics: a) mean; b) fractile 5%; median; d) fractile 95%.

The non-linear time-history analysis has been conducted on the same structure according to FEMA-356 recommendations adopted to define the plastic hinges. The non-linear model associated to the moment-rotation is shown in Figure 4.15.

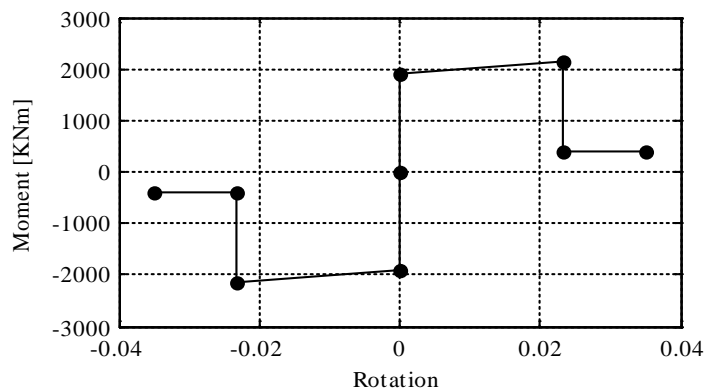


Figure 4.15. Moment-rotation relationship for moment resisting column-beam connection of the analysed node at the roof.

The distributions of the maximum displacements of top floor are reported in Figure 4.16.

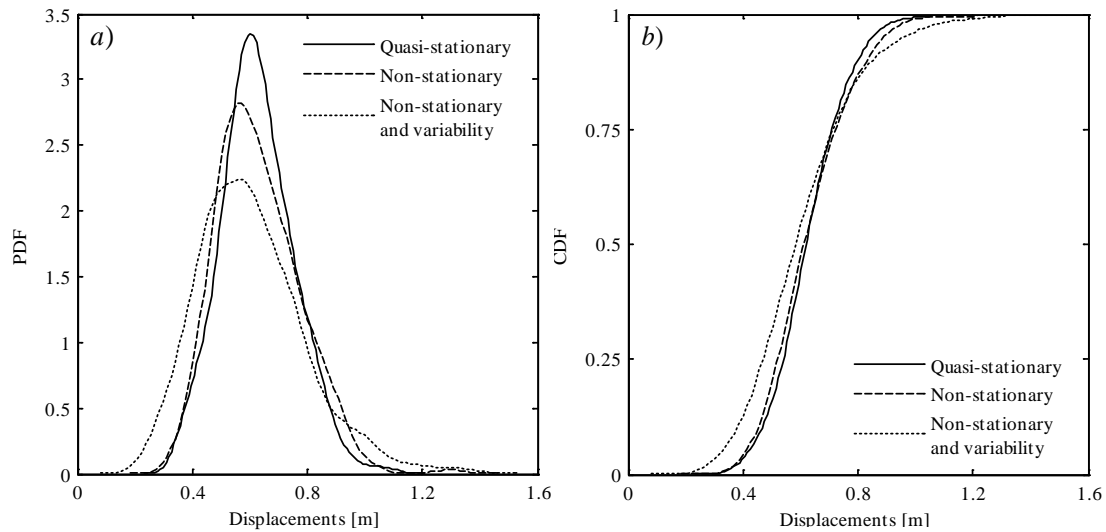


Figure 4.16. SAC building non-linear model output displacements: a) probability density function; b) cumulative density function.

As Table 4.5 summarises, also in this case, significant differences can be observed with respect to the tails especially for the 5% and 95% fractiles. Interestingly for this case, the discrepancies between the 95% fractile in the case of linear and non-linear model are more evident in the linear case, again in opposite of the general view that the non-stationarity of the ground motion models is more relevant for non-linear behaving structures.

SAC building non-linear model	Mean	Fractile 5%	Fractile 50%	Fractile 95%
Quasi-stationary	0.6275	0.4277	0.6183	0.8359
Non-stationary	0.6283	0.4208	0.6064	0.8841
Non-stationary and variability	0.6041	0.3354	0.5861	0.9624
Δ NS %	0.1319	1.6049	1.9261	5.7702
Δ NSV %	3.7272	21.5823	5.2093	15.1320

Table 4.5. SAC building non-linear model structural responses: displacement statistics [m].

Proof of convergence is also reported in Figure 4.17. It is observed that for non-linear time-history analysis the statistics of the response converge more slowly in comparison to the linear case. Remarkably the minimum number of 7 accelerograms for the non-linear time-history analysis to use the average of the response quantities

should be significantly increased (e.g. 100 samples), especially if higher order statistics, such as the fractile 95% is used for design purpose.

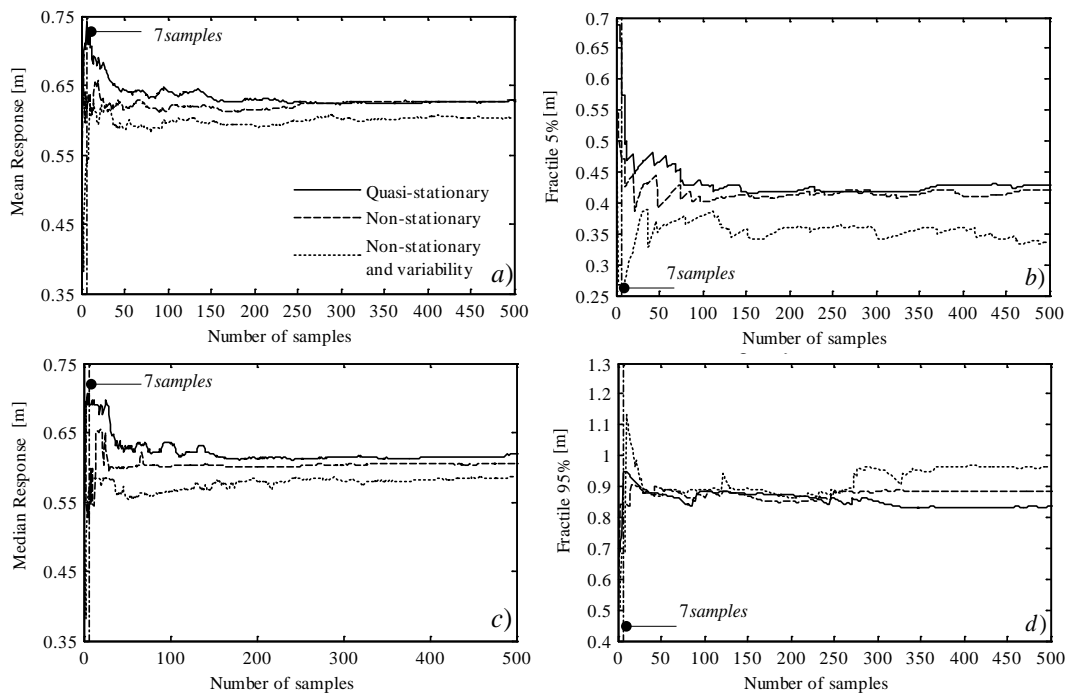


Figure 4.17. SAC building non-linear model convergence of the output displacement statistics: a) mean; b) fractile 5%; median; d) fractile 95%.

4.3 Concluding Remarks

In this Chapter, the seismic analysis of structural systems forced by response-spectrum-compatible accelerograms simulated according to the Eurocode 8 provision has been presented in a numerical comparative study. Three different stochastic ground motion models (i.e. quasi-stationary, non-stationary and non-stationary with imposed variability, without accounting of the spectral correlations a different periods) have been adopted, generated using the proposed simulation technique presented in Chapter 3. The ground motions possess common features, namely: the same mean 5% damping response spectrum, PGA, strong motion phase and the total duration.

By comparing the structural responses of three benchmark buildings forced by sets of accelerograms simulated according to the proposed technique, it has been highlighted that even if the Eurocode 8 provisions have been fulfilled, the

distribution of the relevant response parameters such as the peak displacement are sensibly different for the three models adopted; differences of about 30-40% of the response fractiles are observed. This result manifests the weakness of the response-spectrum-compatible criteria prescribed by international seismic codes.

Moreover, it has been shown that the response of structures having damping ratio smaller than the nominal 5% (used as a target) is sensitive to the non-stationary model adopted in the simulation. Furthermore, the general view that the non-stationarity of the ground motion models is more relevant for non-linear behaving structures than for the linear case should be revised, as the results shown in this Chapter demonstrate that the opposite condition is possible. Finally, the general accepted understanding that quasi-stationary models lead to over-conservative response compared to the non-stationary model should be also revised, as it depends on the strategy used to generate the accelerograms. The findings provided in this Chapter enforce the importance to define reliable non-stationary models for ground motion simulations, which up to now has been highlighted only for non-linear behaving structures and the necessity to review the seismic code provisions with regard to the time-history representation of the ground motion.

The contribution provided in this Chapter has demonstrated the influence of the selection of ground motion processes whether for linear and non-linear system and the different level of sensitivity to the structural damping variation of the structural responses due to the different hypothesis regarding the ground motion models. These considerations are the basis for the investigations following in the next chapters in which the response of Structure-Soil-Structure Interaction (SSSI) systems is analysed under the same stochastic models of earthquake excitation.

5 Structure-Soil-Structure-Interaction

Overview

In Chapter 4 the influence of the non-stationarity of the seismic action on the stochastic response of selected benchmark buildings has been scrutinised. The buildings forced by the simulated response-spectrum-compatible earthquakes have been investigated under the hypothesis of fixed base and rigid soil, i.e. without accounting of the effects of the Soil-Structure-Interaction (SSI). The SSI, phenomenon encompassed by the Structure Soil-Structure-Interaction (SSSI) are presented in this Chapter to provide the background principles on which the Vibrating Barriers' design is funded.

The Vibrating Barriers' design is based on the principle of the SSSI, which is exploited to reduce the response in buildings by taking advantage of the possible beneficial effects that the mutual interaction among neighbouring structures may induce, to one or more structures in the same cluster. To achieve the aim of this work, in the study of multi structure systems (i.e. ViBa and a building to protect), the modelling of the SSSI, as well as the effects induced by the SSI, have been undertaken.

In this Chapter, firstly the fundamentals of the SSI during earthquake ground motion are introduced; the effects induced on engineering systems by the SSI, and the methods adopted to evaluate them are described. Successively the SSSI phenomenon is described in the Chapter along with a literature on the subject. In the review, particular attention is provided to the discrete models, whose formulation is adopted in this research to pursue the investigations. The literature on the discrete SSSI model is attempted along with the works tackling their studies by the experimental and stochastic approach.

5.1 Fundamentals of Dynamic Soil-Structure-Interaction (SSI)

The following sections present the basic principles and methods adopted to study and account of the Soil-Structure-Interaction (SSI) for engineering applications. From the late 19th century the field of SSI has progressed involving a wide range of disciplines as both structural and geotechnical earthquake engineering (see e.g. Kausel 2010). In the last 50 years, the SSI developments have been supported by the growth of powerful computational and numerical methods, enhancing the capability of analysing and predicting the phenomenon for several applications. Particularly, the seismic design of Nuclear Power Plants has considerably encouraged the research on the subject (Roesset 2013).

Principally there are two ways to approach to SSI problems: (i) to represent the structure as an elastic block and to describe the soil as a continuum half space body, (ii) to assume the soil as a bed of springs or by rigid boundaries (see e.g. Woods and Deek 2004). In the next sections both approaches are covered by following the established division of the problem onto static and dynamic SSI.

5.1.1 Overview of SSI in Earthquake Engineering

Two fundamental problems arise for SSI problems during earthquake excitation, the first concerns the soil effects on the dynamic stiffness of the structure soil foundation system, and the second is the evaluation of the effective input motion acting on the foundation.

According to the approach proposed by Wolf (1985), the simplistic model for dynamic analysis of SSI is herein presented; through this approach the global system is assumed to be formed of a SDOF characterized by the mass m , the stiffness k and the hysteretic damping c , placed on a massless L-shaped rigid foundation. The foundation's compliance is described through translational and rotational dashpots represented by the damping coefficients c_h and c_r , and by the translational and

rotational springs respectively with stiffness k_h and k_r (Kramer 1996). Figure 5.1 shows the idealized described discrete system.

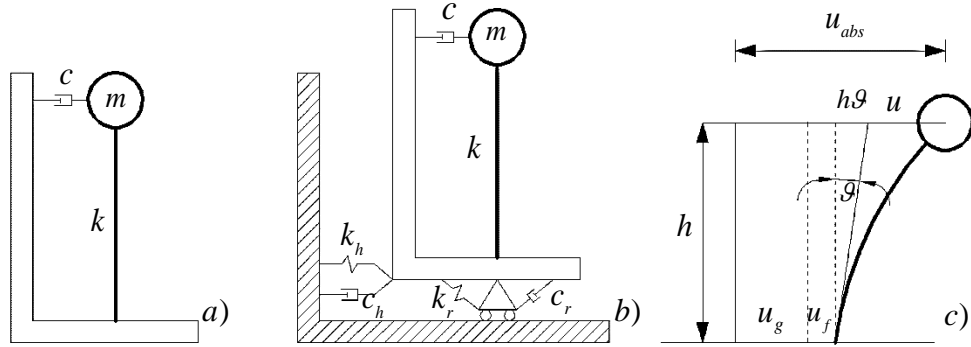


Figure 5.1. Model with: a) SDOF system on elastic soil deposit; b) idealised discrete system with representation of the translational and rotational springs and dashpots; c) components of motion (Kramer 1996).

The equation of motion in the time domain of the SDOF system depicted in Figure 5.1, can be generalized according to equation (1.1) assuming an equivalent stiffness k_e and damping coefficients c_e , that is

$$m\ddot{u}_{abs}(t) + c_e\dot{u}_{rel}(t) + k_e u_{rel}(t) = 0 \quad (5.1)$$

where $u_{rel}(t)$ are the displacements of the lumped mass relatively to the base of the oscillator and $u_{abs}(t)$ the total absolute displacements, that are

$$u_{abs}(t) = u_g(t) + u_f(t) + u_{rel}(t) \quad (5.2)$$

where $u_g(t)$ is horizontal ground displacement, $u_f(t)$ is the horizontal foundation displacement and $u_{rel}(t)$ is

$$u_{rel}(t) = h\vartheta + u(t) \quad (5.3)$$

where $u(t)$ are the horizontal relative displacements of the mass due to the translational motion of the foundation while $h\vartheta$ are the relative displacements due to the rocking of the foundation.

Equation (5.2) can be rewritten as a summation of the mass displacements relative to the base and the displacements of the foundation with respect to the original position

$$u_{abs}(t) = u_{0,abs}(t) + u_{rel}(t) \quad (5.4)$$

where $u_{0,abs}(t)$ are the absolute displacements of the foundation equal to

$$u_{0,abs}(t) = u_g(t) + u_f(t) \quad (5.5)$$

Therefore substituting equation (5.4) into (5.1), it follows that

$$m[\ddot{u}_{0,abs}(t) + \ddot{u}_{rel}(t)] + c_e \dot{u}_{rel}(t) + k_e u_{rel}(t) = 0 \quad (5.6)$$

In the frequency domain, the dynamic equilibrium of the equivalent SDOF system for which translational and rocking motion are accounted, is obtained after taking the Fourier Transform of (5.6) and rearranging the terms as follows

$$(-m\omega^2 + i\omega c_e + k_e)U_{rel}(\omega) = m\omega^2 U_g(\omega) \quad (5.7)$$

where $U_g(\omega)$ according to the Fourier Transform of equation (5.5) represents the equivalent seismic input motion given by the combination of the horizontal ground displacement $U_{0,abs}(\omega)$ and the foundation displacement $U_f(\omega)$; $U_{rel}(\omega)$ are the relative displacements of the lumped mass with respect to the original configuration of the foundation.

It has to be noticed that the equivalent system does not take into account the mass of the foundation.

The equivalent natural frequency of the system described, can be expressed as the frequency at which the response of the system goes to infinity when $\zeta_e = 0$; for which the following expression holds

$$\frac{1}{\omega_e^2} = \frac{1}{\omega_0^2} + \frac{1}{\omega_h^2} + \frac{1}{\omega_r^2} \quad (5.8)$$

where the natural frequencies ω_e , ω_0 , ω_h and ω_r are respectively for: the equivalent system, the fixed-base system, the translational motion and the rocking motion.

The natural frequency for translational vibration ω_h can be determined assuming the condition of infinitely rigid structure and the foundation is unable to rotate, therefore the frequency would depend on the translational stiffness of the foundation only according to the following equation

$$\omega_h = \sqrt{\frac{k_h}{m}} \quad (5.9)$$

Whereas, in order to express the natural frequency for rocking ω_r , the case of infinitely rigid structure on foundation unable to translate has to be considered, from which the natural frequency of the system would depend only on the rotational stiffness of the foundation according to the following

$$\omega_r = \sqrt{\frac{k_r}{mh^2}} \quad (5.10)$$

where h is the position of the lumped mass with respect to the foundation.

By substituting the expressions of the natural frequencies in equation (5.8), according to equation (2.4), (5.9) and (5.10), equation (5.8) becomes

$$\omega_e = \frac{\omega_0}{\sqrt{1 + k/k_h + kh^2/k_r}} \quad (5.11)$$

The equation above shows the first important effect of the SSI of reducing the frequency of the system with respect to the system with fixed base.

Hysteretic damping

The damping is defined as the mechanism of removal of energy from an oscillating system, it is conveniently measured by the loss factor, which represents the energy lost per cycle of motion with respect to the peak potential energy stored in the systems, that reads

$$\eta = \frac{\Pi}{2\pi V} \quad (5.12)$$

where Π and V are respectively the total energy lost in a cycle and the peak potential energy stored in the system in that cycle.

The energy of a system dissipated in a cycle of harmonic vibration under the hypothesis of linear viscous damping, with damping force $f_D = c\dot{u}$, is given as follows (Chopra 2007)

$$\begin{aligned} \Pi &= \int f_D du = \int (c\dot{u})u dt = \\ &= c \int_0^{2\pi/\omega} [\omega u_0 \cos(\omega t - \phi)]^2 dt = \pi c \omega u_0^2 = 2\pi \zeta \frac{\omega}{\omega_0} k u_0^2 \end{aligned} \quad (5.13)$$

where the energy dissipated results to increase linearly with excitation frequency.

Commonly the actual structural damping is idealised by linear viscous dampers or dashpots since these allow the governing differential equation of motion to maintain linearity, this advantage balances the approximation on the mechanism of energy dissipation which is highly complex.

The damping is due partially to the phenomena of radiation energy, for instance related to the geometry of the system and to the coupling with external factors. Moreover, the dissipation of energy is influenced by the material properties and their characteristics, as the plasticity and viscosity, and importantly also by the frequency of the oscillations. Major difficulties are involved to model the damping effects on the response of dynamic systems, for which the linear hysteretic damping model is widely employed if the non-casualty requirement is satisfied (Crandall 1969).

Mainly, this complex phenomenon classifies in two main mechanisms, the first is called geometrical damping, which depends on the extension of the material, the second is the material damping, related to the intrinsic characteristic of the medium.

Concerning the material damping in soils, the Kelvin-Voight model is usually considered under the hypothesis of visco elastic wave propagation. The Kelvin-Voight model consider the resistance to shearing deformation as the sum of an elastic spring k and a viscous dashpot c , which establishes the proportionality between the dissipative force and the velocity. The model assumes the energy dissipation to be proportional to the frequency of the loading, real soils however dissipate energy hysterically, with energy dissipation insensitive to the frequency.

The simplest way to model rate independent linear damping during harmonic motion is assuming the damping force at frequency ω as follows (Chopra 2007)

$$f_D = \frac{\eta k}{\omega} \dot{u} \quad (5.14)$$

which compared to the viscous damping force implies the viscous damping coefficient is

$$c = \frac{\eta k}{\omega} \quad (5.15)$$

Substituting equation (5.14) into (5.13), the energy lost per cycle for frequency independent linear damping is

$$\Pi = \pi \eta k u_0^2 \quad (5.16)$$

which is independent of the forcing frequency and that satisfies equation (5.12).

For ideal dampers under harmonic excitation in resonant or near-resonant motion the damping coefficient for viscous damping equivalent to the actual damping can be expressed by equating (5.13) with equation (5.12), that gives

$$\zeta_e = \frac{\Pi}{4\pi V} \quad (5.17)$$

Considering that the potential energy stored in a cycle of motion is $V = ku_0^2 / 2$, and substituting it along with equation (5.16) into equation (5.17), it follows that

$$\eta = \frac{c\omega}{k} = 2\zeta_e \quad (5.18)$$

The frequency independent damping η is real, non-negative and even and associated to the equivalent viscous damping ratio ζ_e through a constant value.

Considering the equivalent SDOF system involved in the SSI in Figure 5.1, under the assumption of hysteretic damping both material and the radiation damping can be modelled; the damping ratio relatively to the material damping is named ζ_g and ζ_x for the radiation damping in the horizontal direction. The equivalent viscous damping coefficient c_e in equations (5.1) according to equation (5.18) reads

$$c_e = \frac{2k_e\zeta_e}{\omega} \quad (5.19)$$

in which $k_e = m\omega_e^2$.

Being the damping assumed to be influenced by the radiation and material mechanism, the damping coefficient relatively to the horizontal direction of the motion can be written as

$$c_h = c_x + \frac{2}{\omega} \zeta_g k_x \quad (5.20)$$

where c_x correspond to the radiation damping and the second part of the expression is the contribution of the material damping.

The damping coefficient for the rotational component of the SDOF response can be written as

$$c_r = c_\theta + \frac{2}{\omega} \zeta_g k_\theta \quad (5.21)$$

where c_θ is the contribution of the radiation damping and in the second part of the expression represents of the radiation damping.

The equivalent hysteretic damping by neglecting the second order terms is

$$\zeta_e = \frac{\omega_e^2}{\omega_0^2} \zeta_0 + \left(1 - \frac{\omega_e^2}{\omega_0^2}\right) \zeta_g + \frac{\omega_e^2}{\omega_h^2} \zeta_x + \frac{\omega_e^2}{\omega_r^2} \zeta_\theta \quad (5.22)$$

Another important effect of the SSI is expressed by the above equation, which shows that the damping ratio of the equivalent system is larger than the damping ratio of the structure with fixed base.

5.1.2 Soil-Structure-Interaction Effects and Methods of Analysis

In the context of engineering analysis and design, the SSI effects are categorised in

- Inertial interaction: related to the mass of the structure whose vibrations determine shear and moment inducing the displacements of the foundation relatively to the free field.
- Kinematic interaction: associated with the stiffness of the structure, which specifically causes deviation from the free field motion.

Two are the general methods adopted in earthquake engineering to perform SSI analysis, these are the direct approach and the substructure approach. By direct methods the soil and the structure are analysed in a single step, whereas via the substructure approach, the problem is broken down leading to a multistep method's typology.

Direct analysis

Once the soil has been discretized according to finite element modelling the equation of motion of the combined system structure and supporting soil; these analyses allow

to model non-linearities although the expensive computational costs and the small advantages compared to equivalent linear methods (see e.g. Stewart et al. 1999).

The equation of motion for the combined SSI system can be expressed in a matrix form as follows

$$\begin{bmatrix} \mathbf{M} & \mathbf{M}_g \end{bmatrix} \begin{bmatrix} \ddot{\mathbf{u}}(t) \\ \ddot{\mathbf{u}}_g(t) \end{bmatrix} + \begin{bmatrix} \mathbf{C} & \mathbf{C}_g \end{bmatrix} \begin{bmatrix} \dot{\mathbf{u}}(t) \\ \dot{\mathbf{u}}_g(t) \end{bmatrix} + \begin{bmatrix} \mathbf{K} & \mathbf{K}_g \end{bmatrix} \begin{bmatrix} \mathbf{u}(t) \\ \mathbf{u}_g(t) \end{bmatrix} = \mathbf{0} \quad (5.23)$$

where the vectors of the motion are partitioned by input and output as well as the mass, stiffness and damping matrices, whose subscript g denotes the partition for representing the coupled forces due to the motion of the supports.

A review of the art regarding the direct methods is available in the work of Shah et al. (2011) enlightening the efficiency of the direct methods for simple analysis while for non-linear analysis the substructure methods, presented in the next paragraphs, are more effective as well as simple to apply.

Substructure analysis

The substructure approach adopts the superposition method in order to combine the effects for the overall system broken down into parts. The substructure approach can be divided into the following steps:

- Expressing the equations of motion of the global system according to the principle of superposition of the effects by determining the equilibrium for each substructures; the unknowns, as many as the number of equations to describe the global equilibrium, are: the mass displacements $u(t)$ of the mass m of the SDOF relative to the base, as seen in equation (5.3), the rotation \mathcal{G} is of the foundation with mass m_0 and the basement's displacement induced by the SSI, $u_0(t)$.
- Evaluating the impedance functions (dynamic stiffness functions) from the equations of motion obtained from step 1. The impedance functions are complex valued, these can be expressed as follows

$$\mathbf{K}_{dyn}(\omega) = \text{Re}[\mathbf{K}_{dyn}(\omega)] + \text{Im}[\mathbf{K}_{dyn}(\omega)] \quad (5.24)$$

where $\text{Re}[\cdot]$ and $\text{Im}[\cdot]$ are respectively the real and the imaginary part.

By inverting the impedance functions, the compliance functions are defined to characterise the dynamic flexibility the SSI system.

5.2 State of the Art of Structure-Soil-Structure-Interaction (SSSI)

Several authors observed that during earthquakes closely spaced buildings mutually influence their structural responses (Clouteau and Aubry 2001, Wang et al 2013), this phenomenon may impact on dense populated cities. The interaction among neighbouring buildings is activated by the soil deposit of the site under consideration motivating the site-city interaction studies, which focus on the modification of the urban wave field during the earthquake (Semblat et al. 2002, Kham et al. 2006). The site-city interaction represents a challenging trend of investigations in earthquake engineering, supported and encouraged by the development of numerical methods for analysis of structures and by powerful commercial software. The cross interaction among neighbouring buildings is not considered for analysis and design of structures by any design code; however due to the present urban growth, the implication of the SSSI in cities creates motivation for overcoming the current knowledge limitations of the phenomenon.

Up to now the dynamic cross interaction among structures has been observed analytically, numerically and experimentally mostly in a small scale, a recent review of the state of the art of the topic can be found in the work of Lou et al. (2011). Warburton et al. (1971) and Luco and Contesse (1973) are the pioneers of this field of study having established the mathematical foundation of the dynamic mutual interaction among structures. The theories of Warburton et al. (1971) and Luco and Contesse (1973) are based on the principles of wave propagation. Warburton et al. (1971) developed a theory by which the responses of two identical masses attached upon an elastic medium is evaluated; one of the two masses is excited by a vertical harmonic force, and the dynamic responses of both masses have been observed. Successively Luco and Contesse (1973) enabled the analytical prediction of the

responses of two infinite shear walls, which were investigated when singularly excited firstly and when simultaneously subjected to the seismic loading. The response of the systems was evaluated and compared through a parametric study in which stiffness, height and distance between the walls are varying; the investigation discloses that the displacements of the smaller mass are significant when the taller mass is placed in its proximity. The taller system induces disadvantageous effects on the response of the smaller wall, the sway broadcasting on the wave field amplifies the vibrations of the smaller and reduces the response of the taller structure. This is the beneficial effect that the SSSI may induce to structural systems under vibrations within the same wave field. The dynamical characterization of the soil structure cross interaction was pursued also by Kobori et al. (1973). The authors defined the dynamical ground compliance matrix of two type of structural system of masses supported on a multi foundation. The cross interaction effects result to be influenced by the fundamental frequency of the soil, the type of excitation and the dynamical characteristics of the structures. After Luco and Contesse (1973), Wong and Trifunac (1975) studied the vibrations of nearby shear walls; the last mentioned authors extended the number of the systems involved in the mechanism of interaction under SH-type vibrations. Successively the numerical investigations of Betti (1977) examined the effects of the dynamic interaction among multiple three dimensional embedded foundations. The authors' formulation evidences the effects of the distance on the interaction mechanism; it is by increasing the distance between the foundations that respective structural responses tend to the isolated case of single foundations. From all the presented studies emerges that several are the factors influencing the mechanism of cross interaction in neighbouring buildings (e.g. the size, height, distance, soil type, base of the foundations), and that this field of research is a wide area to explore.

Mulliken and Karabalis (1998) proposed a discrete formulation to capturing the effect of the interaction between two foundations, the FSFI, and among a set of three adjacent buildings coupled by SSSI. The buildings are SDOF with lumped masses, placed on separate rigid foundations connected through frequency-independent springs. The damping is modelled by dashpots and the soil-foundation interaction is

accounted in the model. The frequency-independent stiffness and damping coefficients to describe the stiffness and the viscous elements coupling the foundations of the set building-foundation systems are calibrated for two identical 3D square foundations to define the coupling terms in order to account of the SSSI phenomenon. Mulliken and Karabalis (1998) assume the mutual independency of each mode of vibration and consider independent SFI among the foundations underneath each building. In order to consider the non-linearity of soil and structures a modified Wilson θ -method is employed to solve the equations of motion of the structural systems forced by dynamic loading. Results show that each of the coupled structures are significantly altered by the presence of the neighbouring structures. Naserkhaki and Pourmohammad (2012) investigated the effects on the response of two shear buildings taking into account SSI and SSSI effects; the buildings are modelled by assuming lumped masses for each floor, the underlying soil by a discrete visco-elastic homogenous half space. The authors propose an analytical approach to perform numerical analyses in which the equilibrium of the system is considered with respect to the translation and rotation around the centre of gravity of the soil. The mass, damping and stiffness values characterising the SSSI and SSI effects were assumed according to the work of Mulliken and Karabalis (1998). The numerical study presented has been pursued by Newmark's linear acceleration step-by-step procedure which investigated the soil effect on the buildings period and on the responses as well as the SSI and SSSI effects on them. With regard to the latter, the authors estimated dominant effects due to the SSI than SSSI on the structural responses. By varying the inter-building distance, the SSSI showed to be beneficial: the effects of the soil on the response are reduced for closer distances, while by incrementing the separation distance the SSSI and SSI determine similar responses. Therefore, the mutual interaction among the buildings can reduce the consequences due to SSI. The authors carried out investigation also on a group of buildings, for which it is shown that the buildings responses are more influenced by the adjacent structure. The evidences provided by the theory proposed by Luco and Contesse (1973) have been recently considered in the investigations of Alexander et al. (2012). The authors developed a discrete analytical model of a pair of closely spaced building placed on superficial foundations. In this work the SSSI mechanism

is encountered through a rotational spring governed by an inverse cubed power law fitted by means of computer simulations (i.e. FE analysis with PLAXIS and MATLAB CALFEM toolbox). In this section, further details on the model proposed by the authors are provided with regard to the use of discrete models for SSSI analysis.

In the last 20 years, the nuclear industry has shown particularly interest on understanding the possible implications of the *cross dynamic interaction* on adjacent buildings. Massive auxiliary structures often stand close to reactor buildings, hence experimental and shaking table tests have been supported. In order to assess the adequacy of nuclear power plants in Japan, in 1994 the Nuclear Power Engineering Corporation (NUPEC) launched a project which at the earliest stage aimed to investigate the Soil-Structure-Interaction (SSI) phenomenon. Model and shaking table tests have been carried out to understand the influence on the response of a turbine building after the construction of a bigger sized reactor building placed nearby (Kitada et al. 1999). The Cross Dynamic Interaction mechanism is proven by the alteration of the resonance curves relatively to the first building initially standing alone. Furthermore, the considerable change in the energy content of the earthquake acceleration observed at the top of embedded twin buildings has been observed and further investigated by Clouteau et al. (2012). Clouteau and co-authors validated with FEM and FE/BE coupled methods in the context of both SSI and “dynamic cross interaction” the experimental results from the NUPEC project. Their numerical studies confirmed the importance of the stiffness of the first soil layer underneath the buildings, which results to be governing the cross interaction; their models confirmed the different effects between embedded and superficial closely spaced foundations. Specifically, considering the coupled system, a reduction of the 30% has been detected at the top of the second building with respect to the response obtained for the same building by forcing the first building only considering uncoupled conditions.

5.2.1 Discrete Models

In this section, among the analytical discrete models presented in the introduction to the state of the art on SSSI, the works of Mulliken and Karabalis (1998) and Alexander et al. (2012) are elucidated. Specifically, the review of discrete models hereafter poses particular attention on the formulation of the coupling coefficients for the foundation-soil-foundation interaction; as the model analysed by Naserkhaki and Pourmohammad (2012) adopted the coupling coefficients according to Mulliken and Karabalis (1998), the authors' work is not explained in further details in this section.

Generally, discrete structural models for analysis of structures are formulated to reduce the computational costs with respect to those involved in continuous analytical and numerical solutions by FEM or BEM; however discrete models still guarantee a suitable level of accuracy. In the case of analysis of SSSI system, the use of discrete systems results highly advantageous considering the complexity of the problem formulation and the high number of variables involved. It has to be noticed that several approximations are considered in order to reduce complex systems to discrete models and that the main challenge is to define the parameters that characterise the interaction. The SSI (i.e. foundation-soil interaction) is generally included in the formulations.

Mulliken and Karabalis (1998) developed a model for dynamic cross interaction among adjacent rigid foundations using a translational spring models. The discrete rigid surface square foundations have frequency independent springs and dashpots and are placed on homogeneous isotropic linear elastic half space, whose mass, stiffness and viscous damping matrices are characterised in order to perform time domain analysis. In order to perform the integration of the equations of motion in the time domain, the authors proposed a modified Wilson θ method. The traditional step-by-step procedure was modified to cope with the following assumption: (i) the static stiffness of each foundation is unchanged by the presence of the other foundations, (ii) a time lag is assumed between the response of one foundation and the response induced by the same foundation on the other ones. Mulliken and

Karabalis (1998) based their discrete model on the following hypotheses: (i) the coupling between the foundations for each mode is independent of the others' DOF, (ii) the static stiffness of each foundation-soil system is not affected by the presence of the other foundations, (iii) the time lag of the response is related to the shear or longitudinal wave velocity, i.e. dependency on the shear wave velocity for the vertical, rocking and torsional motion, on the longitudinal wave velocity for horizontal motion. In order to model the SSI relative to each foundation, the authors adopted a combination of coefficients from the literature for defining pertinent mass, stiffness and damping matrices. In Table 5.1 inertia of the soil, the stiffness and damping coefficients are presented.

Motion	Inertia ratio β	Equivalent radius r_0	Virtual soil mass m_v	Static stiffness K	Damping C
Vertical	$\frac{(1-\nu)}{4} \frac{m}{\rho r_0^3}$	$\frac{2a}{\sqrt{\pi}}$	$\frac{0.27m}{\beta}$	$\frac{4.7Ga}{1-\nu}$	$\frac{0.8G}{v_s} K$
Horizontal	$\frac{(7-8\nu)}{32(1-\nu)} \frac{m}{\rho r_0^3}$	$\frac{2a}{\sqrt{\pi}}$	$\frac{0.095m}{\beta}$	$\frac{9.2Ga}{2-\nu}$	$\frac{0.163Ga}{v_s}$
Rocking	$\frac{3(1-\nu)}{8} \frac{m}{\rho r_0^5}$	$\frac{2a}{\sqrt[4]{3\pi}}$	$\frac{0.24m}{\beta}$	$\frac{4.0Ga}{1-\nu}$	$\frac{0.6a}{v_s} K$
Torsional	$\frac{m}{\rho r_0^5}$	$\frac{2a}{\sqrt[4]{3\pi}}$	$\frac{0.045m}{\beta}$	$8.31Ga^3$	$\frac{0.127a}{v_s} K$

Table 5.1. Stiffness coefficients for one-dimensional discrete foundation soil-interaction (Richart et al. 1970, Gazetas 1983, Wolf 1988).

The static stiffness and damping coefficients proposed by Wolf (1988) presented in Table 5.1, depend on the parameter a which represents the half-width of a square foundation and on the shear wave velocity $v_s = \sqrt{G/\rho}$ where G and ρ are the shear modulus and the density of the soil.

Concerning the damping model, the authors modified the coefficients proposed by Wolf (1988) through a procedure of best fitting in which the damping coefficients, in combination with the mass and stiffness values, were assumed to be fixed; the best fitting was performed with reference to data available for SDOF systems. Successively the authors undertook the computation of the coupling between the soil and the adjacent foundations by developing new expressions for the stiffness and the

damping constant coefficient introduced by Wolf (1988) and seen in Table 5.1. Then, in order to take into account the distance between the foundations, the authors proposed the continuous functions reported in Table 5.2.

Motion	Stiffness Γ	Damping Ψ
Vertical	$1.614 \times 10^{-0.16257(d/a)}$	8.504
Horizontal	$3.7561 \times 10^{-0.18995(d/a)}$	13.2875
Rocking	$-(0.04234 - 0.2396 \times \log_{10}(d/a))$	$7.3823 - 6.775 \times \log_{10}(d/a)$
Torsional	0.05931	$4.4429 - 2.9125 \times \log_{10}(d/a)$

Table 5.2. Expression of coupling functions for foundation-soil-foundation interaction (Mulliken and Karabalis 1998).

The coupling stiffness proposed and damping coefficients relatively to two nearby foundations for vertical, horizontal, rocking and torsional motion were introduced to be used in place of the constant values in Table 5.1.

The SSSI coupling functions proposed depend on the foundation distance and their size, these were calibrated by an iterative procedure adopting the modified Wilson θ method; the proposed modification for integrating the equations of motion was employed to evaluate both foundation's responses in the case of a single loaded foundation, and the functions Γ and Ψ calibrated by comparing the responses obtained with BEM time domain analysis. The BEM solutions employed for the calibration are in accordance with Huang (1993) model which conforms with the investigated case of two identical square foundations placed on half space. The expressions of the coupling functions proposed by the authors are presented in Table 5.2. For foundations placed at distances ratios $d/a \leq 0.5$ the coupling function in Table 5.2 are more accurately defined as follows

$$\begin{aligned}\Gamma &= -(0.967 - 0.880(d/a)) \\ \Psi &= 0.204\end{aligned}\tag{5.25}$$

Mulliken and Karabalis (1998) applied their methodology for numerical investigations on the cross interaction among three structures placed on rigid square foundations under harmonic and earthquake loading. The buildings, shown in Figure 5.2 were modelled as SDOF systems with lumped masses, the foundations were then

assumed to have frequency independent translational, rotational springs and dashpots.

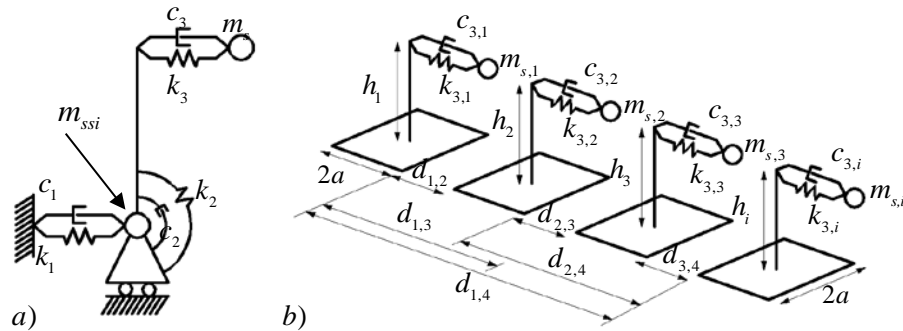


Figure 5.2. a) Lumped parameters representation of the building and its foundation; b) SDOF systems placed on independent foundations according to Mulliken and Karabalis (1998).

The SSI coefficient and SSSI coupling functions characterising the mass, stiffness and damping matrices for the system, were evaluated according to models chosen from literature and to the proposed functions. The authors' investigations highlighted that the peak of the response of a selected building forced by a number of harmonic functions over a range of frequencies, is sensitive to the presence of the others. From the analyses, the authors observed a reduction of the selected building response in correspondence of its first natural frequency when coupled with the others. On the other hand, in coupled conditions the system shows higher peaks relatively to a range of frequencies. By varying the building position with respect to the other structures, a higher reduction of its response was reported for building placed between the others than when located at the end of the row of buildings.

Alexander et al. (2012) presented a 2D formulation to model the SSSI between two structures placed on rigid foundations are connected by a rotational spring representing the interaction due to the soil underneath the oscillators.

The buildings and the soil are discretised, respectively as 2 DOF linear elastic oscillators and a rotational spring depicted in Figure 5.3.

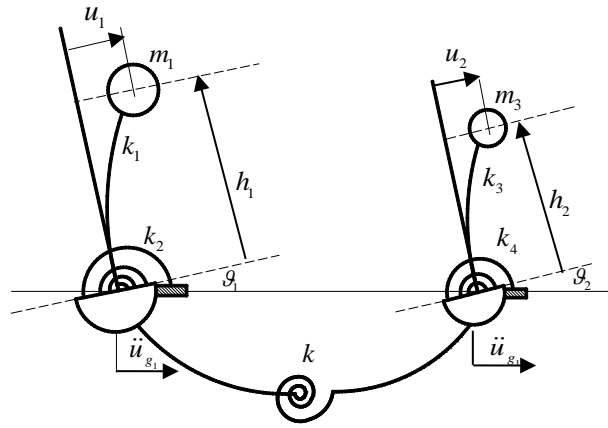


Figure 5.3. Discrete model for structure-soil-structure-interaction according to Alexander et al. (2012).

The 2 DOF of each building correspond to the horizontal translation of the lumped mass and to the rotation of the foundation. The foundations are considered to be superficial and rigid. The limit cases of the interaction conditions for the system are: (i) zero value of the rotational stiffness of the soil spring, i.e. absence of the interaction, uncoupled conditions, (ii) infinite rotational stiffness of the soil spring, i.e. the oscillators are fixed at the base then the DOF reduce to the translation of the lumped mass only.

The authors derived the Euler-Lagrange equations of motion of the system under investigation in a matrix form in terms of non-dimensional parameters. For the sake of clarity, the model's equations of motion are hereafter derived.

According to Hamilton's principle, the Euler-Lagrange equations of motion can be written in the following form

$$\frac{d}{dt}(\nabla_{\dot{\mathbf{u}}}K) - \nabla_{\mathbf{u}}K + \nabla_{\mathbf{u}}V + \frac{1}{2}\nabla_{\dot{\mathbf{u}}}\Pi = \mathbf{f}(t) \quad (5.26)$$

where K , V and Π are respectively the total kinetic, potential and the dissipated energy of the system; $\mathbf{f}(t)$ is the vector of the non-conservative external forces, and $\nabla_{\mathbf{u}}$ and $\nabla_{\dot{\mathbf{u}}}$ are the divergences which in a compact form can be written as follows

$$\nabla_{\mathbf{Y}}^T = \left[\frac{\partial}{\partial Y_1} \frac{\partial}{\partial Y_2} \dots \frac{\partial}{\partial Y_n} \right] \quad \mathbf{Y} = \mathbf{U}, \dot{\mathbf{U}} \quad (5.27)$$

where \mathbf{U} and $\dot{\mathbf{U}}$ are the vectors of the generalised displacements and velocities.

Under the hypothesis of small oscillations, the kinetic energy depends on the vector $\dot{\mathbf{U}}$ only, meaning that $\nabla_{\mathbf{U}} K = 0$; moreover for conservative systems $\frac{1}{2} \nabla_{\dot{\mathbf{U}}} \Pi = 0$, as a consequence equation (5.26) reduces to

$$\frac{d}{dt} (\nabla_{\dot{\mathbf{U}}} T) + \nabla_{\mathbf{U}} V = \mathbf{f}(t) \quad (5.28)$$

where

$$K = \frac{1}{2} \dot{\mathbf{U}}^T \mathbf{M} \dot{\mathbf{U}} \quad V = \frac{1}{2} \mathbf{U}^T \mathbf{K} \mathbf{U} \quad (5.29)$$

which substituted into equation (5.28) lead to the dynamic equilibrium for MDOF systems seen in equation (2.41) in absence of dissipation. It has to be noticed that the dissipation matrix can be assigned a posteriori.

In order to write the dynamic equilibrium of the system, equation (5.28) is particularised for the DOF involved in the motion. Firstly the generalised DOF are assigned according to a rotating coordinate frame, in which the generalised displacements of the mass of building 1 and 2 named u_1 and u_3 , relate to the original Cartesian coordinates, x_1 , and x_3 ; the displacement of the ground u_g relates to the original ground displacement x_g , and the generalised rotations u_2 and u_4 coincide with the original rotations \mathcal{G}_1 and \mathcal{G}_2 . In a matrix form the generalisation of the 2D Cartesian coordinates in the rotational system is

$$\begin{bmatrix} x_1 \\ \theta_1 \\ x_2 \\ \theta_2 \end{bmatrix} = \begin{bmatrix} r_1 & 0 & 0 & 0 \\ 0 & 1 & 0 & 0 \\ 0 & 0 & r_2 & 0 \\ 0 & 0 & 0 & 1 \end{bmatrix} \begin{bmatrix} u_1 \\ u_2 \\ u_3 \\ u_4 \end{bmatrix} = \begin{cases} x_1 = r u_1 \\ \mathcal{G}_1 = u_2 \\ x_2 = r_2 u_3 \\ \mathcal{G}_2 = u_4 \end{cases} \quad (5.30)$$

where r_1 and r_2 are the soil foundation masses radius of gyration respectively of building 1 and 2.

The problem can be divided into two parts defining

- i) the quantity $\frac{d}{dt}(\nabla_{\dot{u}}T)$, which takes into account the kinetic energy due to the masses velocities of the buildings and the foundations.

Mass of building 1 and 2

The velocity of the mass m_1 due to the anticlockwise rotation ϑ_1 is the first derivative of the displacement of the mass $h_1\vartheta_1$, which is displayed in Figure 5.4 a).

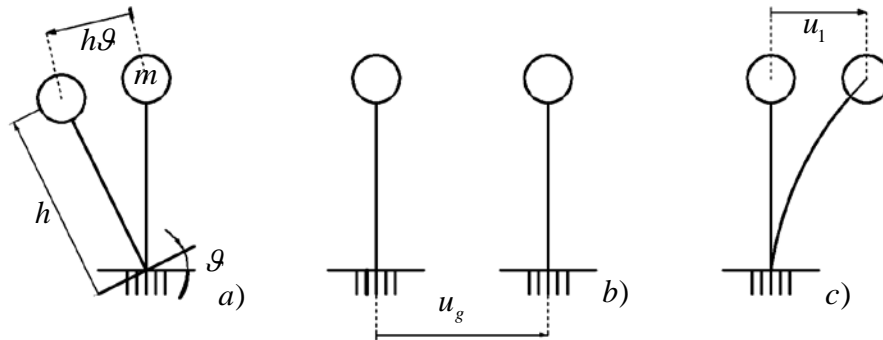


Figure 5.4. Effect on the translational DOF of the building due to: a) the rotation of the foundation; b) the horizontal acceleration at the base; c) the deformation of the structure.

According the generalised coordinate system gives

$$\frac{d}{dt}(-h_1\vartheta_1) = -h_1\dot{u}_2 \quad (5.31)$$

In analogy for building 2 it follows that

$$\frac{d}{dt}(-h_2\vartheta_2) = -h_2\dot{u}_4 \quad (5.32)$$

where h_1 and h_2 are the heights of the two buildings.

The velocity of the mass m_1 due to the displacement of the ground, see Figure 5.4 b), is

$$\frac{d}{dt}(x_g = r_1 u_g) = r_1 \dot{u}_g \quad (5.33)$$

Analogously for m_3 of building 2 follows

$$\frac{d}{dt}(x_g = r_1 u_g) = r_1 \dot{u}_g \quad (5.34)$$

The velocity of the mass m_1 due to the deformation of the building, see Figure 5.4 c), is

$$\frac{d}{dt}(x_1 = r_1 u_1) = r_1 \dot{u}_1 \quad (5.35)$$

Similarly, for the mass m_3 it follows

$$\frac{d}{dt}(x_2 = r_2 u_3) = r_2 \dot{u}_3 \quad (5.36)$$

Mass of foundation 1 and 2

The velocity of the rotating mass m_2 of the foundation 1 is

$$\mathcal{G}_1 r_1 = \dot{u}_2 r_1 \quad (5.37)$$

and for the foundation 2 the velocity assumed by m_4 is

$$\mathcal{G}_2 r_2 = \dot{u}_4 r_2 \quad (5.38)$$

where r_1 and r_2 are the soil-foundation masses radius of gyration of building 1 and 2.

Finally summing all the contributions given by equations (5.31)-(5.38) and substituting into the first of equation (5.29), that for each DOF is $K = \frac{1}{2}m_i\dot{u}_i^2$, it follows

$$K = \frac{1}{2} \left\{ m_2 \dot{u}_2^2 r_1^2 + m_1 (r_1 \dot{u}_1 + r_1 \dot{u}_g - h_1 \dot{u}_2)^2 + m_4 \dot{u}_4^2 r_2^2 + m_3 (r_2 \dot{u}_3 + r_1 \dot{u}_g - h_2 \dot{u}_4)^2 \right\} \quad (5.39)$$

ii) The values $\nabla_{\mathbf{u}}V$ have to be determined, for which the stiffness of the building and the foundations are accounted according to the second of equation (5.29).

Stiffness of both buildings and rotational stiffness of the foundations

According to the transformation in equation (5.30) and for the definition of potential energy given by equation (5.29) which for each DOF is $V = \frac{1}{2}k_i u_i^2$, it follows

$$V_{b,f} = \frac{1}{2} \left\{ k_1 r_1^2 u_1^2 + k_3 r_2^2 u_3^2 + k_2 u_2^2 + k_4 u_4^2 \right\} \quad (5.40)$$

Interaction stiffness between foundation 1 and 2

The contribution to the potential energy relatively to the interaction stiffness between the soil and the foundations is given by

$$V_{SSSI} = \frac{1}{2} k (u_4 - u_2)^2 \quad (5.41)$$

From the equation above it can be observed that rotating the foundations of the angle $\mathcal{G}_1 = u_2$ or $\mathcal{G}_2 = u_4$ a consequent opposite rotation is transferred to the other foundation equal to $u_2 u_4$.

Therefore, summing the contributes in equation (5.40) and (5.41) the total contribution to the potential energy of the system is

$$V = \frac{1}{2} \left\{ k_1 r_1^2 u_1^2 + k_3 r_2^2 u_3^2 + k_2 u_2^2 + k_4 u_4^2 + k (u_4^2 + u_2^2 - 2u_2 u_4) \right\} \quad (5.42)$$

In order to identify the elements of the mass and stiffness matrices, equation (5.28) needs to be fulfilled.

After deriving equations (5.39) for u_1, u_2, u_3, u_4 the first part of equation (5.28) is rewritten by substituting the following equations

$$\frac{d}{dt} \left(\frac{dT}{du_1} \right) = r_1^2 \ddot{u}_1 m_1 + r_1^2 \ddot{u}_g m_1 - r_1 h_1 m_1 \ddot{u}_2 \quad (5.43)$$

$$\frac{d}{dt} \left(\frac{dT}{du_2} \right) = m_2 r_1^2 \ddot{u}_2 + m_1 h_1^2 \ddot{u}_2 - m_1 r_1 h_1 \ddot{u}_g - r_1 h_1 m_1 \ddot{u}_1 \quad (5.44)$$

$$\frac{d}{dt} \left(\frac{dT}{du_3} \right) = m_3 r_2^2 \ddot{u}_3 + m_3 r_1 r_2 \ddot{u}_g - m_3 r_2 h_2 \ddot{u}_4 \quad (5.45)$$

$$\frac{d}{dt} \left(\frac{dT}{du_4} \right) = m_4 r_2^2 \ddot{u}_4 + m_3 h_2^2 \ddot{u}_4 - m_3 r_2 h_2 \ddot{u}_g - m_3 r_2 h_2 \ddot{u}_3 \quad (5.46)$$

Equations (5.43)-(5.46) in matrix form are obtained by ordering the elements of the equations row by row, according to order of the elements of vector $\ddot{u} = [\ddot{u}_1 \quad \ddot{u}_2 \quad \ddot{u}_3 \quad \ddot{u}_4]^T$, that gives

$$\mathbf{M} = \begin{bmatrix} r_1^2 m_1 & -r_1 h_1 m_1 & 0 & 0 \\ -r_1 h_1 m_1 & h_1^2 m_1 + r_1^2 m_2 & 0 & 0 \\ 0 & 0 & r_2^2 m_3 & -r_2 h_2 m_3 \\ 0 & 0 & -r_2 h_2 m_3 & h_2^2 m_3 + r_2^2 m_4 \end{bmatrix} \quad (5.47)$$

The influence vector is obtained by separating from equations (5.43)-(5.46) the terms proportional to \ddot{u}_g , that is

$$\mathbf{Q} = -\mathbf{M}\boldsymbol{\tau} = \begin{bmatrix} -r_1^2 m_1 & r_1 h_1 m_1 & -m_3 r_1 r_2 & h_2 r_2 m_3 \end{bmatrix}^T \quad (5.48)$$

which is obtained for the following incidence vector

$$\boldsymbol{\tau} = [-1 \quad 0 \quad -1 \quad 0]^T \quad (5.49)$$

By substituting the first derivative of the potential energy in equation (5.42) with respect to the generalised displacements to the second part of equation (5.28) the equation of motion can be explicated, these are

$$\frac{d}{du_1} V = k_1 r_1^2 u_1 \quad (5.50)$$

$$\frac{d}{du_2} V = k_2 u_2 + k u_2 - k u_4 \quad (5.51)$$

$$\frac{d}{du_3} V = k_3 r_2^2 u_3 \quad (5.52)$$

$$\frac{d}{du_4} V = k_4 u_4 + k u_4 - k u_2 \quad (5.53)$$

From equations (5.50)-(5.53) the stiffness matrix can be cast row by row following the order of the displacements $u = [u_1 \quad u_2 \quad u_3 \quad u_4]^T$, that gives

$$\mathbf{K} = \begin{bmatrix} r_1^2 k_1 & 0 & 0 & 0 \\ 0 & k_2 + k & 0 & -k \\ 0 & 0 & r_2^2 k_3 & 0 \\ 0 & -k & 0 & k_4 + k \end{bmatrix} \quad (5.54)$$

Assembling equations (5.47),(5.48) and (5.54) into the equations of motion in compact form in equation (2.41) in absence of dissipation the Euler-Lagrangian equations of motion in the time domain assume the form

$$\begin{aligned}
& \begin{bmatrix} r_1^2 m_1 & -r_1 h_1 m_1 & 0 & 0 \\ -r_1 h_1 m_1 & h_1^2 m_1 + r_1^2 m_2 & 0 & 0 \\ 0 & 0 & r_2^2 m_3 & -r_2 h_2 m_3 \\ 0 & 0 & -r_2 h_2 m_3 & h_2^2 m_3 + r_2^2 m_4 \end{bmatrix} \begin{bmatrix} \ddot{u}_1 \\ \ddot{\theta}_1 \\ \ddot{u}_2 \\ \ddot{\theta}_2 \end{bmatrix} + \\
& + \begin{bmatrix} r_1^2 k_1 & 0 & 0 & 0 \\ 0 & k_2 + k & 0 & -k \\ 0 & 0 & r_2^2 k_3 & 0 \\ 0 & -k & 0 & k_4 + k \end{bmatrix} \begin{bmatrix} u_1 \\ \theta_1 \\ u_2 \\ \theta_2 \end{bmatrix} = \begin{bmatrix} -r_1^2 m_1 \\ r_1 h_1 m_1 \\ -m_3 r_1 r_2 \\ h_2 r_1 m_3 \end{bmatrix} \ddot{u}_g
\end{aligned} \tag{5.55}$$

By writing the equations of motion with respect to the rotating reference frame enabled the authors to non-dimensional the matrices in equation (5.55) and after some algebra reduced them to a parametric form.

To characterise the SSI effects due to the foundation rocking motion and the SSSI interaction between the two foundations, the authors established a methodology by static and dynamic FEM analyses using the software PLAXIS. Through the computer software the SSI effects are investigated by considering the model for rotational soil foundation stiffness according to Gorbunov-Possadov (Brinkgreve et al 2010). The foundations are modelled by 2D analysis according to the Mindlin plates model (Bathe 1982) under the assumptions of: (i) identical geometry (i.e. with identical stiffness, $k_2 = k_4$), (ii) to be perfectly rigid and (iii) to be placed on the same soil at arbitrary distance; whereas in order to validate the model, perfectly rigid line elements were implemented in MATLAB.

The FE model was used to determine the rotations of the foundations due to the applied static moment M . By the relation among internal strain energy to the potential energy obtained from the Euler-Lagrange relation and the applied moment, the expressions for the rotational foundation spring and the rotational interaction spring are obtained in closed-form by the following equations

$$k_2 = \frac{\mathcal{G}_1}{\mathcal{G}_1 + \mathcal{G}_2} k_s; \quad k = \frac{\mathcal{G}_2}{\mathcal{G}_1 - \mathcal{G}_2} k_2; \quad k_s = \frac{M}{\mathcal{G}_1}; \tag{5.56}$$

where k is the rotational interaction spring, k_2 is the rotational foundation spring of the second building and k_s is the foundation rotation spring.

By using the FE model, the authors performed an empirical procedure by which k and k_2 were established as functions of the non-dimensional inter-building distance z , i.e. ratio of the buildings' distance and their width. The FE analysis was employed to obtain the values of the foundations' rotations \mathcal{G}_1 and \mathcal{G}_2 , relative to building 1 and building 2 for a given applied moment M . The empirical soil foundation spring and the rotational interaction spring obtained from the FEM model in conjunction with equation (5.56) were fitted to an inverse power relationship, that are

$$k = q_k(z)k_2; \quad k_2 = q_2(z)k_s; \quad q_k(z) = \frac{c_3}{(z+1)^3}; \quad q_2(z) = 1 + \frac{c_4}{(z+1)^3} \quad (5.57)$$

where $q_2(z)$ is the stiffening of the rotational springs k_2 and k_4 , c_3 and c_4 are constant parameters.

The authors pointed out that the smaller building acts as a localised energy absorber (i.e. tuned mass dampers), and observed that the presence of taller buildings next to an existing smaller one may induce detrimental effects to the smaller. The results were evaluated from observing the change in power of the total response for building 1 under analysis in coupled and uncoupled conditions, from which an amplification of the 85% and reduction of 30% were observed.

5.2.2 Experimental Approach

The lack of empirical data regarding the SSSI phenomenon is bringing researchers to intensify the experimental works. The early contributions in experimental SSSI investigations, can be addressed to the Nuclear Power Engineering Corporation (NUPEC), which carried out several tests from 1994 until 2002. During the NUPEC research project, the SSSI involving nuclear power plant buildings was explored through field tests. Kitada et al. (1999) described the status of the project conducted

in order to ensure the adequacy of structural systems in nuclear power plants in Japan. Models and shaking table tests were performed to study the response of the reactors buildings according to three conditions. The authors created the models of two pairs of buildings; for each pair a single building was analysed before and after second one, such to study the dynamic interaction of the pair by comparing the results in term of peaks of the response displacement. The laboratory tests reproduced the structures and the soil respectively with aluminium and silicon rubber. The real buildings were forced with an exciter acting at the top and at the base. Kitada et al. (1999) simulated the effect of the ground modelled on shaking table. By numerical models Niwa et al. (1988) investigated also the influence of the variation of the distance among the buildings on the SSSI effect, and validated their experimental results with satisfactory consistency of the results obtained in the field investigations.

As part of the NEESR-SG: *city block* project, lunched to establish case histories by use of large scale centrifuge, Trombetta et al. (2012) performed tests carried out at the NEES at UC Davis to understand both Structure-Foundation-Structure-Interaction and the modified SSSI response. The tests were performed by using one-dimensional ground motions selected from databases of recorded earthquakes forcing structures placed on superficial foundations, in order to investigate inelastic behaviour in a variety of boundary conditions due to SSSI effects. The buildings studied under: (i) in-plane shaking, relatively to a 2 DOF and 1 DOF system, (ii) anti-plane shaking of the same structural systems, and (iii) combined in-plane and anti-plane shaking for two identical 2 DOF systems and a smaller 1 DOF structure. The correlation of the PGA and chosen demand parameter for the case of study presented showed the SSSI to modify the inelastic structure-foundation demand. Within the same project, Jones (2013) confirmed the significant effects of the SSSI on the dynamic response the of moment resisting frames by tests performed with centrifuge. The frames, placed on shallow and deep foundations, were studied in adjacent and solitary conditions, and in resonance motion. Whereas for the study of rocking of a shear wall on a shallow mat, selected ground motions were employed.

The works demonstrated by experimental evidences that neighbouring buildings mutually influences the dynamic response of the other. As observed from the transfer functions, typically used to analysis the problem, the effects are identified to be either beneficial or detrimental.

5.3 Stationary Stochastic Analysis of SSSI Systems

In this section, a review of the stationary stochastic model for SSSI prior to the studies on the ViBa, is presented. To this regard, the review of the state of the art is of particular importance for the development of this work, in which the stochastic approached is undertaken. Investigations of the stochastic response of SSSI system have been performed only by few authors so far. As in the investigations pursued by this research to design the ViBa device, Behnamfar and Sugimura (1999) and Alexander et al. (2012) scrutinised the dynamic response of a SSSI system of two structures under input modelled as stationary random process.

Behnamfar and Sugimura's (1999) studies accounted of the spatial variation of the ground motion considering the coherency between the locations of the two structures and the wave passage effect; homogenous and layered visco-elastic medium half space is investigated under the effect of surface and body waves' propagation, which determines therefore both horizontal and vertical motion; the P, SV and Rayleigh waves are separately considered for the study of an idealised 2D system which configuration was changed to analyse different types of structures, from low to high rise buildings, and a stiffer reactor building. SSI effects are also taken into account and the hysteretic damping model is assumed. The stochastic response is compared to deterministic analysis in the frequency domain for the surface and body waves' considered and derived from methods for propagation of harmonic for the cases of uniform and layered half space from stiff to soft soils. The investigations revealed that the cross interaction reduces the response for the taller building and amplifies it for the smaller structures, with maxima values under Rayleigh's waves input that contrarily to the shear waves present noticeable difference from deterministic input assumption. Regarding the effects of the spatial variability the authors pointed out that for slender structures, for which the rocking motion is predominantly

transmitted and induces higher responses with respect to the horizontal motions, the loss of coherency reduces the structural responses in comparison to the case of perfect coherency. Moreover, larger responses for inclined incidence body waves are observed compared to vertically incident waves and that top shallow layers influence the SSSI effects with differences up to the 20% than the uniform case. The dynamic stiffness matrix of the coupled foundations was calibrated through a procedure by which these are derived from the dynamic stiffness matrix of the site.

The model proposed by Alexander et al. (2012) has been introduced in section 5.2.1 more in depth. The authors analysed the response of the system under stationary input ground motion in the frequency domain. The equations of motion for SDOF systems seen in equation (2.107) for unilateral PSD, can be expanded for MDOF system and particularised for the case of bilateral PSD functions as follows

$$\mathbf{S}_{UU}(\omega) = |\mathbf{H}(\omega)|^2 S_{\ddot{u}_g \ddot{u}_g}(\omega) \quad (5.58)$$

where $\mathbf{H}(\omega) = [H_1(\omega) \ H_2(\omega) \ H_3(\omega) \ H_4(\omega)]^T$ is the vector of the transfer functions for the 4 DOF of the system, and the input process $S_{\ddot{u}_g \ddot{u}_g}(\omega) = S_{KT}(\omega)$ is assumed pertinently to the Kanai-Tajimi spectrum.

According to equation (2.63) the vector of the transfer functions is obtained by equation

$$\mathbf{H}(\omega) = (\mathbf{K} - \omega^2 \mathbf{M} + i\omega \mathbf{C})^{-1} \mathbf{Q} \quad (5.59)$$

where the dissipation matrix \mathbf{C} is modelled according to the Rayleigh viscous damping model assuming 5% damping for the first two modes and the influence vector, $\mathbf{Q} = -\mathbf{M}\boldsymbol{\tau}$, is obtained from the mass matrix presented in equation (5.47) and the incidence vector in equation (5.49).

The total response displacements of the buildings' masses are presented in terms of power spectral density functions of the total sway, which is the sum of two contributions: the displacements the buildings masses due to the horizontal

translational DOF of the masses and the translation due to the rotation of the foundations. Therefore, the PSD of the total displacements for building 1 and 2 respectively are

$$\begin{aligned} S_{11}(\omega) &= \left(H_1^{sway} - H_2^{rotation} \right) \left(H_1^{sway} - H_2^{rotation} \right)^* S_{KT}(\omega) \\ S_{22}(\omega) &= \left(H_3^{sway} - H_4^{rotation} \right) \left(H_3^{sway} - H_4^{rotation} \right)^* S_{KT}(\omega) \end{aligned} \quad (5.60)$$

where S_{KT} is the Kanai-Tajimi spectrum, H_1^{sway} is the pure sway term and $H_2^{rotation}$ is the rotational sway term.

Alexander et al. (2012) presented a numerical application in which the response power spectra of the total sway for building 1 and 2 in Figure 5.3 are evaluated. The characteristics of the two structures correspond to: identical base $b = 10 \text{ m}$, heights $h_1 = 20 \text{ m}$ and $h_2 = 22 \text{ m}$; distance between the buildings $d = 1 \text{ m}$ in loose sand soil conditions; the ground frequency of the KT spectrum is considered to be coincident with the first natural frequency of the system in uncoupled conditions.

For the system under analysis, the response is evaluated for coupled and uncoupled conditions in the frequency domain as Figure 5.5 displays, in which the PSD functions relatively to the total sway of the two buildings are shown.

To quantify the variation of the response the authors introduced the percentage change in power of the total response according to equation

$$\chi_{ii} = \frac{\int S_{ii}^{coupled} - S_{ii}^{uncoupled} d\omega}{\int S_{ii}^{uncoupled} d\omega} \times 100 \quad (5.61)$$

where $S_{ii}^{coupled}$ and $S_{ii}^{uncoupled}$ are the bilateral stationary PSD function relatively to a selected DFO of the system under investigation.

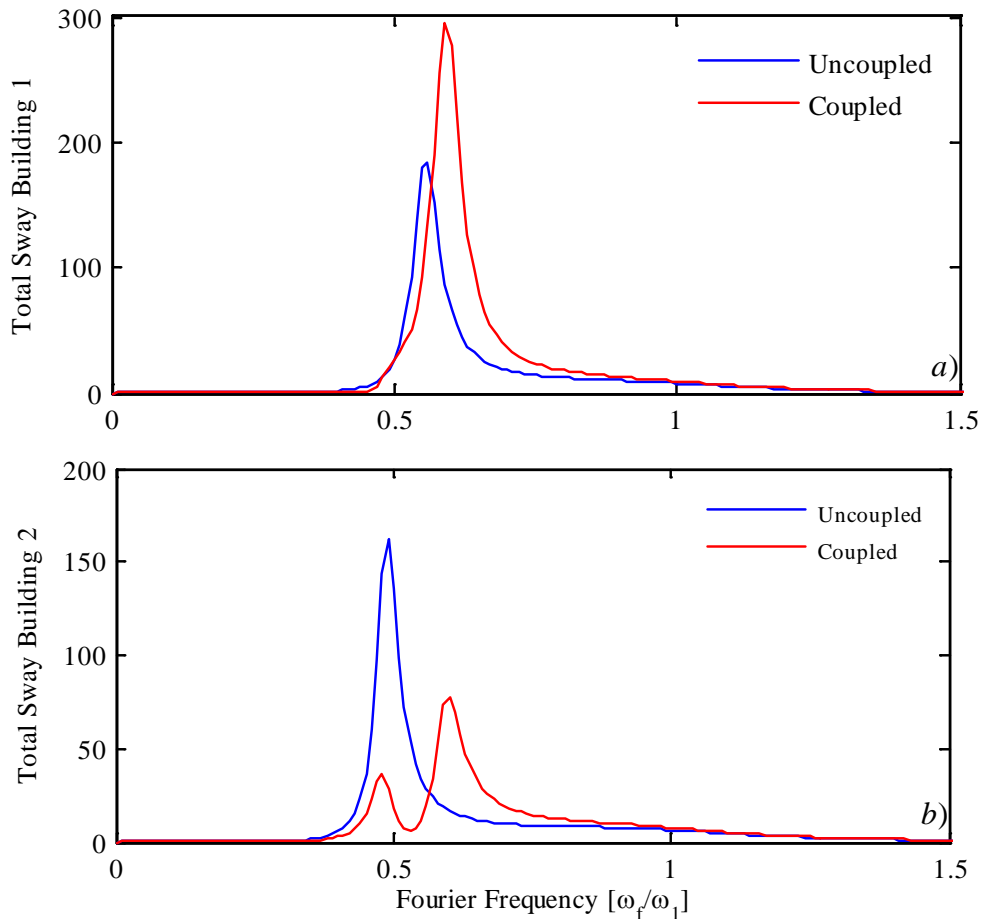


Figure 5.5. Power Spectral Density functions of the response for a) building 1; b) building 2 according to Alexander et al. (2012).

According to the PSD function in Figure 5.5, which has been reproduced following Alexander et al. (2012), the authors demonstrated for their case study that by means of equation (5.61) the power increases of the 63% for buildings 1 and decreases of the 19 % for building 2.

Aldaikh et al. (2015) and Aldaikh et al. (2016) extended the work of Alexander et al. (2012) to investigate the adverse and beneficial effects due to the SSSI when three buildings are under the effect of seismic ground acceleration. The investigations have been carried out numerically and experimentally for the case of selected real records for which the results showed that the central building acts as a tuned mass damper and suffers higher detrimental effects in comparison to the case of only two buildings.

The work presented in this section has been reference also for the investigations of D'Amico et al. (2014), with respect to non-stationary stochastic analysis of the SSSI, specifically regarding the studies on multicorrelated vector processes, through which the authors attempted to determine the statistics of the second order of the system response by an approximation of the well-known mathematical structure for the case of stationary input motion.

5.4 Concluding Remarks

In this Chapter an overview of the problem of the SSSI is addressed through a literature review on the subject, with premises on the SSI. The significance of the SSI in the seismic assessment of structures is well-testified, therefore according to the purpose of this Chapter only the fundamentals concept and comprehensive contributions have been reviewed. Instead, more attention has been given to the problem of the SSSI, particularly to the existing discrete models, in line with the approach chosen in this work, in which the ViBa is modelled within discretised SSSI systems.

Investigations on the SSSI phenomenon can be tackled by: the rigorous continuous approach by means of the theory of the wave propagation, by numerical study or experimental approaches. According to the literature, the majority of the analyses carried out have been performed numerically, justified by the complexity of the phenomenon which is influenced by several factors, e.g. the shape and dimension of the buildings' foundations, the soil characteristics, the distance between the structures. From the state of the art, it can be noted that up to date a restricted number of contributions have been provided in the framework of stochastic analysis of SSSI systems, specifically only structural models under the effect of stationary stochastic process have been identified. Accounting of the non-stationarity of the stochastic input in the evaluation of the response of SSSI system implies to take into account the transient response. To this regard, for multi-correlated non-stationary Gaussian stochastic processes, Damico et al. (2014) studied the problem of the SSSI by extending the model proposed by Alexander et al. (2012). To simplify the problem, Damico et al. (2014) approximated the evaluation of the time-variant

second order moments by means of the well-known simplified expressions for the stationary case, whose validity has been demonstrated by the authors for the case of rigid structures (see Appendix). Alternatively, the more rigorous approach to evaluate the second order statistics through the NGSMs of the response, could be undertaken (see e.g. Di Paola 1985, Cacciola and Muscolino 2011, Barbato 2011). In light of the insight provided by this certainly non-exhaustive review of the state of the art of the SSSI, in the next Chapter the design of the ViBa for discretised structural systems under stationary Gaussian stochastic ground motion processes is introduced.

6 Vibration Control of a Single Structure through the Vibrating Barrier

Vibration control strategies in civil engineering are well-established solutions, which reduce the structural response due to the motion induced by external dynamic actions, such as earthquakes and wind excitation (see e.g. Den Hartog 1956, Warburton 1982, De Silva 2007, Preumont and Seto 2008, Marian and Giaralis 2014). These solutions can be classified as: passive, which do not require external energy supply; active, involving the supply of external energy and consist of sensors (measure either the structural response or the external excitation, or both), the device evaluating the control force and the actuators to produce the force required; semi-active, which use passive and active control, specifically in the latter, the actuators do not add mechanical energy directly to the structure, contrarily to the hybrid systems, which combining active and passive control, require less energy being a portion of the control objective performed by the passive system (Soong and Spencer 2002).

In the area of passive vibration control, the available solutions encompass the energy dissipation techniques, tuning devices and the base isolation systems, which have shown marked development world-wide in recent decades. Among passive control systems, base isolation has been predominantly employed, consisting of groups of bearings placed at the base of the buildings and elongating the period of the structure. Base isolation is conveniently installed in new constructions whilst to retrofit into existing buildings may be an invasive process. Similarly, some energy dissipative systems such as: visco-elastic dampers, yielding steel inner frames and frictional dampers, encounter restrictions in their use for protecting existing structures e.g. historical masonries and heritage buildings. Among passive control devices, tuned mass dampers provide a practical solution widely used for protecting buildings and bridges. Tuned mass dampers are particularly efficient to adsorb the structural vibrations due to narrow band excitations, such as for wind engineering applications. However, under highly uncertain broadband input, the tuned mass

dampers efficiency may present some limitations; in such a case their drawback can be compensated by introducing active control elements, therefore creating hybrid solutions. The latter solutions rely on the implementation of adjustable active control elements, which increase the device's response sensitivity to the original external input by introducing an additional active force exciting the system.

The vibration adsorption solution investigated in this Chapter, the Vibrating Barrier (ViBa), enables the control of the structural responses of a building and thus protection of the structure by proper design of the control device's mass, stiffness and damping. These being established in accordance with the characteristics of the structure to be protected and with regard to the dynamic interaction between the ViBa, the soil deposit and the building. Effectively, the ViBa and the structure to be protected are subsystems, part of a global structures-soil system, whose behaviour is governed by the Structure-Soil-Structure-Interaction phenomenon. The ViBa does not require external energy to be activated, in similarity with the currently available *passive* control strategies, from which it crucially differs being embedded into the soil instead of being locally attached to the structural members.

The investigations in this chapter concern the ViBa design performed in the time domain under broadband input, modelled according to the techniques proposed in Chapter 3. In order to establish a reliable procedure to design the ViBa, the quasi-stationary, non-stationary and non-stationary with imposed variability response-spectrum-compatible stochastic ground motion models are adopted to force the global structure-soil-ViBa system. Specifically, the system under investigation is the analytical discrete model proposed by Cacciola and Tombari (2015) and hereafter extended in the time domain. Firstly, the formulation proposed by Cacciola and Tombari (2015) is explained in detail. The original formulation proposed by the authors accounts of the frequency-independent hysteretic damping. In this Chapter from the hysteretic model of Cacciola and Tombari (2015), an equivalent viscous model is estimated. Finally, the design of the ViBa under stochastic excitation is presented, where the device is calibrated through an optimization procedure aimed to reduce the mean of the largest peak of the relative horizontal displacement of the building, i.e. relative displacement between the

absolute top displacement of the structure and its foundation, forced by stationary stochastic input. The design procedure is successively verified by evaluating the structural response under the more advanced ground motion introduced in Chapter 3. The investigations are conducted by analyses of the structural response via pertinent Monte Carlo Simulation. To conclude, the proposed procedure to design the ViBa is applied to protect a benchmark structure, the 20-storey SAC building presented in Chapter 4.

The main contributions of this Chapter are the following: (i) defining the dynamic equilibrium of the investigated SSSI system in the time domain, (ii) the methodology to design the ViBa for broadband stochastic excitation by using derived simplified discretised models, and (iii) the MCS study to validate the efficiency of the ViBa calibrated through the design approach proposed. Moreover, to perform the analyses of the response in the time domain, enables a deeper insight in the influence of the input non-stationarity on the structural response of the buildings investigated. Besides, the assessment of the ViBa efficiency under advanced non-stationary input motion, provides the basis for future investigations on non-linear buildings-soil-ViBa systems.

6.1 Literature Review

In this Chapter, the novel ViBa device is investigated as a solution that is able to reduce the vibrations in buildings under earthquake ground motion in a “global” manner. In the context of this research, global control devices, by way of explanation, are systems that enable to protect more than one structure simultaneously. In this section, a review of these devices is attempted, explicitly with regard to the studies on the screening of waves, which may be categorised as the available “global” solutions by the potential of their application to reduce the response of multiple structural systems.

Regarding the reduction of earthquake induced vibrations in a “global” manner, one of the earliest contributions dates back to the field tests carried out by Woods’ (1968). The author examined the problem of footing isolation by probing into the effectiveness of wave screening through open trenches and sheet walls. These field investigations were conducted through a parametric study, whose variables were the trench dimensions, their position and some characteristic parameters governing the problem of wave propagation. The following cases were investigated in the study: the case of an isolated source and the case of source at distance. The barriers under study were placed into the ground modifying the wave field, which was triggered by a vibration exciter. Importantly, from the tests for isolated source, which were performed by full circle trenches around the vibration source, the minimum required length of the barrier was pointed out for the first time. Whereas for the case of source at distance, the application of trenches and sheet walls resulted in being appropriate for a shorter distance of the wave propagation source to the point of sought maximum screening. Successive original investigations on the screening of waves were carried out by Beskos et al. (1986). By means of BEM investigations, Beskos et al. (1986) laid the basis for the expansion of numerical studies on the subject. To test the effectiveness of linear elastic concrete piles and the soil as vibration-screening solution, Kattis et al. (1999) scrutinised a 3D problem by means of BEM models in the frequency domain. Through the authors’ investigation, the efficiency of trenches and piles were compared, and the influence

of the cross-section, length, depth and width on the isolation effectiveness highlighted. These studies showed similar effects for the aforementioned cases. Recently, Kumar et al. (2014) addressed an analytical formulation, along with numerical studies, on the isolation of anisotropic layered soil from horizontal waves through water-saturated trenches. The authors' numerical investigations showed drastic reductions of the shear waves and improved performances of the investigated trenches by adopting softer backfill material. The effect of softer backfill material for vibration-screening has been studied in more depth by Saikia (2014) in studies on dual in-filled trenches. These analyses were carried out by using models on PLAXIS 2D, under the assumption of linear elastic, isotropic, and homogeneous half-space subjected to steady-state vertical excitation. The influence of the trenches' geometry and the in-fill material on the trenches' effectiveness was observed by comparing the scheme proposed to the case of single trench, which disadvantageously may require a higher depth's extension.

Applications of vibration-screening through trenches or piles has generally been the objective of investigations for protection of structures from ground-borne vibrations due to trains, blasting or machine foundations. Screening of waves to reduce ground-borne vibrations induced by trains has been demonstrated to be efficient in the protection of a 6-storey building by Adam et al. (2005), who observed reductions in the structural vibrations of the building nearby open and in-filled trenches modelled by BEM and FEM in the time domain. The authors provided an insight into the direct effects that the trenches have on the structural response of the building under examination by comparing the cases with no trench against those with empty and in-filled ones. The results showed that by increasing the depth and width of the trenches, and the softness of the backfill material, the isolation effects improved predominantly due to the increase in depth rather than in width. Celebi and Kirtel (2013) undertook investigations to train-induced ground-borne vibrations accounting for the case of non-linear response by studying a 2D finite element model. The authors' work focused on accounting for the effect of the local plastic deformation of the soil on the dynamic response of the vibrating structural system by a rail embankment. From time and frequency domain analyses, the investigations

pointed out a significant reduction of the structural vertical vibrations due to open trenches and amplification of the response for in-filled trenches. The highest levels of protection are achieved when the barriers are close to the source, which is to be expected from initial studies on the subject. The effects of the train velocity are also accounted for and observed in relation to the soil conditions. In the last decade, the increasing urbanisation of cities and the consequent proliferation of underground trains and their induced tremors have advanced developments of studies concerning ground-borne vibration. This urbanisation magnifies the risks related to the strikes of earthquakes, however, earthquake vibration-screening is not documented as a possible solution to reduce effects on structures due to the seismic waves.

6.1.1 Passive Vibration Control Solution for Structures under Seismic Ground Motion: Vibrating Barriers

The Vibrating Barriers have been proposed by Cacciola (2012) as a novel passive control strategy able to reduce the vibrations of one or more adjacent structures. Detached from the structure to protect and embedded into the soil, the ViBa solution is thought as massive devices vibrating with the soil according to the wave propagation phenomenon. By controlling the mutual interaction between structures and the ViBa, the designer can impose beneficial effects to the structures intended to be protected, i.e. reducing the responses of the buildings, to the detriment of the control device, i.e. increasing the vibrations of the ViBa. To establish the dynamic mutual influence among structures via the available analytical formulation on the wave propagation, may be a burdensome process. Even for simple continuous structural SSSI systems, the expressions of the dynamic equilibrium as well as for closed-form expression of the ViBa's design parameters could be onerous. On the other hand, discrete models are more practical; these have been tested by the use of numerical models by FEM and BEM showing the accuracy and effectiveness of the approach. Then the calibration of the ViBa device has been tackled by means of discrete formulations of the SSSI system under analysis and verified through FEM and BEM.

The first ViBa design was attempted in order to protect a monopiled-structure through a monopiled-ViBa and is presented in the work of Cacciola et al. (2015) with the design performed through an optimization procedure. In their study the response of the ViBa-soil-structure systems is evaluated under the effect of response-spectrum-compatible Gaussian zero-mean quasi-stationary ground motion. The system ViBa-soil-structure described by analytical formulation was derived for discretised visco-elastic medium and linearly behaving structures neglecting the vertical displacements and as a discrete system modelled by joints with 2 DOF in the frequency domain. The design effectiveness has been scrutinized both by numerical and experimental investigations. The selected parameter to be minimized in the proposed optimization procedure was the largest value of the peak of the horizontal displacement of the structure to protect, i.e. relative displacement between the absolute top displacement and the foundation, whereas the stiffness and the damping of the ViBa were the parameters to be calibrated. Moreover, in a parametric study, the building response reductions have been presented for variations of the mass of the ViBa, the distance of the structures and the type of soil pertinent to the EC8 prescriptions. For fixing the optimal ViBa parameters, the parametric study shows that the higher the mass of the ViBa, the higher the reduction of the structural response. By analyses on the influence of the separation distance between the mono-piled structures it is demonstrated that for larger separation distance the effects of the ViBa are vanish more rapidly for stiffer rather than softer soils. In the latter scenarios, the response reduction is considerably more sensitive to the distance variation, especially in the initial range from 1 to 10 m of separation distance. Notably the optimum values obtained by the optimization procedure enabled a reduction in the stochastic response of the monopiled building of up to 44%.

The impact of the uncertainty of the model parameters on the evaluation of the structural response has been investigated by Tombari et al. (2016), who investigated the sensitivity of the stochastic response of a single building protected by the ViBa. The sensitivity of the structural response of the building was analysed with reference to selected structural parameters of the ViBa and the structure protected.

In their investigation, Tombari et al. (2016) analysed the response of an industrial building subjected to a zero-mean Gaussian quasi-stationary stochastic input. The sensitivity of the response has been observed for the case study with regard to the values of the rotational stiffness of the structure adopted in their work.

Important to the development of the investigations presented in this Chapter, is the work of Cacciola and Tombari (2015). The authors proposed for the case of ViBa-soil-structure systems under deterministic harmonic input the closed-form expressions to design the control device, tested in the scenario of a recorded earthquake forcing a real structure. Details on the formulation and the findings of the authors are reported in the following section.

6.1.2 Design of the Vibrating Barrier under Harmonic Base Excitation: Frequency Domain Approach

In this section, the formulation proposed by Cacciola and Tombari (2015) for frequency domain analysis of the structure-soil-structure interaction is presented. The authors established the generalized equations of motion for multi-structural systems coupled with ViBa. The multi-structure systems are assumed to behave linearly on linear elastic medium and, as customary for frequency domain analyses, the hysteretic damping model was adopted.

Accounting for both SSI and SSSI effects, Cacciola and Tombari (2015) proposed: (i) an optimization procedure for reducing the vibrations of coupled multi-buildings-ViBa systems under generic dynamic action, and (ii) a closed-form solution to design the control device for protecting up to two buildings under harmonic excitation. The authors proved the effectiveness of the ViBa device designed to protect one single 2 DOF building under harmonic force by experimental tests and numerical models. From the experimental tests carried out on a shake table, reductions of 87% of the structure response were achieved. The ViBa performances were also analysed in the case of vibration control of a real nuclear reactor building, by means of BEM/FEM numerical analyses. The building was forced by harmonic loading in steady state analysis firstly, from which a significant reduction of 75% of the absolute displacement at the top of the building

was obtained. Further to this, the nuclear building was forced by a real earthquake showing the significant reduction of 43.2% of the displacements at the top of the structure

This section reports the equations of motion as introduced by Cacciola and Tombari (2015) for the case of ViBa coupled with a single structure. The general dynamic equilibrium for a global SSSI system in terms of absolute displacements proposed by the authors is expressed as

$$\left(\tilde{\mathbf{K}} - \omega^2 \mathbf{M}\right) \mathbf{U}(\omega) = \mathbf{Q} U_g(\omega) \quad (6.1)$$

where $\mathbf{U}(\omega)$ is the $n \times 1$ vector of the absolute displacements relatively to the translational DOF, $\tilde{\mathbf{K}}$ and \mathbf{M} are respectively the complex global stiffness matrix and the real global mass matrix of $n \times n$ dimensions; \mathbf{Q} is the influence matrix, which relates to the incidence vector $\boldsymbol{\tau}$ as follows

$$\mathbf{Q} = \tilde{\mathbf{K}} \boldsymbol{\tau} \quad (6.2)$$

The influence matrix includes for each structure the soil-foundation stiffness, which detain the SSI effects.

From equation (6.1) the complex dynamic stiffness matrix for the systems is given as follows

$$\tilde{\mathbf{K}}_{dyn} = \left(\tilde{\mathbf{K}} - \omega^2 \mathbf{M}\right) \quad (6.3)$$

and according to equations (6.1) and (6.3), the $n \times 1$ vector of the transfer function of the systems is obtained by

$$\mathbf{H}_{hyst}(\omega) = \tilde{\mathbf{K}}_{dyn}^{-1} \mathbf{Q} \quad (6.4)$$

The subscript of the transfer function expressed above refers to the hysteretic damping assumption by which the dissipation is embedded to the elements of the global stiffness matrix as follows

$$\tilde{k}_{ij} = k_{ij} (1 + i\eta_{ij}) \quad (i, j = 1, 2, \dots, n) \quad (6.5)$$

where $\sqrt{-i}$ is the imaginary unit, \tilde{k}_{ij} and k_{ij} are respectively the elements of the hysteretic and real stiffness matrix and η_{ij} are the loss factors.

Finally, by combining equations (6.1)-(6.4) the absolute displacement vector follows as

$$\mathbf{U}(\omega) = \mathbf{H}_{hyst}(\omega) \mathbf{U}_g(\omega) \quad (6.6)$$

Once the equations of motion are cast for the system ViBa-soil-structures, the optimization procedure proposed for designing the ViBa structural parameters is introduced; specifically, the optimization procedure consists of solving the following problem of minimum search

$$\left. \begin{aligned} \min \{U_i^{r, \max}(\boldsymbol{\alpha})\} \quad i = 1, \dots, n, \\ \boldsymbol{\alpha} = \{k_{ViBa}, m_{ViBa}, \eta_{ViBa}\} \in \mathfrak{R}_0^+ \end{aligned} \right\} \quad (6.7)$$

where $U_i^{r, \max}(\boldsymbol{\alpha})$ is the maximum horizontal relative to the foundation, of the i -th structure obtained from equation (6.6) and $\boldsymbol{\alpha}$ is the vector of the unknown design parameters, namely the ViBa's stiffness k_{ViBa} , its mass m_{ViBa} and loss factor η_{ViBa} .

Moreover, the authors restated the optimization procedure in equation (6.7) in terms of the transfer functions of the structure to protect as follows

$$\left. \begin{aligned} \min \{H(\boldsymbol{\alpha}, \omega_0)\} \\ \boldsymbol{\alpha} = \{k_{ViBa}, m_{ViBa}, \eta_{ViBa}\} \in \mathfrak{R}_0^+ \end{aligned} \right\} \quad (6.8)$$

where $H(\boldsymbol{\alpha}, \omega_0)$ is the transfer function of the DOF to be controlled, which depends on the design parameters k_{ViBa} , m_{ViBa} , η_{ViBa} and the fundamental frequency ω_0 of the structure to protect.

By finding the zeros of the transfer function in equation (6.8) for the specified value of the first natural frequency of the building to protect, Cacciola and Tombari (2015) derived the closed-form expressions for k_{ViBa} and η_{ViBa} ; due to design constraints (e.g. bearing capacity of the soil deposit) the mass of the ViBa is therefore a priori assigned.

Based on the presented analytical formulation, Cacciola and Tombari (2015) performed experimental and numerical investigations on the discrete model depicted in Figure 6.1.

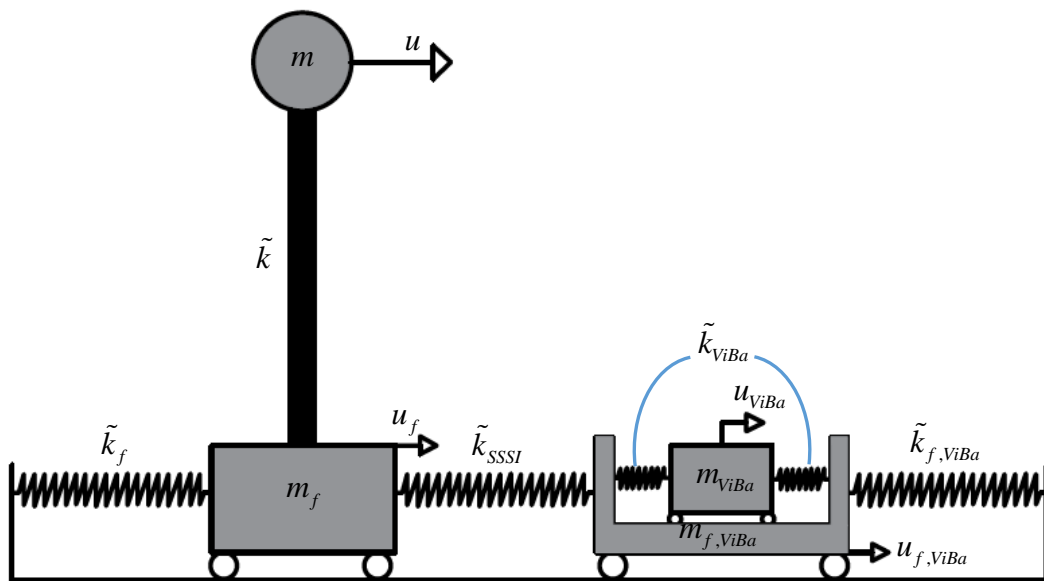


Figure 6.1. Discrete model used for the vibration control of a single structure through ViBa according to Cacciola and Tombari (2015).

The system is formed by two oscillators with 2 DOF each, which are the translations at the level of the lumped masses of the ViBa and the structure and their foundations, with a total number of 4 DOF of the global system. The stiffness coefficients of the foundations of the ViBa and the building capture the SSI effects through two linear translational springs. Similarly, the SSSI is taken into account by means of a linear elastic spring, which connects the building foundation to the ViBa's base restraint. The mass of the ViBa is placed inside the ViBa's foundation oscillating unit as Figure 6.1 illustrates.

By expression combining equation (6.1) and equation (6.2) and accounting for the incidence $\tau = [1 \ 1 \ 1 \ 1]^T$, the dynamic equilibrium of the system in matrix form follows as

$$\begin{aligned}
 & \begin{bmatrix} \tilde{k} & -\tilde{k} & 0 & 0 \\ -\tilde{k} & \tilde{k} + \tilde{k}_f + \tilde{k}_{SSSI} & 0 & -\tilde{k}_{SSSI} \\ 0 & 0 & \tilde{k}_{ViBa} & -\tilde{k}_{ViBa} \\ 0 & -\tilde{k}_{SSSI} & -\tilde{k}_{ViBa} & \tilde{k}_{ViBa} + \tilde{k}_{f,ViBa} + \tilde{k}_{SSSI} \end{bmatrix} \begin{bmatrix} U(\omega) \\ U_f(\omega) \\ U_{ViBa}(\omega) \\ U_{f,ViBa}(\omega) \end{bmatrix} + \\
 & -\omega^2 \begin{bmatrix} m & 0 & 0 & 0 \\ 0 & m_f & 0 & 0 \\ 0 & 0 & m_{ViBa} & 0 \\ 0 & 0 & 0 & m_{f,ViBa} \end{bmatrix} \begin{bmatrix} U(\omega) \\ U_f(\omega) \\ U_{ViBa}(\omega) \\ U_{f,ViBa}(\omega) \end{bmatrix} = \begin{bmatrix} 0 \\ \tilde{k}_f \\ 0 \\ \tilde{k}_{f,ViBa} \end{bmatrix} U_g(\omega) \quad (6.9)
 \end{aligned}$$

where m , m_f , m_{ViBa} and $m_{f,ViBa}$ are respectively the mass of the building, of the building foundation, of the ViBa and of the ViBa foundation; k , k_f , k_{ViBa} and $k_{f,ViBa}$ are respectively the complex stiffness of the building, of the building foundation, of the ViBa and its foundation.

The experimental tests performed on shake table were carried out on a model in aluminium of the structure and acrylic ViBa and building's rigid foundations, which were connected through steel elastic springs. The calibration of the ViBa's parameters was pursued according to the authors' proposed closed-form formulae; the solutions were presented for the case of one and two-buildings coupled with single ViBa device. Specifically, for the case of single structure and ViBa system, the complex optimal design ViBa's stiffness, $\tilde{k}_{ViBa}^{optimal}$, is given by

$$\tilde{k}_{ViBa}^{optimal}(\omega_0) = \frac{(\omega_0^2 m_{ViBa}) \left[\tilde{k}_{f,ViBa} + \tilde{k}_{SSSI} \left(1 + \tilde{k}_{f,ViBa} / \tilde{k}_f \right) - \omega_0^2 m_{f,ViBa} \right]}{\tilde{k}_{f,ViBa} + \tilde{k}_{SSSI} \left(1 + \tilde{k}_{f,ViBa} / \tilde{k}_f \right) - \omega_0^2 (m_{f,ViBa} + m_{ViBa})} \quad (6.10)$$

The separable real and the imaginary part of $\tilde{k}_{ViBa}^{optimal}(\omega_0)$ depends on the natural frequency of the structure to protect, ω_0 and on the values related to the

foundations and the SSSI, which are $m_{f,ViBa}$, k_f , k_{SSSI} , $k_{f,ViBa}$, η_f , $\eta_{f,ViBa}$ and η_{SSSI} . The optimal ViBa loss factor $\eta_{ViBa}^{optimal}$ is derivable from the optimal ViBa stiffness presented in equation (6.10) by the followings

$$\left. \begin{aligned} k_{ViBa}^{optimal} &= \operatorname{Re} \left[\tilde{k}_{ViBa}^{optimal}(\omega_0) \right] \\ \eta_{ViBa}^{optimal} &= \frac{\operatorname{Im} \left[\tilde{k}_{ViBa}^{optimal}(\omega_0) \right]}{\operatorname{Re} \left[\tilde{k}_{ViBa}^{optimal}(\omega_0) \right]} \end{aligned} \right\} \quad (6.11)$$

where $\operatorname{Re}[\cdot]$ and $\operatorname{Im}[\cdot]$ denote the real and imaginary part.

According to equation (6.5), in the case of undamped systems (i.e. for every $\eta = 0$) for which $\tilde{k} = k$, equation (6.10) reduces to the following

$$k_{ViBa}(\omega_0) = \frac{(\omega_0^2 m_{ViBa}) \left[k_{f,ViBa} + k_{SSSI} \left(1 + k_{f,ViBa} / k_f \right) - \omega_0^2 m_{f,ViBa} \right]}{k_{f,ViBa} + k_{SSSI} \left(1 + k_{f,ViBa} / k_f \right) - \omega_0^2 (m_{f,ViBa} + m_{ViBa})}. \quad (6.12)$$

The above expression is the optimal value for systems which hold a real valued stiffness matrix, therefore valid under the hypothesis of viscous damping.

In order to test the ViBa in critical conditions for the structure (i.e. at resonant motion), the global system under analysis was forced by harmonic input with circular frequency $\omega_0 = 22.62$ rad/s. The first two natural frequencies of the system in coupled and uncoupled conditions are reported in Table 6.1.

Natural frequencies	$\omega_{1,coup}$	$\omega_{2,coup}$	$\omega_{1,unc}$	$\omega_{2,unc}$
[rad/sec]	20.45	26.00	19.84	22.62

Table 6.1. First two natural frequencies of the system one building-soil-ViBa under investigation.

The design value of the ViBa stiffness and the pertinent loss factor were derived from the presented formulas; the loss factors of the structure and the foundations as well the stiffness and loss factor of the SSSI interaction spring, were determined though an identification procedure by minimizing the differences between the experimental transfer functions and the analytical transfer functions of the building

for both coupled and uncoupled conditions (see equation (6.4)). In Table 6.2 the mechanical characteristics of the prototype are summarised.

	Mass [kg]	Stiffness [N/m]	Loss factor
Building	$m = 0.5965$	$k = 9.0985 \times 10^2$	$\eta = 0.09$
Building foundation	$m_f = 0.353$	$k_f = 640$	$\eta_f = 0.046$
ViBa device	$m_{ViBa} = 0.629$	$k_{ViBa} = 440$	$\eta_{ViBa} = 0.18$
ViBa foundation	$m_{f,ViBa} = 0.491$	$k_{f,ViBa} = 760$	$\eta_{f,ViBa} = 0.04$
SSSI parameters	-	$k_{SSSI} = 315$	$\eta_{SSSI} = 0.02$

Table 6.2. Mechanical parameters for the experimental tests on a single structure protected through ViBa device (Cacciola and Tombari 2015).

Figure 6.2 and Figure 6.3 show the transfer functions relatively to the ViBa and the building to protect, the plots enable to address the effects of the ViBa mass variation on the building responses reduction in both coupled and uncoupled conditions.

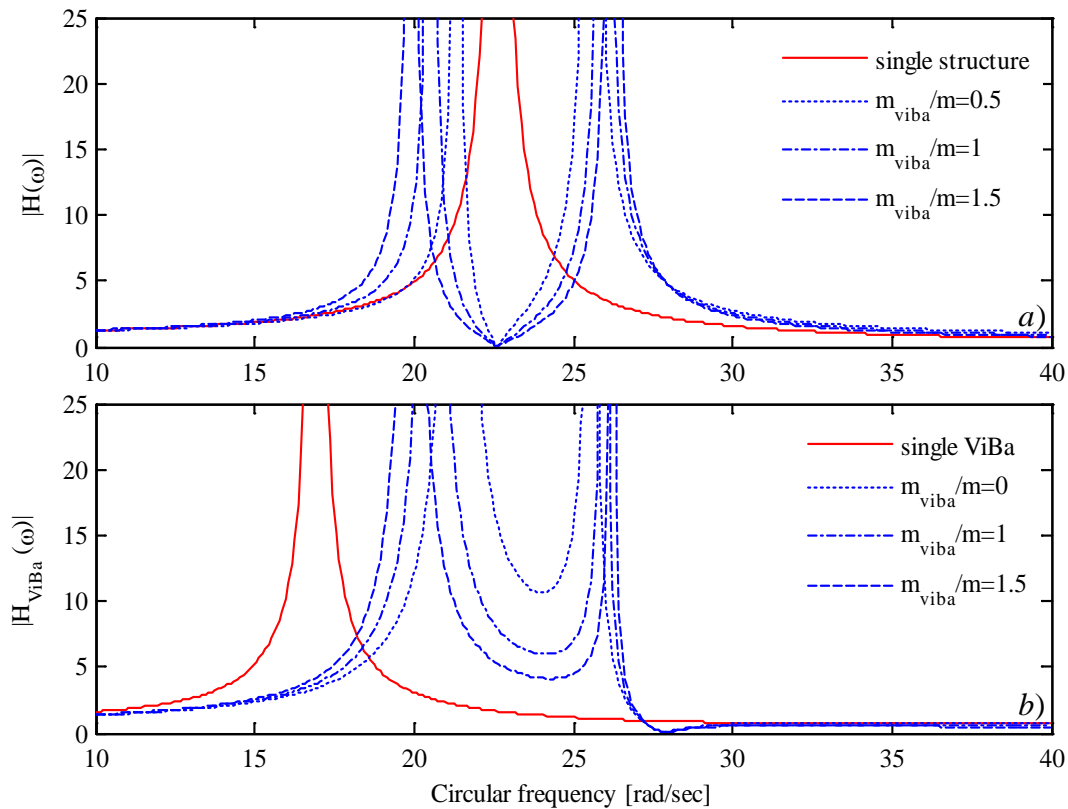


Figure 6.2. Transfer functions of the undamped for different mass ratios system of the: a) structure; b) ViBa (Cacciola and Tombari 2015).

Figure 6.2 displays the modulus of the transfer functions of the building and the ViBa for the undamped case. The red curves refer to the single building and ViBa in uncoupled conditions (i.e. $\tilde{k}_{SSSI} = 0$), whereas the blue curves denote the coupled conditions in which the SSSI effects are taken into account (i.e. $\tilde{k}_{SSSI} = 0$).

Figure 6.3 presents the transfer functions' modulus in damped conditions according to the loss factors measured from the prototype and presented in Table 6.2 in ideal conditions of ViBa with zero damping (i.e. $\eta_{ViBa} = 0$).

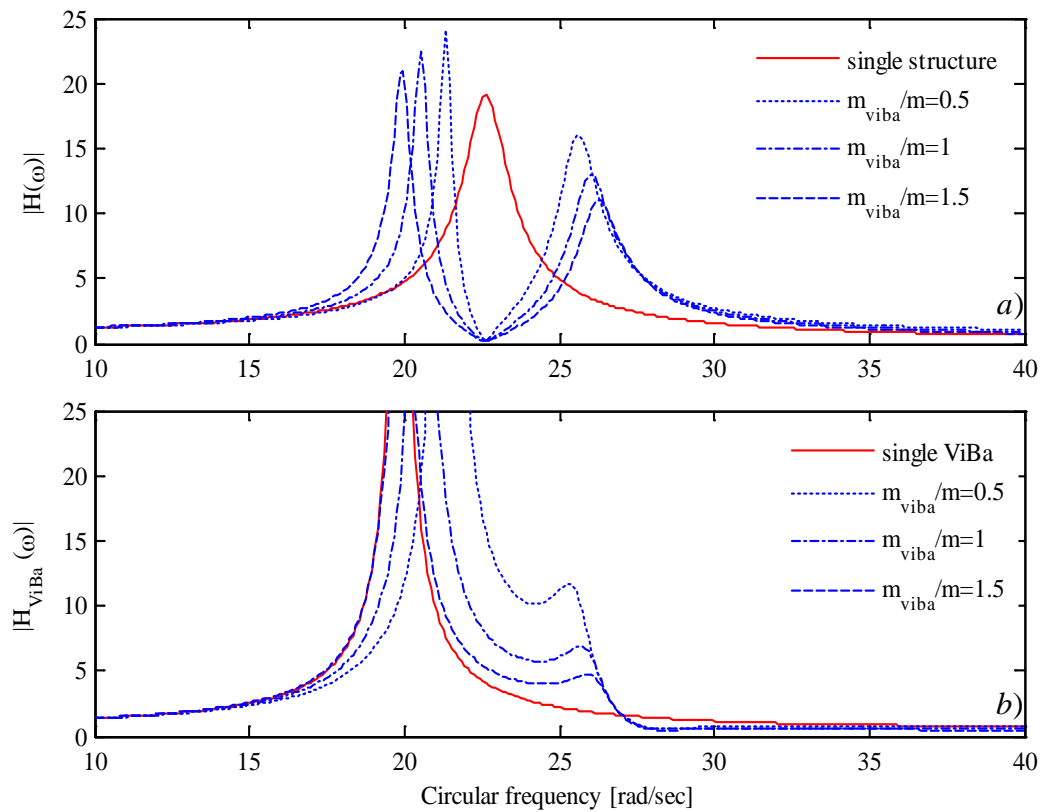


Figure 6.3. Transfer functions of the damped system for different mass ratios and null ViBa loss factor of the: a) structure; b) ViBa (Cacciola and Tombari 2015).

As Figure 6.3 displays, the numerical results pointed out that in ideal conditions of zero damping (i.e. $\eta_{ViBa} = 0$), the ViBa reduces the building response of the 100%, while in damped conditions, the reductions achieved are of the 87%, in accordance with the experimental tests.

6.2 Time Domain Analysis of Single Structures under Harmonic Input Protected through the Vibrating Barrier

In this section, the formulation of a single building-soil-ViBa system proposed by Cacciola and Tombari (2015) in the frequency domain is extended to the time domain. In order to determine the dynamic equation of motion of the system of Cacciola and Tombari (2015), from the hysteretic damping model presented for their prototype, an equivalent viscous damping matrix has been obtained. Hereafter the procedure to determine the equivalent viscous damping model is presented and validated by comparing the results in the frequency and time domains.

The assumption of hysteretic damping, described by a complex valued stiffness matrix is generally accepted to be accurate in some circumstances, but holds the drawback to be directly applicable in the frequency domain only (Henwood 2002). When hysteretic models are directly adopted in the time domain, the use of complex technics to approximate the equation of motion may be required (Inaudi and Makris 1996). However, the validity of hysteretic damping models for time domain analyses has been extensively discussed in literature since the hysteretic model can be rigorously adopted only in the frequency domain otherwise determining the non-causality flaw, i.e. response prior to excitation (see e.g. Muscolino et al. 2005). To this regard, Spanos and Zeldin (2000) argued that when hysteretic damping and frequency-dependent parameters are considered, for both time-domain and random-vibration analyses of non-causal systems, caution must be paid.

The classical viscous damping assumption modelled with viscous dashpots, enables to solve the dynamic equilibrium of light damped vibrating systems by simple mathematical solutions. When the damping is light, the dissipative forces are predominant in resonant motions, for which the loss factor at resonance relates to the viscous damping coefficient by equation (5.18).

The general dynamic equilibrium in the time domain of n -DOF systems subjected to ground motion excitation under the assumption of hysteretic dissipation, are provided by the following set of differential equations

$$\mathbf{M}\ddot{\mathbf{u}}_{abs}(t) + \tilde{\mathbf{K}}\mathbf{u}_{rel}(t) = \mathbf{0} \quad (6.13)$$

where respectively \mathbf{M} and $\tilde{\mathbf{K}}$ are the $n \times n$ real global mass matrix and the complex global stiffness matrix, $\ddot{\mathbf{u}}_{abs}(t)$ and $\mathbf{u}_{rel}(t)$ are the $n \times 1$ vector of the absolute accelerations and the relative displacement of the mass with respect to the foundation.

Specifically, according to the relationship between the absolute and relative displacements. the vector $\ddot{\mathbf{u}}_{abs}(t)$ is rewritten as

$$\ddot{\mathbf{u}}_{abs}(t) = \ddot{\mathbf{u}}_{rel}(t) + \ddot{\mathbf{u}}_g(t) \quad (6.14)$$

and the relative displacement vector $\mathbf{u}_{rel}(t)$ as

$$\mathbf{u}_{rel}(t) = \mathbf{u}_{abs}(t) - \mathbf{u}_g(t) \quad (6.15)$$

By substituting equation (6.15) into equation (6.13), this reads

$$\mathbf{M}\ddot{\mathbf{u}}_{abs}(t) + \tilde{\mathbf{K}}[\mathbf{u}_{abs}(t) - \mathbf{u}_g(t)] = \mathbf{0} \quad (6.16)$$

Moving the unknowns of equation (6.16) to the left hand side it can be rewritten as

$$\mathbf{M}\ddot{\mathbf{u}}_{abs}(t) + \tilde{\mathbf{K}}\mathbf{u}_{abs}(t) = \tilde{\mathbf{K}}\mathbf{u}_g(t) \quad (6.17)$$

where the input ground motion vector is

$$\mathbf{u}_g(t) = \boldsymbol{\tau}u_g(t) \quad (6.18)$$

in which $\boldsymbol{\tau}$ is the incidence vector.

By substituting equation (6.18) into equation (6.17) this becomes

$$\mathbf{M}\ddot{\mathbf{u}}_{abs}(t) + \tilde{\mathbf{K}}\mathbf{u}_{abs}(t) = \tilde{\mathbf{K}}\boldsymbol{\tau}u_g(t) \quad (6.19)$$

After taking the Fourier Transform of equation (6.19) the algebraic equations of the dynamic equilibrium in the frequency domain leads to the equations of motion as presented by Cacciola and Tombari (2015) in equation (6.1).

Equation (6.19) cannot be solved in the time domain being the stiffness matrix $\tilde{\mathbf{K}}$ based on the hysteretic model which is non-casual. Therefore, the solution of equation (6.19) is pursued in the frequency domain through the equations of motion seen in equation (6.1). According to the expression of the dynamic equilibrium in the frequency domain, the hysteretic stiffness matrix $\tilde{\mathbf{K}}$ can be rewritten in the following classical form

$$\tilde{\mathbf{K}} = \mathbf{K} + i\omega\mathbf{C} \quad (6.20)$$

where \mathbf{C} is the equivalent viscous damping matrix, which has been sought in this work through the procedure presented in the next section.

Equation (6.20) above leads to the rheological scheme in Figure 6.4.

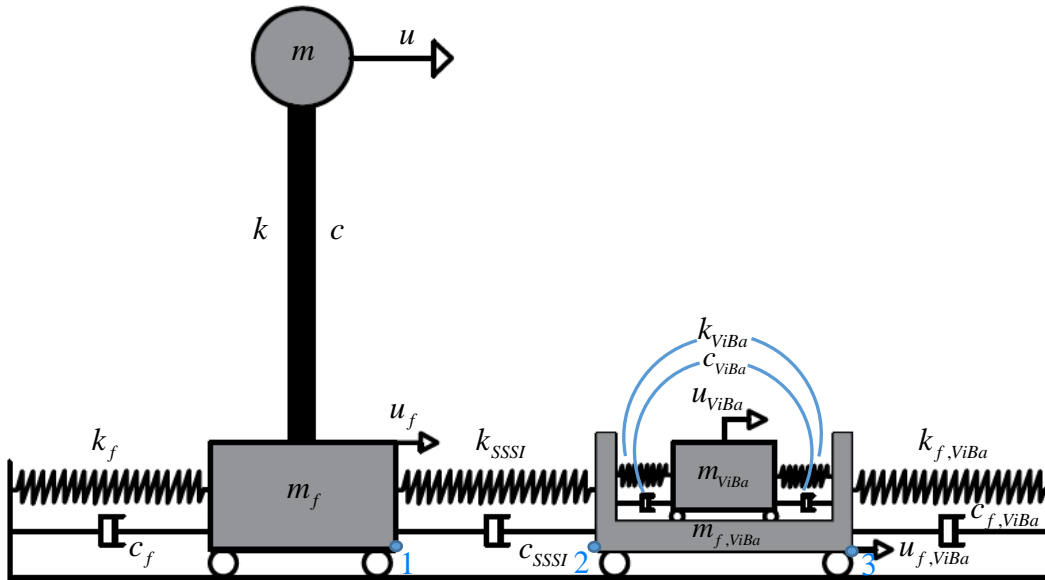


Figure 6.4. Discrete model adopted to study in the time domain the vibration control of a single structure through ViBa.

Considering the system depicted in Figure 6.4 under the action of seismic ground motion, the dynamic equilibrium in terms of absolute displacement, velocity and acceleration is presented hereafter.

The dynamic motion of the system in Figure 6.4 is determined by solving the following system of equations

$$\begin{aligned}
& \begin{bmatrix} m & 0 & 0 & 0 \\ 0 & m_f & 0 & 0 \\ 0 & 0 & m_{ViBa} & 0 \\ 0 & 0 & 0 & m_{f,ViBa} \end{bmatrix} \begin{bmatrix} \ddot{u}_1 \\ \ddot{u}_f \\ \ddot{u}_{ViBa} \\ \ddot{u}_{f,ViBa} \end{bmatrix} + \\
& + \begin{bmatrix} c & -c & 0 & 0 \\ -c & c + c_f + c_{SSSI} & 0 & -c_{SSSI} \\ 0 & 0 & c_{ViBa} & -c_{ViBa} \\ 0 & -c_{SSSI} & -c_{ViBa} & c_{ViBa} + c_{f,ViBa} + c_{SSSI} \end{bmatrix} \begin{bmatrix} \dot{u}_1 \\ \dot{u}_f \\ \dot{u}_{ViBa} \\ \dot{u}_{f,ViBa} \end{bmatrix} + \\
& + \begin{bmatrix} k & -k & 0 & 0 \\ -k & k + k_f + k_{SSSI} & 0 & -k_{SSSI} \\ 0 & 0 & k_{ViBa} & -k_{ViBa} \\ 0 & -k_{SSSI} & -k_{ViBa} & k_{ViBa} + k_{f,ViBa} + k_{SSSI} \end{bmatrix} \begin{bmatrix} u_1 \\ u_f \\ u_{ViBa} \\ u_{f,ViBa} \end{bmatrix} = \\
& = \begin{bmatrix} 0 \\ k_f \\ 0 \\ k_{f,ViBa} \end{bmatrix} \mathbf{u}_g + \begin{bmatrix} 0 \\ c_f \\ 0 \\ c_{f,ViBa} \end{bmatrix} \dot{\mathbf{u}}_g
\end{aligned} \tag{6.21}$$

where c , c_f , c_{SSSI} , c_{SSSI} and $c_{f,ViBa}$ are the viscous damping coefficients relatively to the dashpots representing the energy dissipation for the building, the ViBa and the SSSI; the incidence vector, has been assumed to be $\boldsymbol{\tau} = [1 \ 1 \ 1 \ 1]^T$ pertinently to the 4 DOF of the system.

In order to evaluate the response of the system in Figure 6.4, the unknown coefficient of the viscous damping matrix \mathbf{C} seen in equation (6.21) are identified by a procedure of minimization of the difference between the transfer functions of the system under the hypothesis of hysteretic damping (Cacciola and Tombari 2015) and the transfer functions of the equivalent viscously damped systems.

6.3 Numerical Applications of Time Domain Deterministic Analyses

In the following sections, the methodology to design the ViBa to reduce the vibrations in buildings under deterministic input is applied. Firstly, the model of Cacciola and Tombari (2015) extended to perform the time domain analyses is investigated. The procedure proposed to define a viscous damping matrix equivalent to the hysteretic model used by Cacciola and Tombari (2015) is explained, and the analysis of the structural response for the system is undertaken. Successively, the methodology to design the ViBa as proposed by Cacciola and Tombari (2015) is applied to protect a real benchmark building, whose response is also analysed in the time domain by means of FEM solutions. In the latter numerical application, a constant modal viscous damping model is adopted.

6.3.1 Design of the ViBa for the Control of the Simplified Structure of Cacciola and Tombari (2015)

In this section, the identification of the viscous damping matrix equivalent to the hysteretic model adopted by Cacciola and Tombari (2015) is presented. The coefficients of the viscous dissipation matrix for the system under investigation were sought by solving an unconstrained minimisation problem using the penalty function method. The minimisation problem can be stated as

$$\begin{aligned} \text{Min } f(\mathbf{x}) \\ \mathbf{x} \in \mathfrak{R} \end{aligned} \tag{6.22}$$

Several algorithms are available in literature to solve minimization problems (see e.g. Friswell and Mottershead 2010). In this work, the solution to minimize a non-linear equation of several variables was provided by the algorithm “*fsolve*” available in MATLAB. The algorithm adopted is the “*trust-region-dogleg*” method which basic idea is to approximate the objective function with a simpler function, which reasonably behaves as the objective function in a neighbourhood, the trust region, around the vector \mathbf{x} .

The objective function for the problem tackled in this work has been defined as the difference between the analytical transfer functions for a selected DOF, assuming both the hysteretic and viscous damping models. The identification problem consists of two steps:

- *Step 1: building and ViBa uncoupled*

Firstly, the unknown damping coefficients relatively to building and its foundation, $\boldsymbol{\kappa}_1 = \{c, c_f\} \in \mathfrak{R}_0^+$, have to be evaluated according to equation (6.22), by arranging the minimisation problem for the DOF of the mass of the building in uncoupled conditions., that is

$$\left. \begin{aligned} & \mathbf{H}_{hyst}(\omega, \bar{\boldsymbol{\kappa}}_1) - \mathbf{H}_{visc}(\omega, \boldsymbol{\kappa}_1) = 0 \\ & \bar{\boldsymbol{\kappa}}_1 = \{\eta_1, \eta_f\} \in \mathfrak{R}_0^+ \\ & \boldsymbol{\kappa}_1 = \{c_1, c_f\} \in \mathfrak{R}_0^+ \end{aligned} \right\} \quad (6.23)$$

With reference to the simplified system as proposed by Cacciola and Tombari (2015), whose mechanical properties are summarised in Table 6.2, the solution of the first part of the problem following has led to the following viscous damping coefficients for the building and its foundation, namely $c = 0.2849$ Ns/m and $c_f = 2.1367$ Ns/m.

- *Step 2: building coupled with ViBa*

The evaluation of the unknown damping parameters relatively to the SSSI, the ViBa and the ViBa's foundation, $\boldsymbol{\kappa}_2 = \{c_{SSSI}, c_{ViBa}, c_{f,ViBa}\} \in \mathfrak{R}_0^+$, is achieved by setting the minimization problem for the transfer function of the building DOF in coupled conditions, knowing already the values for c and c_f previously obtained, used to characterise $\mathbf{H}_{visc}(\omega, \boldsymbol{\kappa}_2)$ by satisfying the following system of equations.

$$\left. \begin{aligned} & \mathbf{H}_{hyst}(\omega, \bar{\boldsymbol{\kappa}}_2) - \mathbf{H}_{visc}(\omega, \boldsymbol{\kappa}_2) = 0 \\ & \bar{\boldsymbol{\kappa}}_2 = \{\eta_{SSSI}, \eta_{ViBa}, \eta_{f,ViBa}\} \in \mathfrak{R}_0^+ \\ & \boldsymbol{\kappa}_2 = \{c_{SSSI}, c_{ViBa}, c_{f,ViBa}\} \in \mathfrak{R}_0^+ \end{aligned} \right\} \quad (6.24)$$

To this regard, the values of the damping coefficients found are: $c_{SSSI} = 1.5062$ Ns/m, $c_{ViBa} = 1.6640$ Ns/m and $c_{f,ViBa} = 3.2872$ Ns/m. Figure 6.5 presents the moduli of the analytical transfer functions obtained by assuming the target hysteretic damping model and the equivalent viscous damping model, respectively denoted with \mathbf{H}_{hyst} and \mathbf{H}_{visc} .

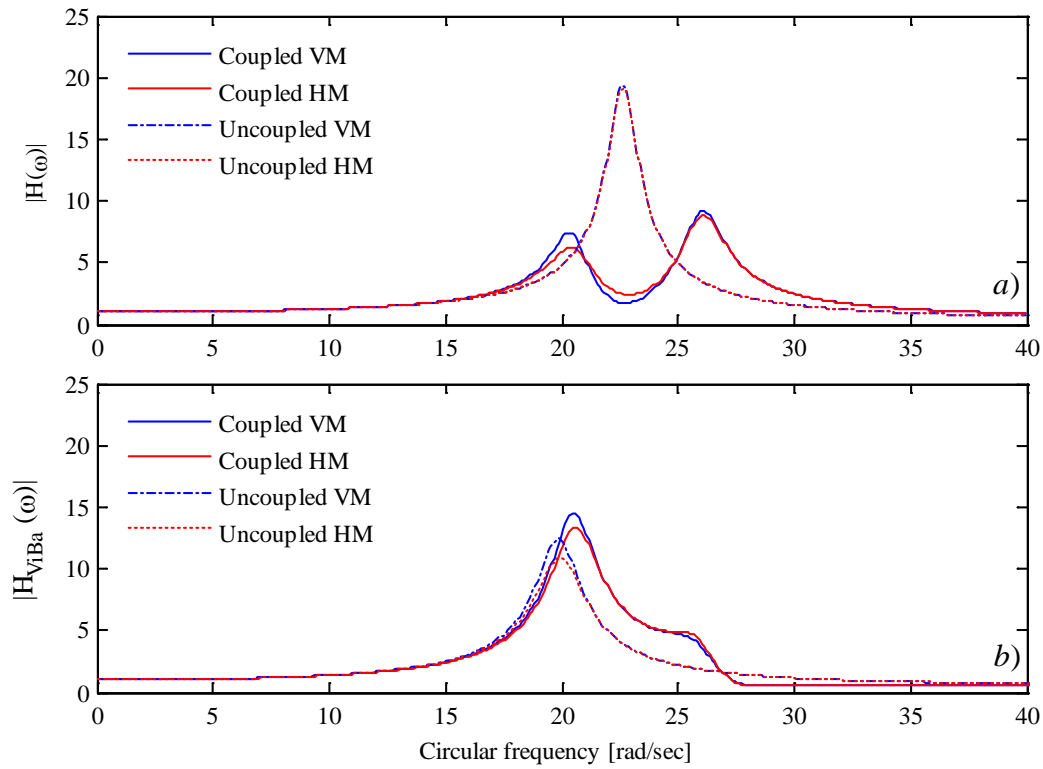


Figure 6.5. Comparison of the transfer functions of the: (a) structure and (b) ViBa for the Viscous Model (VM) and Hysteretic model (HM).

The proposed two step minimisation problem can be summarised in the following flowchart.

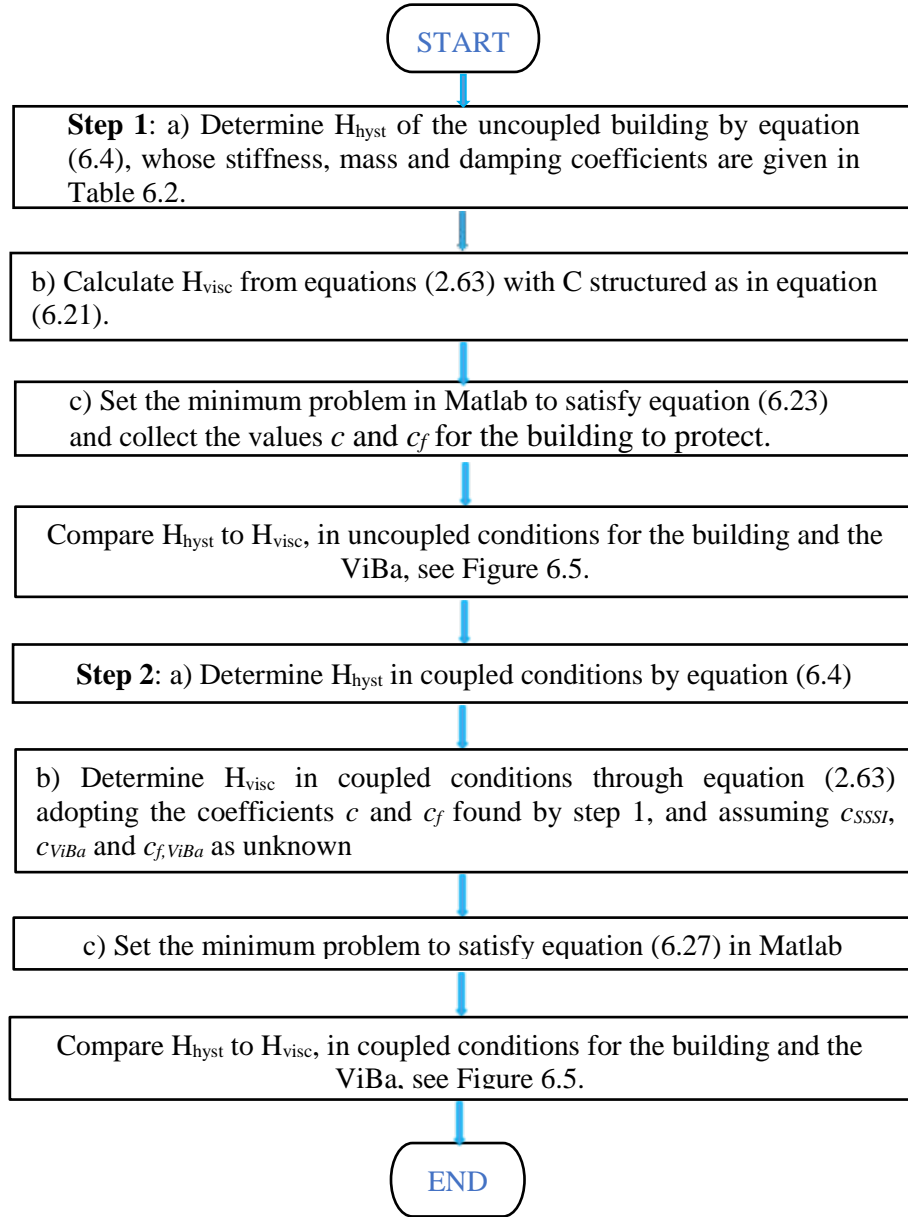


Figure 6.6. Flowchart of the proposed procedure to establish the equivalent viscous damping model of the investigated system from the hysteretic model of Cacciola and Tombari (2015).

In Figure 6.5 a) the moduli of the transfer functions relatively to the horizontal DOF of the building in uncoupled conditions, $H_{hyst}(\omega, \eta_1, \eta_f)$ and $H_{visc}(\omega, c, c_f)$ are displayed along with the corresponding functions for coupled conditions, denoted as $H_{hyst}(\omega, \eta_1, \eta_f, \eta_{SSSI}, \eta_{ViBa}, \eta_{f,ViBa})$ and with $H_{visc}(\omega, c, c_f, c_{SSSI}, c_{ViBa}, c_{f,ViBa})$. Whereas in Figure 6.5 b), the moduli of the transfer functions of the ViBa horizontal DOF in

uncoupled conditions, $H_{hyst}^{ViBa}(\omega, \eta_{SSSI}, \eta_{ViBa}, \eta_{f,ViBa})$ and $H_{visc}^{ViBa}(\omega, c_{SSSI}, c_{ViBa}, c_{f,ViBa})$ are displayed along with the transfer functions determined for coupled conditions, which are $H_{hyst}^{ViBa}(\omega, \eta_1, \eta_f, \eta_{SSSI}, \eta_{ViBa}, \eta_{f,ViBa})$ and $H_{visc}^{ViBa}(\omega, c, c_f, c_{SSSI}, c_{ViBa}, c_{f,ViBa})$.

The identification of the viscous damping coefficients for the system under investigation has been successfully achieved. The effectiveness of the procedure is confirmed by the plots in Figure 6.5 a) and b), from which the differences between the moduli of the transfer functions in comparison are found to be small. Specifically, Figure 6.5 a) highlights the accuracy of the optimisation procedure in relation to the buildings' transfer functions $H_{hyst}(\omega, \eta_1, \eta_f)$ and $H_{visc}(\omega, c, c_f)$ in uncoupled conditions, for which the unknowns of the minimisation problem are c and c_f . In the same figure, the comparison between the moduli of the transfer functions $H_{hyst}(\omega, \eta_1, \eta_f, \eta_{SSSI}, \eta_{ViBa}, \eta_{f,ViBa})$ and $H_{visc}(\omega, c, c_f, c_{SSSI}, c_{ViBa}, c_{f,ViBa})$ in coupled conditions is presented; in this case the minimisation problem was performed to minimise the difference between the two functions through the problem of optimisations with a number of three unknowns, c_{SSSI} , c_{ViBa} and $c_{f,ViBa}$. The agreement between the transfer functions $H_{hyst}(\omega, \eta_1, \eta_f, \eta_{SSSI}, \eta_{ViBa}, \eta_{f,ViBa})$ and $H_{visc}(\omega, c, c_f, c_{SSSI}, c_{ViBa}, c_{f,ViBa})$ is satisfactory although less precise than between $H_{hyst}(\omega, \eta_1, \eta_f)$ and $H_{visc}(\omega, c, c_f)$, for which the unknown for the optimisations problem where less.

A significant result is shown in Figure 6.5 b), where $H_{hyst}^{ViBa}(\omega, \eta_{SSSI}, \eta_{ViBa}, \eta_{f,ViBa})$ and $H_{hyst}^{ViBa}(\omega, c_{SSSI}, c_{ViBa}, c_{f,ViBa})$ relatively to the uncoupled conditions are in good agreement although c_{SSSI} , c_{ViBa} and $c_{f,ViBa}$ have been derived by the minimisation problem set for the building DOF in coupled conditions. The level of accuracy achieved for the moduli of the transfer functions for the ViBa in coupled conditions, $H_{hyst}^{ViBa}(\omega, \eta_1, \eta_f, \eta_{SSSI}, \eta_{ViBa}, \eta_{f,ViBa})$ and $H_{visc}^{ViBa}(\omega, c, c_f, c_{SSSI}, c_{ViBa}, c_{f,ViBa})$, satisfactorily is comparable to the accuracy achieved for the uncoupled case.

Reasonably, as shown by Figure 6.5, the response's reduction obtained through the ViBa calibrated for harmonic input, with frequency $\omega_0 = 22.62$ rad/s, under the hypothesis of viscous damping are of the 90%, slightly different from the reduction of the 87% originally obtained under the hypothesis of hysteretic damping.

As sought, the calibration of the equivalent viscous damping matrix from the loss factors derived empirically by Cacciola and Tombari (2015), has enabled to perform the time domain analyses for the systems under investigation presented hereafter. The equations of motion in the time domain, seen in equation (6.21), are solved assuming the mechanical parameters in Table 6.2 and the damping coefficients derived from the presented optimisation procedure. The equations of motion have been integrated by the step-by-step procedure in equations (2.54) and (2.55) for absolute motion. The system is forced by several harmonic base input, whose frequencies have been selected from Figure 6.5 in accordance to those values of the transfer functions that show significant effects of the ViBa. Harmonic input motions in terms of displacements of unitary amplitude are used. It has to be noticed that the control device may induce either beneficial or detrimental effects, depending on the input frequency forcing the system.

The values of the building's transfer function for a selected number of frequencies in coupled and uncoupled conditions presented in Figure 6.5 a) are listed in Table 6.3.

Labels	a	b	c	d	e	f	g	h
ω [rad/s]	15.05	20.35	21.05	22.62	24.95	26.15	27.95	30.05
$H^{unc}(\omega)$	1.908	5.471	7.552	19.3	5.054	3.365	2.215	1.573
$H^{coup}(\omega)$	1.917	7.448	5.096	1.743	5.402	9.196	4.4	2.449

Table 6.3. Values of the transfer function of the building's horizontal DOF at selected frequencies in coupled and uncoupled conditions under the hypothesis of viscous damping.

The steady state responses obtained from the Frequency Domain Analysis (FDA) reported in Table 6.3 are pertinently traced in Figure 6.7, where these can be compared to the steady state of the displacements time-histories to appreciate the agreement between the response obtained in the dual domains.

Noticeably, Figure 6.7 demonstrates the effectiveness of the calibration procedure used to derive the coefficients of the equivalent viscous damping matrix from the hysteretic model of Cacciola and Tombari (2015). Furthermore, Figure 6.7 d) shows the efficacy of the ViBa in reducing the response of the building by presenting the time-history of the response displacements in uncoupled and coupled conditions, being the latter obtained according to the closed-form formula to design the ViBa proposed by Cacciola and Tombari (2015).

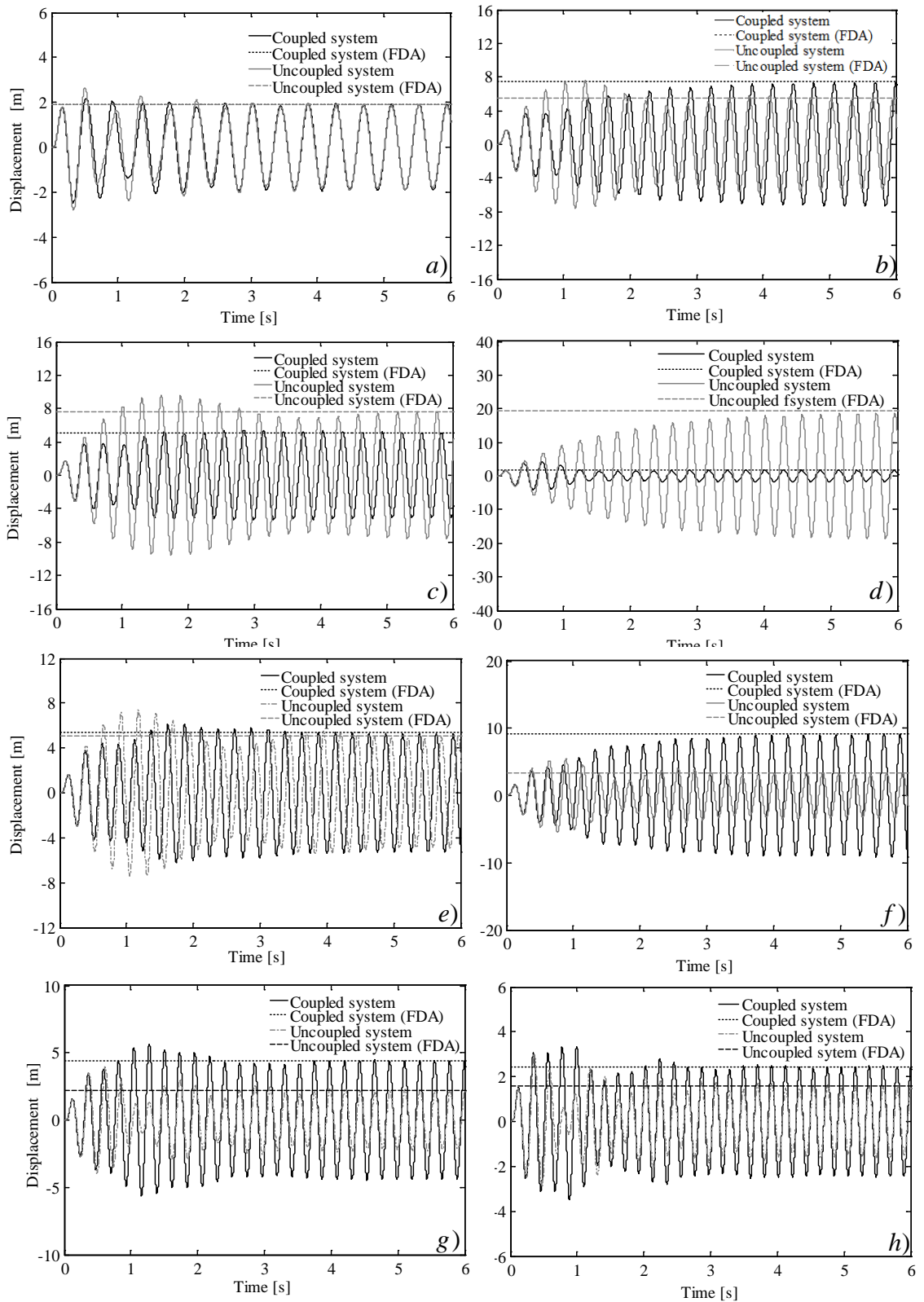


Figure 6.7. Displacement time-histories of the simplified structure of Cacciola and Tombari (2015) under harmonic input in coupled and uncoupled conditions.

6.3.2 Design of the ViBa for the Control of the SAC building 20-Storey Steel Frame

In this section, an application for passive vibration control of a 2D structure protected through the ViBa is presented. The control device is applied to reduce the vibrations of the linear benchmark structure, the SAC building 20-storey steel frame, forced by harmonic input. The building under investigation is the benchmark structure described in Chapter 4. The ViBa has been designed by following the procedure proposed by Cacciola and Tombari (2015) and reported in section 6.1.2. The analyses are carried out on two models: (i) a simplified discrete numerical model implemented in MATLAB, and (ii) a Finite Element model defined on SAP2000. The coupled and uncoupled responses of the building and ViBa under differently selected harmonic motions for both models are compared. By comparing the time-histories obtained from the two models the implications of adopting simplified discrete models to capture the SSSI and the SSI effects are observed. The SSSI and the SSI are accounted by linear elastic springs as conventional for the Winkler approach for modelling linear elastic soils. For both models the modal structural damping is considered with constant value of the 5% for all modes. Finally, the reduction of the structural displacements of a selected point, (i.e. roof displacements) of the building are observed from the difference of the steady state response of the time-histories in coupled and uncoupled conditions.

The simplified system comprising the SAC building, soil and ViBa device placed on rigid foundations on deformable soil, is modelled in MATLAB according to Figure 6.4, as a global 4 DOF system. By the knowledge of the mass and the first natural frequency of the building for fixed base, which is obtained from the numerical FE model, the stiffness of the simplified SAC building is inversely derived through the fundamental relation between mass, stiffness and natural frequency in equation (2.4). The mass of the building foundation has been assigned pertinently to the description of Othori et al. (2004). The foundation is assumed as rigid with 7.30 m embedment according to the benchmark. The mass of ViBa and the building's mass are considered identical as well as their foundations.

The ViBa stiffness has been calibrated by means of equation (6.12), in order to fulfil the design via the closed-form solution proposed by Cacciola and Tombari (2015) the soil-interaction and the SSSI stiffness coefficients have to be defined. The SSI an SSSI stiffness coefficients have been derived through a numerical technique applied on SAP2000, by which the matrix stiffness method for static analysis has been applied to the coupled foundations-soil-foundation system in Figure 6.4 . Specifically, since the soil is assumed linearly behaving, the coefficients were obtained with reference to Figure 6.4 by the followings: (i) assignment of fictitious supports to restrain the horizontal displacements at point 1 and 2 or 3, (ii) imposition of an unitary horizontal displacement to point 2 or 3, (iii) evaluation of the horizontal reactions at point 1 and 2 or 3, which respectively give the values: k_{SSSI} , the sum $k_{SSSI} + k_{SSI}$, from which k_{SSI} is found. The spacing between the foundation of the ViBa and of the building has been assumed 10 m. The mechanical characteristics of the SAC building and ViBa for the simplified model implemented in MATLAB are presented in Table 6.4.

	Mass [kg]	Stiffness [N/m]
Building	$m = 5.8 \times 10^6$	$k = 8.28 \times 10^7$
Building foundation	$m_f = 9.7 \times 10^5$	$k_f = 6.85 \times 10^7$
ViBa device	$m_{ViBa} = m$	$k_{ViBa} = 4.1695 \times 10^7$
ViBa foundation	$m_{f,ViBa} = m_f$	$k_{f,ViBa} = 6.85 \times 10^7$
SSSI parameters	-	$k_{SSSI} = 9.16 \times 10^7$

Table 6.4. Mechanical parameters for the SAC building and ViBa device.

The first two natural frequencies of the global system in coupled and uncoupled conditions are displayed in Table 6.5, where the frequencies $\omega_{1,unc}$ and $\omega_{2,unc}$ are respectively the first natural frequency of the single ViBa and SAC building, whereas $\omega_{1,coup}$ and $\omega_{2,coup}$ are the natural frequencies at which ViBa and building vibrate in coupled conditions.

Natural frequencies [rad/s]	$\omega_{1,coup}$	$\omega_{2,coup}$	$\omega_{1,unc}$	$\omega_{2,unc}$
Simplified model	2.18	2.97	2.08	2.47

Table 6.5. First two natural frequencies of the simplified SAC building-soil-ViBa system modelled on MATLAB.

The transfer functions for the simplified SAC building and ViBa in both coupled and uncoupled conditions are shown in Figure 6.8.

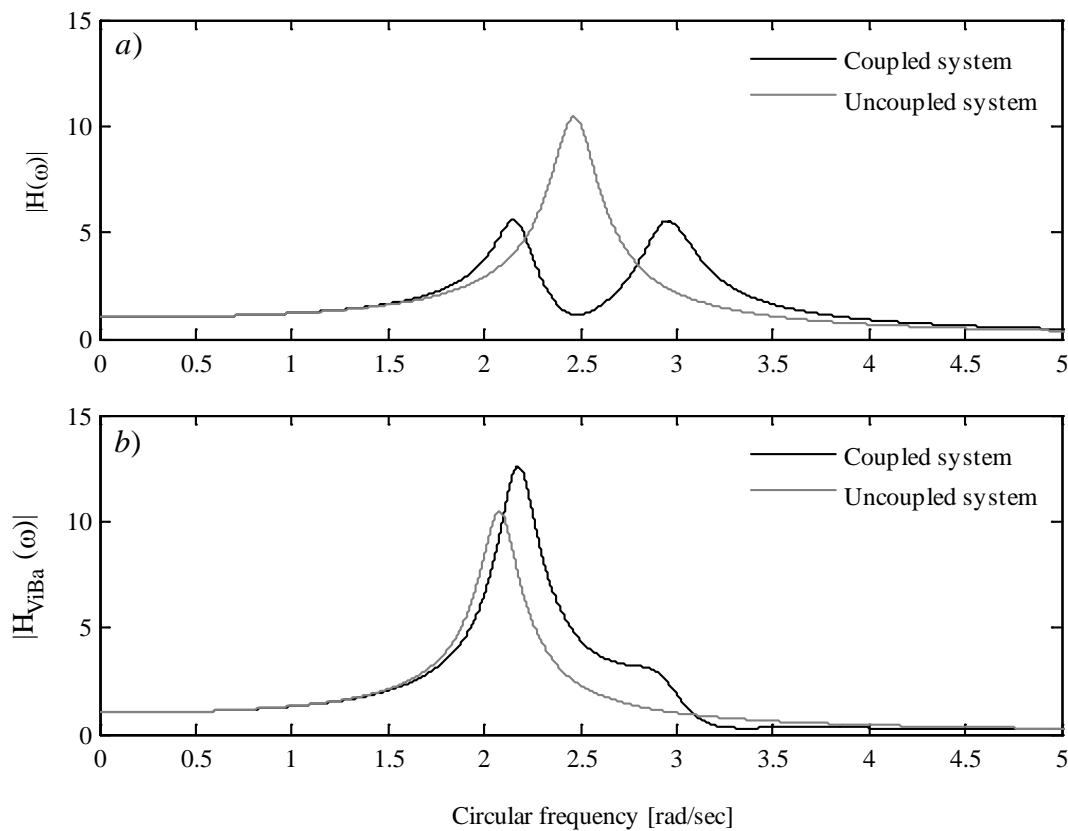


Figure 6.8. Transfer functions of: a) simplified SAC building; b) ViBa.

From Figure 6.8 a), in correspondence of the frequency of the uncoupled building, the significant reduction of 89% is achieved, whereas from Figure 6.8 b) the increase of the transfer function of the ViBa is observed.

In Figure 6.8 a) the two peaks of the transfer function in coupled conditions are respectively at the frequency of the ViBa in uncoupled conditions and of the building in coupled conditions, see values in Table 6.5. For the coupled system, in Figure 6.8 b), the two peaks of the curve are at the frequencies of the ViBa and of the building in coupled conditions.

In the second part of the design study, the benchmark model, which is depicted in Figure 6.9, has been implemented in SAP2000.

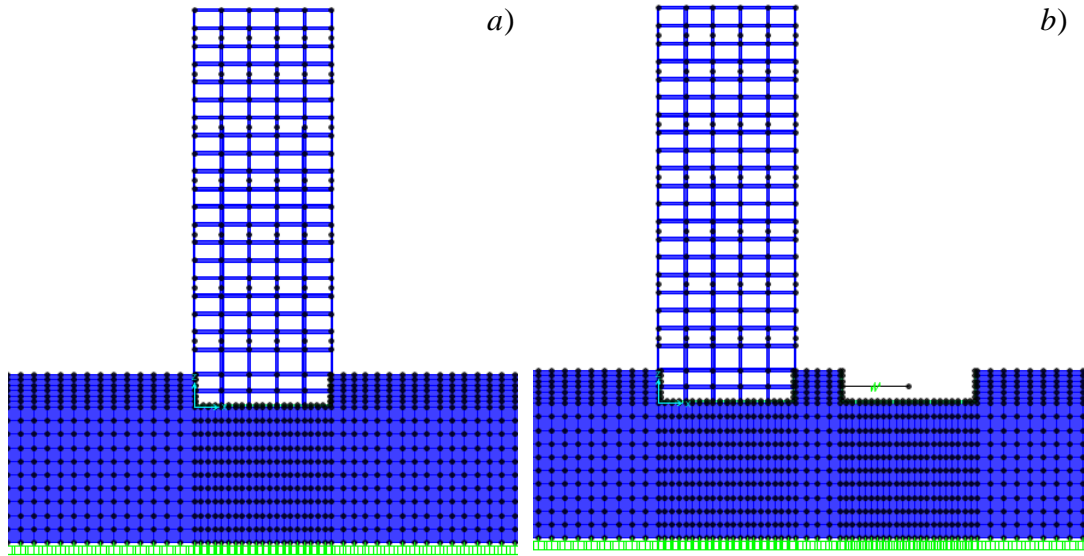


Figure 6.9. FE model in SAP2000 of the SAC building and soil underneath: a) uncoupled; b) coupled with ViBa.

The building and ViBa are placed on a soil deposit 30 m deep, value chosen in conformity to the Eurocode 8 recommendation for soils' characterisation.

Shear wave velocity v_s [m/s ²]	Soil mass density ρ_s [kg/m ³]	Poisson ratio ν	Shear Modulus G [Pa]
150	1300	0.2	29.25×10^6

Table 6.6. Geotechnical properties of the soil deposit adopted to model the SAC building-Soil-ViBa system in SAP2000.

In Table 6.7 the natural frequencies for the coupled and uncoupled SAC building and ViBa from the FE models are shown.

Natural frequencies				
[rad/s]	ω_{ViBa}^{coup}	ω_{Sac}^{coup}	ω_{ViBa}^{unc}	ω_{Sac}^{unc}
SAP2000 model	2.29	3.06	2.20	2.74

Table 6.7. First two natural frequencies of the SAC building-soil-ViBa system modelled on SAP2000 in coupled and uncoupled conditions.

It is worth to observe that the first natural frequency for the SAC building for the model on MATLAB and SAP2000 in uncoupled conditions differ less than 9.85%. Being the first mode of vibration in SAP2000 purely translational, as only the horizontal DOF are considered in the analysis, the difference depends on the

accuracy of the numerical method used for determining the SI and SSSI coefficients.

In order to control the vibrations of the structure the design has been performed according to the closed-form expression for the ViBa stiffness proposed by Cacciola and Tombari (2015) for harmonic input, calibrated for $\omega_0 = 2,74$ rad/s, which leads to the value $k_{ViBa} = 5.1471 \times 10^7$. Considering harmonic motions of unitary amplitude in terms of acceleration, whose frequencies are listed in Table 6.8, both the simplified model and the building implemented in SAP2000 are analysed.

Labels	a	b	c	d	e	f	g	h
ω [rad/s]	1	1.5	2.47	2.1	2.74	2.96	3.5	4

Table 6.8. Values of the selected frequencies of the harmonic input forcing the system SAC building-soil-ViBa.

Figure 6.10 presents the time-histories of the displacements of the SAC building modelled through the simplified system implemented in MATLAB. It can be noticed that the steady state of the time-histories in Figure 6.10 reflects the values of the transfer functions seen in Figure 6.8. Figure 6.11 shows the time-histories of the displacements of the roof of the SAC building implemented in SAP2000. For the simplified model implemented in MATLAB, the input is directly applied underneath the building and the ViBa unit. Contrarily, in the model in SAP2000 the input propagates from the bedrock to the free field.

The effects of the wave propagation are not significant as shown by comparing Figure 6.10 c) and Figure 6.11 e), for which the displacements due to the harmonic input relatively to the resonant frequencies are in good agreement.

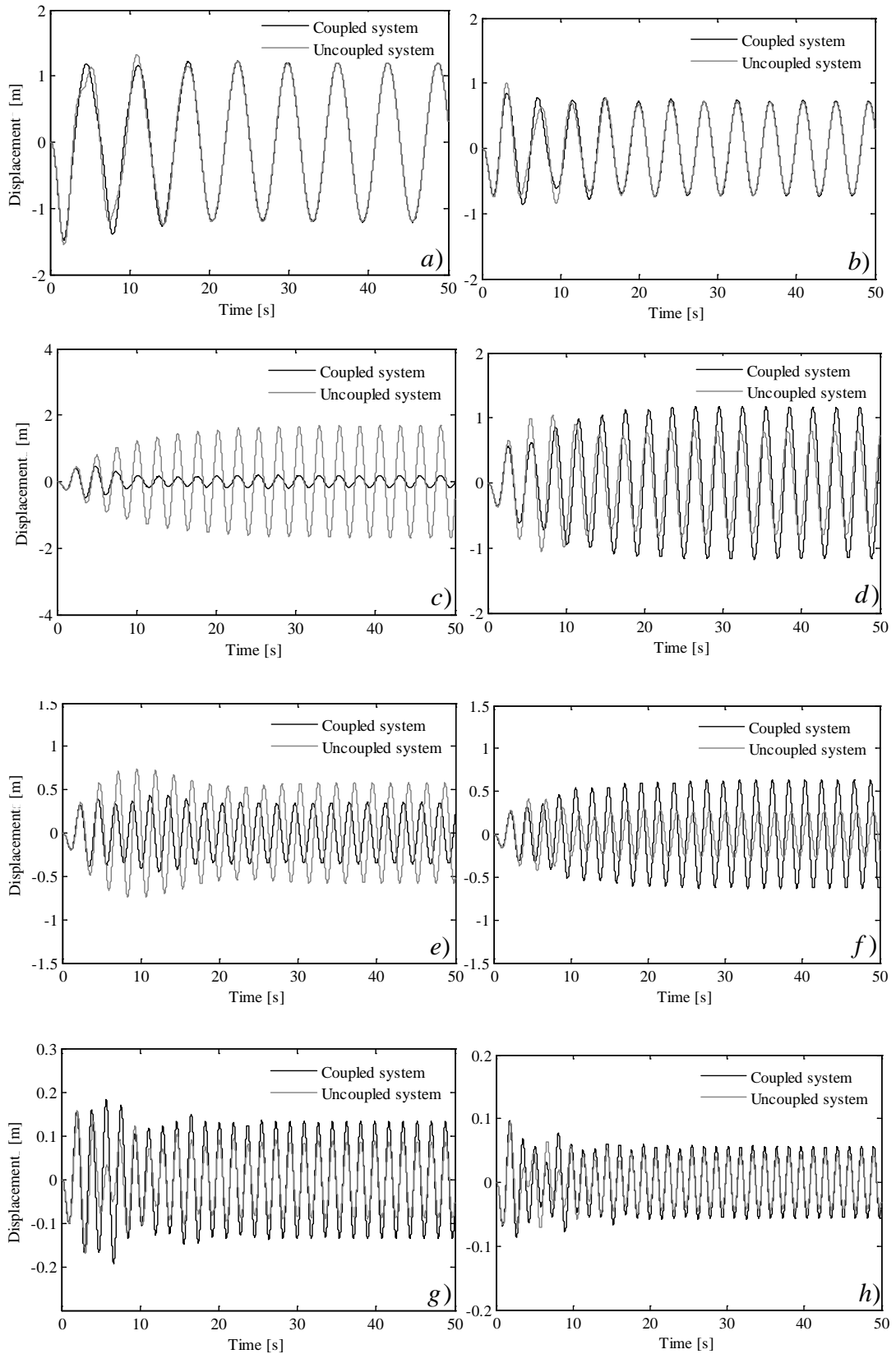


Figure 6.10. Displacement time-histories of the SAC building modelled on MATLAB under harmonic input in coupled and uncoupled conditions.

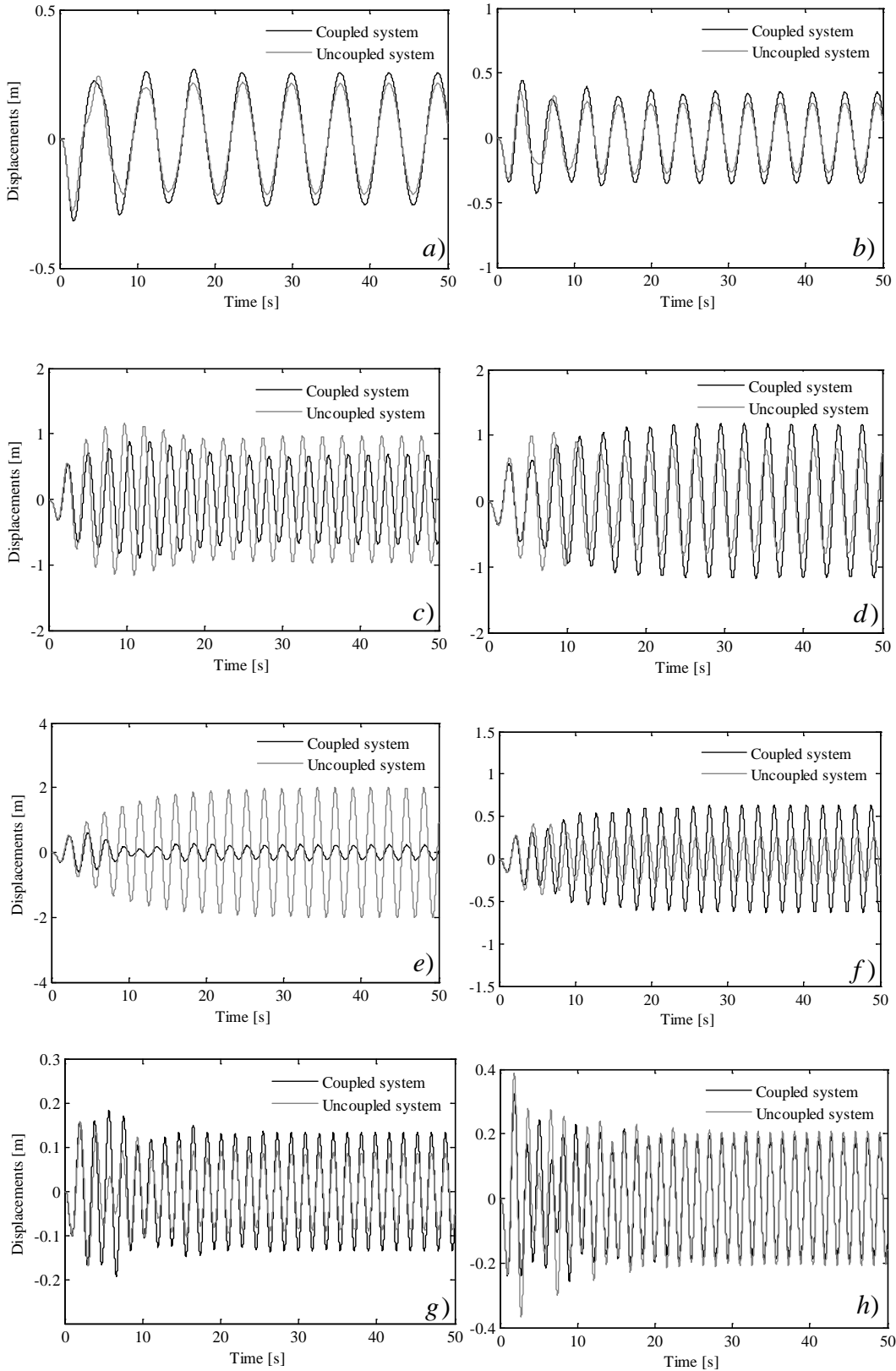


Figure 6.11. Displacement time-histories of the SAC modelled on SAP2000 under harmonic input in coupled and uncoupled conditions.

6.4 Design of the Vibrating Barrier for Stationary Stochastic Excitation

The design and effectiveness of the Vibrating Barriers to protect buildings under harmonic loading, has been proven by the investigations based on frequency domain analyses and reviewed in this Chapter. Specifically, to expand the formulation of Cacciola and Tombari (2015) to the time domain as proposed, enables to design the ViBa for stochastic earthquake ground motions and to perform pertinent Monte Carlo Simulation, by which, insight into transient analysis of the structural response is additionally gained.

In this section, the stochastic analysis in the time domain for the system SSSI depicted in Figure 6.4 is presented. In order to state the dynamic equilibrium of the system, the deterministic differential equations of motion seen in equation (2.50) are extended for input ground motion modelled as zero-mean Gaussian stochastic process, which is represented by the vector

$$\mathbf{U}_g(t) = \boldsymbol{\tau}U_g(t) \quad (6.25)$$

The stochastic equations of motion for MDOF systems in terms of absolute displacements under deterministic initial conditions $P[U(0) = 0 \cap \dot{U}(0) = 0] = 1$, are expressed by the following system

$$\mathbf{M}\ddot{\mathbf{U}}(t) + \mathbf{C}\dot{\mathbf{U}}(t) + \mathbf{K}\mathbf{U}(t) = \mathbf{K}\boldsymbol{\tau}U_g(t) + \mathbf{C}\boldsymbol{\tau}\dot{U}_g(t) \quad (6.26)$$

where $\mathbf{U}(t)$, $\dot{\mathbf{U}}(t)$ and $\ddot{\mathbf{U}}(t)$ are respectively the $n \times 1$ stochastic displacements, velocity and acceleration vectors, $U_g(t)$ and $\dot{U}_g(t)$ are the ground displacement and velocity stochastic process.

By solving the dynamic equilibrium stated above, the peak of the absolute maxima of the building's response is evaluated according to the following definition

$$X_{U_b} = E[\max|U_b(t)|] \quad (6.27)$$

where $E[\cdot]$ is the expectation operator and $U_b(t)$ is the stochastic response process for the degree of freedom of the building to protect.

Specifically, the design of the ViBa's structural parameters is studied for the case of stationary input via the procedure described hereafter.

In this section, the first passage problem of the response displacement process presented in Chapter 2, is rewritten for the DOF of the building to protect, that is

$$X_{U_b}(T_s, p) = \eta_{U_b}(T_s, p) \sqrt{\lambda_{0, U_b}} \quad (6.28)$$

where U_b is the response process of the horizontal displacements of the top floor of the building to protect, X_{U_b} is the fractile of the peak distribution with probability p of not exceedance, T_s is the time observing window, λ_{0, U_b} is the zero-th order geometrical spectral moment of the response process η_{U_b} is the peak factor seen in equation (2.142) defined by the with bandwidth factor given in equations (3.5) and the number of out-crossings obtained by substituting equation (2.99) into (2.131).

The expression for the geometrical spectral moments is given by the general formula in equation (2.108), which expanded for MDOF reads

$$\lambda_{i, U} = \int_0^{+\infty} \omega^i \mathbf{G}_{UU}(\omega) d\omega \quad (6.29)$$

where $\mathbf{G}_{UU}(\omega)$ is the PSD matrix of the response in terms of absolute displacements.

The expression for the PSD matrix $\mathbf{G}_{UU}(\omega)$ is obtained from the stochastic response in the frequency domain by taking the following expectation

$$\mathbf{G}_{UU}(\omega) = E[\mathbf{U}(\omega)\mathbf{U}^*(\omega)] \quad (6.30)$$

where $\mathbf{U}(\omega)$ is the stochastic response of the system in the frequency domain under the hypothesis of viscous damping, that expanded gives

$$E[\mathbf{U}(\omega)\mathbf{U}^*(\omega)] = E\left[\left(\mathbf{H}_{visc}(\omega)U_g(\omega)\right)\left(\mathbf{H}_{visc}(\omega)U_g(\omega)\right)^*\right] \quad (6.31)$$

$$E[\mathbf{U}(\omega)\mathbf{U}^*(\omega)] = \mathbf{H}_{visc}(\omega)\mathbf{H}_{visc}^*(\omega)E[U_g(\omega)U_g^*(\omega)] \quad (6.32)$$

where according to the definition of PSD function $E[U_g(\omega)U_g^*(\omega)] = G_{U_g}(\omega)$, that substituted in the above equation gives

$$E[\mathbf{U}(\omega)\mathbf{U}^*(\omega)] = \mathbf{H}_{visc}(\omega)\mathbf{H}_{visc}^*(\omega)G_{U_g}(\omega) \quad (6.33)$$

Therefore comparing equation (6.30) and (6.33), accounting for the definition of the viscous transfer function by equations (6.3), (6.4) and (6.20), the PSD of the stochastic response process reads

$$\mathbf{G}_{UU}(\omega) = \mathbf{H}_{visc}(\omega)\mathbf{H}_{visc}^*(\omega)G_{U_g}(\omega) \quad (6.34)$$

The PSD of the input process is selected according to the soil conditions, and the transfer function $\mathbf{H}_{visc}(\omega)$, which depends on the SSSI system's factors, is therefore a function of the design parameters to be optimized.

The methodology proposed in this work tackles the design of the ViBa under stochastic stationary excitation for the selected DOF of the structure to protect by: (i) defining the peak of the maxima horizontal displacements relative to the foundation, with the not exceeding probability p (Cacciola et al 2015), for which

$$G_{U^r U^r}(\omega) = G_{U^T U^T}(\omega) + G_{U^F U^F}(\omega) - G_{U^F U^T}(\omega) - G_{U^T U^F}(\omega) \quad (6.35)$$

and (ii) reducing the peak of the response from solving a problem of minimization, that reads

$$\left. \begin{aligned} &\min \left\{ X_{U_b}^r(T_S, p, \boldsymbol{\beta}) \right\} \\ &\boldsymbol{\beta} \left\{ k_{ViBa}, m_{ViBa}, c_{ViBa} \right\} \in \mathfrak{R}_0^+ \end{aligned} \right\} \quad (6.36)$$

where $\boldsymbol{\beta}$ is the vector listing the ViBa design parameters.

The problem of minimisation of the stochastic response for the building-soil-ViBa systems is undertaken by a parametric study in which the unknowns of the problem are obtained by varying the ViBa parameters over a fixed range $\beta_{\min} < \beta < \beta_{\max}$.

The optimisation problem has been performed by calculating for a fixed value of m_{ViBa} and every pair $k_{ViBa} - c_{ViBa}$ listed in β , the peak factors and response root mean square values, such to obtain for every pair, the fractile 50% of the peak distribution. Finally, the optimal design parameters are found by identifying the pair associated to the minimum fractiles 50 % of the peak distribution obtained.

6.5 Numerical Application of Stochastic Analysis and Design of the Vibrating Barrier

In the next sections, the parametric study presented in equation (6.36) is performed. The study consists of evaluating the peak of the building response to be minimised given a range of ViBa's structural parameters a priori assigned, which are the stiffness and the viscous damping coefficient. For the SSSI system calibrated with the established ViBa's design parameters, the mean peak of the response of the building to protect is evaluated via Monte Carlo Simulation, i.e. solving the equation of motion in (6.26), for the sets of accelerograms simulated from different ground motion models. Therefore, the results of the investigations are presented in terms of the reductions of the mean peak of the displacements of the building, obtained by comparison of the response in uncoupled and coupled conditions.

6.5.1 Ground Motion Models Specifications

In this section, the stochastic ground motion models defined for loading the SSSI systems investigated in this Chapter are specified. Three models, namely the quasi-stationary (QS), non-stationary (NS) and non-stationary with imposed variability (NSV) are generated by Spectral Representation Method (SRM). The sets of accelerograms fulfil the spectrum compatibility criteria prescribed by the Eurocode 8 (EC8).

The ground motion stochastic processes used for the investigations have been modelled according to the procedure presented in Chapter 2, see section 4.1. The evolutionary power spectral density functions of the stochastic processes are presented in Figure 6.12, which displays the functions obtained after a number of iterations performed in order to meet the spectrum compatibility criteria, which has been achieved by following the scheme presented in equation (3.47).

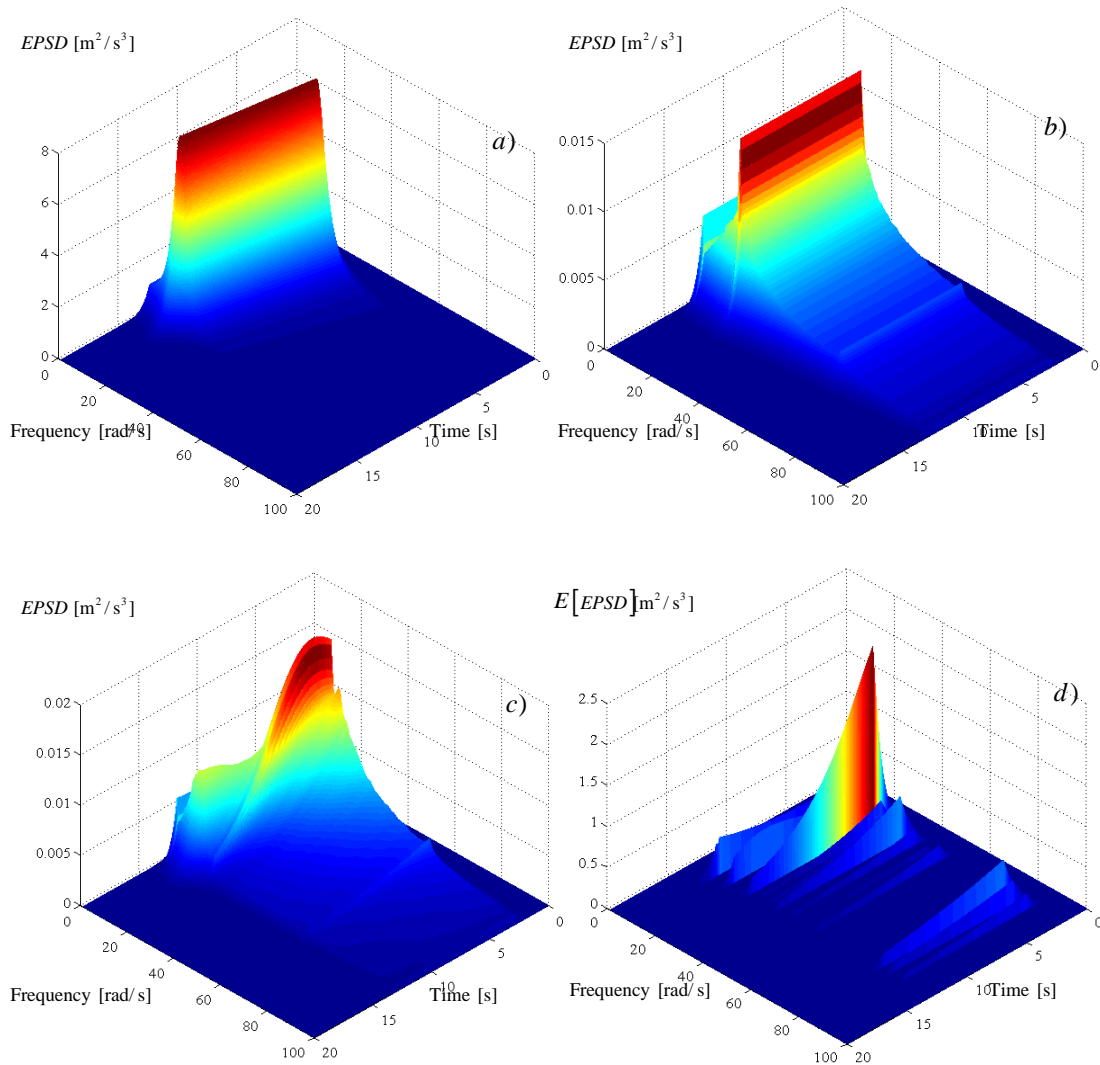


Figure 6.12. Evolutionary PSD functions: a) C&P model, b) quasi-stationary; c) non-stationary; d) non-stationary and imposed variability.

The stationary PSD function adopted to implement the ground motion models is the PSD proposed by Cacciola et al. (2004), for the soil characteristics specified by the EC8 and presented in the Table 6.9.

Parameter	Value
S	1.8
a_g	0.102 g
T_B	0.1 s
T_C	0.3 s
T_D	1.2 s

Table 6.9. Target response spectrum parameters of definition: Type 2, soil D.

For the non-stationary and non-stationary with variability stochastic processes, the non-stationary frequency content has been established by modelling the time frequency variation of the CP evolutionary spectrum according to the parameters defined by equation (4.2), that are: the frequency at the initial time, $\omega_{t_0} = 25$ rad/s, the frequency limit at the final time $\omega_{t_f} = 10$ rad/s, the parameter of the second filter, $\omega_f(t)$, which has been set according to equation (3.73), and the damping ratios $\zeta_g = 0.2$ and $\zeta_f = 0.6$, selected according to Der Kiureghian and Neuenhofer (1992).

The mean instantaneous frequency content of the three ground motion stochastic processes is estimated according to equation (2.105) and displayed in Figure 5.12.

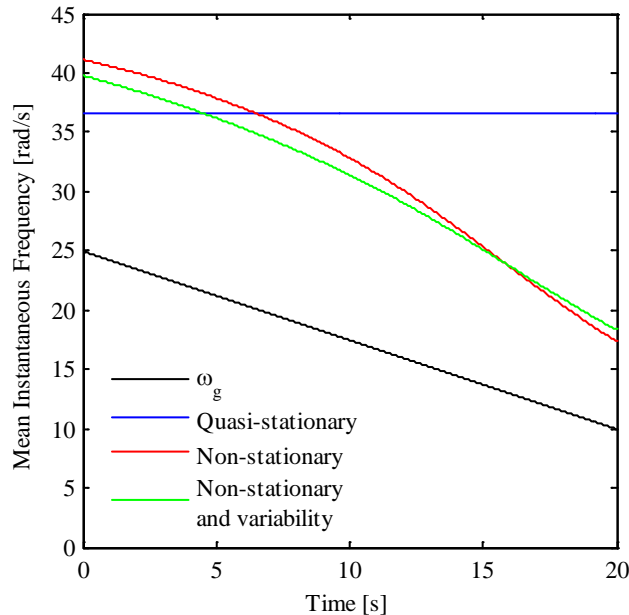


Figure 6.13. Mean instantaneous frequency of the response-spectrum-compatible ground motion models adopted in the SSSI investigations.

The three sets of simulated accelerograms are compatible with the EC8 response spectrum presented in equation (3.44). In order to meet the recommendations mandated by the EC8, the matching between the mean response spectrum of the simulated time-histories and the target spectrum is guaranteed within the prescribed tolerance, both along the prefixed range of periods according to equation (3.45), and relatively to the value of the simulated mean response spectral acceleration at $T_0 = 0$ according to equation (3.46).

From the evolutionary power spectral density function in Figure 6.12, a number of 500 ground motion time-histories have been simulated via SRM through equation (3.43). The time-histories were simulated by superposing a number of 1000 harmonics sampled with a frequency step of $\Delta\omega = 0.1$ rad/s. The total duration of the signal is equal to 20 s and the strong motion phase selected according to the minimum value of 10 s required by EC8. In Figure 6.14, the trajectories of the simulated time-histories are shown.

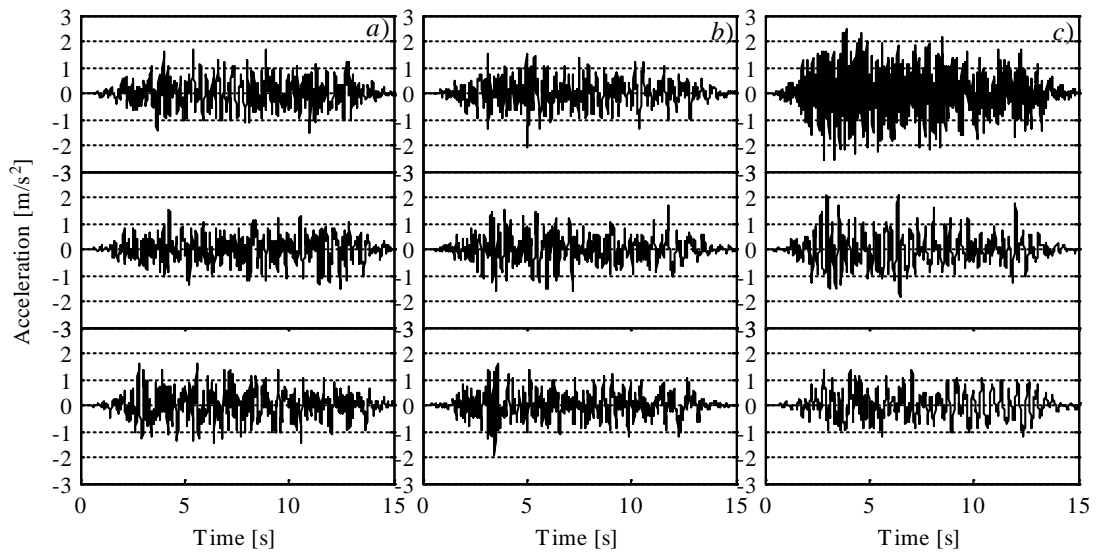


Figure 6.14. Trajectories of simulated ground motion accelerograms: a) quasi-stationary; b) non-stationary; c) non-stationary with imposed variability.

From the selected time-histories in Figure 6.14, the frequency non-stationarity of the evolutionary power spectral density functions from which the samples are generated can be observed. The simulated ground motion time-histories have been

adjusted by baseline correction, through the scheme presented in equation (4.3), in order to yield realistic velocity and displacement functions.

The set of simulated quasi-stationary, non-stationary and non-stationary with imposed variability accelerograms, present a mean value of their PGA respectively of: 1.81, 1.80 and 2.21 m/s^2 ; these values are to be compared with the PGA of the target response spectrum, which is $Sa_g=1.8 \text{ m/s}^2$.

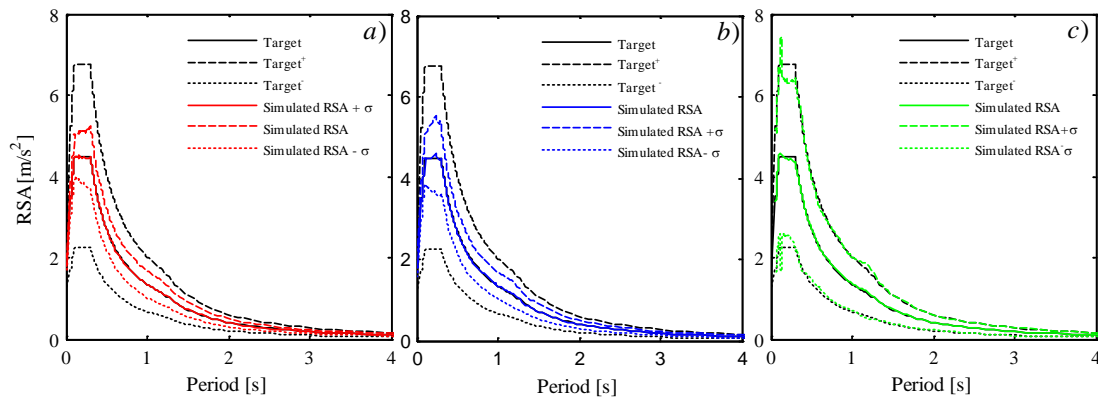


Figure 6.15. Comparison between simulated and target response spectra: a) stationary; b) non-stationary; c) non-stationary with imposed variability.

From Figure 6.15 the fulfilment of the spectrum compatibility requirements is shown. Notably, the mean response spectra present a satisfactory achievement of the spectrum compatibility requirement for all the three models. From Figure 6.15 c), the reference plots relatively to the $\pm\sigma$ spectral accelerations at the plateau level, show that the non-stationary model with variability has not reached the imposed value of standard deviation of $\sigma = 0.5$. The number of iterations set to achieve the matching between the simulated and the target $\pm\sigma$ response spectra have been limited in order to reduce the computational costs.

Figure 6.16 shows the convergence of the statistics of the PGA for the three sets of ground motion models. The mean, 50% and 95% fractile of the distribution of the PGA relatively to the ground motion with imposed variability differs especially regarding the 5% and 95% fractiles from the other two ground motion models considered. From Figure 6.17 b), differences between the ground motions with and without variability are observed above the 50% fractile. Above the median value of

the distributions of the PGA values, the higher the fractile the higher the differences between ground motion with imposed variability and the quasi-stationary and non-stationary models.

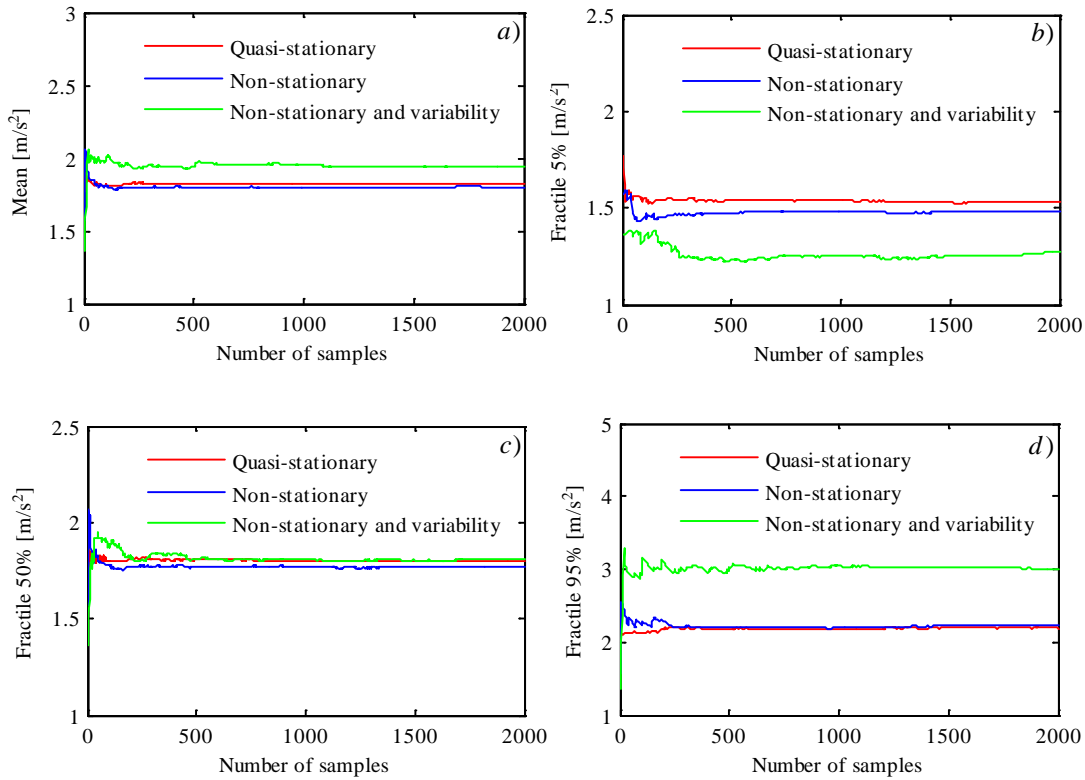


Figure 6.16. Ground motion models' peak ground acceleration: a) mean; b) fractile 5%; c) median; d) fractile 95%.

In Figure 6.17 the probability density function and the cumulative density function of the distribution of the PGA are shown.

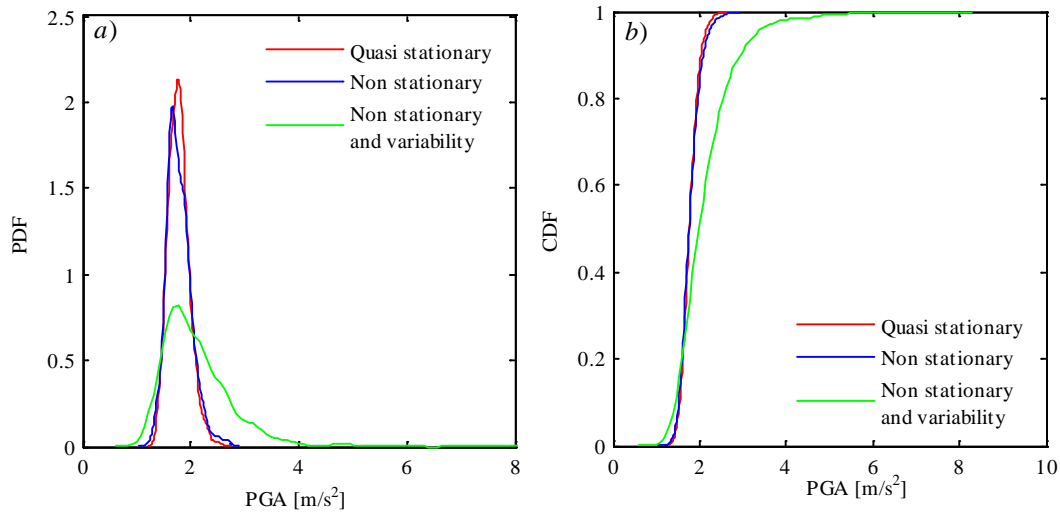


Figure 6.17. a) Probability density function and b) cumulative density function of the peak ground acceleration of the quasi-stationary, non-stationary and non-stationary with variability ground motions.

6.5.2 Parametric Study to Calibrate the ViBa and Monte Carlo Simulation Study

In this section, the methodology introduced in section 6.4 to determine the optimal design parameters for the ViBa is applied by a parametric study. In order to solve the problem of minimum search presented in equation (6.36), once the stationary PSD function to model a stationary earthquake ground motions is selected, the procedure has been performed by the following steps:

- To establish the range for the unknowns of the problem, which are the stiffness and the viscous damping coefficient of the ViBa, listed in the vector $\boldsymbol{\beta} = \{k_{ViBa}, c_{ViBa}\}$.
- To compute the transfer function $\mathbf{H}_{visc}(\omega, \boldsymbol{\beta})$ for every pair of unknowns, through which the stochastic responses of the building to protect is evaluated according to equation (6.34).
- To calculate the zero-th order spectral moment of the response by equation (6.29).
- To determine the value of the largest peak of the response, $X_{U_b}(T_S, p)$ with associated not exceeding probability p , for the assigned couples $\{k_{ViBa}, c_{ViBa}\}$ varying over a prefixed range.
- To evaluate the distribution of the peak of the response from equation (6.34) with a probability of not exceedance $p=0.5$, i.e. fractile 50%.
- To establish the reduction of the structural response for the DOF of the building to protect, as the percentage difference for the peak of the maxima of the response obtained in coupled and uncoupled conditions, that is

$$Reduction\% = \left[\frac{X_{U_b}^{coup}(T_S, p, \boldsymbol{\beta}) - X_{U_b}^{uncoup}(T_S, p, \boldsymbol{\beta})}{X_{U_b}^{uncoup}(T_S, p, \boldsymbol{\beta})} \right] \times 100 \quad (6.37)$$

where $X_{U_b}^{coup}(T_s, p, \boldsymbol{\beta})$ is the largest peak of the response of the global system for ViBa coupled with the structure and $X_{U_b}^{uncoup}(T_s, p, \boldsymbol{\beta})$ for uncoupled conditions. The interaction stiffness and damping coefficient seen in equation (6.21) in uncoupled conditions are set as: $k_{SSSI} = 0$, $c_{SSSI} = 0$.

In the following sections, the methodology proposed to design the ViBa is applied to address the effectiveness of the procedure established for stationary stochastic input. The design of the ViBa is tested for systems under the simulated earthquakes ground motions that, more realistically than stationary models, characterise the seismic action. The Monte Carlo Simulation method has been employed to predict the response of the structural systems under investigation, which are the model proposed by Cacciola and Tombari (2015) and the SAC benchmark building (Othori et al. 2004). The reduction of the mean peak displacement for the buildings is addressed by MCS considering the ground motions models presented in section 6.5. Finally, the reductions of the response of the different building-soil-ViBa systems forced by the sets of accelerograms are compared.

6.5.2.1 Design of the ViBa for the Control of the Simplified Structure of Cacciola and Tombari (2015) under Gaussian Stochastic Excitation

In this section, for the simplified structure of Cacciola and Tombari (2015), the results of the calibration of the ViBa's stiffness and viscous damping coefficient are presented. The parametric study has been performed for different mass ratios of the mass of the ViBa and the building. As Table 6.10 shows, four scenarios are investigated for selected ratios m_{ViBa} / m .

m_{ViBa} / m	k_{ViBa} [N/m]	c_{ViBa} [Ns/m]	Reduction [%]
0.5	195	1.30	24.74
1.05	450	4.50	33.10
1.5	710	10.6	37.42
2	1055	23.50	41.07

Table 6.10. ViBa's parameters for different ratios m_{ViBa} / m obtained by the design under stationary stochastic excitation for the protection of the structure of Cacciola and Tombari (2015) through ViBa.

Table 6.10 displays the ViBa's design parameters obtained by the optimization procedure, in which the input is modelled as the stationary stochastic ground motion process as specified in section 6.5. Specifically, the ratio $m_{ViBa} / m = 1.05$ corresponds to the prototype studied by Cacciola and Tombari (2015).

Figure 6.18 shows the surfaces plots representing the reduction of the building's peak response $X_{U_b}(T_s = 10 \text{ s}, p = 0.5)$.

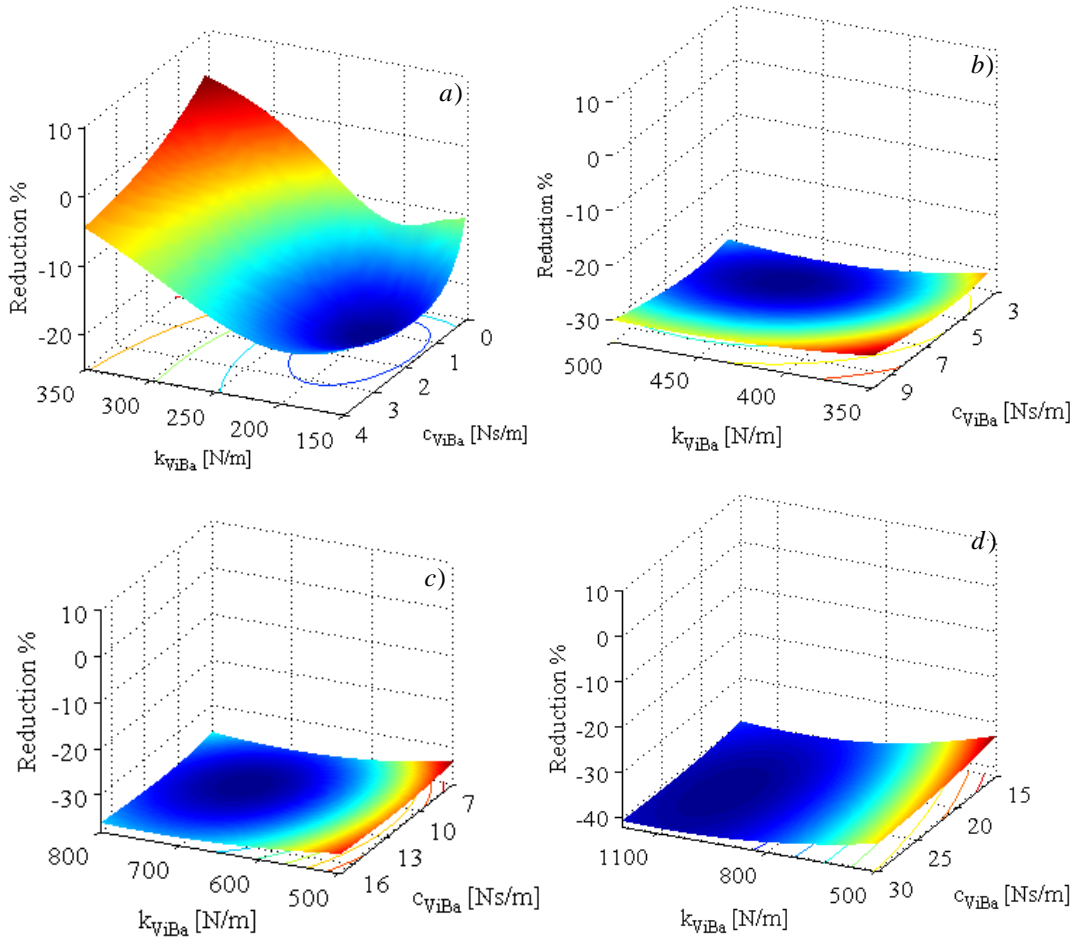


Figure 6.18. Surface plots of the parametric study to reduce the displacements relative to the foundation of the structure of Cacciola and Tombari (2015) for: a) $m_{viBa}/m = 0.5$; b) $m_{viBa}/m = 1.05$; c) $m_{viBa}/m = 1.5$; d) $m_{viBa}/m = 2$.

From Figure 6.18 it is observed that the higher the ratio m_{viBa}/m the flatter the parametric surface, which reflects the case in which a wider range of values determines reductions of close magnitude, while for $m_{viBa}/m = 0.5$ the response reduction is obtained for couple of values $\{k_{viBa}, c_{viBa}\}$ which are concentrated about a smaller range of coordinates. This implies that for such a scenario the efficiency of the device is more sensitive to perturbations of the values of the design parameters.

6.5.2.2 Stochastic Response of the Simplified Structure of Cacciola and Tombari (2015) Protected with the ViBa

The response of the prototype of the one building-soil-ViBa system formulated by Cacciola and Tombari (2015) to the simulated GMMs is presented hereafter. The values of the ViBa's stiffness and viscous damping coefficient in Table 6.10 characterise the SSSI systems in four opportunely selected mass ratios, m_{ViBa} / m . The systems have been forced by the three sets of accelerograms simulated from the quasi-stationary (QS), non-stationary (NS) and non-stationary with imposed variability (NSV) ground motion stochastic processes.

The natural frequencies of the numerical models calibrated with the ViBa's design parameters from the proposed procedure, are reported in Table 6.11.

Natural frequencies [rad/s]								
m_{ViBa} / m	$\omega_{1,unc}$	$\omega_{1,coup}$	$\omega_{2,unc}$	$\omega_{2,coup}$	$\omega_{3,unc}$	$\omega_{3,coup}$	$\omega_{4,unc}$	$\omega_{4,coup}$
0.5	21.83	22.02	22.62	25.84	46.06	51.24	73.51	79.17
1.05	19.95	20.56	22.62	26.04	52.74	56.87	73.51	79.33
1.5	18.92	19.75	22.62	26.15	58.55	61.90	73.51	79.56
2	17.92	18.92	22.62	26.21	65.26	67.59	73.51	80.10

Table 6.11. Coupled and uncoupled natural frequencies of the system building-soil-ViBa for different ratios m_{ViBa} / m .

The model proposed by Cacciola and Tombari (2015) agrees with the ratio $m_{ViBa} / m = 1.05$. For the case of ViBa designed for deterministic input, the natural frequencies of the system proposed by Cacciola and Tombari (2015) in coupled conditions are presented in Table 6.1, which compared with the values in Table 6.11 in coupled conditions, show differences less than the 1%.

The first natural frequency of the SSSI system in coupled conditions, $\omega_{1,coup}$, is smaller than the first natural frequency of the uncoupled building, $\omega_{2,unc}$, and it diminishes as the mass ratio m_{ViBa} / m increases. Whereas, the second natural frequency of the coupled system, $\omega_{2,coup}$, is higher of the fundamental frequency of the uncoupled building $\omega_{2,unc}$ and it tends to larger values as the mass ratio increases.

The first and the second natural frequency of the coupled system are respectively representative of the motion of the ViBa and the building. The natural frequencies variation is visualised in Figure 6.19.

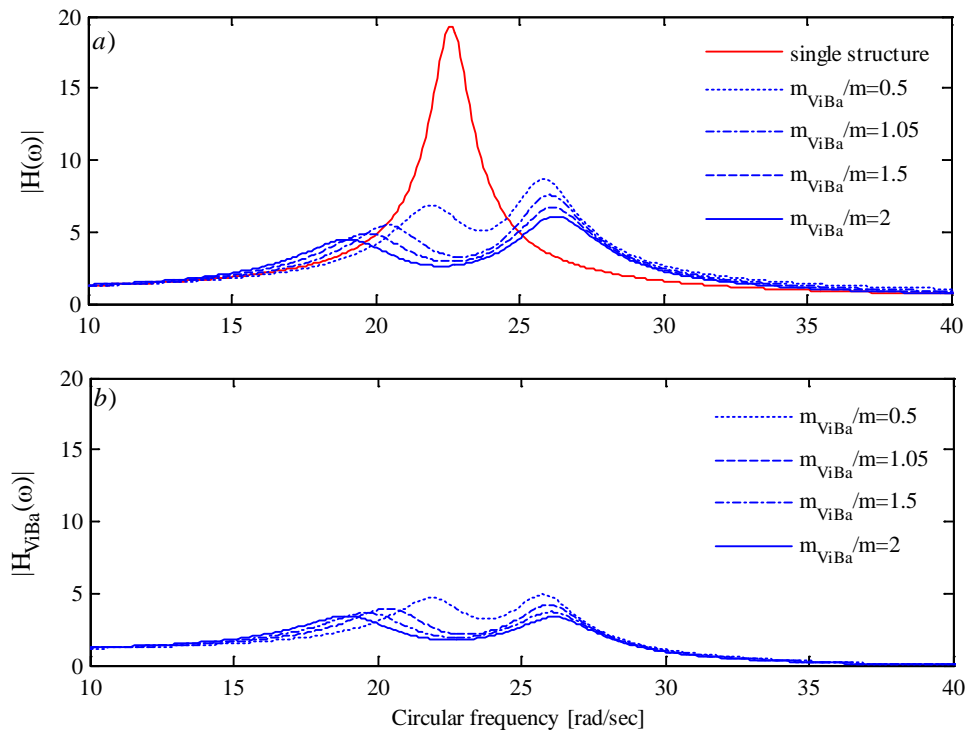


Figure 6.19. Transfer functions of the ViBa and the modified Cacciola and Tombari (2015) prototype building for different values of m_{ViBa} / m .

According to the observations made and the illustrations in Figure 6.19 a), in coupled conditions the systems' stiffness increases the higher the mass ratio. Therefore, the higher the mass ratio, the shorter the transient of the response of the building to protect. This might justify the discrepancies between the reductions obtained from the MCS study, see Table 6.12-Table 6.27 and those determined under stationary stochastic input, presented in Table 6.28, which reduce by increasing the mass ratio.

In Table 6.12-Table 6.15 the statistics of the displacements of the mass of the building according to the scenario $m_{ViBa} / m = 0.5$ are reported; in this case, the displacements' reduction determined in the design's phase (i.e. fractile 50%) is of 24.74%.

Mean [m]	QS	NS	NSV
Coupled	0.0794	0.0808	0.0805
Uncoupled	0.0964	0.0969	0.0932
Reduction %	17.6313	16.6372	13.6261

Table 6.12. Monte Carlo Simulation: mean of the displacements of the building protected with ViBa for $m_{ViBa} / m = 0.5$.

Fractile 5% [m]	QS	NS	NSV
Coupled	0.0627	0.0597	0.0465
Uncoupled	0.0715	0.0676	0.0508
Reduction %	12.3077	11.6864	8.4646

Table 6.13. Monte Carlo Simulation: fractile 5% of the displacements of the building protected with ViBa for $m_{ViBa} / m = 0.5$.

Fractile 50% [m]	QS	NS	NSV
Coupled	0.0783	0.0789	0.0740
Uncoupled	0.0941	0.0952	0.0849
Reduction %	16.7906	17.1218	12.8386

Table 6.14. Monte Carlo Simulation: fractile 50% of the displacements of the building protected with ViBa for $m_{ViBa} / m = 0.5$.

Fractile 95% [m]	QS	NS	NSV
Coupled	0.1002	0.1085	0.1352
Uncoupled	0.1282	0.1352	0.1621
Reduction %	21.8409	19.7485	16.5947

Table 6.15. Monte Carlo Simulation: fractile 95% of the displacements of the building protected with ViBa for $m_{ViBa} / m = 0.5$.

From the tables, the highest reduction of the displacements relative to the foundation is obtained for the fractile 95%, with a value of 21.84% under the action of the set of QS simulated accelerograms.

In Figure 6.20 the convergence of the statistics of the peak displacements of the building to protect in coupled conditions are presented.

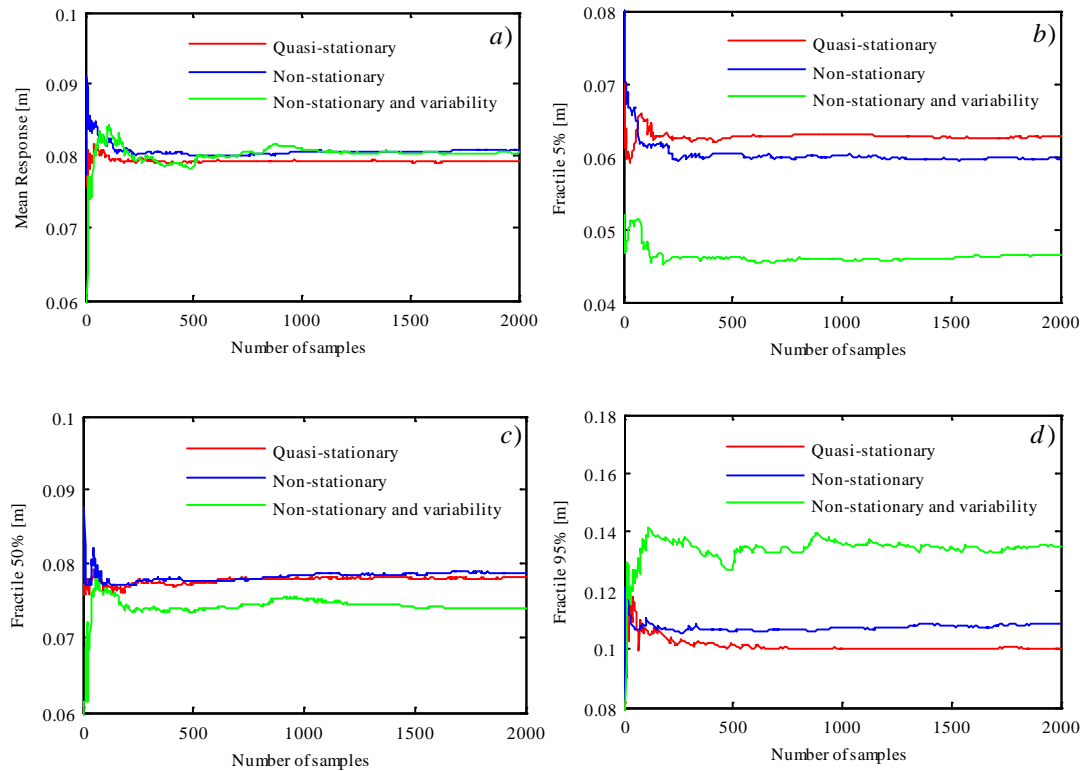


Figure 6.20. Convergence of the response of the building protected with ViBa: a) mean; b) fractile 5%; c) median; d) fractile 95% for $m_{ViBa} / m = 0.5$.

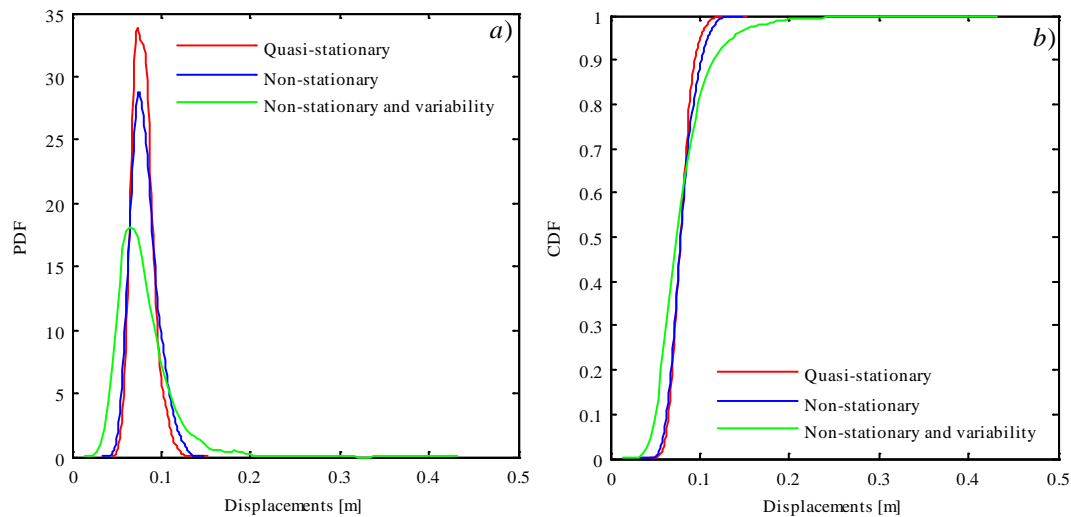


Figure 6.21. a) Probability density function; b) cumulative density function of the response of the building protected with ViBa for $m_{ViBa} / m = 0.5$.

In Table 6.16-Table 6.15 the results of the MCS analysis are presented for the scenario relatively to the mass ratio $m_{ViBa} / m = 1.05$, for which the reduction obtained by direct stochastic design is 33.10 %.

Mean [m]	QS	NS	NSV
Coupled	0.0697	0.0702	0.0707
Uncoupled	0.0964	0.0969	0.0932
Reduction %	27.6639	27.5343	24.1202

Table 6.16. Monte Carlo Simulation: mean of the displacements of the building protected with ViBa for $m_{ViBa} / m = 1.05$.

Fractile 5% [m]	QS	NS	NSV
Coupled	0.0555	0.0523	0.0412
Uncoupled	0.0715	0.0676	0.0508
Reduction %	22.3776	22.6331	18.8976

Table 6.17. Monte Carlo Simulation: fractile 5% of the displacements of the building protected with ViBa for $m_{ViBa} / m = 1.05$.

Fractile 50% [m]	QS	NS	NSV
Coupled	0.0688	0.0687	0.0650
Uncoupled	0.0941	0.0952	0.0849
Reduction %	26.8863	27.8361	23.4393

Table 6.18. Monte Carlo Simulation: fractile 50% of the displacements of the building protected with ViBa for $m_{ViBa} / m = 1.05$.

Fractile 95% [m]	QS	NS	NSV
Coupled	0.0877	0.0936	0.1184
Uncoupled	0.1282	0.1352	0.1621
Reduction %	31.5913	30.7692	26.9587

Table 6.19. Monte Carlo Simulation: fractile 95% of the displacements of the building protected with ViBa for $m_{ViBa} / m = 1.05$.

Also in this case, by comparing the reductions of the fractile of the peak of the response displacements, the highest reductions shown is relative to the fractile 95%, which is of the 31.59% under the action of the QS simulated accelerograms.

The convergence of the statistics of the responses is illustrated in Figure 6.22, the PDF and CDF in Figure 6.23.

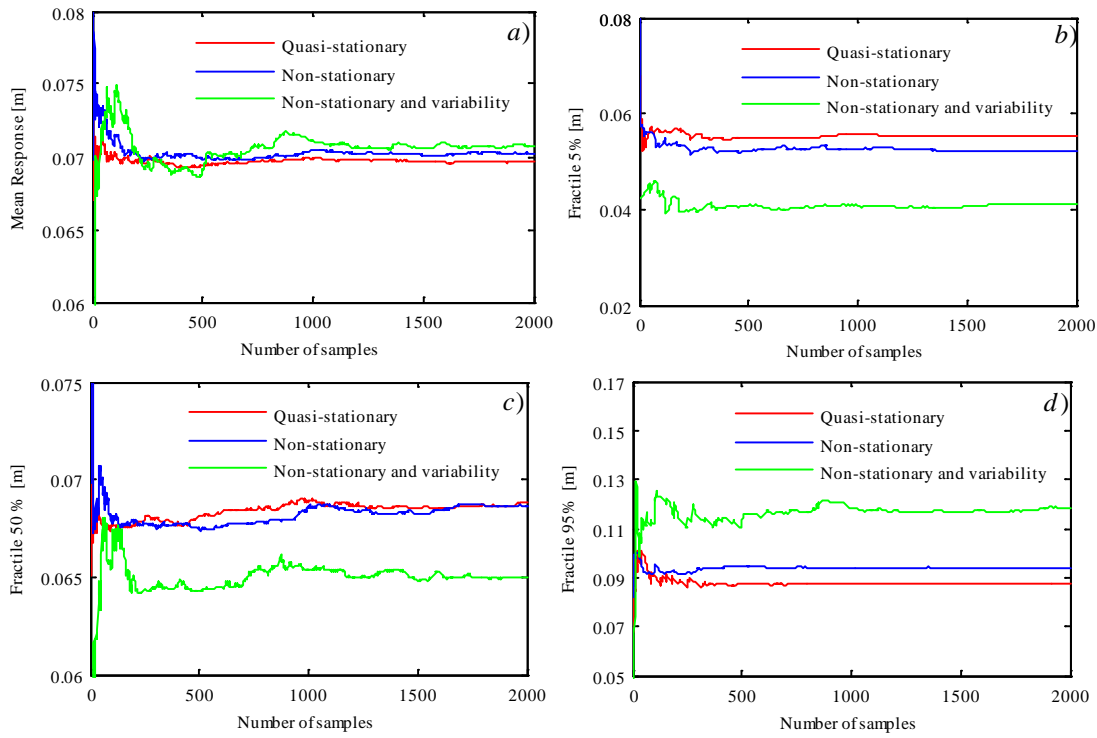


Figure 6.22. Convergence of the response of the building protected with ViBa: a) mean; b) fractile 5%; c) median; d) fractile 95% for $m_{ViBa} / m = 1.05$.

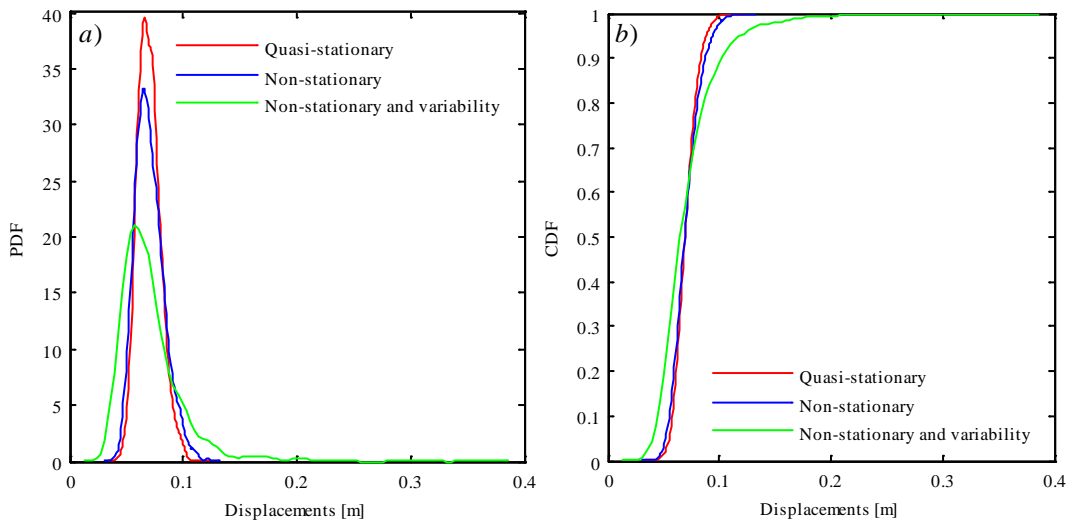


Figure 6.23. a) Probability density function; b) cumulative density function of the response of the building protected with ViBa for $m_{ViBa} / m = 1.05$.

For the ratio $m_{ViBa} / m = 1.5$ the reduction corresponding to the direct stochastic design for stationary input are of 37.42 %, Table 6.20-Table 6.23 show the statistics of the reductions of the displacements obtained from the MCS analyses.

Mean [m]	QS	NS	NSV
Coupled	0.0646	0.0648	0.0658
Uncoupled	0.0964	0.0969	0.0932
Reduction %	32.9660	33.1186	29.4414

Table 6.20. Monte Carlo Simulation: mean of the displacements of the building protected with ViBa for $m_{ViBa} / m = 1.5$.

Fractile 5% [m]	QS	NS	NSV
Coupled	0.0517	0.0486	0.0388
Uncoupled	0.0715	0.0676	0.0508
Reduction %	27.6923	28.1065	23.6126

Table 6.21. Monte Carlo Simulation: fractile 5% of the displacements of the building protected with ViBa for $m_{ViBa} / m = 1.5$.

Fractile 50% [m]	QS	NS	NSV
Coupled	0.0636	0.0632	0.0607
Uncoupled	0.0941	0.0952	0.0849
Reduction %	32.4123	33.6134	28.4862

Table 6.22. Monte Carlo Simulation: fractile 50% of the displacements of the building protected with ViBa for $m_{ViBa} / m = 1.5$.

Fractile 95% [m]	QS	NS	NSV
Coupled	0.0812	0.0856	0.1093
Uncoupled	0.1282	0.1352	0.1621
Reduction %	36.6615	36.6864	32.5808

Table 6.23. Monte Carlo Simulation: fractile 95% of the displacements of the building protected with ViBa for $m_{ViBa} / m = 1.5$.

The highest reduction is obtained for the fractile 95% of the distribution of the peak of the simulated response displacements, which is of the 36.68% for the system forced by NS accelerograms.

In Figure 6.24 and Figure 6.25 respectively the convergence of the statistics of the response relative displacements, the PDF and CDF are shown.

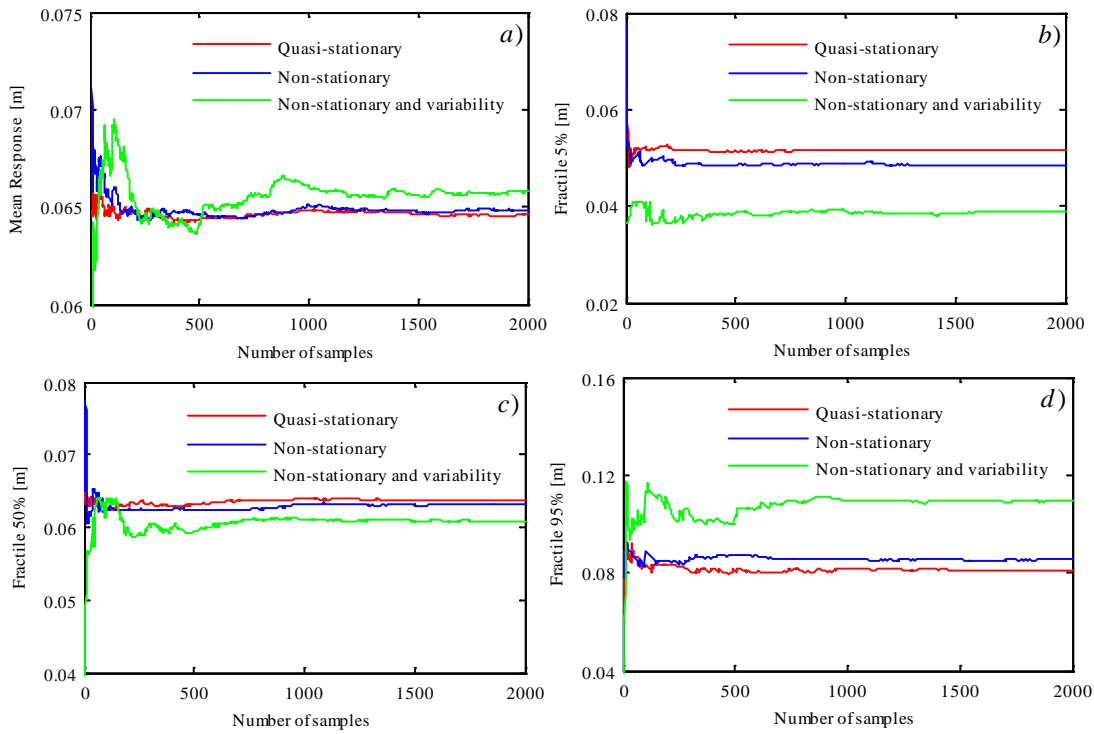


Figure 6.24. Convergence of the response of the building protected with ViBa: a) mean; b) fractile 5%; c) median d) fractile 95% for $m_{ViBa} / m = 1.5$

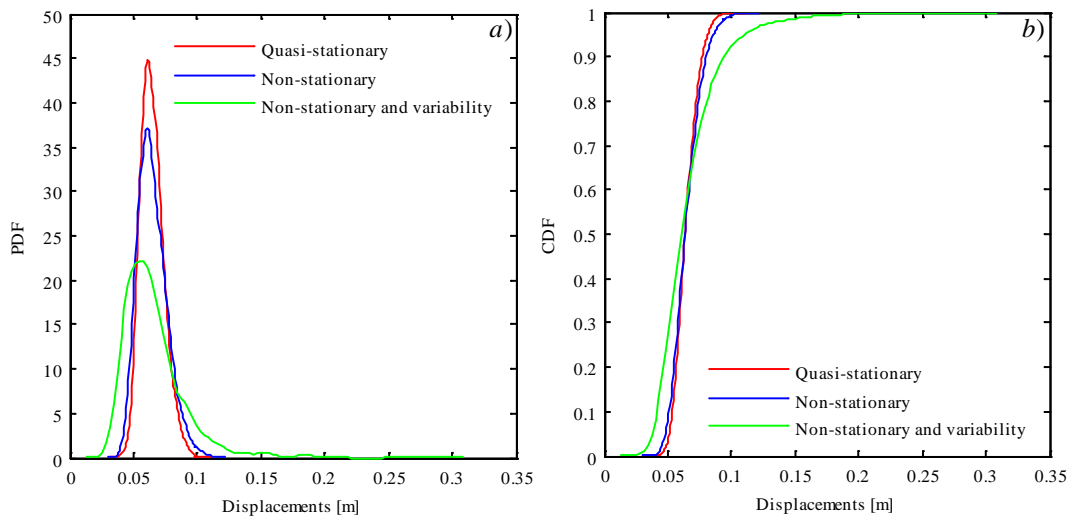


Figure 6.25. a) Probability density function; b) cumulative density function of the response of the building protected with ViBa for $m_{ViBa} / m = 1.5$.

For the case of mass ratio $m_{ViBa} / m = 2$, the reductions obtained according to the stochastic design are 41.07 %, while the reductions of the mean relative displacements of the building obtained by MCS are displayed in the following tables.

Mean [m]	QS	NS	NSV
Coupled	0.0602	0.0603	0.0616
Uncoupled	0.0964	0.0969	0.0932
Reduction %	37.5036	37.8041	33.9748

Table 6.24. Monte Carlo simulation: mean of the displacements of the building protected with ViBa for $m_{ViBa} / m = 2$.

Fractile 5% [m]	QS	NS	NSV
Coupled	0.0484	0.0455	0.0367
Uncoupled	0.0715	0.0676	0.0508
Reduction %	32.3077	32.6923	27.7559

Table 6.25. Monte Carlo simulation: fractile 5% of the displacements of the building protected with ViBa for $m_{ViBa} / m = 2$.

Fractile 50% [m]	QS	NS	NSV
Coupled	0.0592	0.0589	0.0570
Uncoupled	0.0941	0.0952	0.0849
Reduction %	37.0882	38.1303	32.8622

Table 6.26. Monte Carlo simulation: fractile 50% of the displacements of the building protected with ViBa for $m_{ViBa} / m = 2$.

Fractile 95% [m]	QS	NS	NSV
Coupled	0.0755	0.0791	0.1029
Uncoupled	0.1282	0.1352	0.1621
Reduction %	41.1076	41.4941	36.5207

Table 6.27. Monte Carlo simulation: fractile 95% of the displacements of the building protected with ViBa for $m_{ViBa} / m = 2$.

The highest reduction of the peak displacements is obtained for the fractile 95%, which shows a reduction of 41.49 % under the action of simulated NS accelerograms.

Proof of the convergence of the response statistic, the PDF and CDF are presented in Figure 6.26 and Figure 6.27.

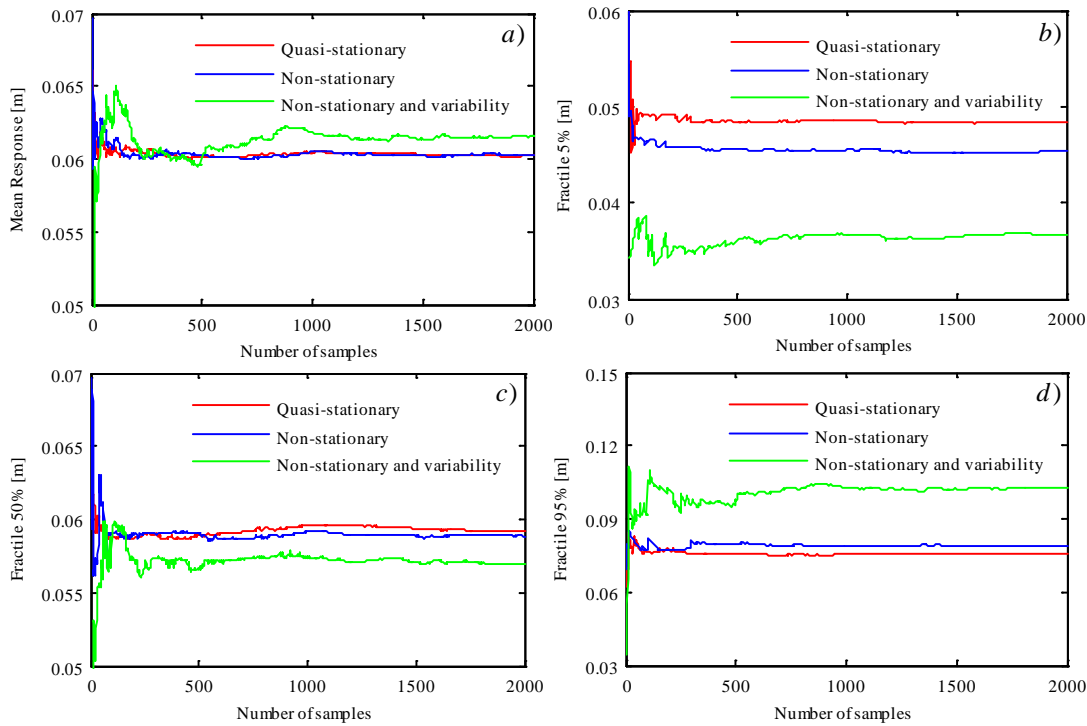


Figure 6.26. Convergence of the response of the building protected with ViBa: a) mean; b) fractile 5%; c) median d) fractile 95% for $m_{ViBa} / m = 2$.

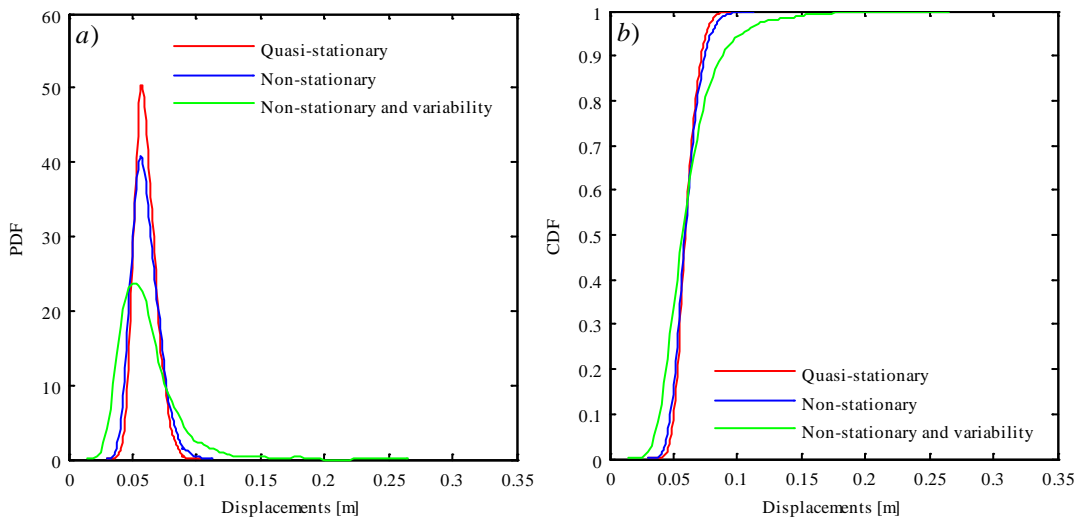


Figure 6.27. a) Probability density function and b) cumulative density function of the response of the building protected with ViBa $m_{ViBa} / m = 2$.

Table 6.12-Table 6.24 displayed the reductions obtained by the MCS study of the response, in which the relative displacements of the systems under investigation to each ground motion model have been simulated. From the analyses of the results, comparisons between the reductions obtained in the design phase seen in Table 6.10, and the MCS results seen in Table 6.12-Table 6.27, are elucidated hereafter. Specifically, Table 6.28 presents the differences between the reduction of the 50% fractile of the peak displacements of the building obtained via direct evaluation of the stationary stochastic response in the design phase, and the reduction of the mean peak displacements determined via MCS. The comparison of the response reductions is presented as the percentage difference relative to the three ground motions with respect to the reductions estimated assuming the stationary input model.

m_{ViBa} / m	Quasi stationary	Non-stationary	Non-stationary and variability
0.50	40.31 %	48.70 %	81.56 %
1.00	19.65 %	20.21 %	37.23 %
1.50	13.51 %	12.98 %	27.10 %
2.00	9.50 %	9.63 %	20.88 %

Table 6.28. Percentage differences between the reductions predicted through the design under stationary stochastic excitation and Monte Carlo Simulation study of the response of Cacciola and Tombari (2015) structure.

For the four scenarios under investigation in which the mass of the ViBa varies, Table 6.28 shows that the difference relatively to the quasi stationary and non-stationary models in all the scenarios are comparable, whereas the differences estimated with regard to the non-stationary model with imposed variability are significant.

In order to facilitate the interpretation of the results and to address the influence of the frequency content of the ground motions on the structural response, the Figure 5.1, and Table 6.11 are observed in conjunction, which respectively show the variation of the frequency content of the three ground motions, and the natural frequencies of the building protected.

Considering the time-evolution of the mean instantaneous frequency in Figure 5.1, it can be observed that the frequency content of the ground motion model with imposed variability tends towards the first two natural frequencies of the coupled SSSI system, while the mean instantaneous frequency in the first 6.5 s of motion relatively to the non-stationary model influences the response less than the other two ground motions. In Table 6.29 the modal participation coefficients for the mode of vibration of the structural systems are shown.

m_{viBa} / m	1 st mode	2 nd mode	3 rd mode	4 th mode
0.50	68.47 %	19.75 %	0.87%	10.90%
1.00	78.62%	14.36%	0.64%	6.36%
1.50	83.84%	11.38%	0.47%	4.29%
2.00	87.12%	9.61%	0.24%	3.01%

Table 6.29. Modal participation coefficients for the SSSI systems under investigation.

According to the mass contributing at each mode provided by Table 6.29, it can be noticed that the case with the highest discrepancies presented in Table 6.28, is for the lowest m_{viBa} / m to which the contribution of the first mode is the lesser, therefore the non-stationarity of the ground motion effects also the higher modes with frequency closer to the frequency content carried by the three ground motion processes.

The comparison of the highest reductions obtained for the mean value and the fractiles of the distribution of the peak response displacements obtained in the MCS study are summarised in Table 6.30; the results relatively to the four scenarios for different mass ratios under the specified set of accelerograms are shown.

m_{viBa} / m	Mean	50% fractile	5% fractile	95% Fractile
0.50	17.6313(QS)	17.1218 (NS)	12.3077 (QS)	21.8409 (NS)
1.05	27.6639 (QS)	27.8361 (NS)	22.6331 (NS)	31.5913(NS)
1.50	33.1186 (NS)	33.6134 (NS)	28.1065 (NS)	36.6864 (NS)
2.00	37.8041 (NS)	38.1303 (NS)	32.6923 (NS)	41.4941 (NS)

Table 6.30. Summary of the highest reductions of the mean value and fractiles of the distribution of the peak displacements of the simplified system of Cacciola and Tombari (2015).

The MCS study performed has shown the following outcomes: (i) close mean and median values of the peak response displacements are obtained as expected, (ii) the

reduction of the fractile 95% of the response are higher than the reduction of the mean, median and fractile 5% for the four scenarios investigated, (iii) the highest reduction of the response displacement is relatively to the fractile 95%, with a value of 41.49% and for the mean value of 37.80%, both obtained for the case scenario $m_{ViBa} / m = 2$ and under the action of the non-stationary ground motion.

6.5.2.3 Design of the ViBa for the Control of the SAC Building 20-Storey Steel Frame under Gaussian Stochastic Excitation

In this section, the methodology proposed to design of the ViBa is applied to a linear SSSI system formed by: the SAC benchmark building, the ViBa device and the soil underneath them. Both the building and the ViBa are modelled as a 2 translational DOF system and forced by stationary input ground motion defined pertinently to the soil conditions described in section 6.5.

The optimal ViBa's design parameters enabling the control of the SAC building's peak displacements relative to the foundation, $X_{U_b}(T_s = 10s, p = 0.5)$, are reported in Table 5.31.

m_{ViBa} / m	k_{ViBa} [N/m]	c_{ViBa} [Ns/m]	Reduction [%]
0.5	25×10^6	1.5×10^6	13.21
1	50×10^6	3.5×10^6	27.11
1.5	80×10^6	7.5×10^6	34.32
2	115×10^6	13.5×10^6	38.93

Table 6.31. ViBa's parameters for different ratios m_{ViBa} / m obtained by the design under stationary stochastic excitation for the protection of the structure of the SAC building through ViBa.

Figure 6.18 shows the surfaces plots representing the reduction of the peak of the response of the building for the four scenarios in which m_{ViBa} / m varies.

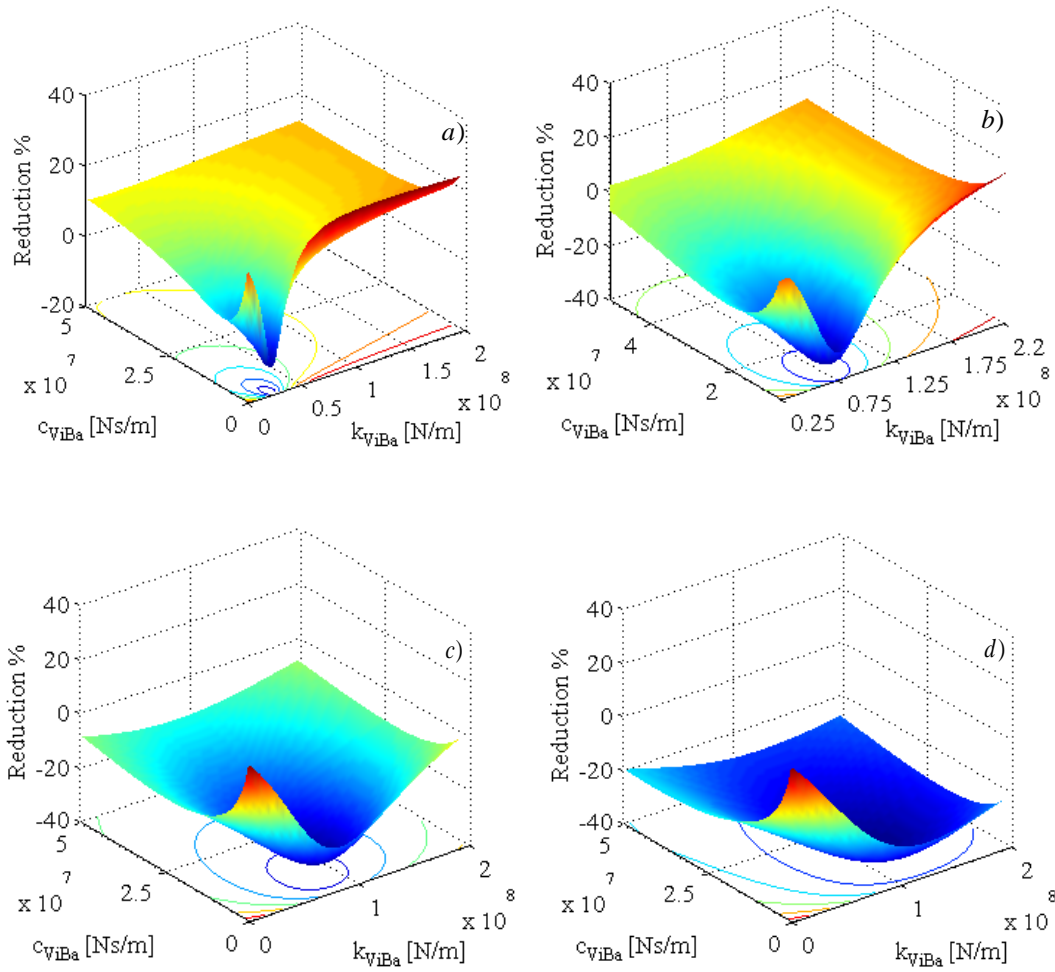


Figure 6.28. Surface plots of the parametric study to reduce the displacements relative to the foundation of the SAC building for: a) $m_{viBa} / m = 0.5$ b) $m_{viBa} / m = 1$; c) $m_{viBa} / m = 1.5$; d) $m_{viBa} / m = 2$.

6.5.2.4 Stochastic Response of the SAC Building 20-Storey Steel Frame Protected with the ViBa

In this section, the stochastic response of the SAC benchmark building represented in Figure 6.4. forced by the sets of response-spectrum-compatible ground motion model discussed is analysed. The SAC building modelled in MATLAB as discrete simplified 2 DOF system has been coupled with ViBa modelled according to the design parameters presented in Table 6.31.

Natural frequencies [rad/s]								
m_{ViBa} / m	$\omega_{1,unc}$	$\omega_{1,coup}$	$\omega_{2,unc}$	$\omega_{2,coup}$	$\omega_{3,unc}$	$\omega_{3,coup}$	$\omega_{4,unc}$	$\omega_{4,coup}$
0.5	2.47	2.47	2.47	2.99	9.95	11.25	12.81	17.96
1.05	2.19	2.28	2.47	3.00	11.23	11.97	12.81	18.23
1.5	2.02	2.15	2.47	3.03	12.58	12.69	12.81	18.61
2	1.88	2.06	2.47	3.04	13.98	13.36	12.81	19.14

Table 6.32. Natural frequencies of the simplified SAC building-soil-ViBa system for different ratios m_{ViBa} / m .

The ViBa has been calibrated for the four scenarios reported in Table 6.32, in which the four natural frequencies of the systems are shown. The transfer functions of the structural systems evaluated according to the proposed methodology are presented in Figure 6.29, where consistency to the values listed in Table 6.32 is shown.

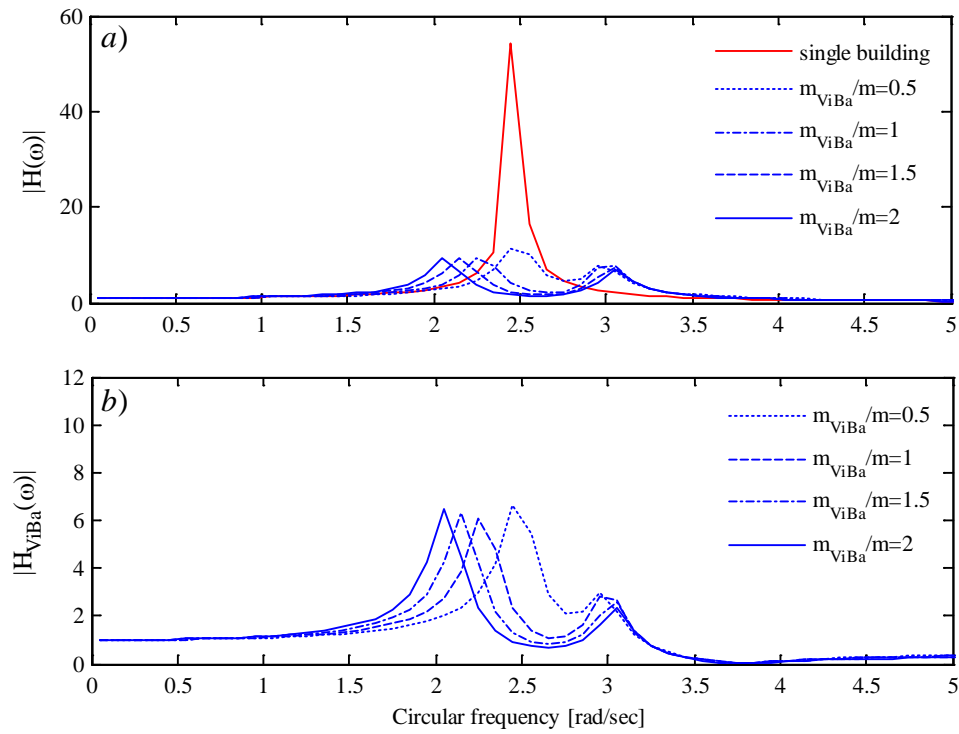


Figure 6.29. Transfer functions for the ViBa and the simplified SAC building benchmark for different values of m_{ViBa} / m .

The reductions of the peak displacements relative to the foundation are reported in the following tables. The statistics have been obtained by analysis of the SAC building via MCS, in which the building is forced by the ground motion models presented in this numerical application.

Relatively to the scenario $m_{ViBa} / m = 0.5$, the results are shown in Table 6.33-Table 6.36, the results are to be compared to Table 6.10, in which the prediction of the reductions determined during the design's phase is 13.21% for the 50% fractile.

Mean [m]	QS	NS	NSV
Coupled	0.1150	0.1151	0.1197
Uncoupled	0.1260	0.1261	0.1299
Reduction %	8.7402	8.6910	7.7881

Table 6.33. Monte Carlo Simulation: mean of the displacements of the simplified SAC building protected with ViBa for $m_{ViBa} / m = 0.5$.

Fractile 5% [m]	QS	NS	NSV
Coupled	0.0870	0.0597	0.0718
Uncoupled	0.0941	0.0676	0.0753
Reduction %	7.5567	11.6864	4.6386

Table 6.34. Monte Carlo Simulation: fractile 5% of the displacements of the simplified SAC building protected with ViBa for $m_{ViBa} / m = 0.5$.

Fractile 50% [m]	QS	NS	NSV
Coupled	0.1133	0.1136	0.1116
Uncoupled	0.1245	0.1242	0.1193
Reduction %	9.0208	8.5408	6.3921

Table 6.35. Monte Carlo Simulation: fractile 50% of the displacements of the simplified SAC building protected with ViBa for $m_{ViBa} / m = 0.5$.

Fractile 95% [m]	QS	NS	NSV
Coupled	0.1488	0.1507	0.1968
Uncoupled	0.1628	0.1677	0.2169
Reduction %	8.6480	10.1501	9.2422

Table 6.36. Monte Carlo Simulation: fractile 95% of the displacements of the simplified SAC building protected with ViBa for $m_{ViBa} / m = 0.5$.

From the tables above, the highest reduction of the peak of the relative displacements is obtained for the fractile 5%, with a value of 11.69% under the action of the set of NS simulated accelerograms.

Figure 6.30 and Figure 6.31 show respectively the convergence of the fractiles of the distributions of the peak response and the PDF and CDF.

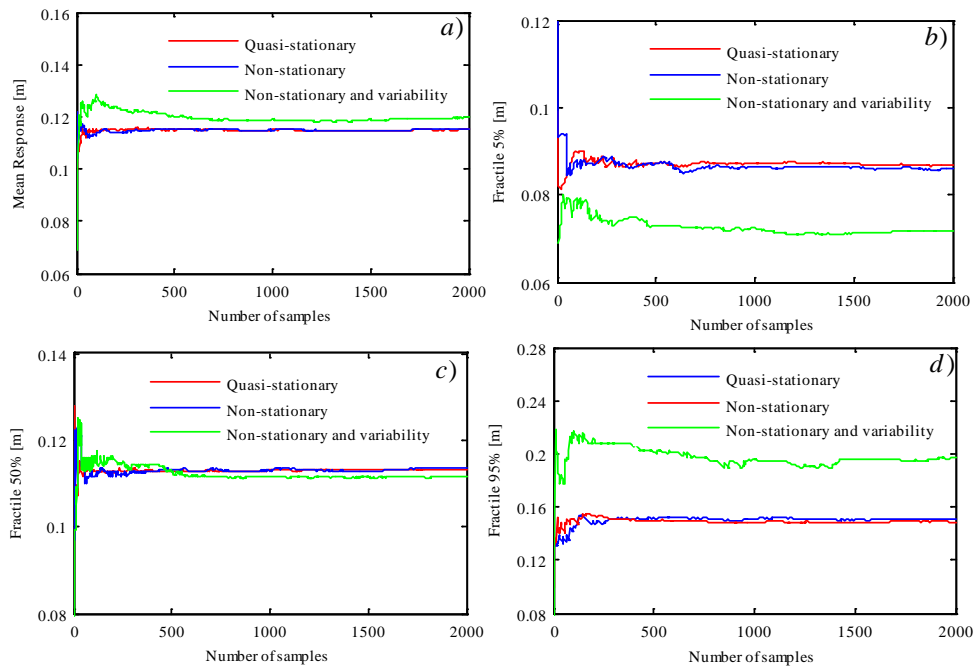


Figure 6.30. Convergence of the response of the simplified SAC building protected with ViBa: a) mean; b) fractile 5%; c) median d) fractile 95% for $m_{ViBa} / m = 0.5$.

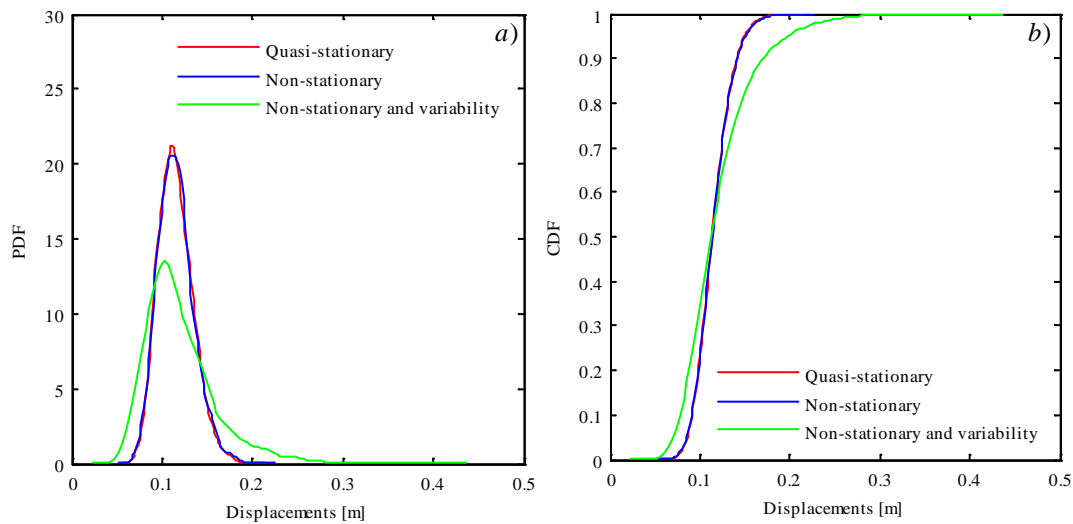


Figure 6.31. a) Probability density function; b) cumulative density function of the response of the simplified SAC building simplified model protected with ViBa for $m_{ViBa} / m = 0.5$.

In Table 6.37-Table 6.40 the reductions of the statistics' displacements of the mass of the SAC building forced by the simulated ground motions are shown for the scenario $m_{ViBa} / m = 1$. The reductions obtained by means of the parametric study performed to calibrate the ViBa are 27.11%.

Mean [m]	QS	NS	NSV
Coupled	0.0979	0.0987	0.1034
Uncoupled	0.1260	0.1261	0.1299
Reduction %	22.3562	21.7576	20.3920

Table 6.37. Monte Carlo simulation: mean of the displacements of the simplified SAC building protected with ViBa for $m_{ViBa} / m = 1$.

Fractile 5% [m]	QS	NS	NSV
Coupled	0.0748	0.0757	0.0628
Uncoupled	0.0941	0.0926	0.0753
Reduction %	20.4614	18.2620	16.4936

Table 6.38. Monte Carlo Simulation: fractile 5% of the displacements of the simplified SAC building protected with ViBa for $m_{ViBa} / m = 1$.

Fractile 50% [m]	QS	NS	NSV
Coupled	0.0962	0.0966	0.0976
Uncoupled	0.1245	0.1242	0.1193
Reduction %	22.7563	22.2191	18.1982

Table 6.39. Monte Carlo Simulation: fractile 50% of the displacements of the simplified SAC building protected with ViBa for $m_{ViBa} / m = 1$.

Fractile 95% [m]	QS	NS	NSV
Coupled	0.1261	0.1275	0.1665
Uncoupled	0.1628	0.1677	0.2169
Reduction %	22.5520	23.9884	23.2399

Table 6.40. Monte Carlo Simulation: fractile 95% of the displacements of the simplified SAC building protected with ViBa for $m_{ViBa} / m = 1$.

The MCS analysis shows the highest reduction of the fractile 95% of the peak displacements with a value of 23.99% under the action of the accelerograms simulated according to the NS model.

The convergence of the statistics of the response, the PDF and CDF evaluated by MCS are displayed in Figure 6.32 and Figure 6.33.

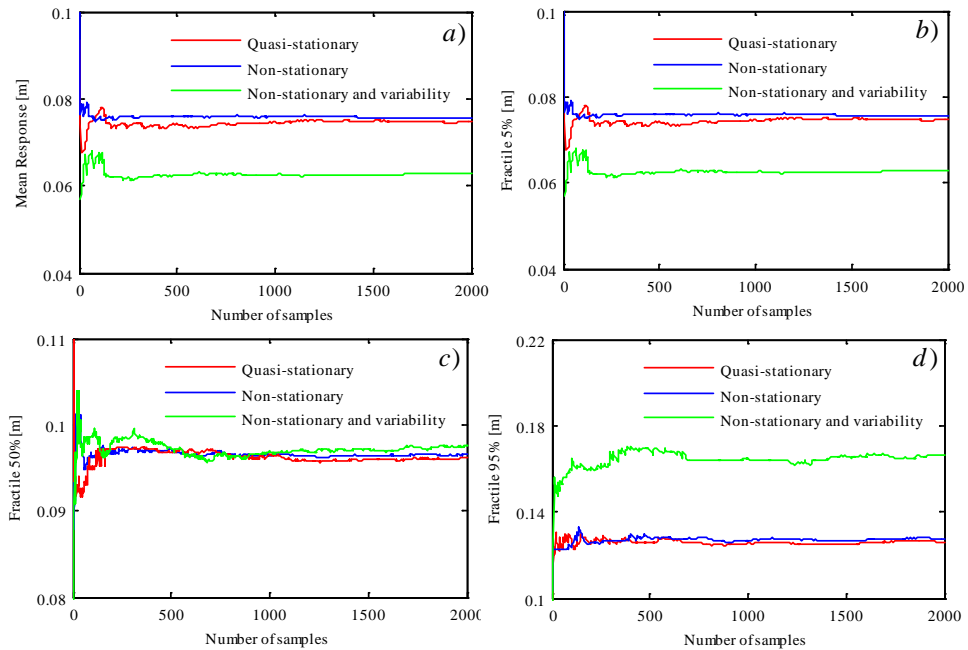


Figure 6.32. Convergence of the response of the simplified SAC building protected with ViBa: a) mean; b) fractile 5%; c) median d) fractile 95% for $m_{ViBa} / m = 1$.

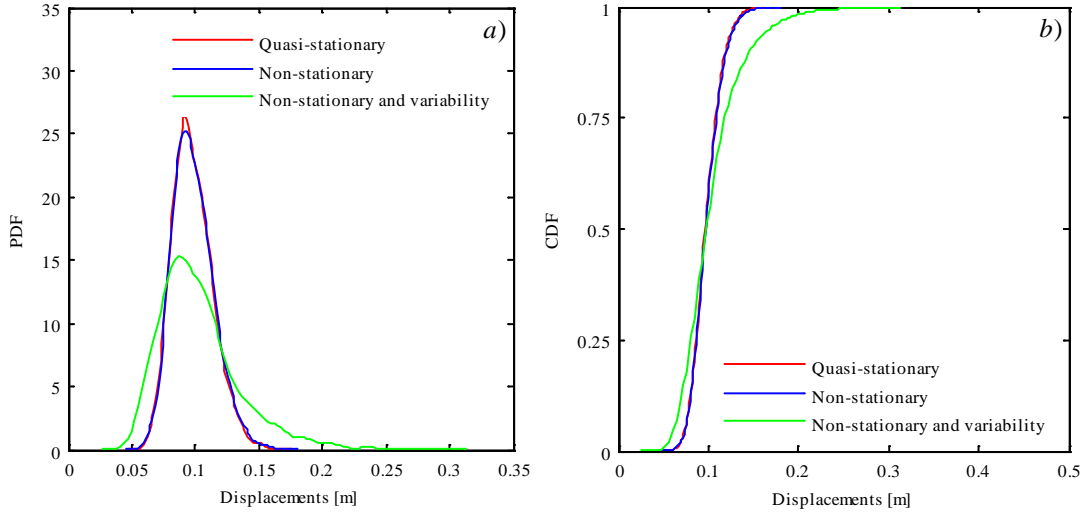


Figure 6.33. a) Probability density function; b) cumulative density of the response of the simplified SAC building simplified model protected with ViBa for $m_{ViBa} / m = 1$.

Table 6.41-Table 6.44 present the results for the ratio $m_{ViBa} / m = 1.5$. The reductions evaluated by means of simulation of the structural responses can be compared to the reduction obtained by design under stationary stochastic excitation which is 34.31% (i.e. fractile 50%).

Mean [m]	QS	NS	NSV
Coupled	0.0874	0.0882	0.0933
Uncoupled	0.1260	0.1261	0.1299
Reduction %	30.6145	30.0712	28.1846

Table 6.41. Monte Carlo simulation: mean of the displacements of the simplified SAC building protected with ViBa for $m_{ViBa} / m = 1.5$.

Fractile 5% [m]	QS	NS	NSV
Coupled	0.0682	0.0668	0.0574
Uncoupled	0.0941	0.0926	0.0753
Reduction %	27.4675	27.7870	23.7072

Table 6.42. Monte Carlo simulation: fractile 5% of the displacements of the simplified SAC building protected with ViBa for $m_{ViBa} / m = 1.5$.

Fractile 50% [m]	QS	NS	NSV
Coupled	0.0861	0.0867	0.0881
Uncoupled	0.1245	0.1242	0.1193
Reduction %	30.8673	30.1976	26.1285

Table 6.43. Monte Carlo simulation: fractile 50% of the displacements of the simplified SAC building protected with ViBa for $m_{ViBa} / m = 1.5$.

Fractile 95% [m]	QS	NS	NSV
Coupled	0.1113	0.1130	0.1484
Uncoupled	0.1628	0.1677	0.2169
Reduction %	31.6314	32.6365	31.5626

Table 6.44. Monte Carlo simulation: fractile 95% of the displacements of the simplified SAC building protected with ViBa for $m_{ViBa} / m = 1.5$.

From the results displayed in the tables above, the highest reduction of the fractile 95% of the peak displacements is of 32.64%, due to the action of the NS ground motion.

The convergence of the statistics of the peak displacements of the SAC building are shown in Figure 6.34 and the PDF and CDF in Figure 6.35.

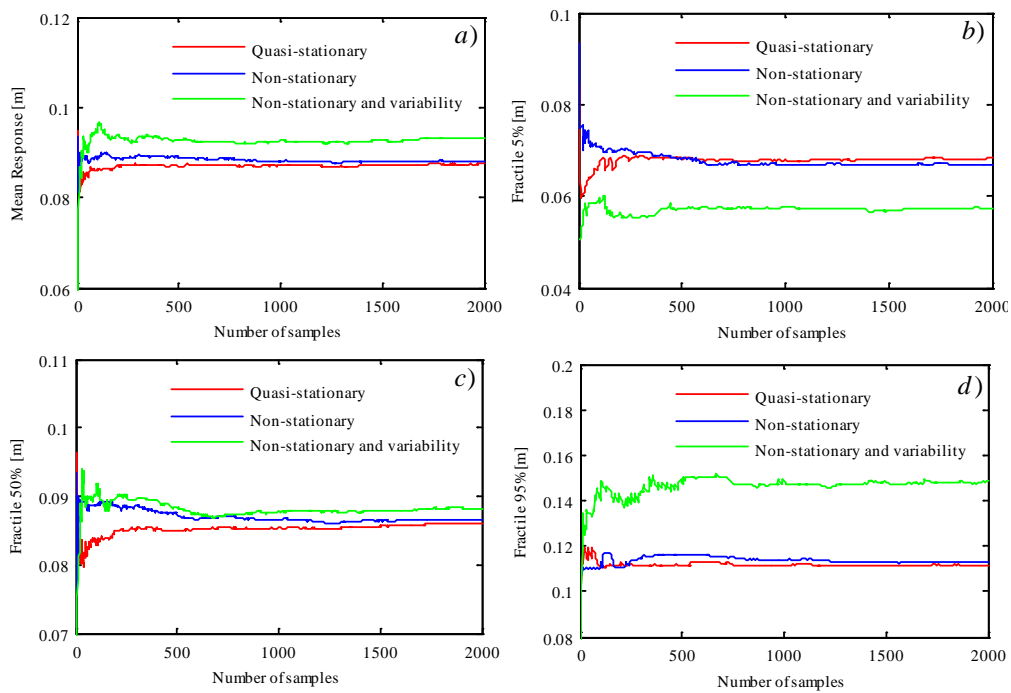


Figure 6.34. Convergence of the response of the simplified SAC building protected with ViBa: a) mean; b) fractile 5%; c) median d) fractile 95% for $m_{ViBa} / m = 1.5$.

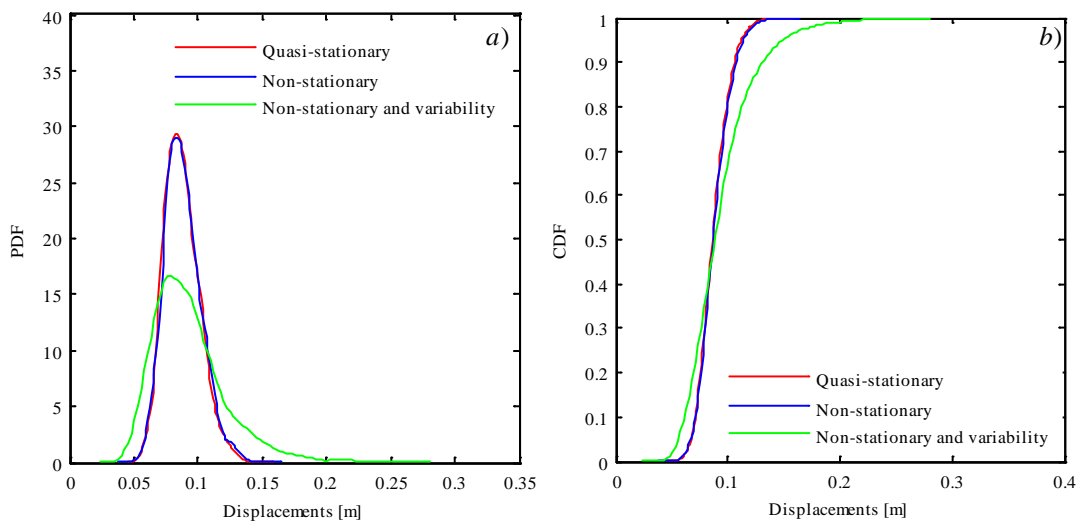


Figure 6.35. a) Probability density function; b) cumulative density of the response of the simplified SAC building simplified model protected with ViBa for $m_{ViBa} / m = 1.5$.

The results obtained from performing MCS for the case in which $m_{ViBa} / m = 2$ are shown in Table 6.45-Table 6.48. The reductions obtained in the design under stationary stochastic input presented in the previous section is 38.93 %.

Mean [m]	QS	NS	NSV
Coupled	0.0823	0.0830	0.0879
Uncoupled	0.1260	0.1261	0.1299
Reduction %	34.7284	34.2021	32.3470

Table 6.45. Monte Carlo simulation: mean of the displacements of the simplified SAC building protected with ViBa for $m_{ViBa} / m = 2$.

Fractile 5% [m]	QS	NS	NSV
Coupled	0.0641	0.0635	0.0538
Uncoupled	0.0941	0.0926	0.0753
Reduction %	31.8935	31.3694	28.4999

Table 6.46. Monte Carlo simulation: fractile 5% of the displacements of the simplified SAC building protected with ViBa for $m_{ViBa} / m = 2$.

Fractile 50% [m]	QS	NS	NSV
Coupled	0.0809	0.0815	0.0828
Uncoupled	0.1245	0.1242	0.1193
Reduction %	35.0452	34.4097	30.5505

Table 6.47. Monte Carlo simulation: fractile 50% of the displacements of the simplified SAC building protected with ViBa for $m_{ViBa} / m = 2$.

Fractile 95% [m]	QS	NS	NSV
Coupled	0.1041	0.1064	0.1395
Uncoupled	0.1628	0.1677	0.2169
Reduction %	36.0666	36.5773	35.6532

Table 6.48. Monte Carlo simulation: fractile 95% of the displacements of the simplified SAC building protected with ViBa for $m_{ViBa} / m = 2$.

The study has shown the highest reduction of the peak displacements relatively to the fractile 95%, with a value of 36.58%, due to the time-histories simulated according to the NS model.

Convergence of the response of the SAC building protected with ViBa, the PDF and CDF are shown in the plots in Figure 6.36 and Figure 6.37.

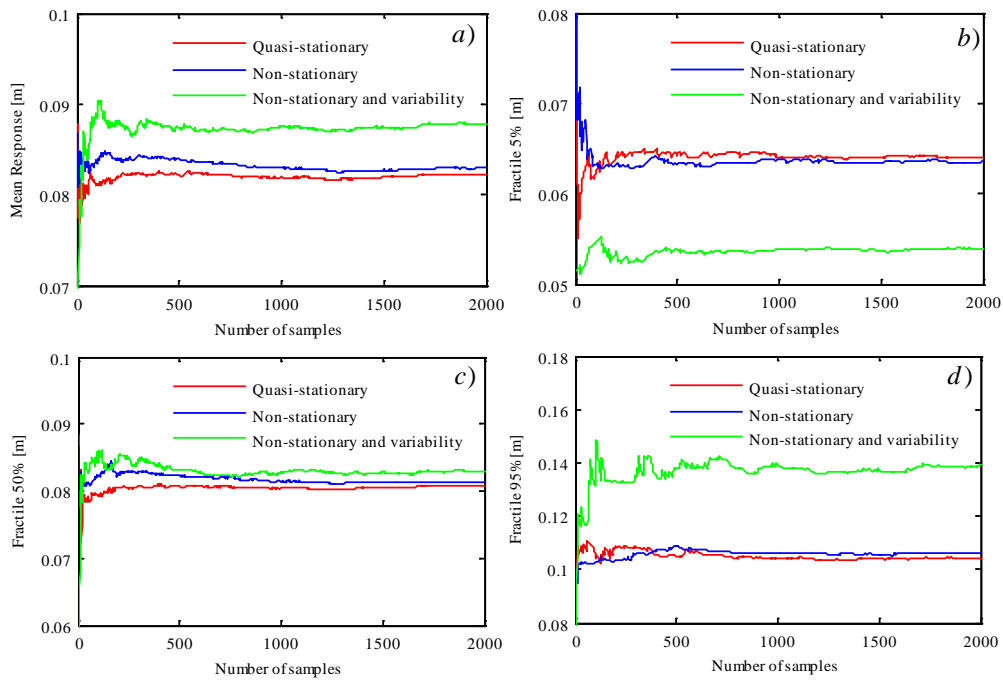


Figure 6.36. Convergence of the response of the building protected with ViBa: a) mean; b) fractile 5%; c) median d) fractile 95% for $m_{ViBa} / m = 2$.

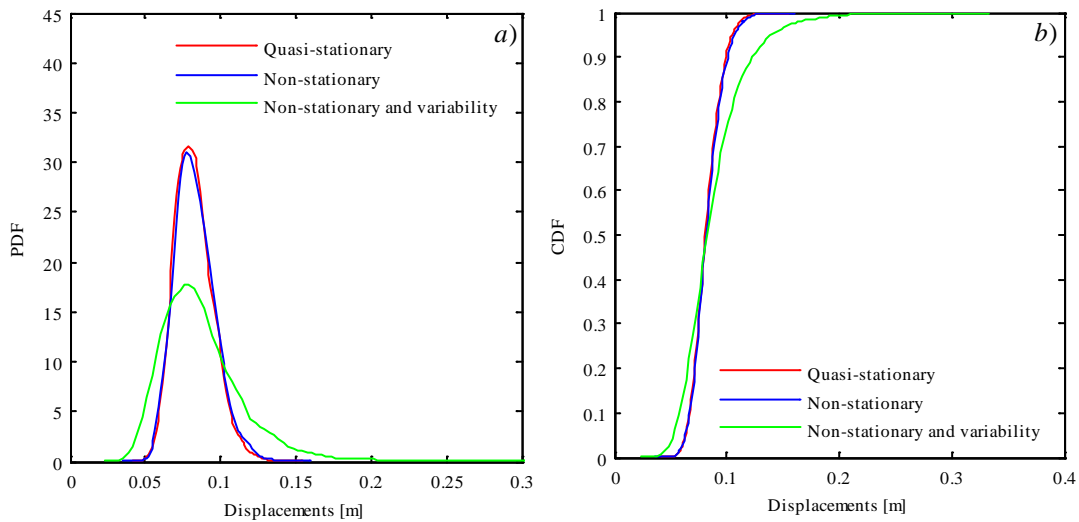


Figure 6.37. a) Probability density function; b) cumulative density function of the response of the simplified SAC building simplified model protected with ViBa for $m_{ViBa} / m = 2$.

For the analysed SSSI system, Table 6.49 shows the difference between the reduction established by Monte Carlo Simulation and those predicted via design for stationary stochastic input.

$m_{ViBa} / m .$	Quasi-stationary	Non-stationary	Non-stationary and variability
0.50	51.14%	51.00%	69.62%
1.00	21.26%	24.60%	32.95%
1.50	12.10%	14.13%	21.77%
2.00	12.09%	13.82%	20.35%

Table 6.49. Percentage differences between the reductions predicted through the design under stationary stochastic excitation and Monte Carlo Simulation study of the response of the simplified SAC building model.

In Table 6.49 the percentage differences between the reduction of the 50% fractile of the peak response displacements obtained by stationary stochastic analysis and the mean values obtained from the Monte Carlo Simulation are presented. The quasi-stationary model and the non-stationary model presents similarities for all the scenarios taken into account in the analyses, whereas the reductions of the peak obtained for non-stationary ground motions with imposed variability are higher than for the other simulated inputs. Being a system flexible, and therefore its frequencies are within a range of lower values compared to stiffer structures, the dynamic transitory response assumes the features typical of high rise building. For the global system formed by the 20-storey SAC building coupled with ViBa, the modal frequencies are higher than the frequencies of the uncoupled building, and the ViBa. The ground motions frequency content of the simulated time-histories carries energy at higher frequencies than the frequencies of the modes of vibration of the system. Nevertheless, the effects of the variability imposed to the fully non-stationary model are noticeable.

In analogy to the observation from Figure 6.29 for the prototype system of Cacciola and Tombari (2015), also Table 6.31 shows that the higher the mass ratio, the higher the frequency of the coupled system, which might be the justification for the decrease in the discrepancies between the reductions obtained for stationary input in the design phase and the reductions from the MCS study.

In order to present the comparison of the highest reductions obtained for the mean value, median, 5% and 95% fractiles of the distribution of the peak response displacements, Table 6.50 shows the reductions for the case scenarios under investigation, specifying which set of the simulated ground motions determines the reductions displayed.

m_{ViBa} / m	Mean	50% fractile	5% fractile	95% Fractile
0.50	8.7402 (QS)	9.0208 (QS)	11.6864 (NS)	10.1501 (NS)
1.00	22.3562 (QS)	22.7563(QS)	20.4614 (QS)	23.9884 (NS)
1.50	30.6145 (QS)	30.8673 (QS)	27.7870 (NS)	32.6365 (NS)
2.00	34.7284 (QS)	35.0452 (QS)	31.8935 (QS)	36.5773 (NS)

Table 6.50. Summary of the highest reductions of the mean value and fractiles of the distribution of the peak displacements of the simplified SAC building model.

Pertinently to the first study on the simplified structure proposed by Cacciola and Tombari (2015), the statistics of the reduction of the building displacements computed in the MCS study presented in this section show: (i) close results of the mean and median values, (ii) the fractile 95% of the displacements' reduction are higher than the reduction of the mean, median and fractile 5% for the four case scenarios investigated, (iii) the highest reduction of the peak response displacement is relatively to the fractile 95% with a value of 36.58%, under the effect of the non-stationary ground motion, and for the mean value of 34.72%, obtained for the quasi-stationary ground motion, both reductions refers to the case of mass ratio $m_{ViBa} / m = 2$.

6.5.3 Concluding Remarks

In this Chapter the design of the ViBa under stochastic excitation to protect two different structural systems is presented. Namely, the buildings investigated are: the structural system studied by Cacciola and Tombari (2015), which is the first prototype of the ViBa to protect single buildings on rigid embedded foundations, and the SAC building benchmark, simplified as a MDOF system according to the analytical formulation proposed by Cacciola and Tombari (2015). The objective successfully accomplished in the investigations presented in this Chapter are: (i) the extension of the dynamic equilibrium of the system proposed by Cacciola and

Tombari (2015) from the frequency to the time domain, by the proposed procedure to calibrate a viscous damping matrix equivalent to the original hysteretic model experimentally derived by the authors, (ii) to apply the methodology to design the ViBa under stochastic stationary ground motion for the extended model of Cacciola and Tombari (2015) and for the benchmark building, the SAC 20-storey steel frame, (iii) to demonstrate by MCS study the efficiency of the ViBa device calibrated through the proposed methodology and tested under the action of quasi-stationary, non-stationary and non-stationary with imposed variability ground motion models.

The results have been presented in terms of the reduction of the fractiles of the peak relative displacement distribution of the buildings to protect. The analyses have demonstrated that the ViBa calibrated for stationary stochastic input reduces the response of the two benchmark structures investigated also under the action of stochastic earthquake ground motions modelled more realistically than the stationary model. The simulated sets of accelerograms adopted in the MCS study have been simulated according to the theory of random vibrations, specifically the non-stationary with imposed variability accelerograms have been generated by means of a proposed technique accounting of a parametrised EPSD function with random coefficients.

The Monte Carlo Simulation study has shown the following results with regard to the reductions of the peak displacement of the mass of the building controlled through the ViBa: (i) for the prototype system of Cacciola and Tombari (2015), the highest reductions have been obtained for a mass of the ViBa twice the mass of the building. A reduction of the 37.80% of the mean peak displacement has been observed for the non-stationary ground motion, whereas an higher reduction of the 41.49% has been achieved for the 95% fractile, under the non-stationary ground motion, (ii) the SAC building has shown the maximum reduction of the mean peak displacements for a mass of the ViBa twice the mass of the SAC building, with the value of 34.73% for the case of simulated quasi-stationary ground motions, and of 36.58% for the fractile 95% under the non-stationary ground motion.

In this Chapter four case scenarios have been investigated, which consider different ratios of the mass of the ViBa and the building to protect. From the analysis carried out on both systems under investigation, differences between the reductions predicted during the phase of design of the ViBa under stationary stochastic excitation, and the reductions obtained via MCS have been observed. These differences reduce as the mass of the ViBa increases. The discrepancies are higher for the modified system of Cacciola and Tombari (2015), whose natural frequencies are closer to the frequency content of the simulated earthquakes. Therefore, the non-stationarity of the simulated ground motion models influences the response of the structural system under investigation. In the second case study, the discrepancies between the reductions achieved for stationary input ground motion against quasi-stationary, non-stationary and non-stationary with variability, confirm the influence of the transient part of the response, which is neglected in the stationary stochastic formulation to determine the mean value of the peak displacements of the response (i.e. approximated to the fractile 50%), pursued by means of geometrical spectral moments. For the SAC building model, the discrepancies are less compared to the results obtained for the simplified system of the Cacciola and Tombari (2015) extended model, due to the frequency content of the simulated earthquake ground motions.

From the numerical applications presented in this Chapter, which have been carried out in order to test the efficacy and validity of the simplified approach to design the ViBa under stochastic excitation, it is proved that the proposed methodology is efficient for those systems whose dynamic response is governed by the steady state, i.e. for which the influence of the transient on the statistics of the response is negligible.

7 Conclusions

Despite of the rapid advancement in research and technology, the growth of sophisticated computer software and the innovative methodologies for engineering design, the seismic ground motion remains one of the most unpredictable cause of structural damage, threatening cities as well as small urban centres especially in developing areas. The seismic risk is related to the unpredictability of the earthquake phenomenon, its magnitude and frequency content. Additionally, in dense populated cities, the dynamic interaction among closely spaced structures, which is triggered by the wave propagating throughout the soil, known as Structure-Soil-Structure-Interaction, complicates further the analysis of the structural response to ground motion excitation. The phenomenon has been recognised decades ago and only recently has gained more attention by researchers, also motivated by the empowerment of computer technologies.

In this research an effort has been devoted to fill a gap in knowledge with regard to the problem of vibration control by furthering the investigations on a novel solution called Vibrating Barriers (ViBas). The ViBas have been proposed to be modelled as part of a SSSI global system, which is formed by the device itself, the soil and the structure to protect. The solution has been recognised as a possible vehicle to tackle the protection of structures by controlling their structural vibrations by opportune calibration of the device, which is placed nearby the structure to protect, embedded into the soil, and designed to undergo the effects of the SSSI.

This work has focused on assessing the efficiency of a Vibrating Barrier designed by adopting advanced methods of Stochastic Dynamics, in order to understand and put forward the development of the device by using a probabilistic approach. Moreover, in this research, the ViBa has been tested under response-spectrum-compatible simulated earthquakes modelled realistically according to the current developments in ground motion modelling, also furthered in this work.

The modelling of the ground motion has been mainly undertaken during the first stage of the project; the capability to capture the natural feature of real earthquakes

propagating from the fault to the site where the buildings stands, is a matter of major concern for seismic engineers and seismologists. The approach pursued in this work is supported by the necessity to promote the use of more reliable techniques and provide a versatile technique to simulate ground motion model that can capture both the non-stationarity of amplitude and frequency content of earthquakes, as well as the natural variability typical of the response spectral coordinates of recorded accelerograms. On the other hand, the limits of the stochastic approach concern the computational costs required and the complexity of the mathematical formulation. Therefore, in order to reduce the computational efforts and the formulations for future studies, a simple methodology to design the ViBa has been proposed and tested by means of Monte Carlo Simulation study. The simulated ground motion time-histories adopted in the MCS analyses have been simulated via Spectral Representation Method under the assumption of quasi-stationary, non-stationary and non-stationary with imposed variability stochastic processes.

At the onset of this thesis, the adoption of the time domain formulation for SSSI investigations has been recognised of primary importance in order to understand the implications of the transient of the structural response. Preliminary investigations to this regards have been presented by means of Finite Element Model of the ViBa and the SAC benchmark building under harmonic functions. Moreover, in this project the use of time-history analysis has been motivated also by the sensitivity of structural response of systems on the hypothesis concerning the structural damping, which has been demonstrated in the first part of the investigations. The preliminary investigations assessed the structural response of benchmark buildings, encompassing flexible and rigid structures, linearly and non-linearly behaving. The initial studies have been purposely carried out without accounting of the SSSI phenomenon, in order to understand the implications of the selection of stochastic ground motions holding different hypotheses, firstly in relation to linear systems. According to the outcomes of the comparative study presented in Chapter 4, although the accepted knowledge that the non-stationarity of the earthquake ground motion affects significantly only non-linear structures, the frequency non-stationarity has shown to influence also linear systems, therefore linear SSSI systems to non-

stationary ground motions are investigated. From the comparative study on the structural response in Chapter 4, a major understanding of the effects of the variability of the spectral accelerations on structures has been gained.

The simplified approach to model the ViBa design parameters by means of the parametric study presented in Chapter 6, is based on the assumption of stationary Gaussian stochastic excitation. Although the design of the ViBa tackled with the proposed methodology is certainly approximated, it may be considered as a valuable tool to perform a computationally more efficient design of the ViBa, however to be rigorously supported by MCS studies.

Within this research the problem of defining the damping model of the SSSI systems for time domain analyses is highlighted by the effort to obtain a viscous damping matrix from experimentally calibrated hysteretic models. The procedure adopted in this work is recommended for the simplicity and accuracy demonstrated.

7.1 Review of research aim and objectives

In the presented work, the formulation of a methodology to design the ViBa under Gaussian stochastic excitation to protect single buildings, has been achieved by means of the methods of structural dynamics presented in Chapter 2. The aim has been accomplished by successfully completing the objectives set out at the beginning of the investigations. In this section, a review of the objectives is exposed.

From the review of the state of the art on response-spectrum-compatible stochastic ground motion models, a comprehensive description of the techniques to feature realistic earthquake stochastic processes has been achieved. With regard to the modelling of the amplitude non-stationarity of simulated time-histories, closed-form solutions of the parameters characterising the time modulating function of Jennings et al. (1969) have been derived and effectively applied.

Regarding the modelling of the non-stationarity of the frequency content, the model proposed by Cacciola and Zentner (2012) and D'Amico et al. (2012) has been extended in this work in order to investigate the effects of the frequency non-

stationarity with imposed variability of the earthquake ground motions on linear and non-linear systems. In this regard, a comparative study on the structural response of benchmark buildings has been performed and presented in Chapter 4. From the investigations, the differences among the evolutionary power spectral density functions of the quasi-stationary, non-stationary and non-stationary with imposed variability models are appreciable. Precisely, the non-stationarity model and the non-stationary model with imposed variability, derived from the single parametrical evolutionary power spectral density function, show differences in their mean value, nevertheless a common linear decay of the frequency content variation and amplitude modulation is set identical.

To verify the seismic code recommendation and their implications on the analysis of the structural response under different ground motion models, response-spectrum-compatible earthquakes have been simulated according to common features, namely: the same mean 5% damping response spectrum, PGA, strong motion phase and the total duration. The structural responses of three benchmark buildings, SMART 2008, IASC 1996 and the SAC building 1996 joint Venture, forced by three simulated sets of accelerograms have been determined by pertinent Monte Carlo Simulation. From the investigations, a method of analysis has been set in order to assess the influence of the structural damping on the response of systems and to generalise the results observed for the benchmark models. The method of analysis introduced, consist in determining the response spectral accelerations over a range of periods, due to the three sets of ground motions adopted, by varying the structural viscous damping for selected values, higher and lower of the nominal 5% recommended by the seismic codes (e.g. EC8). The highest differences among the response spectral accelerations due to the different ground motions have been obtained for the lowest values of the damping ratio (i.e. 1%).

Within this research, some limitations of the current Eurocodes 8 have been identified regarding the stochastic response analysis of structural systems. Specifically, the convergence of the response statistics has been scrutinized in order to identify the implications of using the minimum mandatory number of accelerograms required for time-history analysis. The convergence of the statistics

for the stochastic buildings' response have shown that: (i) for the ground motion adopted, the number of 7 accelerograms is not sufficient to obtain statistically significant outputs from the analyses, and (ii) although the Eurocode 8 provisions fulfilment, i.e. the spectrum compatibility of the mean simulated response spectra of the ground motion models, the distribution of the relevant response parameters, such as the peak displacements are sensibly different for the three models adopted.

In this work a review of the literature on the Structure-Soil-Structure-Interaction (SSSI) developments and its modelling has been undertaken with focus on discrete models, according to the approach undertaken in this work to design the ViBa according to the literature on the novel control solution. The literature review on the SSSI discrete models has been observed with particular attention to the beneficial effects of the SSSI.

In Chapter 6 the numerical results relative to the modelling of SSSI systems have been presented. The application of the methodology to design the Vibrating Barriers proposed in this research has been performed for a prototype structural model and a benchmark structure. The proposed simplified design methodology requires the definition of viscous damping matrices to characterise the damping of the systems under investigation. For the prototype model of Cacciola and Tombari (2015), the viscous damping matrix has been calibrated from the hysteretic model originally proposed by the authors. The implementation of the procedure to establish the damping model has been achieved.

The design of the ViBa has been successfully finalised by means of a parametric study. The stochastic analysis of the structural response of the SSSI systems under investigation has been undertaken via Monte Carlo Simulation in order to evaluate the response of the systems under the different sets of simulated earthquake time-histories. The results have shown to be pertinent to the predictions of the response in the design phase and presented differences based upon the non-stationarity of the input. The estimation of the reductions by the simplified methodology has significant discrepancies compared to the MCS study, with reduced stiffness of the global SSSI system, i.e. for larger duration of the transient of the response.

The methodology to design the ViBa for protecting single structures has been scrutinised for different scenarios, which consider a variable mass of the ViBa proportional to the mass of the building to protect. The study has highlighted the advantages of adopting higher values of the mass of the device. The maximum reductions have been obtained for mass of the ViBa the double of the mass of the building. The limitation of the design methodology, due to the simplified hypotheses on the spectral characteristics of the response, i.e. characterisation of the response by geometrical spectral moments, have been elucidated. The non-geometrical spectral moments should be adopted for avoiding discrepancies with MCS and for a likely more accurate calibration of the ViBa device.

7.2 Summary of the Main Findings

The aim of this research has been to propose a methodology enabling the design of Vibrating Barriers for protecting single buildings forced by earthquake ground motions modelled as non-stationary Gaussian stochastic processes. The methodology presented within this project is proposed to be used for further investigations on vibration control of structures through the Vibrating Barriers.

The previous investigations on the ViBa for protecting single structures modelled as discrete systems, have been carried out by Cacciola and Tombari (2015), Cacciola et al. (2015), Tombari et al. (2016). As in Cacciola and Tombari (2015), the studies on the design and optimisation of the ViBa performed in this research, focus on the reduction of the response of MDOF buildings placed on embedded rigid foundations.

The work of Cacciola and Tombari (2015) presented the first results identifying the ViBa as a possible solution for passive control of vibrations in building under seismic ground motions. The authors proposed a methodology enabling in the frequency domain, the design of ViBa devices to protect single and multi-structural linear systems forced by harmonic load. This research points out the need to investigate the response of linear structural systems in the time domain, under the action of simulated ground motion modelled with advanced techniques able to capture the non-stationarity of the frequency content of real earthquakes (Cacciola et

al. 2014). Therefore, the investigations undertaken in this research extend the SSSI system proposed Cacciola and Tombari (2015) for time domain analyses.

In this research the main findings relate to: (i) the design of the ViBa under stochastic excitation and, (ii) the study of the efficiency of the control device via Monte Carlo Simulation study of the structural response to simulated ground motions, among which the technique proposed to model fully non-stationary stochastic process is comprised. On the basis of the validity of the Monte Carlo Simulation method, extensively adopted in earthquake engineering and herein employed to test the efficiency of the ViBa, the crucial results found are:

- For the prototype system proposed by Cacciola and Tombari (2015) the highest reductions of the mean peak of the relative displacements of the mass of the building to protect is of 37.80%, value determined from the response to the response-spectrum-compatible non-stationary ground motion. Under the effect of the same input, the highest reduction of the 95% fractile of the peak distribution achieved is of 41.49%.
- With regard to the 20-storey moment resisting frame, the SAC benchmark building, the highest reduction of the mean peak of the relative displacements of the mass of the building obtained is of 34.73% due to the response-spectrum-compatible quasi-stationary ground motions. Relatively to the 95% fractile of the peak distribution, the maximum reduction obtained is of 36.58% under the action of the non-stationary ground motion.

7.3 Further developments of the research

Ground motion arising from seismic waves is a phenomenon that by its nature varies with time and in space. In this work, spatially variable and three-dimensional ground motions have not been taken into account. The formulation of a multi-correlated ground motion model capturing the natural variability of real earthquakes is recommended as further development of the ground motion simulation technique proposed in this work. The further development would be the definition of randomized PSD matrix with uncertain parameters related to the coherency function.

For these models the ensemble-averaged simulated coherency functions consistent to the prescribed original model (i.e. without variability) has to be guaranteed. Initial investigations on this topic have been undertaken over the course of this research and have not been included due to the limited number of works that has been found to address the variation of frequency dependant standard deviation functions, thus to impede a realistic characterisation of the variability of the existing frequency dependant coherency models.

The hypothesis of stationary Gaussian stochastic ground motions for ViBa's design underpinning the proposed methodology is particularly suitable for rigid systems, whereas the duration of the transient counterpart of the response is negligible. However, for systems with predominant transient response and for highly non-stationary response, the formulation based on non-geometrical spectral moments of the response appears to be the most appropriate. Nevertheless, this approach can be extremely challenging from both a computational and theoretical point of view and requires further "ad hoc" investigations.

The discrete models adopted in the formulation of the SSSI systems under investigation in the presented work, assume the simplistic hypothesis of soil linearity by means of linear springs. To further the development of the Vibrating Barriers, the modelling of the investigated building-soil-ViBa systems should be improved by adopting non-linear spring models for the soil, and therefore the effectiveness of the proposed calibration methodology tested under these conditions. The proposed methodology should be adopted in line with FEM analyses modelling the soil deposit, in order to address and take into account not only the soil non-linearity but also the effects of the wave propagation thus to enhance insight in the SSSI phenomenon. Moreover, the 3D modelling of the presented scenarios for protection of single and more buildings through the ViBa device is recommended.

Among the further developments pointed out, it is recommended to prioritise the enhancement of the models by including the soil and structural non-linearity firstly, and proceed with the assessment of the ViBa according to the proposed procedure,

instead of extending the methodology by employing the formulation of the non-geometrical spectral moments.

The major limitation of the ViBa as viable solution to control the vibrations of structures is the large mass of the device needed to achieve significant reductions. To put in place a massive structure as the ViBa calibrated in this work may induce high costs for materials and excavation. On the other hand, the ViBa can be designed to protect more buildings therefore its costs can be spread for the advantage of an entire neighbourhood, nevertheless future investigations aiming to reduce the mass need to be undertaken. For instance, the use of a ViBa modelled with similar working principle of the recently proposed Tuned Mass Damper Inerter (Marian and Giaralis 2014), could be the approach to tackle the problem.

References

- Adam, M., and Estroff von O. (2005) "Reduction of train induced building vibration by using open and filled trenches." *Computer and Structures*, 83, 11-24.
- Ahmadi, G. (1979). "Generation of artificial time-histories compatible with given response spectra: a review," *SM archives*, 4(3), 207-239.
- Alexander, N. A., Ibraim, E., and Aldaikh, H. (2012). "A simple discrete model for interaction of adjacent buildings during earthquakes." *Computer and Structures*, 124, 1-10.
- Aldaikh, H., Alexander, N. A., Ibraim, E., and Oddbjornsson, O. (2015). "Two dimensional numerical and experimental models for the study of structure-soil-structure-interaction involving three buildings." *Computers and Structures*, 150, 79-91.
- Aldaikh, H., Alexander, N. A., Ibraim, E., and Knappett, J. (2016). "Shake table testing of the dynamic interaction between two and three adjacent building (SSSI)." *Soil Dynamics and Earthquake Engineering*, 89, 219-232.
- Amin, M., and Gungor, I. (1971). "Random Vibration in Seismic Analysis: an evaluation." *ASCE National meeting on Structural Engineering, Baltimore, MD*, 19-23.
- Baker, J. W. (2007). "Correlation of ground motion intensity parameters used for predicting structural and geotechnical response." *Applications of Statistics and Probability in Civil Engineering*, Kanda, Takada & Furuta (eds) Taylor & Francis Group, London.
- Baker, J.W. and Cornell, C. A. (2005). "A vector-valued ground motion intensity measure consisting of spectral acceleration and epsilon." *Earthquake Engineering and Structural Dynamics* 34,1193-1217.

Baker, J.W., and Jayaram, N. (2008). "Correlation of spectral acceleration values from NGA ground motion models." *Earthquake Spectra*, 24(1), 299-317.

Barbato, M., and Conte, J. (2008). "Spectral characteristics of non-stationary random processes: theory and application to linear structural models." *Probabilist. Eng. Mech.*, 23, 416-426

Barbato, M., and Vasta, M. (2010). "Closed form solutions for the time-variant spectral characteristics of non-stationary random processes." *Probabilist. Eng. Mech.*, 25, 9-17.

Barbato, M., (2011). "Use of Time-Variant Spectral Characteristics of Nonstationary Random Processes in the First-Passage Problem for Earthquake Engineering Applications." *Computational Methods in Stochastic Dynamics*, 22, 67-88.

Bathe, K. J. (1996), *Finite Element Procedures*. Prentice-Hall, Upper Saddle River, New Jersey.

Beck, J. L., and Papadimitriou, C. (1993). "Moving resonance in nonlinear response to fully non stationary stochastic ground motion." *Probabilist. Eng. Mech.*, 8(3-4), 157-167.

Behnamfar, F. and Sugimura Y. (1999). "Dynamic response of adjacent structures under spatially variable seismic waves." *Probabilist. Eng. Mech.*, 14, 33-44.

Beskos, D. E., Dasgupta, B., and Vardoulakis, I. G. (1986) "Vibration isolation using open or filled trenches Part 1: 2-D homogeneous soil." *Comput Mec*, 1(1), 43-63.

Betti, R. (1977). "Effects of the dynamic cross interaction in the seismic analysis of multiple embedded foundations." *Earthquake Engineering and Structural Dynamics*, 26, 1005-1019.

- Bogdanoff, J. L., Goldberg, J. E., and Bernard M. C. (1961). "Response of a simple structure to a random earthquake-type disturbance." *Bull. Seismological Soc. America*, 51(2), 293-310.
- Boore, D. M. (2003). "Simulation of Ground Motion Using the Stochastic Method." *Pure appl. geophys.* 160, 635–676.
- Boore, D. M., and Bommer, J. J. (2005). "Processing of strong-motion accelerograms, needs options and consequences." *Soil Dynamics and Earthquake Engineering*, 25(2), 93-115.
- Borino, G., and Muscolino, G. (1986). "Mode-superposition methods in dynamic analysis of classically and non-classically damped linear systems." *Earthquake Eng. Struct. Dyn.*, 14, 705-717.
- Brinkgreve, R. B. J., Kumarswamy, S., and Swolfs W. M. (2010). *PLAXIS 2D manual*, Delft University of Technology and PLAXIS BV, the Netherlands.
- Cacciola, P. (2010). "A stochastic approach for generating spectrum compatible fully non-stationary earthquakes." *Computers and Structures*, 88(15-16), 889-901.
- Cacciola, P. (2011). "Stochastic ground motion modelling for the seismic analysis of structures: a review." *Computational technologies reviews*, 4, 65-91.
- Cacciola, P. (2012) "*Vibrating Barriers for the control of seismic waves (ViBa)*." EPSRC First Grant EP/K004867/1.
- Cacciola, P., Colajanni, P., and Muscolino, G. (2004). "Combination of modal responses consistent with seismic input representation." *Journal of Structural Engineering* (ASCE), 130(1), 47-55.
- Cacciola, P., and Deodatis, G. (2011) "A method for generating fully non-stationary and spectrum-compatible ground motion vector processes." *Soil Dyn. and Earthq Eng.*, 31(3), 351-360.

Cacciola, P., and Muscolino, G. (2011) “Stochastic seismic analysis of large linear structural systems under fully non-stationary spectrum compatible ground motion” In: Padrakakis, M., Stefanou, G. and Papadopoulos, V., eds. *Computational Mechanics in Stochastic Dynamics. Computational Methods in Applied Sciences*, Springer, 22, 89-109.

Cacciola P., and Zentner I. (2012). “Generation of response spectrum compatible artificial earthquake accelerograms with random joint time frequency distributions.” *Probabilist. Eng. Mech.*, 28, 52-58.

Cacciola, P., and D'Amico, L., (2015). “Response-Spectrum-Compatible Ground Motion Processes” In: Beer, M., Kougoumtzoglou, I.A., Patelli, E. and Au, I., eds. *Encyclopaedia of Earthquake Engineering*. Springer, Berlin Heidelberg, 1-27. ISBN 9783642361975.

Cacciola, P., D'Amico L., and Zentner, I. (2014). “New insights in the analysis of the structural response to spectrum-compatible accelerograms”. *Eng. Struct.*, 78, 3-16. ISSN 0141-0296.

Cacciola, P. and Tombari, A. (2014). “Vibration Control of Structures through Structure-Soil-Structure-Interaction”. *Proceedings of the 9th International Conference on Structural Dynamics, Eurodyn 2014*, Porto, Portugal.

Cacciola, P., Espinosa, M. G., and Tombari, A. (2015). “Vibration control of piled-structures through structure-soil-structure-interaction.” *Soil Dyn. Earthq. Eng.*, 77, 47-57. ISSN 0267-7261.

Cacciola, P., and Tombari, A. (2015). “Vibrating barrier: a novel device for the passive control of structures under ground motion.” *Proceedings of the Royal Society A: Mathematical, Physical and Engineering Sciences*, 471. ISSN 1364-5021.

Caddemi, S., Colajanni, P., Duca, I, and Muscolino, G. (2004). “Non-geometric spectral moments for frequency varying filtered input processes.” *Probabilist. Eng. Mech.*, 19, 21-31.

- Caddemi, S., Colajanni, P., and Muscolino, G. (2001). "On the non-stationary spectral moments and their role in structural safety and reliability." *Structural Engineering Mechanics and Computation*, 1, 1113-1120.
- Celebi, E., and Kirtel, O. (2013). "Non-linear 2-D FE modelling for prediction of screening performance of thin-walled trench barriers in mitigation of train-induced ground vibrations." *Construction and Building Materials*, 42, 122-131.
- Chopra, A. K. (2007). *Dynamics of structures, theory and applications to earthquake engineering*, 3rd Ed., Pearson.
- Clough, R.W., and Penzien, J. (1975). *Dynamics of Structures*. MacGraw-Hill.
- Clouteau, D., Broc, D., Devesa, G., Guyonvarh, V., and Massin, P. (2012). "Calculation methods of Structure Soil Structure Interaction (3SI) for embedded buildings: Application to NUPEC tests." *Soil Dyn. Earthq. Eng.*, 32, 129-142.
- Clouteau, D., and Aubry D. (2001). "Modifications of the ground motion in dense urban areas". *Journal of Computational Acoustics*, 9, 1659-1675.
- Cohen, L., (1989). "Time-Frequency Distributions-A review", *Proceedings of the IEEE*, 77(7), 941-981.
- Conte, J.P., and Peng, B.F. (1997). "Fully non-stationary analytical earthquake ground-motion model." *Journal of Engineering Mechanics*, 123(1), 15-24.
- Corotis, R.B., Vanmarcke, E.H., and Cornell, C.A. (1972). "First passage of non-stationary random processes." *Journal of Engineering Mechanic Division*, 98, 401-414.
- Crandall, S. H (1969). "The role of damping in vibration theory." *Journal of Sound and Vibration*, 11(1), 3-11.
- D'Amico, L. (2012). *Simulated Ground Motions and Correlated Spectral Accelerations: Compatibility with Eurocode 8 Response Spectra*, Report, EDF R&D AMA, France.

D'Amico, L., Zentner, I., and Cacciola, P. (2012). "Simulation of spectral acceleration correlated and response spectrum compatible ground motion accelerograms." *15th World Conference on Earthquake Engineering 15 WCEE*, Lisbon, Portugal.

D'Amico, L., Tombari, A., and Cacciola, P. (2014). "Non-stationary stochastic analysis of the Structure Soil Structure Interaction." *Computational Stochastic Mechanics, Proc. of the 7th International Conference (CSM-7)*, G. Deodatis and P.D. Spanos (eds.) Santorini, Greece.

Davenport, A. G. (1964). "Note on the distribution of the largest value of a random function with application to gust loading." *Proceedings of the institution of Civil Engineers*, 28, 187-196.

Deodatis, G. (1996). "Non-stationary stochastic vector processes: seismic ground motion applications." *Probabilistic Engineering Mechanics*, 11, 149-168.

Deodatis, G., and Shinozuka, M. (1988). "Autoregressive model for non-stationary stochastic processes." *Journal of Engineering Mechanics*, ASCE, 114, 1995-2012.

Den Hartog, J. P. (1956). *Mechanical vibrations*, 4th Ed., McGraw-Hill, New York.

Der Kiureghian, A. (1980). "Structural response to stationary excitation." *Journal of the engineering mechanics division*, 106, 1195-1211.

Der Kiureghian, A. and Neuenhofer, A. (1992). "A response spectrum method for multiple-support seismic excitation." *Earthquake Engineering and structural Dynamics*, 21(8), 713-740.

Di Paola, M. (1985) "Transient spectral moments of linear systems." *Solid Mechanics Archives*, 10(3), 225-43.

Di Paola, M., and Petrucci, G. (1990). "Spectral moments and pre envelope covariances of non-separable processes." *Journal of Applied Mechanics*, Transaction ASME, 57, 218-224.

Di Paola, M., and Navarra, G. (2009). “Stochastic seismic analysis of MDOF structures with nonlinear viscous dampers.” *Structural Control and Health Monitoring*, 16, 303-318.

Djajakesukma, S.L., Samali, B., and Nguyem, H. (2002), “Study of a semi-actiovestiffness damper under various earthquake inputs ” *Earthquake Engineering and Structural Dynamics*, 31, 1757-1776.

Eurocode 8 (2010). “Design of structures for earthquake resistance, Part 1: General rules, seismic actions and rules for buildings”.

Eurocode 8 (2010). “Design of structures for earthquake resistance, Part 2: Bridges”.

Fan, F. G., and Ahmadi, G. (1990). “Nonstationary Kanai-Tajimi models for El Centro 1940 and Mexico City 1985 earthquake.” *Probabilist. Eng. Mech.*, 5(4), 171-181.

Freedman, D., Pisani, R. and Purves, R. (1978). *Statistics*. Norton, New York.

Friswell, M. I., and Mottershead, J. E. (2010). *Finite element model updating in structural dynamics*, Kluwer Academic Publishers.

Gazetas, G. (1983). “Analysis of machine foundation vibration: state of the art review.” *Soil Dynamics and Earthquake Engineering*, 2, 2-42.

Giaralis, A., and Spanos, P. D. (2009). “Wavelets based response spectrum compatible synthesis of accelerograms- Eurocode application (EC8).” *Soil Dynamics and Earthquake Engineering*, 29, 219-235.

Giaralis, A., and Spanos, P. D. (2010). “Effective linear damping and stiffness coefficients of nonlinear systems for design spectrum based analysis.” *Soil Dynamics and Earthquake Engineering*, 30, 798-810.

Giaralis, A., and Spanos, P. D (2012). "Derivation of response spectrum compatible non-stationary stochastic processes relying on Monte Carlo-based peak factor estimation." *Earthquakes and Structures*, 3(3-4), 581-609.

Gasparini D. A., and Vanmarcke E. H. (1976). "Simulated earthquake motions compatible with prescribed response spectra. Evaluation of seismic safety of buildings." Report number 2.

Grigoriu, M. (1995). "Probabilistic models and simulation methods for seismic ground acceleration." *Meccanica: An International Journal of Theoretical and Applied Mechanics AIMETA*, 30(1), 105-124.

Hancock, J., Bommer, J.J., and Stafford P. J. (2008). "Numbers of scaled and matched accelerograms required for inelastic dynamic analyses." *Earthquake Engineering and Structural Dynamics*, 37, 1585-1607.

Henwood, D. J. (2002). "Approximating the hysteretic damping matrix by a viscous matrix for modelling in the time domain." *Journal of Sound and Vibration*, 254(3), 575-593.

Hilber, H. M, Hughes, T. J. R, and Taylor, R. L. (1977). "Improved Numerical Dissipation for Time Integration Algorithms in Structural Dynamics" *Earthquake Engineering and Structural Dynamics*, 5, 282-292.

Houbolt, J.C. (1950). "A recurrence matrix solution for the dynamic response of elastic aircraft" *Journal of the Aeronautical Sciences*, 17, 540-550.

Housner, G. W. (1947) "Characteristics of Strong Motion Earthquakes" *Bulletin of Seismological Society of America*, 37, 19-31.

Housner, G. W., and Jennings, P.C. (1982). *Earthquake design criteria*. Oakland, Calif.: Earthquake Engineering Research Institute.

Huang, C. F. D. (1993). "Dynamic soil foundation and foundation-soil-foundation interaction in 3D." Ph.D. Dissertation, Dept. Civil Eng., University South Carolina, Columbia.

Huang N. E., Shen Z., Long S. R., Wu M. C., Shih H. H., Zheng Q., Yen, N. C., Tung C. C., and Liu, H. H. (1998). "The empirical mode decomposition and the Hilbert spectrum for nonlinear and non-stationary time series analysis." *Proc. R. Soc. London*, 454, 903-995.

Iervolino, I. De Luca, F. and Cosenza, E. (2010). "Spectral shape-based assessment of SDOF nonlinear response to real, adjusted and artificial accelerograms." *Engineering and Structures*, 30, 2776-2792.

Iwan., W. D., and Hou, Z. K. (1989). "Explicit solutions for the response of simple systems subjected to non-stationary random excitation." *Structural Safety*, 6, 77-86.

Inoue, T., and Cornell, C. A. (1990). "Seismic hazard analysis of multi-degree-of-freedom structures." RMS-8, Reliability of Marine structures: Stanford, CA, 70

Jennings, P. C., Housner, G. W., and Tsai, C. (1969). "Simulated earthquake motions for design purpose." *Proc. 4th World Conference Earth. Engineering Santiago, A*, 1, 145-160.

Kanai, K. (1957). "Semi empirical formula for the seismic characteristics of the ground", University of Tokyo, *Bulletin of the Earthquake research institute*, 35, 309-325

Kattis, S. E., Polyzos, D., and Beskos, D. E. (1999). "Modelling of pile wave barriers by effective trenches and their screening effectiveness." *Soil Dynamics and Earthquake Engineering*, 18, 1-10.

Katsanos, E. I., Sextos, A. G., and Manolis G. D. (2010) "Selection of earthquake ground motion records: A state-of-the-art review from a structural engineering perspective." *Soil Dynamics and Earthquake engineering*, 30(4), 157-169.

Kaul, M. J. (1978). "Stochastic Characterization of earthquakes through their response spectrum." *Earthquake Engineering and Structural Dynamics*, 6, 497-509.

Kausel, E. (2010). "Early history of soil structure interaction." *Soil Dynamics and Earthquake Engineering*, 30, 822-832.

- Kham, M., Semblat, J. F., Bard, Y. P., and Dangla, P. (2006). "Seismic site city interaction: main governing phenomena through simplified numerical models." *Bulletin of seismological society of America*, 96(5), 1934-1951.
- Kitada, Y., Hirotsu, T., and Iguchi, M. (1999). "Models test on dynamic structure-structure interaction of nuclear power plant buildings." *Nuclear Engineering and Design*, 192, 205-216.
- Kobori, T., Minai, R., and Kusabe, K. (1973). "Dynamical characteristics of Soil-Structure Cross-Interaction System, I." *Bulletin Disas. Prev. Res. Inst., Kyoto Univ.*, 22(2), 113-151.
- Kostic, S., Vasovic, N., Perc, M., Toljic, M., and Nikolic, D. (2013). "Stochastic nature of earthquake ground motion." *Physica A*, 392, 4134-4145.
- Kramer, S. L. (1996). *Geotechnical Earthquake Engineering*. Prentice Hall.
- Kumar, P., Sandhu, H. K., and Chakrabortya, S. K., (2014). "Isolation of plane shear wave using water saturated trench barrier." *Soil Dynamics and Earthquake Engineering*, 59, 42-50.
- Lermitte, S., Chaudat, T., Payen, T., Vandeputte, D., and Viallet, E. (2008). "SMART 2008: seismic design and best estimate methods assessment for RC buildings subjected to torsion." *14th World Conf. on Earthquake Eng.*, Beijing, China.
- Luco, J. E. and Contesse, L. (1973). "Dynamic Structure-Soil-Structure Interaction." *Bulletin of seismological society of America*, 63(4), 1289-1303.
- Lutes, L. D. and Sarkani, S. (2004). *Random Vibration, Analysis of structural and mechanical systems*, 1st.Ed., Elsevier Butterworth-Heinemann.
- Marian, L., and Giaralis, A. (2014). "Optimal design of a novel tuned mass-damper-inerter (TMDI) passive vibration control configuration for stochastically support-excited structural system". *Probabilistic Engineering Mechanics*, 38, 156-164.

Meirovitch, L. (1980). *Computational methods in structural dynamics*. Sijthoff and Noordhoff, Alphen aan den Rijn, The Netherlands.

Lou, M., Wang, H., Chen, X., and Zhai, Y. (2011). "Structure soil structure interaction: literature review." *Soil Dynamics and Earthquake Engineering*, 31, 1724-1731.

Mikealov, G., Sarkani, S., and Lutes, L. D. (1999a). "Spectral characteristics of non-stationary random processes- a critical review." *Structural Safety*, 21, 223-244.

Mikealov, G., Sarkani, S., and Lutes, L. D. (1999b). "Spectral characteristics of non-stationary random processes: response of a simple oscillator." *Structural Safety*, 21, 245-267.

Mulliken, J. S., and Karabalis, D. L. (1998). "Discrete model for dynamic through-the-soil coupling of 3-D foundations and structures." *Earthquake Engineering and Structural Dynamics*, 27(7), 687-710.

Muscolino, G., Palmeri, A., and Ricciardelli, F. (2005). "Time-domain response of linear hysteretic systems to deterministic and random excitations." *Earthquake Engineering and Structural Dynamics*, 34, 1129-1147.

Muscolino, G., and Alderucci, T. (2015). "Closed form solution for the evolutionary frequency response function of linear systems subjected to separable or non-separable non-stationary stochastic excitation." *Probabilistic Engineering Mechanics*, 40, 75-89.

Naeim, F., and Lew, M. (1995). "On the use of design spectrum compatible time histories." *Earthquake Spectra*, 11(1), 111-127.

Naserkhaki, S., and Pourmohamad, H. (2012). "SSI and SSSI effects in seismic analysis of twin buildings: discrete model." *Journal of Civil Engineering and Management*, 18(6), 890-898.

Newland, D. E. (1989). *Mechanical vibration analysis and computation*, New York; London: Longman Scientific & Technical.

- Newmark, N. M. (1959). "A method of computation for structural dynamics." *Journal of Engineering Mechanics Division*, 85(3), 67-94.
- Ni, S. H, Xie, W.C., and Pandey M. D. (2011). "Tri-directional spectrum compatible earthquake time-histories for nuclear energy facilities." *Nuclear Engineering Design*, 241, 2732-2743.
- Ni, S. H, Xie, W.C., and Pandey M. D. (2013). "Generation of spectrum-compatible earthquake ground motions considering intrinsic spectral variability using Hilbert-Huang transform." *Structural Safety*, 42, 45-53.
- Ohtori, Y., Christenson R. E., Spencer B. F., and Dyke S. J. (2004). "Benchmark control problems for seismically excited nonlinear buildings." *Journal of Engineering Mechanics* (ASCE), 130(4), 366-85.
- Papadimitriou, K., and Beck, J. L. (1990). "Stochastic characterisation of ground motion and application to structural response." *Earthquake engineering, Tenth World Conference*, Balkema, Rotterdam ISBN 90 5410 0605.
- Park, Y. (1995). "New conversion method from Response Spectrum to PSD functions." *Journal of Engineering Mechanics*, 121(12), 1391-1392.
- Peng, Y., and Li, L. (2013). "A univariate phase spectrum model for simulation of non stationary earthquake ground motions." *Journal of Earthquake and Tsunami*, 10.1142/S1793431113500255, 1350025.
- Pfaffinger, D. D. (1983). "Calculation of power spectra from response spectra." *Journal of Engineering Mechanics*, 109(1), 357-372.
- Pousse, G., Bonilla, L. F., Cotton, F., Margerin, L. (2006). "Nonstationary Stochastic Simulation of String Ground Motion Time Histories Including Natural Variability: Application to the K-Net Japanes Database." *Bulletin of the Seismological Society of America*, 96(6), 2103-2117.
- Preumont, A. (1980). "A method for the generation of artificial earthquake accelerograms." *Nuclear Engineering and Design*, 59, 357-368.

Preumont, A. (1984). "The generation of spectrum compatible accelerograms for the design of nuclear power plants." *Earthquake Engineering and Structural Dynamic*, 12, 481-497.

Preumont, A. (1985). "The generation of non-separable artificial earthquake accelerograms for the design of nuclear power plants." *Nuclear Engineering and Design*, 88, 59-67.

Preumont, A., and Seto, K. (2008). *Active control of structures*. John Wiley & Sons, Ltd. ISBN: 978-0-470-03393-7.

Priestley, M. B. (1965) "Evolutionary Spectra and Non-Stationary Processes." *Journal of the Royal Statistical Society. Series B. (Methodological)*, 27(2), 204-237.

Priestley, M. B. (1981). *Spectral Analysis and Time Series*, Academic Press.

Rezaeian, S., and Der Kiureghian, A. (2008). "A stochastic ground motion model with separable temporal and spectral nonstationarities." *Earthquake Engineering and Structural Dynamics* 37, 1565-1584.

Rezaeian, S., and Der Kiureghian, A. (2010). "Simulation of synthetic ground motions for specified earthquake and site characteristics." *Earthquake Engineering and Structural Dynamics* 39, 1155-1180.

Richart, F. E., Hall, J. R., and Woods, R. D. (1970). *Vibrations of Soil Foundations*, Prentice-Hall, Englewood Cliffs, N.J.

Rofooei, F. R., Mobarake, A., Agmadi, G. (2001). "Generation of artificial records with a nonstationary Kanai-Tajimi model." *Engineering Structures*, 23(7), 827-837.

Rosenblueth, E., and Elorduy, J. (1969). "Response of linear systems to certain transient disturbances." *Proceeding 4th World Conference Earthquake Engineering, Santiago, Chile*, A-1, 185-196.

Sabetta, F., and Pugliese, A. (1996). "Estimation of response spectra and simulation of nonstationary earthquake ground motions." *Bulletin of Seismological Society of America*, (86)3,337-352.

Samali B. (2007). "System identification of a five story benchmark model using modal analysis." *Proceedings of the Asia Pacific Vibration Conference*, 701-706.

Saragoni, G. R., and Hart G. C., (1974). "Simulation of artificial earthquakes". *Earthquake Engineering and Structural Dynamics*, 2, 249-267.

Sarkar K., and Gupta, V. K. (2005). "Wavelet based simulation of spatially correlated and spectrum compatible accelerograms." *Proceedings of the national symposium on structural dynamics, random vibration and earthquake engineering, Bangalore*, 69-78.

Semblat, J. F., Kham, M., Guéguen, P., Bard, P. Y., and Duval, A. M. (2002). "Site-City Interaction through Modifications of Site Effects." *7th US Conference on Earthquake Engineering*, Boston: United States.

Shinozuka. M., and Jan D. M. (1972) "Digital simulation of random processes and its applications." *Journal of Sound and Vibration*, 25, 111–128.

Shinozuka, M., and Sato, Y. (1967). "Simulation of no-stationary random process." *Journal of Engineering mechanics (ASCE)*, 93, 11-40.

Shinozuka, M. (1987). "Stochastic fields and their digital simulation." *Stochastic methods in Structural Dynamics*, Martinus Nijhoff Publishers, Boston, M. Shinozuka, Editor, 93-133.

Shinozuka M. (1988) "State of the art report engineering modelling of ground motion." *Proceedings of Nineth Conference on Earthquake Engineering*, Tokyo-Kyoto, Japan.

Shinozuka, M. and Deodatis, G. (1988). "Stochastic Process Models for Earthquake Ground Motion." *Probabilistic Engineering Mechanics*, 3, 114-123.

- Shinozuka, M., and Deodatis, G. (1991) "Simulation of Stochastic Processes by Spectral Representation". *App. Mech. Rev.*, 44(4), 191-204.
- Shinozuka, M., and Deodatis, G. (1996) "Simulation of multi-dimensional Gaussian stochastic fields by spectral representation." *App. Mech. Rev.*, 49(1), 29-53.
- Shinozuka, M., Deodatis, G., Zhang, R., Papageorgiou, A. S. (1999). "Modeling, synthetics and engineering applications of strong earthquake wave motion." *Soil Dynamics and Earthquake Engineering*, 18, 209-228.
- Shrinkhande, M. and Gupta, V. K. (2011). "On the Characterisation of the Phase Spectrum for Strong Motion Synthesis." *Journal of Earthquake Engineering*, 5(04), 465-482.
- Saikia, A. (2014). "Numerical study on screening of surface waves using a pair of softer backfilled trenches." *Soil Dynamics and Earthquake Engineering*, 65, 206-213.
- Sha, S. G., Solanki, C. H., Desai, J. A. (2011). "Soil Structure interaction analysis methods- State of art Review." *International journal of Civil and Structural Engineering*, 2(1), 176-204.
- Silva de, C. W. (2007). *Vibration Damping, Control, and Design*, CRC press.
- Somerville, P. (1993). "Engineering applications of strong ground motion simulation." *Tectonophysics*, 218 195-219, Elsevier Science Publishers B.V., Amsterdam.
- Soong, T. T., and Spencer Jr, B. F. (2002). "Supplemental energy dissipation: state-of-the-art and state-of-the-practice." *Engineering Structures*, 24(3), 243-259.
- Spanos, P. D., and Giaralis, A. (2013). "Third-order statistical linearization-based approach to derive equivalent linear properties of bilinear hysteretic systems for seismic response spectrum analysis." *Structural safety*, 44,59-69.

Spanos, P. D., Kougioumtzoglou, I. A. (2011). "Harmonic wavelets based statistical linearization for response evolutionary power spectrum determination." *Probabilistic Engineering Mechanics*, 27, 57-68

Spanos, P., and Miller, S. (1993). "Hilbert transform generalisation of a classical random vibration integral." *American Society of Mechanical Engineers, Design Engineering Division*, 54, 195-203.

Spanos, P. D., and Vargas Loli, L. M. (1985). "A statistical approach to generation of design spectrum compatible earthquake time histories." *Soil Dynamics and Earthquake Engineering*, 4(1), 2-8.

Spanos, P., and Zeldin, B. (2000). "Pitfalls of Deterministic and Random Analyses of Systems with Hysteresis." *Journal of Engineering Mechanics*, 126(10), 1108-1110.

Spanos, P. D., Giaralis, A., and Politis, N. P. (2007a). "Time- frequency representation of earthquake accelerograms and inelastic structural response records using the adaptive chirplet decomposition and empirical mode decomposition." *Soil Dynamics and Earthquake Engineering* 27, 675-689.

Spanos, P., Tezcan, J., and Failla, G. (2002). "Wavelets applications in structural Dynamics." *Structural Dynamics, EURO DYN200*, Grundmann and SchutJller (eds.). 185-196.

Spanos, P., Tezcan, J., and Tratzkas, P. (2005). "Stochastic processes evolutionary estimation via harmonic wavelets." *Computer Methods in Applied Mechanics and Engineering*, 194, 1367-1383.

Spanos, P.D., Giaralis, A., Politis, N.P. and Roessett, J.M. (2007b). "Numerical treatment of seismic accelerograms and of inelastic seismic structural responses using harmonic wavelets." *Computer-Aided Civil and Infrastructure Engineering*, 22, 254-264.

Stewart, J. P., Fenves, G. L. and Seeds, R. B. (1999). "Seismic soil structure Interaction in buildings I: analytical methods." *Journal of geotechnical and Geoenvironmental Engineering*, 125, 26-37.

Sundararajan, C. (1980). "An iterative method for generation of seismic power spectral density functions." *Nuclear Engineering and Design*, 61, 13-23.

Thomson, W. T. (1993). *Theory of vibration with applications*, 4th Ed., Prentice Hall. ISBN 0-7487-4380-4.

Tombari, A., Zentner, I., and Cacciola, P. (2016). "Sensitivity of the stochastic response of structures coupled with vibrating barriers" *Probabilistic Engineering Mechanics*, 44, 183-193. ISSN 0266-8920.

Trombetta N. W., Hutchinson, T. C., Mason, H. B., Zupan, J. D., Bray, J. D., Bolisetti, C., Whittaker, A. S., Chen., Z. and Kutter, B. L. (2012). "Centrifuge modelling of structure-soil-structure interaction: Seismic performance of inelastic building models." *15th World Conference on Earthquake Engineering 15 WCEE*, Lisbon, Portugal.

Vanmarke, E. H. (1972). "Properties of spectral moments with applications to random vibration." *Journal of the Engineering Mechanics Division*, ASCE, 425-446.

Vanmarke, E. H. (1976). *Structural Response to Earthquake: Seismic Risk and Engineering Decisions*, Lomnitz, C. and Rosenblueth, E., editors, New York: Elsevier.

Vanmarcke, E. H., and Gasparini, D. A. (1977). "Simulated earthquake ground motions." *Proc. 4th Int. Conf. on Smirt*, K1/9, San Francisco.

Vanmarke, E. H. (1996). "Random processes and random fields in earthquake engineering." *Eleventh World Conference on Earthquake Engineering, Acapulco, Mexico*, paper No. 2170, ISBN 0 08 0428223.

Vetter, C., and A.A. Taflanidis (2014). "Comparison of alternative stochastic ground motion models for seismic risk characterization". *Soil Dynamics and Earthquake Engineering*, vol. 58, 48-65.

Watson-Lamprey, J., and Abrahamson, N. (2006). "Selection of ground motion time series and limits on scaling." *Soil Dynamics and Earthquake Engineering*, 26, 477-482.

Warburton, G. B., Richardson, J. D., and Webster, J. J. (1971). "Forced Vibration of Two Masses on an Elastic Space." *Journal of Applied Mechanics*, Transaction of the ASME, 148-156.

Warburton, G. B. (1982). "Optimum absorber parameters for various combinations of response and excitation parameters." *Earthquake Engineering and Structural Dynamics*, 10(3), 381-401.

Wang, G. (2011). "A ground motion selection and modification method capturing response spectrum characteristics and variability of scenario earthquakes." *Soil Dynamics and Earthquake Engineering*, 31,611-625.

Wang, H., Lou, M., Chen, X., and Zhai, Y. (2013). "Structure-Soil-Structure-Interaction between underground structure and ground structure." *Soil Dynamics and Earthquake Engineering*, 54, 31-38.

Wang, J., Fan Qian, L. S., and Zhou, J. (2002). "Simulations of non-stationary frequency content and its importance to seismic assessment of structures." *Earthquake Engineering and Structural Dynamics*, 31, 993-1005.

Wilson, E. L. (1968). "A computer program for the dynamic stress of underground structures." SESM Report 68-1, University of California, Berkley.

Wolf, J. P. (1985). *Dynamic Soil Structure Interaction*, Prentice-Hall.

Wolf, J. P. (1988). "Soil-Structure-Interaction Analysis in Time Domain." Prentice-Hall, Englewood Cliffs, N.J.

Wolf, J. P. and Deeks, A. J. (2004). *Foundation Vibration Analysis: a strength of material approach*. Elsevier, Burlington, MA.

Wong, H. L., and Trifunac, M. D. (1975). "Two dimensional, anti-plane, building-soil-building interaction for two or more buildings and for incident plane SH waves". *Bulletin of the Seismological society of America*, 65(6), 1863-1885.

Woods, R. D., (1968). "Screening of surface waves in soil." Report of The university of Michigan, Industry program of the college of engineering.

Yeh, C. H., and Wen, Y. K. (1990). "Modelling of non-stationary ground motion and analysis of inelastic structural response". *Structural Safety*, 8(1-4), 281-298.

Zentner, I., D'Amico, L., and Cacciola, P. (2013). "Simulation of non-stationary ground motion compatible with NGA-spectra". *11th International Conference on Structural Safety & Reliability, ICOSSAR 2013*, Columbia University New York, NY.

Appendix

NON STATIONARY STOCHASTIC ANALYSIS OF THE STRUCTURE SOIL STRUCTURE INTERACTION

LAURA D'AMICO, ALESSANDRO TOMBARI and
PIERFRANCESCO CACCIOLA

This paper investigates the dynamic response of structures under stochastic seismic input taking into account the Structure-Soil-Structure-Interaction (SSSI) mechanism. The wave field in urban environment is strongly affected by the presence of vibrating structures, this interaction and the consequent modification of the ground motion at the free field have not been scrutinized in detail yet. In this paper the response of two adjacent structures on superficial foundations forced by the ground acceleration processes is investigated. To this aim the ground motion is modelled as a Gaussian fully-non stationary spectrum compatible vector process satisfying the seismic codes requirements. A methodology for generating spatially variable response-spectrum compatible ground motions is presented by introducing a procedure of filtering in series of a non-separable power spectral density (PSD) function. The solution for determining the second order moments for multivariate and multicorrelated stationary processes is adapted to the case of non-stationary power spectral density matrix. Comparisons with pertinent Monte Carlo study will show the effectiveness of the approximate procedure adopted. The responses of both coupled and uncoupled conditions of the overall system are analyzed and specifically the impact of a non-stationary spatially variable ground motion in comparison with a quasi-stationary stochastic vector process is examined.

Keywords: Structure-Soil-Structure-Interaction, ground motion model, spatial variability, Monte Carlo Simulation, non-stationary vector process.

1 Introduction

Several authors observed that during earthquakes closely spaced buildings mutually affect their structural responses (Menglin et al. 2011). This cross dynamic interaction can influences the response of buildings especially in dense populated cities, for which the use of Structure-Soil-Structure-Interaction (SSSI) analyses is not accounted in the design practice. The interaction among neighboring buildings is triggered by the

soil deposit, motivating the site-city interaction studies, whose investigations have been recently enabled by the digital evolution.

Kham et al. (2006) revealed through numerical investigations that during earthquakes the energy released at the free field is reduced due to the perturbations generated by the structures in resonance with the soil deposit. This interaction has not been scrutinized in detail yet and only few contributions can be addressed to the study of discrete models for SSSI. Mulliken and Karabalis (1998) investigated two coupled building-foundation systems, observing the alteration of the structural responses due to the presence of the neighboring structures; more recently, Naserkhaki and Pourmohammad (2012) proposed a discrete model of two shear buildings and underlying soil accounting of both SSI and SSSI. The authors pointed out that heavier buildings influence adjacent lighter buildings more than others. A further contribution was given by Alexander et al. (2012) proposing a simple model of a pair of building with same base placed on superficial foundations. By modeling the SSSI mechanism through a rotational spring, the reduction of the response of the taller building has been observed while the vibrations of the smaller structure increased. Recently Cacciola and Tombari (2014) studied the dynamic cross interaction between two structures on deep foundations (i.e. piles), aiming to control the response of one of the two buildings by exploiting the vibrations of the other acting as a Vibrating Barriers (ViBa) opportunely calibrated.

In this paper the Structure-Soil-Structure-Interaction (SSSI) problem is tackled through the analysis of the response of the discrete model proposed by Alexander et al. (2012), which is herein extended accounting for the spatial variability of the seismic action. The modeling of a novel fully non-stationary Spectrum-Compatible Ground Motion vector process is proposed and compared to a quasi-stationary spectrum compatible ground motion by a numerical study. The structural response of the system for SSSI investigated considering both the quasi-stationary and non-stationary ground motions. A simplified approach is presented for the evaluation of the second order statistics of the response under the fully non-stationary seismic input. The evaluation of the stochastic response is herein performed by adapting the well-known formulation for the stationary case, to the case of a non-separable power spectral density matrix of the fully non-stationary vector process.

2 Discrete systems for SSSI and spatially variable GMM

In order to take into account for the wave propagation phenomenon in the stochastic analysis of a simple discrete model of SSSI, a suitable coherency model has to be considered for ground motion simulation. Herein the model proposed by Alexander et al. (2012) and depicted Figure 1, is presented and extended in order to account of the spatial variability of the seismic action.

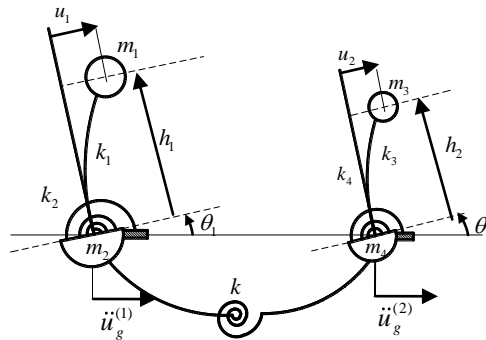


Figure 1 Discrete model for Structure Soil Structure Interaction after Alexander et al. (2012)

The model proposed by Alexander et al. (2012) is a 2D linear elastic system of two buildings including the soil underneath them. The buildings have 2 Degree Of Freedom (DOF) each, which are the translation of the lumped mass and the rotation of the foundation. The foundations are superficial and rigid and the interaction through the soil is represented by a rotational spring with stiffness k . The rotational stiffness is described as a function of the inter-building distance obtained empirically by modelling the foundations and soil with FEM software. By considering a pair of identical foundations placed on the same soil type at arbitrary distance, an inverse power law for k has been fitted. The absence of the rotational spring represents the condition of uncoupled buildings. The equations of motion of discrete SSSI model under spatially variable ground motion and un-damped conditions are the following

$$\begin{aligned} \mathbf{M}\ddot{\mathbf{u}}(t) + \mathbf{K}\mathbf{u}(t) &= -\mathbf{M}\mathbf{T}\ddot{\mathbf{u}}_g(t); \\ \mathbf{u}(t) = \mathbf{0}; \quad \dot{\mathbf{u}}(t) &= \mathbf{0}; \end{aligned} \quad (1)$$

where \mathbf{M} is the mass matrix, \mathbf{K} is the stiffness matrix, $\mathbf{u}(t), \dot{\mathbf{u}}(t), \ddot{\mathbf{u}}(t)$ are the vectors of the nodal displacements, velocities and accelerations and \mathbf{T} is the influence matrix given as

$$\mathbf{T} = \begin{bmatrix} -1 & 0 & 0 & 0 \\ 0 & 0 & -1 & 0 \end{bmatrix}^T \quad (2)$$

and the $\ddot{\mathbf{u}}_g(t)$ is the input vector for different input motion at the base of the two buildings.

Specifically Eq.(1) can be expressed for the system studied as follows

$$\begin{aligned}
& \begin{bmatrix} m_1 & -h_1 m_1 & 0 & 0 \\ -h_1 m_1 & h_1^2 m_1 + r_1^2 m_2 & 0 & 0 \\ 0 & 0 & m_3 & -h_2 m_3 \\ 0 & 0 & -h_2 m_3 & h_2^2 m_3 + r_2^2 m_4 \end{bmatrix} \begin{bmatrix} \ddot{u}_1(t) \\ \ddot{\theta}_1(t) \\ \ddot{u}_2(t) \\ \ddot{\theta}_2(t) \end{bmatrix} + \\
& + \begin{bmatrix} k_1 & 0 & 0 & 0 \\ 0 & k_2 + k & 0 & -k \\ 0 & 0 & k_3 & 0 \\ 0 & -k & 0 & k_4 + k \end{bmatrix} \begin{bmatrix} u_1(t) \\ \theta_1(t) \\ u_2(t) \\ \theta_2(t) \end{bmatrix} = \\
& = \begin{bmatrix} m_1 & 0 \\ -h_1 m_1 & 0 \\ 0 & m_3 \\ 0 & -h_2 m_3 \end{bmatrix} \begin{bmatrix} \ddot{u}_g^{(1)}(t) \\ \ddot{u}_g^{(2)}(t) \end{bmatrix} \quad (3)
\end{aligned}$$

where respectively u_1 and u_2 are the relative translational displacements of the building 1 and building 2 of mass m_1 and m_3 ; θ_1 and θ_2 are the rotations of the foundations masses m_2 and m_4 ; h_1 and h_2 are the buildings heights, r_1 and r_2 are the soil foundation masses radii of gyration, k_1 and k_2 are the stiffness and the rotational spring of building 1, k_3 and k_4 are stiffness and the rotational spring stiffness of building 2, \ddot{u}_{g_1} and \ddot{u}_{g_2} are the seismic input underneath building 1 and 2.

The equations of motion in Eq. (1) can be written in in terms of state variables $\mathbf{y}(t) = [\mathbf{u}(t) \quad \dot{\mathbf{u}}(t)]^T$ solved in the state variable in the following form

$$\dot{\mathbf{y}}(t) = \mathbf{D}\mathbf{y}(t) + \mathbf{v}\ddot{\mathbf{u}}_g(t); \quad \mathbf{y}(t_0) = \mathbf{0} \quad (4)$$

where

$$\mathbf{D} = \begin{bmatrix} \mathbf{0} & \mathbf{I}_n \\ -\mathbf{M}^{-1}\mathbf{K} & -\mathbf{M}^{-1}\mathbf{C} \end{bmatrix}; \quad \mathbf{v} = \begin{bmatrix} \mathbf{0} \\ \mathbf{T} \end{bmatrix} \quad (5)$$

in which the dissipation matrix \mathbf{C} is also introduced for sake of completion, which can be constructed in the modal space by assigning a constant value of damping to each mode.

3 Stochastic response

The second order statistical moments $\mathbf{m}_{2,Y}(t) = E[\mathbf{Y}(t) \otimes \mathbf{Y}(t)]$ are given as the solution of the following system of differential equations

$$\dot{\mathbf{m}}_{2,Y}(t) = \mathbf{D}_2 \mathbf{m}_{2,Y}(t) + \mathbf{f}_2(t) \quad (6)$$

in which \mathbf{D}_2

$$\mathbf{D}_2 = \mathbf{D} \otimes \mathbf{I}_{2n} + \mathbf{I}_{2n} \otimes \mathbf{D} \quad (7)$$

and

$$\begin{aligned} \mathbf{f}_2(t) = \\ = \mathbf{v} \otimes E[\ddot{\mathbf{u}}_g(t) \otimes \mathbf{Y}(t)] + E[\mathbf{Y}(t) \otimes \ddot{\mathbf{u}}_g(t)] \otimes \mathbf{v} \end{aligned} \quad (8)$$

The cross correlation terms in Eq.(8), expressed in the frequency domain for non-stationary input $\mathbf{S}_{i_g}(\omega, t)$, are herein approximated according to the expression

$$\begin{aligned} E[\ddot{\mathbf{u}}_g(t) \otimes \mathbf{Y}(t)] &\cong \int_{-\infty}^{+\infty} [\mathbf{I}_n \otimes \mathbf{H}(\omega)] \text{vec}\{\mathbf{S}_{i_g}(\omega, t)\} d\omega \\ E[\mathbf{Y}(t) \otimes \ddot{\mathbf{u}}_g(t)] &\cong \int_{-\infty}^{+\infty} [\mathbf{H}^*(\omega) \otimes \mathbf{I}_n] \text{vec}\{\mathbf{S}_{i_g}(\omega, t)\} d\omega \end{aligned} \quad (9)$$

where $\mathbf{H}(\omega)$ is the matrix transfer function of the system whose asterisk indicates its complex conjugate, \mathbf{I}_n is the identity matrix of order $n \times n$ and $\mathbf{S}_{i_g}(\omega, t)$ is the matrix of the mult correlated seismic stochastic input.

Note that the approximation introduced in Eq. (9) is assuming that the transfer function $\mathbf{H}(\omega, t)$ to be independent with respect to the time, it follows that the mathematical structure adopted in Eq.(9) is preserved as for the case of stationary input.

4 Simulation of spatially variable ground motion Gaussian time histories

Let assume the seismic ground motion as zero-mean Gaussian stochastic process fully described by the autocorrelation matrix or alternatively by the power spectral density matrix. According to the theory of the evolutionary spectra (Priestley 1965), a non-separable stochastic process can be expressed as follows

$$\begin{aligned} S_{\ddot{u}_g}(\omega, t) &= 0 & \omega < 0, \\ S_{\ddot{u}_g}(\omega, t) &= |a(\omega, t)|^2 S_{\ddot{u}_g}(\omega) & \omega \geq 0; \end{aligned} \quad (10)$$

where $S_{\ddot{u}_g}(\omega)$ is the two-sided power spectral density function, $a(\omega, t)$ is the frequency dependent modulating function, which particularizes in the uniformly modulated stochastic processes $a(\omega, t) = a(t)$.

Considering the one-dimensional multi-variate (1D-mV) zero-mean Gaussian non-stationary ground motion vector process $\ddot{u}_g^{(j)}(t) (j=1, \dots, m)$, the process is described by the cross-spectral density matrix (Deodatis 1996) which is given by

$$\mathbf{S}_{\ddot{u}_g}(\omega, t) = \begin{bmatrix} S_{11}(\omega, t) & \cdots & S_{1m}(\omega, t) \\ \vdots & \ddots & \vdots \\ S_{m1}(\omega, t) & \cdots & S_{mm}(\omega, t) \end{bmatrix} \quad (11)$$

which diagonal elements are real and non-negative functions and the off-diagonal terms are complex functions of ω . The cross spectral Hermitian and satisfies the following condition

$$\mathbf{S}_{\ddot{u}_g}(\omega, t) = \overline{\mathbf{S}_{\ddot{u}_g}}(\omega, t) \quad (12)$$

in which $\overline{\mathbf{S}_f}(\omega, t)$ is the complex conjugate of $\mathbf{S}_{\ddot{u}_g}(\omega, t)$. Therefore $\mathbf{S}_{\ddot{u}_g}(\omega, t)$ can be obtained by Cholesky's decomposition

$$\mathbf{S}_{\ddot{u}_g}(\omega, t) = \hat{\mathbf{H}}(\omega, t) \hat{\mathbf{H}}^{T*}(\omega, t) \quad (13)$$

where $\hat{\mathbf{H}}^{T*}(\omega, t)$ is the transposed conjugate of the lower triangular matrix $\hat{\mathbf{H}}(\omega, t)$ defined as

$$\hat{\mathbf{H}}(\omega, t) = \begin{bmatrix} \hat{H}_{11}(\omega, t) & 0 & \cdots & 0 \\ \hat{H}_{21}(\omega, t) & \hat{H}_{22}(\omega, t) & \cdots & 0 \\ \vdots & \vdots & \ddots & \vdots \\ \hat{H}_{m1}(\omega, t) & \hat{H}_{m2}(\omega, t) & \cdots & \hat{H}_{mm}(\omega, t) \end{bmatrix} \quad (14)$$

which elements are real and non-negative functions and the off-diagonal elements are generally complex functions of ω . After decomposition of the components of matrix $\mathbf{S}_{\ddot{u}_g}(\omega, t)$ according to Eq.(14) the non-

stationary ground motion vector process $\ddot{u}_g^{(j)}(t)$ can be simulated as follows (Shinozuka and Deodatis 1988)

$$\ddot{u}_g^{(j)}(t) = 2 \sum_{r=1}^m \sum_{s=1}^N \left| \hat{H}_{jr}(\omega_s, t) \right| \sqrt{\Delta\omega} \cos[\omega_s t - \mathcal{G}_{jr}(\omega_s, t) + \phi_{rs}] \quad (15)$$

where

$$\mathcal{G}_{jr}(\omega, t) = \tan^{-1} \left(\frac{\text{Im} \left[\hat{H}_{jr}(\omega, t) \right]}{\text{Re} \left[\hat{H}_{jr}(\omega, t) \right]} \right) \quad (16)$$

with $\text{Im}[\square]$ and $\text{Re}[\square]$ respectively the imaginary and real part of the complex function $\hat{H}_{jr}(\omega, t)$ and ϕ_{rs} are the N independent random phase angles uniformly distributed over $[0, 2\pi)$.

For simulating 1D-2V non-stationary ground motions according to Eq. (15), the two components of the vector process are specified as follows

$$\begin{aligned} \ddot{u}_g^{(1)}(t) &= 2 \sum_{s=1}^N \left| \hat{H}_{11}(\omega_s, t) \right| \sqrt{\Delta\omega} \cos[\omega_s t - \mathcal{G}_{11}(\omega_s, t) + \phi_{1s}] \\ \ddot{u}_g^{(2)}(t) &= 2 \sum_{s=1}^N \left| \hat{H}_{21}(\omega_s, t) \right| \sqrt{\Delta\omega} \cos[\omega_s t - \mathcal{G}_{21}(\omega_s, t) + \phi_{1s}] + \\ &+ 2 \sum_{s=1}^N \left| \hat{H}_{22}(\omega_s, t) \right| \sqrt{\Delta\omega} \cos[\omega_s t - \mathcal{G}_{22}(\omega_s, t) + \phi_{2s}] \end{aligned} \quad (17)$$

4.1 Spectrum compatible quasi-stationary stochastic vector processes

Numerous quasi-stationary models have characterized the framework of spectrum compatible ground motion processes in the last 30 years (see e.g. Vanmarcke and Gasparini 1977, Kaul 1978, Sundararajan 1980, Pfaffinger 1983, Park 1995; Cacciola et al. 2004). The designation of spectrum compatible ground motion PSD functions is generally based on the “first passage problem” (Vanmarcke and Gasparini 1977), which is expressed by the following relationship

$$RSA(\omega_0, \zeta_0) = \omega_0^2 \eta_U(T_s; p) \sigma_U \quad (18)$$

where $RSA(\omega_0, \zeta_0)$ is the pseudo-acceleration response spectrum for a given damping ratio ζ_0 and natural circular frequency ω_0 , η_U is the dimensionless peak factor, T_s is the time observing window, p is the not-exceeding probability of the barrier and σ_U is the standard deviation of the displacement.

The recursive formula proposed by Cacciola et al. (2004) for the unilateral response spectrum compatible PSD function will be used in the following

$$\begin{aligned}
 G(\omega_i) &= 0, & \forall 0 \leq \omega \leq \omega_\alpha \\
 G(\omega_i) &= 2S(\omega_i) = \frac{4\zeta_0}{\omega_i\pi - 4\zeta_0\omega_{i-1}} \times \\
 &\times \left(\frac{RSA(\omega_i, \zeta_0)^2}{\bar{\eta}_U^2(\omega_i, \zeta_0)} - \Delta\omega \sum_{k=1}^{i-1} G(\omega_k) \right); \forall \omega > \omega_\alpha
 \end{aligned} \tag{19}$$

where $\bar{\eta}_U$ is the approximated peak factor determined under the hypothesis of barrier out-crossing in clumps and by assuming a smooth shape input and $\zeta_0 \ll 1$

$$\begin{aligned}
 \bar{\eta}_U(\omega_i, \zeta_0) &= \\
 &= \sqrt{2\ln \left\{ 2N_U \left[1 - \exp \left[-\delta_U^{1.2} \sqrt{\pi \ln(2N_U)} \right] \right] \right\}}
 \end{aligned} \tag{20}$$

in which

$$N_U = \frac{T_s}{2\pi} \omega_i (-\ln p)^{-1} \tag{21}$$

and bandwidth factor

$$\begin{aligned}
 \delta_U &= \\
 &= \sqrt{1 - \frac{1}{1 - \zeta_0^2} \left(1 - \frac{2}{\pi} \arctan \frac{\zeta_0}{\sqrt{1 - \zeta_0^2}} \right)^2},
 \end{aligned} \tag{22}$$

also $\omega_\alpha \cong 1$ rad/s is the lowest bound of the existence of the peak factor.

The stationary process determined through Eq. (19)-(22) is time-modulated by using the function of Jennings et al. (1969), which reads

$$a(t) = \begin{cases} \left(\frac{t}{t_1}\right)^2 & t < t_1 \\ 1 & t_1 \leq t \leq t_2 \\ \exp[-\beta(t-t_2)] & t > t_2 \end{cases} \quad (23)$$

which parameters will be (Cacciola et al. 2014)

$$\beta = \frac{9}{T_s}; t_1 = \frac{2.5}{\beta}; t_2 = \frac{11.5}{\beta}. \quad (24)$$

Eqs.(19)-(24) define the stochastic ground motion at a single point in the free field. In order to extend the model above presented for taking into account for spatial variability and wave propagation, the response spectrum compatible cross-spectral density matrix is introduced (see e.g. Deodatis 1996).

By extending the mono-correlated model described above to a multi-correlated vector process, the terms in Eq.(11) are given by the following

$$\begin{aligned} S_{jj}^{SC}(\omega, t) &= |a_j(t)|^2 S_j^{SC}(\omega), \\ S_{jk}^{SC}(\omega, t) &= a_j(t)a_k(t)\sqrt{S_j^{SC}(\omega)S_k^{SC}(\omega)}\Gamma_{jk}(\omega) \end{aligned} \quad (25)$$

where $a_j(t)$ and $S_j^{SC}(\omega)$ are the modulating function and the spectrum compatible PSD function with prescribed response spectrum at the location j given by Eq. (23) and (19) respectively, and $\Gamma_{jk}(\omega)$ the coherency function expressed as

$$\Gamma_{jk}(\omega) = |\gamma_{jk}(\omega)| \exp[i\theta_{jk}(\omega)] \quad (26)$$

in which $|\gamma_{jk}(\omega)|$ is the incoherence effect and $\exp[i\theta_{jk}(\omega)]$ is the imaginary term describing the site response and the wave passage effect (Der Kiureghian 1996).

Once the terms of the spectrum compatible response power spectral density matrix are defined, samples of ground motion time histories compatible with given response spectra can be simulated through Eqs. (17). In order to improve the matching between the prescribed response spectrum and the mean simulated stochastic response spectral accelerations, the following iterative scheme is generally employed

$$S_j^{SC}(\omega_i) = S_j^{SC(k-1)}(\omega_i) \left[\frac{RSA(\omega_i, \zeta_0)}{\overline{RSA}^{(k-1)}(\omega_j, \zeta_0)} \right]^2 \quad (27)$$

where $\overline{RSA}^{(k-1)}$ is the approximate pseudo-acceleration spectrum determined at the k -th iteration and RSA the target response spectrum.

4.2 Spectrum compatible non-stationary stochastic vector processes

International seismic codes do not impose any condition of the non-stationary features of the simulated ground motions, although the non stationarity can be relevant for several cases of engineering interest (see e.g. Cacciola et al. 2014). To evaluate non-stationary spectrum compatible PSD functions from a given response spectrum, the “first passage problem” can be pursued by solving the following high non-linear problem

$$\exp \left[- \int_0^{t_f} \alpha_U (RSA(\omega_0, \zeta_0), t) dt \right] = p \quad (28)$$

where t_f is the time interval in which the ground motion possesses not negligible energy and α_U is the hazard function.

Alternative procedures were proposed in order to simplify the problem presented in Eq. (28) (Spanos & Vargas Loli 1985; Preumont 1985; Cacciola 2010). In the scenario of spectrum compatible ground motion simulation, several authors contributed to the current state of the art with regard to the modelling of both frequency non-stationarity and spatial variability (Hao et al. 1989, Deodatis 1996, Sarkar and Gupta 2005, Cacciola and Deodatis 2011). In particular, Cacciola and Deodatis (2011) proposed a method to simulate fully non-stationary and response spectrum compatible ground motion processes by a correction in parallel of a selected “local” ground motion vector process, that is

$$\begin{aligned} S_{jj}^{SC}(\omega, t) &= S_L^{(j)}(\omega, t) + S_C^{(j)}(\omega, t), \\ S_{jk}^{SC}(\omega, t) &= \sqrt{S_{jj}^{SC}(\omega, t) S_{kk}^{SC}(\omega, t)} \Gamma_{jk}(\omega) \end{aligned} \quad (29)$$

where $S_L^{(j)}(\omega, t)$ is a “local” evolutionary counterpart and $S_C^{(j)}(\omega)$ a stationary “corrective” PSD function.

In this work an alternative approach to define a fully non-stationary spectrum compatible ground motion vector process is proposed. The approach proposed is based on the correction in series of a “local” evolutionary model, which represents seismicity and spatial variability of the original site, through a stationary corrective counterpart, that is

$$\begin{aligned}
 S_{ij}^{SC}(\omega, t) &= S_L^{(j)}(\omega, t) S_C^{(j)}(\omega) \\
 S_{jk}^{SC}(\omega, t) &= \sqrt{S_{ij}^{SC}(\omega, t) S_{kk}^{SC}(\omega, t)} \Gamma_{jk}(\omega)
 \end{aligned} \tag{30}$$

where $S_L^{(j)}(\omega, t)$ is a “local” evolutionary counterpart and $S_C^{(j)}(\omega)$ a stationary “corrective” PSD function.

The corrective term is defined by extending the model proposed by Preumont (1985) and revised by Cacciola and Zentner (2012) to vector processes. Specifically through the energy balance approach the corrective term for each individual component is determined according to the following equation

$$S_C^{(j)}(\omega) = \frac{\int_0^{\infty} a_j^2(t) dt}{\int_0^{\infty} |S_L^{(j)}(\omega, t)|^2 dt} S^{SC(j)}(\omega) \tag{31}$$

where $a_j(t)$ is the modulating function defined in Eq. (23) and $S^{SC(j)}(\omega)$ is the stationary PSD function given in Eq. (19) determined for the j -th response spectrum.

Therefore, the proposed procedure to generate fully non-stationary response-spectrum compatible ground motion vector process requires the following steps:

- (i) definition of a “local” power spectral density matrix $\mathbf{S}_L^{(j)}(\omega, t)$ taking into account of the seismological and geological conditions
- (ii) definition of the target spectra at each location j at the free field
- (iii) evaluation of the quasi-stationary response spectrum compatible PSD function $S^{SC}(\omega_j)$ in Eq. (19) for each response spectrum.
- (iv) evaluation of the corrective term $S_C^{(j)}(\omega)$ in Eq. (31) and definition of the elements of the response spectrum compatible matrix in Eq. (30)
- (v) simulation of the ground motion time histories through the procedure proposed by Deodatis (1996) described in Eqs. (11)-(17)
- (vi) implementation of the iterative scheme in Eq. (27) to enhance the spectrum compatibility of the simulated response spectral accelerations and the target response spectra.

5 Numerical application

In this section the stochastic response of the discrete model for SSSI is determined. The system is forced by both the quasi-stationary and fully non-stationary ground motion models in order to show: (i) the effects of

the SSSI mechanism on the structural response, (ii) the influence of the different hypothesis of quasi-stationarity and non-stationarity of the input on the structural responses. In order to demonstrate the validity of the approximate second order statistics presented in this work, the results of the direct stochastic analysis are compared to the Monte Carlo Simulation of the responses performed in the time domain.

5.1 Ground motion models specifications

The SSSI system under analysis is forced by two sets of 1D-2V ground motions processes simulated by using Eqs. (11)-(17) to model the quasi-stationary and the fully non stationary ground motion vector processes.

In order to generate spectrum compatible accelerograms the Eurocode 8 response spectrum is considered

$$\begin{aligned}
 RSA(T) &= a_g S \left[1 + \frac{T}{T_B} (1.5) \right]; 0 \leq T \leq T_B \\
 RSA(T) &= 2.5 a_g S; \quad T_B \leq T \leq T_C \\
 RSA(T) &= 2.5 a_g S \left[\frac{T_C}{T} \right]; \quad T_C \leq T \leq T_D \\
 RSA(T) &= 2.5 a_g S \left[\frac{T_C T_D}{T^2} \right]; T_D \leq T \leq 4s
 \end{aligned} \tag{32}$$

where a_g is the design peak ground acceleration; S is the soil factor and T is the natural period of a SDOF system.

The code recommends that the mean response-spectrum of the simulated time-histories matches the target response spectrum within a prescribed tolerance along the prefixed range of periods given by

$$\max \left\{ \frac{\overline{RSA}(T) - RSA(T)}{RSA(T)} \times 100 \right\} \leq 10\% \tag{33}$$

where \overline{RSA} is the mean peak response-spectrum of at least three simulated accelerograms and $RSA(T)$ is the target response spectrum. Moreover it has to be verified the following conditions

$$\overline{RSA}(0) > a_g S \tag{34}$$

where $\overline{RSA}(0)$ is the peak ground acceleration of the simulated process.

Two different soil profiles are considered, therefore relevant parameters of the response spectra are summarized in Table 1.

Table 1. Parameters for ground Type A and B Type1 according to the Eurocode 8 provisions

Parameter	Soil A	Soil B
S	1.	1.2
a_g	0.1 g	0.1 g
T_B	0.15 s	0.15 s
T_C	0.4 s	0.5 s
T_D	2.00 s	2.00 s

Furthermore in this study the coherency model of Harichandran and Vanmarke (1986) that is

$$\Gamma_{jk}(\omega) = A \exp\left[-\frac{2d}{a\theta(\omega)}(1-A+aA)\right] + (1-A) \exp\left[-\frac{2d}{\theta(\omega)}(1-A+aA)\right] \quad (35)$$

where $d=50.4$ m is the distance between the two structures, A and a are parameters derived from data records and the angle $\theta(\omega) = k \left[1 + (\omega/\omega_0)^b\right]^{-0.5}$.

In order to implement the quasi-stationary ground motion vector process, the cross-spectral density matrix in Eq. (11) has been specified with Eq. (25), in which the time modulating function $a_j(t)$ is set according to Eq. (23) with values $t_1 = 2.78s$, $t_2 = 12.78s$ and $\beta = 0.9$ determined by Eq. (24) and the spectrum compatible stationary PSD function $S_{jj}^{SC}(\omega)$ pertinently to Eqs (19)-(22).

Table 2. Coherency function parameters from empirical data of SMART 1 dense array event 20.

k	a	A	$\omega_0(\text{Hz})$	b
31200	0.0186	0.636	1.51	2.95

A number of five hundred quasi-stationary ground motion time histories were simulated via Spectral Representation Method by Eq. (17) (Deodatis 1996), by superposing a number of $N_a=1000$ harmonics sampled with a frequency step $\Delta\omega = 0.1 \text{ rad/s}$; the total signal duration is set equal to 20s and the strong motion phase is selected according to the minimum

value required by the code of $T_s = 10s$. The comparison of the simulated averaged response spectral accelerations and the target spectra are displayed in Figure 2. The averaged coherency function evaluated from the accelerograms sampled in comparison to the model is shown in Figure 3.

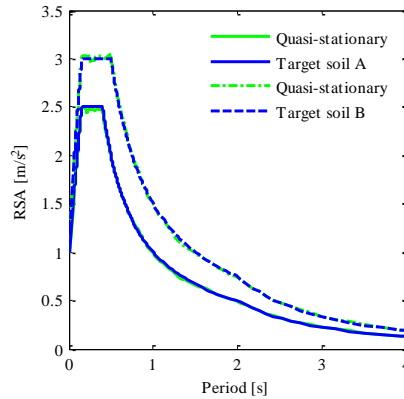


Figure 2. Comparison of the mean ensemble of the simulated response spectra and target spectra.

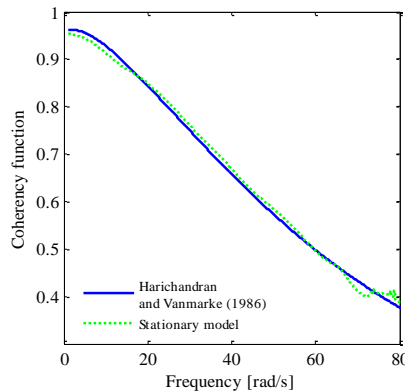


Figure 3. Comparison of the coherency model and simulated coherency function for the simulated quasi-stationary vector process.

It is noted the remarkable accuracy in matching the target functions.

The fully non-stationary vector process according to the prescribed cross spectral density matrix seen in Eq.(11), has been specified though the elements in Eq.(30).

Specifically, in this application the local PSD function $S_L^{(j)}(\omega, t)$ in Eq. (30) is selected as

$$\begin{aligned}
 S_L^{(j)}(\omega, t) &= \\
 &= a(t) \frac{1 + 4\zeta_g^2 \left(\frac{\omega}{\omega_g(t)}\right)^2}{\left\{1 - \left(\frac{\omega}{\omega_g(t)}\right)^2\right\}^2 + 4\zeta_g^2 \left(\frac{\omega}{\omega_g(t)}\right)^2} \times \\
 &\quad \times \frac{\left(\frac{\omega}{\omega_f(t)}\right)^4}{\left\{1 - \left(\frac{\omega}{\omega_f(t)}\right)^2\right\}^2 + 4\zeta_f^2 \left(\frac{\omega}{\omega_f(t)}\right)^2}
 \end{aligned} \tag{36}$$

where $\omega_g(t)$ and $\omega_f(t)$ are the time variant circular frequencies, $\zeta_g(t)$ and $\zeta_f(t)$ the damping ratios of the ground. Also, the circular frequency of the second filter is given by the relation $\omega_f(t) = 0.1\omega_g(t)$ rad/sec.

With regard to the modeling of the frequency content of the process, the filter parameters $\omega_g(t)$ is assumed to be a linear function, which reads

$$\omega_g(t) = \omega_0 - (\omega_0 - \omega_F) \frac{t}{t_F} \tag{37}$$

where ω_g is the predominant frequency of the modelled earthquake, ω_0 is the frequency at the time instant $t=0$, ω_F is the frequency at final time $t_F = 20s$. For illustrative purposes the following values $\omega_0 = 20$ rad/s, $\omega_F = 15$ rad/s, $\zeta_g = 0.2$ and $\zeta_f = 0.6$ have been assumed. The average of the ensemble of the artificial time histories for the novel fully non-stationary ground motion process are in agreement with the target response spectra as Figure 4 shows; in Figure 5 the ensemble average of the simulated coherency functions and the empirical model of Harichandran and Vanmarke (1986) are also compared.

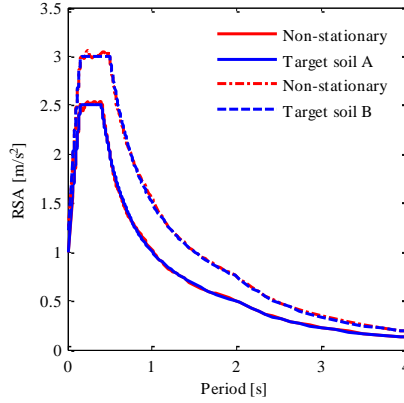


Figure 4. Comparison of the mean ensemble average of the simulated response spectra and target spectra.

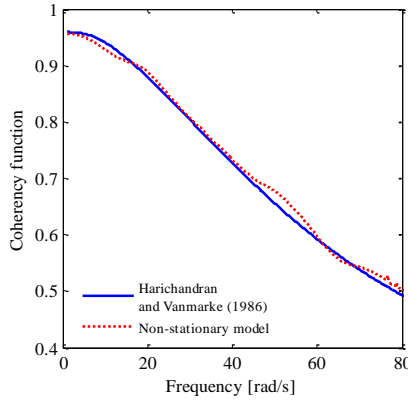


Figure 5. Comparison of the coherency model and ensemble average of the simulated coherency function for the simulated non-stationary vector process.

By the comparison of Figures 2-5 it can be observed that both quasi-stationary and fully non-stationary vector processes are equivalent in terms of response spectra and coherence function.

5.2 Structural response

In this section the stochastic response of the discrete SSSI model is studied, considering both the response spectrum compatible vector processes determined in the previous sections.

The two buildings are modelled as 2 DOF systems with the following values of the mechanical parameters (see Eq. (3)): $m_1=13,107$ Kg, $m_2=11,469$ Kg, $m_3=14,418$ Kg, $m_4=11,469$ Kg, $k_1=4.27 \times 10^7$ N/m, $k_2=3.6 \times 10^7$ N/m, $k_3=1.99 \times 10^{12}$ N/m, $k_4=1.99 \times 10^{12}$ N/m, $k=-2.88 \times 10^{11}$ N/m,

$h_1=84$ m, $h_2=93$ m, $b=42$ m. A constant value of the 5% damping is assumed for all the modes. The first two modal frequencies evaluated for the uncoupled and coupled conditions are $\omega_{1unc} = 45.57$ rad/s, $\omega_{2unc} = 52.19$ rad/s, $\omega_{1c} = 45.80$ rad/s, $\omega_{2c} = 56.60$ rad/s.

The second order statistical moments of the structural response are evaluated through the presented approximated stochastic analysis by Eq. (6)-(9) and compared with Monte Carlo Simulation by solving the dynamic equation of motion for the stochastic input under the hypotheses of quasi-stationary and non-stationary model.

Figure 6 and Figure 7 present the responses in terms of total displacements of the top masses of the two buildings respectively for the quasi-stationary and non-stationary input.

An excellent agreement can be observed between the approximated stochastic response and the Monte Carlo Simulation. This is due to the fact that two structures can be considered rigid in compared to the frequency distribution of the ground motions.

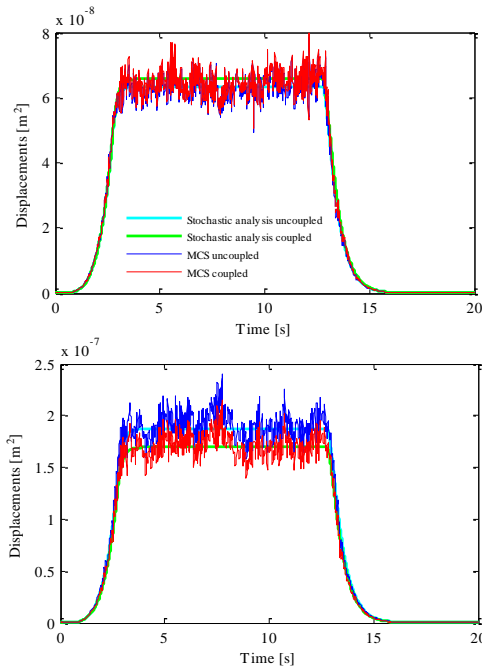


Figure 6. Comparison Monte Carlo Simulation and Direct Stochastic Analysis: a) Second order statistics for building 1; b) Second order statistics for building 2.

Furthermore from Figure 6 a) and Figure 7 a) the increment of the second order statistics for coupled conditions with respect to the uncoupled

response can be observed. On the other hand Figure 6 b) Figure 7b) show a reduction of the response from uncoupled to coupled conditions, demonstrating therefore the exchange of energy between the building 1 and 2. This is in agreement with what has been already observed elsewhere (see e.g. Alexander et al. 2012).

Remarkably from the comparison between Figure 6 and Figure 7, the highest peak of the statistics of the responses are observed in the case of fully non-stationary input in both coupled and uncoupled conditions.

6 Concluding remarks

The seismic analysis of two linear behaving buildings accounting of the SSSI phenomenon and the spatial variability of the ground motion have been investigated. The response to two different 1D-2D stochastic vector processes (i.e. quasi-stationary and fully non-stationary) possessing same mean 5% damping response spectra have been compared.

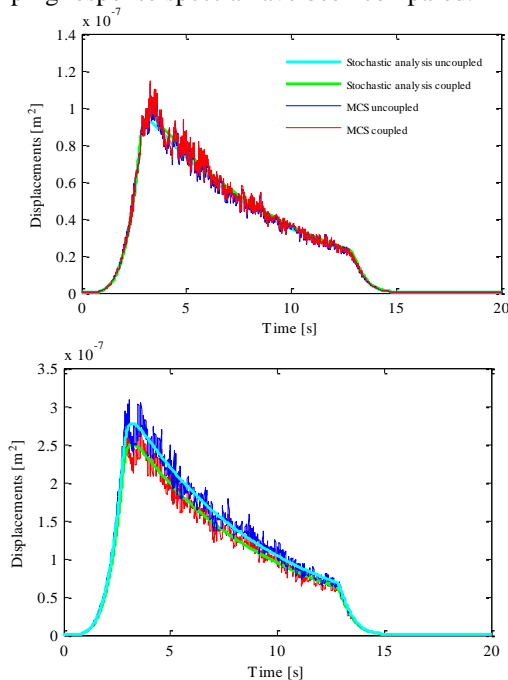


Figure 7. Comparison Monte Carlo Simulation and Direct Stochastic Analysis: a) Second order statistics for building 1; b) Second order statistics for building 2.

The second order statistical moments are determined by approximation of well-known mathematical structures for the case of stationary input motion. Comparison between Monte Carlo Simulation and the results obtained by the approximated procedure show consistency of the results validating the approximate solution of the second order moments. Higher

values of the evolution of the second order statistic of the response of the SSSI systems are observed when this is forced by non-stationary ground motion model. These differences induce to conclude that the quasi-stationary models not always lead to over-conservative results as generally accepted. Remarkably, it has to be observed that when the SSSI is not taken into account an amount of energy exchanged between neighboring structures would be neglected underestimating the response of one of the two structural systems.

References

- Alexander, N.A. Ibraim, E. Aldaikh, H., A simple discrete model for interaction of adjacent buildings during earthquakes, *Computers and Structures*, 124(1-10), 2012.
- Cacciola, P., A stochastic approach for generating spectrum compatible fully non-stationary earthquakes, *Computers and Structures*, 88(15-16), 889-901, 2010.
- Cacciola, P. Colajanni, P. and Muscolino, G., Combination of modal responses consistent with seismic input representation, *J. of Structural Engng ASCE*, 130(1), 47-55, 2004.
- Cacciola, P. and Deodatis, G., A method for generating fully non-stationary and spectrum-compatible ground motion vector processes, *Soil dyn. Earth. Engng.*, 31(3), 351-360, 2011.
- Cacciola, P. and Zentner, I., Generation of response spectrum compatible artificial earthquake accelerograms with random joint time frequency distributions, *J. Prob. Engng. Mech.*, 28, 52-58, 2012.
- Cacciola, P. D' Amico L. and Zentner, I., New insights in the analysis of the structural response to spectrum-compatible accelerograms, *Engineering Structures*, DOI: 10.1016/j.engstruct.2014.07.015.
- Cacciola, P. and Tombari, A., Vibration Control of Structures through Structure-Soil-Structure-Interaction". *Proc. of the 9th International Conference on Structural Dyn. Eurodyn*, Porto, Portugal, 2014.
- Deodatis, G., Non-stationary stochastic vector processes: seismic ground motion applications. *J. Prob. Engng. Mech.*, 11, 149-168, 1996.
- Der Kiureghian, A., A coherency model for spatially varying ground motion, *Earthquake engineering and structural dynamics*, 25, 99-111, 1996
- Eurocode 8, Design of structures for earthquake resistance, Part 1: General rules, 2010.
- Hao, H. Oliveira, C.S. and Penzien, J., Multiple-station ground motion processing and simulation based on SMART-1 array data, *Nuclear Engng. and Design*, 111, 293-310. 1989.
- Jennings, P.C. Housner, G.W. and Tsai, C., Simulated earthquake motions for design purpose, *Proc. 4th World Conference Earth. Engineering Santiago*, A(1), 145-160, 1969.
- Kaul, M.J., Stochastic Characterization of earthquakes through their response spectrum, *Earth. Engng. and Structural Dyn.*, 6, 497-509. 1978.
- Kham, M. Semblat, J.F. Bard, Y.P. Dangla, P., Seismic site city interaction: main governing phenomena through simplified numerical models, *Bulletin. of seismological society of America*, 96(5), 1934-1951, 2006.
- Menglin, L. Huaifeng C. Xi, C. Zhai, Yongmei, Z., Structure soil structure interaction: literature review, *Soil dyn. Earth. Engng.*, 31, 1724-1731, 2011.

- Park, Y., New conversion method from Response Spectrum to PSD functions, *J. of Engng. Mech.*, 121(12), 1391-1392, 1995.
- Pfaffinger, D.D., Calculation of power spectra from response spectra, *J. of Engng. Mech.*, 109(1),357-372.1 983.
- Preumont, A., The generation of non-separable artificial earthquake accelerograms for the design of nuclear power plants. *Nuclear Engng. and Design*, 88, 59-67. 1985.
- Priestley, M.B., Evolutionary Spectra and Non-Stationary Processes, *J. of the Royal Statistical Society, Series B. (Methodological)*, 27(2), 204-237, 1965
- Shinozuka, M. and Deodatis, G., Stochastic Process Models for Earthquake Ground Motion, *Prob. Eng. Mech.*, (3), 114-123, 1988.
- Spanos, P.D. and Vargas Loli L.M., A statistical approach to generation of design spectrum compatible earthquake time histories. *Soil Dyn. and Earth. Engng.*, 4(1):2-8, 1985.
- Sundararajan, C., An iterative method for generation of seismic power spectral density functions, *Nuclear Engng. and Design*, 61,13-23. 1980
- Vanmarcke, E.H. and Gasparini, D.A., Simulated earthquake ground motions, *Proceedings of the 4th International Conference on Smirt*, K1/9, San Francisco, 1977.
- Harichandran, R.S. and Vanmarcke, E.H Stochastic variation of earthquake ground motion in space and time, *J. of Engng. Mech, ASCE*, 112,154-74, 1986.